

THE HISTORY OF SEDIMENTATION AND
ABYSSAL CIRCULATION ON THE
GREATER ANTILLES OUTER RIDGE

by

BRIAN EDWARD TUCHOLKE

B.S., South Dakota School of Mines & Technology
(1968)

SUBMITTED IN PARTIAL FULFILLMENT OF THE
REQUIREMENTS FOR THE DEGREE OF
DOCTOR OF PHILOSOPHY

at the

MASSACHUSETTS INSTITUTE OF TECHNOLOGY

and the

WOODS HOLE OCEANOGRAPHIC INSTITUTION

August, 1973

Signature of Author.....
Joint Program in Oceanography, Massachu-
setts Institute of Technology - Woods Hole
Oceanographic Institution, and Department
of Earth & Planetary Sciences, and Depart-
ment of Meteorology, Massachusetts Insti-
tute of Technology, August, 1973

Certified by.

.....
Thesis Supervisor

Accepted by.....
Chairman, Joint Oceanography Committee in
the Earth Sciences, Massachusetts Insti-
tute of Technology - Woods Hole Oceano-
graphic Institution

Lindgren
~~WITHDRAWN~~
~~FROM~~ 1973
MIT LIBRARIES

THE HISTORY OF SEDIMENTATION AND ABYSSAL CIRCULATION ON THE GREATER ANTILLES OUTER RIDGE

Brian E. Tucholke

Submitted to the Massachusetts Institute of Technology-Woods Hole Oceanographic Institution Joint Program in Oceanography on August 13, 1973, in partial fulfillment of the requirements for the degree of Doctor of Philosophy.

ABSTRACT

The Greater Antilles Outer Ridge is an 1800 km long, submarine sedimentary ridge which lies below 5000 m in the southwestern North Atlantic Ocean. Seismic reflection profiles and core data indicate that the ridge is composed of more than 6×10^4 km³ of acoustically transparent sediment which has accumulated above a sequence of acoustically stratified sediments deposited before late Eocene time.

The sediments consist of low-carbonate, homogeneous, terrigenous lutites which have accumulated at rates of up to 30 cm/1000 yr. since the middle Eocene. Clay-mineral analyses indicate that the chlorite-enriched sediment is derived from the northeastern continental margin of North America.

Abyssal contour-following currents which flow around the Greater Antilles Outer Ridge are interpreted as an extension of the Western Boundary Undercurrent (WBUC) found along the continental rise of eastern North America. This current system is proposed to be the agent which has transported sediment southward for more than 2500 km and deposited it on the Greater Antilles Outer Ridge. Sediment is presently carried in concentrations up to 65 ug/liter in the currents flowing around the outer ridge, and mineral analyses show that the suspended sediment has a northern provenance; it is similar in composition to the bottom sediment and is interpreted as the source of sediment deposited on the Greater Antilles Outer Ridge.

The Puerto Rico Trench began to form in middle Eocene time, and it cut off direct downslope sedimentation to the Greater Antilles Outer Ridge. At the same time, the newly formed WBUC interacted with existing sea-floor topography and the Antarctic Bottom Water (AABW) flowing in from the South Atlantic, and it began to deposit acoustically trans-

parent sediment on the eastern outer ridge. This depositional pattern persisted until the middle or late Miocene, when increased AABW flow diverted the WBUC to the northwest and initiated deposition of the western sector of the Greater Antilles Outer Ridge. Shortly thereafter, decreased AABW flow and lower current speeds allowed rapid deposition of sediment on the Greater Antilles Outer Ridge and on the Caicos Outer Ridge to the west. The bottom topography has controlled the abyssal current pattern, and current-controlled deposition has continued to construct the Greater Antilles Outer Ridge since early Pliocene time.

Thesis Supervisor: Dr. Charles D. Hollister
Title: Associate Scientist

ACKNOWLEDGEMENTS

I thank Charles D. Hollister for his enthusiastic support and guidance, and for serving as my thesis advisor during the course of this research. Support and encouragement from the members of my thesis committee, W.R. Wright, J.D. Milliman, and J.B. Southard, are also gratefully acknowledged.

I have greatly profited by discussions with E.T. Bunce, J.I. Ewing, D.A. Johnson, J.C. Hathaway, A.J. Silva and B. Haq. S. Dawson helped with the carbonate analyses, W.R. Wright made the geostrophic calculations, and D. Habib examined palynomorph assemblages.

The CHAIN 57 cores from the core laboratory at Woods Hole were made available through E.T. Bunce, and other cores were collected with the support of NSF Grant GA 24872 and Contract N00014-66-C0241 NR 083-004 from the Office of Naval Research. Cores and core data collected under contracts ONR (N00014-67-A-0108-0004) and NSF- GA 35454 were made available from the Lamont-Doherty Geological Observatory core laboratory by R. Capo and M. Truchan. Seismic reflection data were kindly provided by J.I. Ewing, E.T. Bunce, C.H. Savit and H. Banks.

I am also indebted to W.R. Wright, A.H. Driscoll, A.J. Silva, M. Stalcup, W. Beloff, and R. Flood for their

efforts in collecting data at sea, and to the officers and crew of R/V ATLANTIS and R/V KNORR for their cooperation during the sampling programs. R. Heinmiller conducted the current meter operations and the data were processed by the WHOI Buoy Group.

G.H. Keller kindly arranged ship time aboard the MSS MT. MITCHELL and OSS RESEARCHER during phases of this study and provided unpublished data on the cores we collected aboard the MT. MITCHELL. Unpublished current data were provided by S. Eittreim, and A.J. Silva furnished unpublished physical-property data on the cores which we collected on cruises ATLANTIS II 60 and KNORR 25. Hydrographic data were supplemented by information from the files of NODC and WHOI.

Collection of all physical oceanographic data and much geological data was made possible by NSF Grant GA 24872. The writer was supported by this grant and by a Teaching Assistantship at Woods Hole during the period of this research.

C.D. Hollister, P.E. Biscaye, E.T. Bunce, J.D. Milliman, K. O. Emery, J.B. Southard, W.R. Wright, J.C. Hathaway, and W.A. Berggren kindly criticized my manuscripts at various stages of the research.

My deepest thanks are to my wife, Anita, who not only put me through graduate school, but also helped with laboratory analyses and typed the manuscript.

TABLE OF CONTENTS

	Page
ABSTRACT.	2
ACKNOWLEDGEMENTS.	4
LIST OF FIGURES	8
LIST OF TABLES.	13
CHAPTER I INTRODUCTION.	14
CHAPTER II BATHYMETRY.	20
General description	20
The scale of sediment swells.	24
Surrounding provinces	26
CHAPTER III STRUCTURE OF THE GREATER ANTILLES	
OUTER RIDGE	28
Previous geophysical work	28
Acoustic basement	34
The stratified layer.	40
The transparent layer	49
CHAPTER IV THE SEDIMENTS	66
General lithology	66
The carbonates.	82
Mineralogy.	89
Methods	89
Results	93
Other sediment tracers.	101
CHAPTER V CHRONOLOGY OF SEDIMENTATION	105
Regional patterns	105
Greater Antilles Outer Ridge.	105
Abyssal plains.	115
North slope - Puerto Rico Trench.	116
CHAPTER VI ABYSSAL CIRCULATION	121
Water masses.	121
Earlier studies of circulation.	122
Methods	124
Current meters.	124
Hydrographic stations	126
Bottom photography.	129

	Page
Results.	130
Hydrography	130
Dynamic calculations.	148
Direct current measurements	156
Current evidence from bottom photographs.	171
Summary.	172
CHAPTER VII SUSPENDED PARTICULATE MATTER	182
Introduction	182
Methods.	182
Concentration and distribution	185
Grain size and general composition	193
Mineralogy	200
Methods	200
Results	207
The depositional conditions.	212
Discussion	215
CHAPTER VIII THE GEOLOGICAL EVOLUTION OF THE GREATER ANTILLES OUTER RIDGE	217
Previous theories.	217
Middle Cretaceous to middle Eocene	218
Middle to late Eocene.	222
Late Eocene to Miocene	230
Pliocene to Recent	238
Comparison with other depositional ridges	242
Suggestions for future work.	245
REFERENCES CITED	247
APPENDIX I SEDIMENT CORES	258
APPENDIX II BOTTOM PHOTOGRAPHS	263
APPENDIX III SUSPENDED PARTICULATE MATTER	278
APPENDIX IV PHYSICAL PROPERTIES OF CORES	285
Water content.	285
Shear strength	285
BIOGRAPHY.	313

LIST OF FIGURES

Figure		Page
1.1	Bathymetry of the Greater Antilles Outer Ridge and vicinity.	16
2.1	Echo-sounding profiles on the Greater Antilles Outer Ridge.	23
3.1	Bathymetric map of the Greater Antilles Outer Ridge showing locations of the seismic profiles.	30
3.2	Seismic reflection profile on the crest of the Greater Antilles Outer Ridge.	32
3.3	Map showing dominant sediment type and sediment thickness above Datum A.	36
3.4	Map showing distribution of Datum A and basement peaks.	38
3.5	Seismic reflection profile on the far eastern sector of the Greater Antilles Outer Ridge	42
3.6	Idealized profile along the topographic axis of the Greater Antilles Outer Ridge.	44
3.7	Seismic reflection profile across the Caicos Outer Ridge and Greater Antilles Outer Ridge	47
3.8	Seismic reflection profile showing Datum A outcrop near southern end of the Silver Abyssal Plain	51
3.9	Seismic reflection profile across the Nares Abyssal Plain and Greater Antilles Outer Ridge	55
3.10	Seismic reflection profile across the Hatteras Abyssal Plain and northwest section of the Greater Antilles Outer Ridge	58
3.11	Seismic reflection profile across the Silver Abyssal Plain and the Greater Antilles Outer Ridge.	60

Figure		Page
3.12	Echo-sounding profile (12 kHz) illustrating layered valley formation	62
3.13	Seismic reflection profile across the Greater Antilles Outer Ridge showing migration of sediment swells	64
4.1	General lithology of cores from the Greater Antilles Outer Ridge	68
4.2	Grain size distribution in cores from the Greater Antilles Outer Ridge and Nares Abyssal Plain.	70
4.3	Organic carbon in cores from the Greater Antilles Outer Ridge and Nares Abyssal Plain.	73
4.4	Bottom photographs taken on the flanks of the Greater Antilles Outer Ridge	75
4.5	Distal turbidite sequences in a core from the Nares Abyssal Plain.	78
4.6	General lithology of cores taken from a layered valley and adjacent sediment swell	81
4.7	Graph of carbonate factors for core KN25-4GPC.	84
4.8	Curves of carbonate content in cores from the Greater Antilles Outer Ridge	86
4.9	Chlorite abundances in samples from abyssal depths in the western North Atlantic Ocean	96
4.10	Chlorite abundances in sediment samples from the continental margin of eastern North America and from the Greater Antilles Outer Ridge.	98
5.1	Abundance of the <u>Globorotalia menardii</u> complex in cores from the Greater Antilles Outer Ridge.	110
5.2	Ages and general lithology of cores from the north slope of the Puerto Rico Trench.	118

Figure		Page
6.1	Bathymetric map of the Greater Antilles Outer Ridge showing positions of hydrographic stations, locations of hydrographic sections, and current meter positions.	128
6.2	Potential-temperature sections for the deep water over the Greater Antilles Outer Ridge and Caicos Outer Ridge	133
6.3	Potential temperature at 5300 m for the Greater Antilles Outer Ridge and vicinity.	140
6.4	Traces of potential temperature, <u>in situ</u> temperature, and salinity versus depth for KNORR Station 55	144
6.5	Diagram of potential temperature versus salinity for water flowing south along the western margin of the North Atlantic basin.	147
6.6	Silicate versus potential temperature for the deep water over the Greater Antilles Outer Ridge and Caicos Outer Ridge	150
6.7	Current pattern and volume transports below 4300 m	155
6.8	Progressive vector diagrams of currents recorded at position A	159
6.9	Polar histograms of currents recorded on the Greater Antilles Outer Ridge	161
6.10	Progressive vector diagrams for currents recorded at position B on the north flank of the Greater Antilles Outer Ridge. . . .	163
6.11	Polar histogram of currents recorded at position C	166
6.12	Progressive vector diagrams for currents recorded on the north and south flanks of the northwestern Greater Antilles Outer Ridge.	169
6.13	Directions and relative intensities of bottom currents on the Greater Antilles Outer Ridge determined from bottom photographs.	174

Figure		Page
6.14	Bottom photograph taken at ATLANTIS II Station K20A.	176
6.15	Summary of direct current measurements and photographic indications of bottom currents in the western North Atlantic Ocean	180
7.1	Locations of suspended-matter sample stations and nephelometer profiles.	184
7.2	Light-scattering profiles and suspended- matter concentrations plotted against potential temperature	187
7.3	Light-scattering profiles plotted against potential temperature for areas affected by the Western Boundary Undercurrent. . . .	190
7.4	Scanning electron micrographs of suspended- matter sample and bottom-sediment sample. .	196
7.5	Scanning electron micrographs of suspended- matter samples.	198
7.6	Relationships between peak areas on x-ray diffractograms and sample concentrations on silver filters	206
7.7	X-ray diffractograms of glycolated suspended matter and bottom-sediment samples	211
8.1	Schematic sketch of sedimentation condi- tions during the early to middle Eocene . .	220
8.2	Synthesis of sea-floor morphology and sedi- mentation conditions in middle to late Eocene time	226
8.3	Schematic diagram of sedimentation on the Greater Antilles Outer Ridge during the late Oligocene.	232
8.4	Sketch showing the development of the Greater Antilles Outer Ridge from the late Miocene to the Recent	236
8.5	Idealized representation of the modern bottom-flow regime over the Caicos Outer Ridge and Greater Antilles Outer Ridge. . .	240

Figure		Page
A4.1	Plots of water content and shear strength for gravity core AII60-8:2GC.	288
A4.2	Plots of water content and shear strength for gravity core 4B, taken on leg 8 of ATLANTIS II Cruise 60	290
A4.3	Plots of water content and shear strength for gravity cores 6A and 6B, taken on ATLANTIS II Cruise 60, leg 8.	292
A4.4	Plots of water content and shear strength for gravity core AII60-8:7GC.	294
A4.5	Plots of water content and shear strength for gravity core 10A (AII60, leg 8) . . .	296
A4.6	Plots of water content and shear strength for gravity core AII60-8:11GC	298
A4.7	Plots of water content and shear strength for gravity core AII60-8:13GC	300
A4.8	Plots of water content and shear strength for gravity core AII60-8:18GC	302
A4.9	Plots of water content and shear strength for giant gravity-core KN25-3GGC.	304
A4.10	Plots of water content and shear strength for giant piston-core KN25-4GPC	306
A4.11	Plots of water content and shear strength for gravity core MM-1GC	308
A4.12	Plots of water content and shear strength for gravity core MM-2GC	310
A4.13	Plots of water content and shear strength for gravity core MM-3GC	312

LIST OF TABLES

Table		Page
4.1	Mineralogy of the $< 2 \mu\text{m}$ Size Fraction. . . .	91
4.2	Mineralogy of the 2-62 μm Size Fraction . . .	102
5.1	Average Rates of Sedimentation for the Greater Antilles Outer Ridge and Surrounding Provinces Since Middle Eocene Time.	106
5.2	Average Rates of Sediment Accumulation During Warm and Cool Periods (cm/1000 yr) . .	111
5.3	Radiocarbon Dates and Calculated Sedimentation Rates	113
6.1	Summary of Current Meter Moorings	125
6.2	Calculated Volume Transports for Reference Levels at 4300 m and 4700 m	151
7.1	Calculated Clay Mineral Composition Versus Sample Concentration.	203
7.2	Mineralogy of Suspended Matter Samples. . . .	208
8.1	Comparison of Sediment Composition Above and Below Datum A at Site 28.	228
A1.1	Data on Cores Studied	260
A2.1	Bottom Photographs.	264
A3.1	Suspended Particulate Matter Samples.	279

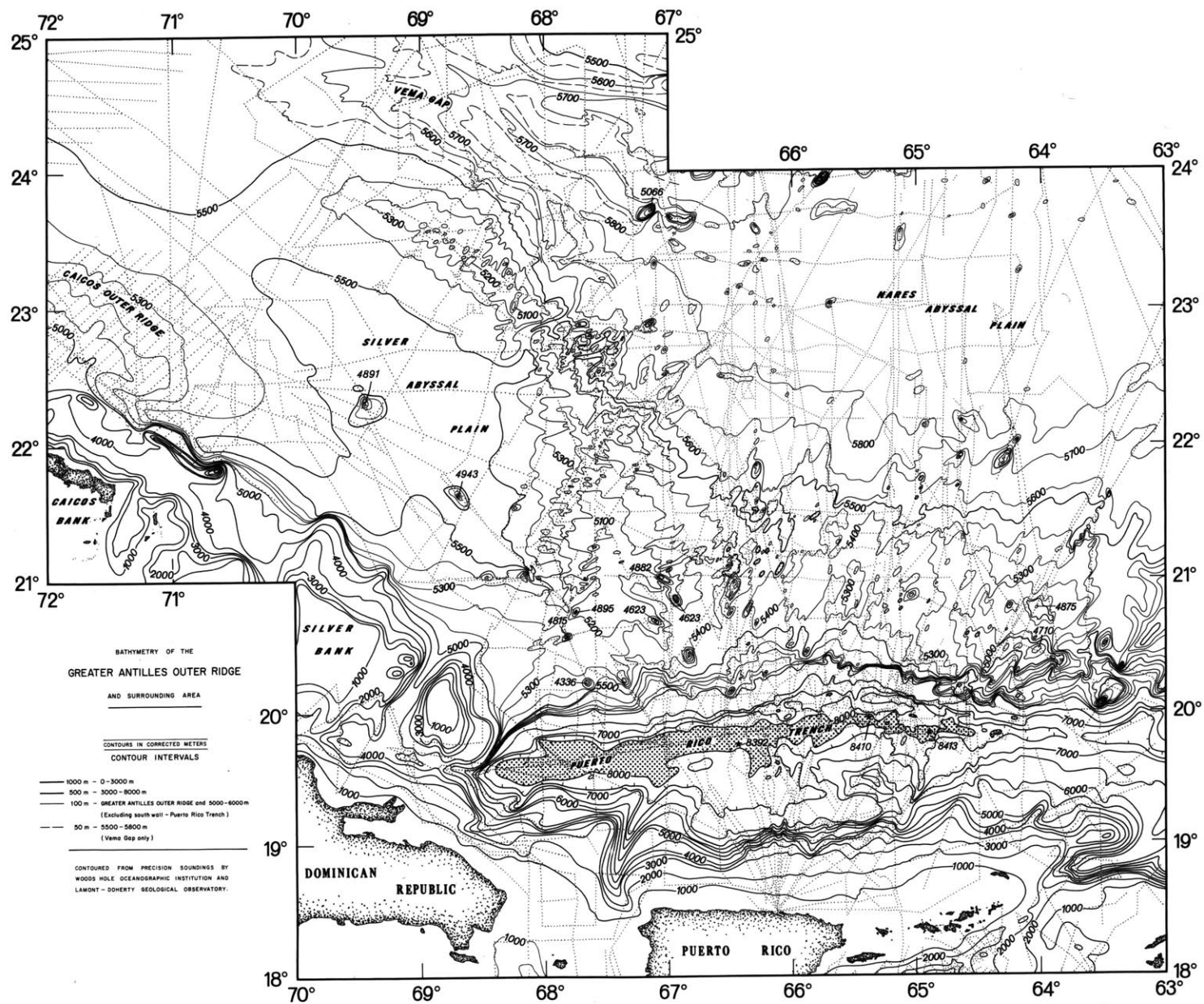
CHAPTER I

INTRODUCTION

The area investigated is the Greater Antilles Outer Ridge north of Puerto Rico in the southwestern North Atlantic Ocean (Fig. 1.1). This broad swell or rise was first recognized on topographic maps by Tolstoy (1951). It can be divided into 1) a western sector which rises from the southern Hatteras Abyssal Plain near 24°N lat., 70°W long. and extends southeast to about 21°N lat., 67°W long.; and 2) an eastern sector which extends along the north side of the Puerto Rico Trench eastward to at least 56°W long. (Ewing and others, 1968). The Greater Antilles Outer Ridge is bounded by the Nares Abyssal Plain, Vema Gap, and the Hatteras Abyssal Plain on the north, the Silver Abyssal Plain on the west, and the Puerto Rico Trench on the south. It is more than 1800 km long, from 110 to 220 km wide, and its crest lies at a depth of 5100-5200 m (up to 700 m above the surrounding sea floor). The Greater Antilles Outer Ridge is thus comparable in length to the more familiar Blake-Bahama Outer Ridge system, but its relief is only about one-third as great.

This study arose during an investigation of the sediments of the Greater Antilles Outer Ridge, which in initial research were determined to be abyssal brown lutites of dominantly terrigenous derivation interbedded with occasional calcareous

Figure 1.1. Bathymetry of the Greater Antilles Outer Ridge and vicinity, contoured from precision soundings of Woods Hole Oceanographic Institution and Lamont-Doherty Geological Observatory. The Greater Antilles Outer Ridge, which extends from 24°N lat., 70°W long. to 21°N lat., 67°W long., and then east along the north side of the Puerto Rico Trench, is not labelled in order to avoid covering contours. Contours are in meters, corrected for sound velocity in water (Matthews, 1939). Contours in Vema Gap are modified from Heezen and Menard (1963), in the Virgin Islands Passage from Frassetto and Northrop (1957), on the Caicos Outer Ridge from Schneider and Heezen (1966), and on the Bahama Banks from HO Charts BC 704 and 804. Control on bathymetry is shown by light dotted lines.



lutites (the word lutite is used in this text as a descriptive term for unconsolidated sediment with grain size less than $2\text{ }\mu\text{m}$, and no genetic associations are implied). Ericson and others (1952) examined cores from the Greater Antilles Outer Ridge and described them as "typical deep-sea red clay throughout" and "entirely red clay". Seismic reflection profiles taken in this region (Ewing and Ewing, 1962; Savit and others, 1964; Bunce and Hersey, 1966) demonstrated that a blanket of acoustically transparent sediment up to 0.8 km thick covers and actually forms the Greater Antilles Outer Ridge in many places. The origin of this accumulation of sediment and the geologic evolution of the Greater Antilles Outer Ridge was chosen as the topic of this research effort.

The most puzzling problem in reconstructing the geological history of the Greater Antilles Outer Ridge is the origin of the upper, acoustically transparent layer, and several working hypotheses can be tested. Extensive accumulations of sediments with a similar acoustic nature occur at numerous other locations in the world oceans, and some are attributed to rapid deposition of biogenous material beneath regions of high surface productivity (see for example, Ewing and others, 1969). This mechanism could provide much of the sediment on the Greater Antilles Outer Ridge; however, sediment cores from the transparent layer contain low-carbonate, texturally homogeneous, variegated, terrigenous silty lutites with only scattered zones enriched in biogenous carbonate.

This is expected since most of the Greater Antilles Outer Ridge lies below the carbonate compensation depth. Furthermore, the surface waters of the overlying southern Sargasso Sea are relatively unproductive (Ryther and Menzel, 1960; Be' and others, 1971). Core data from Site 28 of the Deep Sea Drilling Project on the south flank of the outer ridge (Bader and others, 1970) also indicate that the upper 170 m of sediment, corresponding to the transparent layer, is green-gray and brown lutite nearly devoid of biogenous material; thus accumulation of biogenous material can be ruled out as an important factor in the deposition of the transparent layer.

Bunce and Hersey (1966) suggested that the transparent layer may be the remnant of a continental rise which extended northward from Puerto Rico and pre-dated the formation of the Puerto Rico Trench. However, continental rise sediments in the western North Atlantic typically exhibit numerous strong internal reflectors (Hoskins, 1967; Emery and others, 1970), and cores from true continental rises contain numerous beds of silt and fine sand (Ericson and others, 1961; Hollister and Heezen, 1972). On the Greater Antilles Outer Ridge, such rise-type sediments might also contain rapidly deposited calcarenite layers similar to those found by Schneider and Heezen (1966) on the Caicos Outer Ridge just 200 km to the west. None of these features are observed in the transparent layer.

The working hypothesis chosen to explain the origin of the transparent layer is that near-bottom, contour-following currents transport fine-grained sediment from the continental margin of eastern North America to the topographically isolated Greater Antilles Outer Ridge and deposit the suspended sediment there. Tucholke and Hollister (1970) and Tucholke and others (1972) postulated that the necessary current system might be the southerly extension of the Western Boundary Undercurrent (Heezen and others, 1966; Hollister and Heezen, 1972) which is active along the continental rise of eastern North America, and the ramifications of this hypothesis are tested in this investigation.

The hypothesis of current-controlled sedimentation on the Greater Antilles Outer Ridge was examined by studying:

- 1) the morphology and structure of the sediments on the outer ridge and the chronology of their sedimentation;
- 2) the mineralogy of the sediment in order to determine its provenance; 3) the present abyssal current pattern, and
- 4) the concentration, size distribution, and composition of suspended matter carried in the abyssal currents.

CHAPTER II

BATHYMETRY

GENERAL DESCRIPTION

The initial step in this investigation was to construct an accurate and detailed bathymetric map of the Greater Antilles Outer Ridge and vicinity (Fig. 1.1) using more than thirty thousand kilometers of precision echo-sounding tracks obtained by Woods Hole Oceanographic Institution and Lamont-Doherty Geological Observatory.

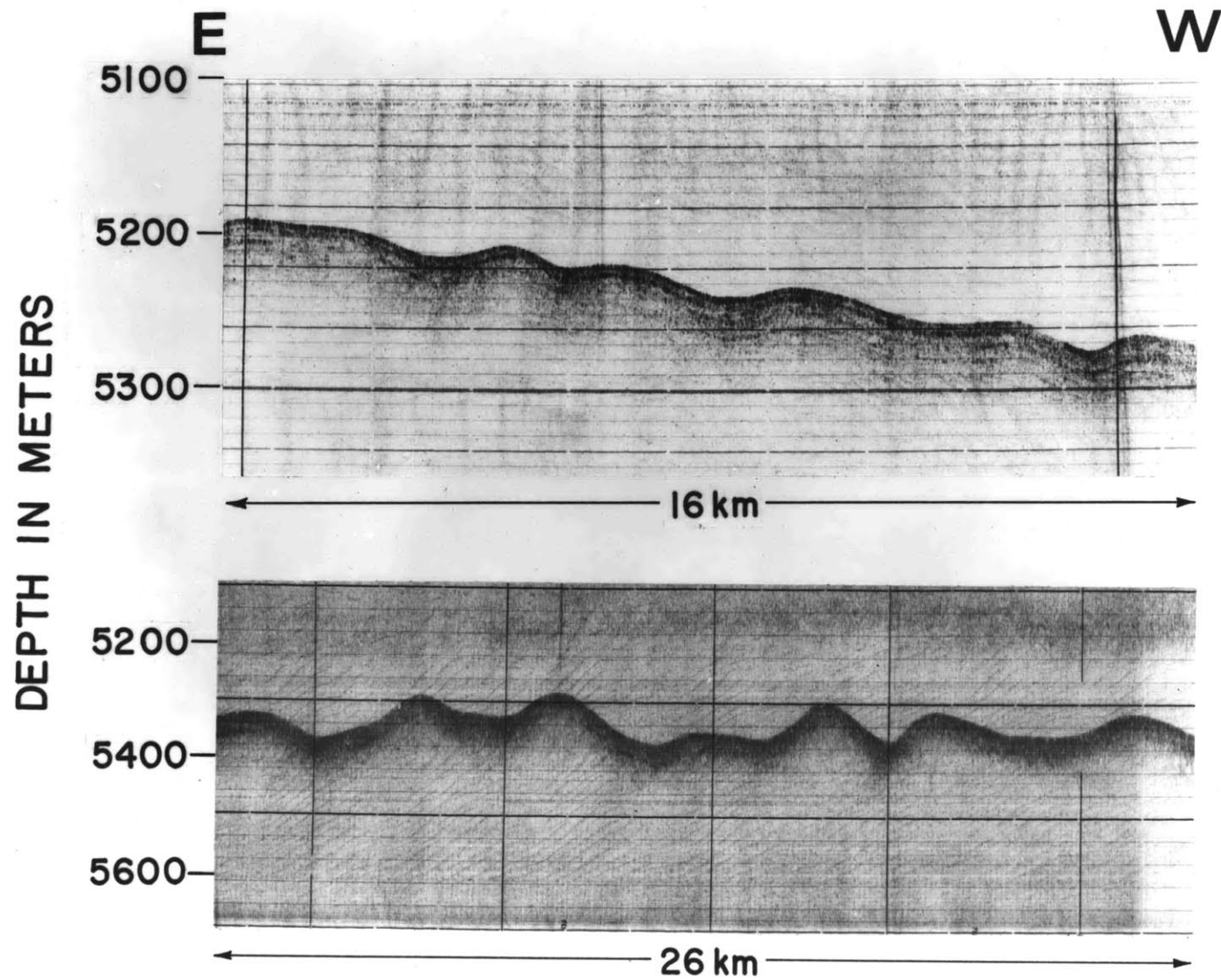
The crest of the ridge is generally at depths of 5100 to 5200 m, although basement peaks commonly interrupt the sea floor and extend to shallower depths just north of the Puerto Rico Trench. The crest is centrally located on the western sector of the ridge but is displaced to the south on the eastern sector. Several saddles or depressions with depths up to 5400 m cross the eastern sector in a north-south direction, and one deep (nearly 5500 m) depression interrupts the western outer ridge near 23°N lat., 68°W long.

The flanks of the Greater Antilles Outer Ridge vary in gradient from about 1:150 to 1:250, the largest gradients being on the north flank of the northwest end of the outer ridge and on the western flank near 68°W long. The south slope of the eastern outer ridge (north slope of the trench) is much steeper, with gradients as high as 1:30.

Most of the western sector of the Greater Antilles Outer Ridge shallower than 5500 m has an undulating surface of regular to irregular small-scale sediment swells with spacing of 1-12 km and amplitudes of 10 to 140 m (Fig. 2.1). The eastern sector of the outer ridge tends to have less well developed swells than the western sector. Subbottom layering detected in 3.5 and 12 kHz echo-sounding profiles is normally parallel to the sea floor, but in some cases differential deposition and small scale migration of the swells can be seen. These swells have been ascribed to possible tectonism or to current-influenced deposition (Ewing and others, 1968; Savit and others, 1964).

Detailed bathymetric surveys were made in the area of 22°N lat., 67°30'W long. to determine the orientation of the swells. Analysis of slope, spacing, and spacing/amplitude versus azimuth failed to show more than a weak elongation of the swells in the east-west direction, nearly perpendicular to the regional contours of the Greater Antilles Outer Ridge in this area. There is further evidence in the general bathymetry of the northwestern section (Fig. 1.1) that the small-scale features trend in a northeast-southwest direction, also at right angles to the axis of the outer ridge. Although the imprecision of echo-sounding surveys made from a surface vessel in mapping these swells limits the reliability of the interpretations, there appears to be a trend toward linearity in the features, with their crests roughly perpendicular to

Figure 2.1. Echo-sounding profiles (12 kHz) on the north-west section of the Greater Antilles Outer Ridge, illustrating the regular (top) and irregular sediment swells (bottom) which trend more or less perpendicular to the regional contours. Note the parallel-bedded layers detected in the upper profile. For locations see Figure 3.1.



regional contours.

An area centered on 22°30'N lat., 67°30'W long. on the northeast flank of the western sector of the outer ridge is referred to as the "layered valley" region by Chase and others (1966) and Bunce and others (1973). Detailed bathymetric surveys conducted by these authors show a series of small ridges and valleys arranged like a dendritic tributary system extending toward the Nares Abyssal Plain. Here again, the swells are oriented roughly at 90° to the outer ridge. The valley floors are flat, and they are thought to be formed by localized turbidity current deposition from the outer ridge.

THE SCALE OF SEDIMENT SWELLS

The following series of sediment swells, listed in order of decreasing size, appears on the Greater Antilles Outer Ridge:

- 1) The largest swells are those that are indicated on the bathymetric map (Fig. 1.1) running generally perpendicular to the axis of the outer ridge. Their spacing ranges from about 6 to 12 km with amplitudes up to 140 m.

- 2) A second set, observed in echo-sounding profiles but generally not shown on the bathymetric map, has spacings of 1-6 km and amplitudes up to 90 m. Detailed bathymetric surveys suggest that these swells have the same orientation as those of 1) above. Mud swells with similar amplitude and spacing were observed on the Caicos Outer Ridge to the west

during leg 8 of ATLANTIS II Cruise 60.

3) Hyperbolic echoes are infrequently observed in echo-sounding profiles taken over the lower flanks of the outer ridge. Their spacing ranges from tens to hundreds of meters and their amplitude is only a few meters. The fact that they are infrequently observed may reflect an actual rarity, or it may result from the insensitivity of the echo-sounding system in detecting weak "side echoes" from small mud swells of fine-grained sediment. The fact that each pulse of the echo-sounding system insonifies roughly 10^6m^2 of sea floor at these depths may also confuse detection of these features.

4) Superimposed on the above are smaller mud swells, probably greater than 10 m in spacing and of < 1 m amplitude. These are not detected in surface echo-sounding records but are well illustrated in many bottom photographs (see Appendix II). Since their size is intermediate between that normally resolved by surface echo sounding and bottom photography, it is not possible to assess their frequency and distribution with the information presently available.

5) Ripples are developed in certain areas of the Greater Antilles Outer Ridge; they are easily recognized in bottom photographs and have wavelengths of 20 to 30 cm and amplitudes of about 5 cm (see Fig. 6.14).

It must be emphasized that none of these patterns is universal on the Greater Antilles Outer Ridge, nor is there reason to believe that the patterns always occur together in

this region. However, all of these features have wavelengths and amplitudes similar to those of other abyssal sediment swells in the deep ocean (see Fig. 9.13 of Heezen and Hollister, 1971).

SURROUNDING PROVINCES

The southern end of the Hatteras Abyssal Plain, about 5500 m deep, bounds the northwest end of the Greater Antilles Outer Ridge. It is connected to the Nares Abyssal Plain by Vema Gap, which slopes toward the east parallel to the northeast flank of the outer ridge with a gradient of 1:1500. The Nares Abyssal Plain provides the northern boundary for the eastern sector of the outer ridge, and it slopes gently to the east from a depth of 5800 m at 67°30'W long. down to 5900 m at 62°30'W long. The outer ridge is bounded on the west by the Silver Abyssal Plain, about 5500 m deep, and on the south by the Puerto Rico Trench with depths of up to 8413 m. The north slope of the trench forms the south flank of the eastern sector of the outer ridge.

Two sills connect the Greater Antilles Outer Ridge with marginal features of the Bahama Banks. The first of these, near 23°30'N lat., 70°30'W long., is only very slightly elevated above the level of the Hatteras and Silver Abyssal Plains. It connects the northwest end of the Greater Antilles Outer Ridge with the Caicos Outer Ridge and has a maximum depth of about 5485 m. The second sill connects the southwest elbow of the Greater Antilles Outer Ridge to the

apron at the base of Navidad Bank and Silver Bank. The maximum depth of this sill is about 5230 m in a narrow passage at the southeast end of the Silver Abyssal Plain.

The Greater Antilles Outer Ridge is thus formed by a low, rolling rise of sediment with a hummocky surface, rising 400-700 m above the surrounding flat abyssal plains. Although the eastern sector bounds the Puerto Rico Trench on the north, the western sector extends away from the trench northwest to the Hatteras Abyssal Plain.

CHAPTER III

STRUCTURE OF THE GREATER ANTILLES OUTER RIDGE

PREVIOUS GEOPHYSICAL WORK

Portions of the Greater Antilles Outer Ridge have been studied extensively by seismic reflection and refraction over the last decade (Ewing and Ewing, 1962; Bunce and Fahlquist, 1962; Northrop and Ransone, 1962; Savit and others, 1964; Ewing and others, 1968; Bunce and Hersey, 1966; Bunce and others, 1969).

In the present study, more than 20,000 km of continuous seismic reflection profiles obtained by Woods Hole Oceanographic Institution and Lamont-Doherty Geological Observatory were examined to determine the structure of the basement and the overlying sedimentary units in the vicinity of the Greater Antilles Outer Ridge. The locations of profiles referred to in this text are shown in Figure 3.1.

The Greater Antilles Outer Ridge is characterized by three main acoustic units recorded in seismic reflection profiles (Figs. 3.2, 3.6, 3.11). The first and uppermost unit is acoustically transparent with thicknesses up to 1.0 sec reflection time. The second unit, which lies immediately beneath the transparent layer, ranges in thickness from 0 to 1.0 sec reflection time, and it appears as flat-lying, acoustically stratified sediment; it has been suggested by Ewing and Ewing (1962) that this reflective

Figure 3.1. Bathymetric map of the Greater Antilles Outer Ridge and vicinity showing locations of profiles discussed in text: lines 1 and 2 are 12 kHz profiles shown in Figure 2.1 (top and bottom respectively), and 3-9 are seismic reflection profiles. The star at $20^{\circ}35.2'N$ lat., $65^{\circ}37.3'W$ long. shows the location of Site 28 of the Deep Sea Drilling Project.

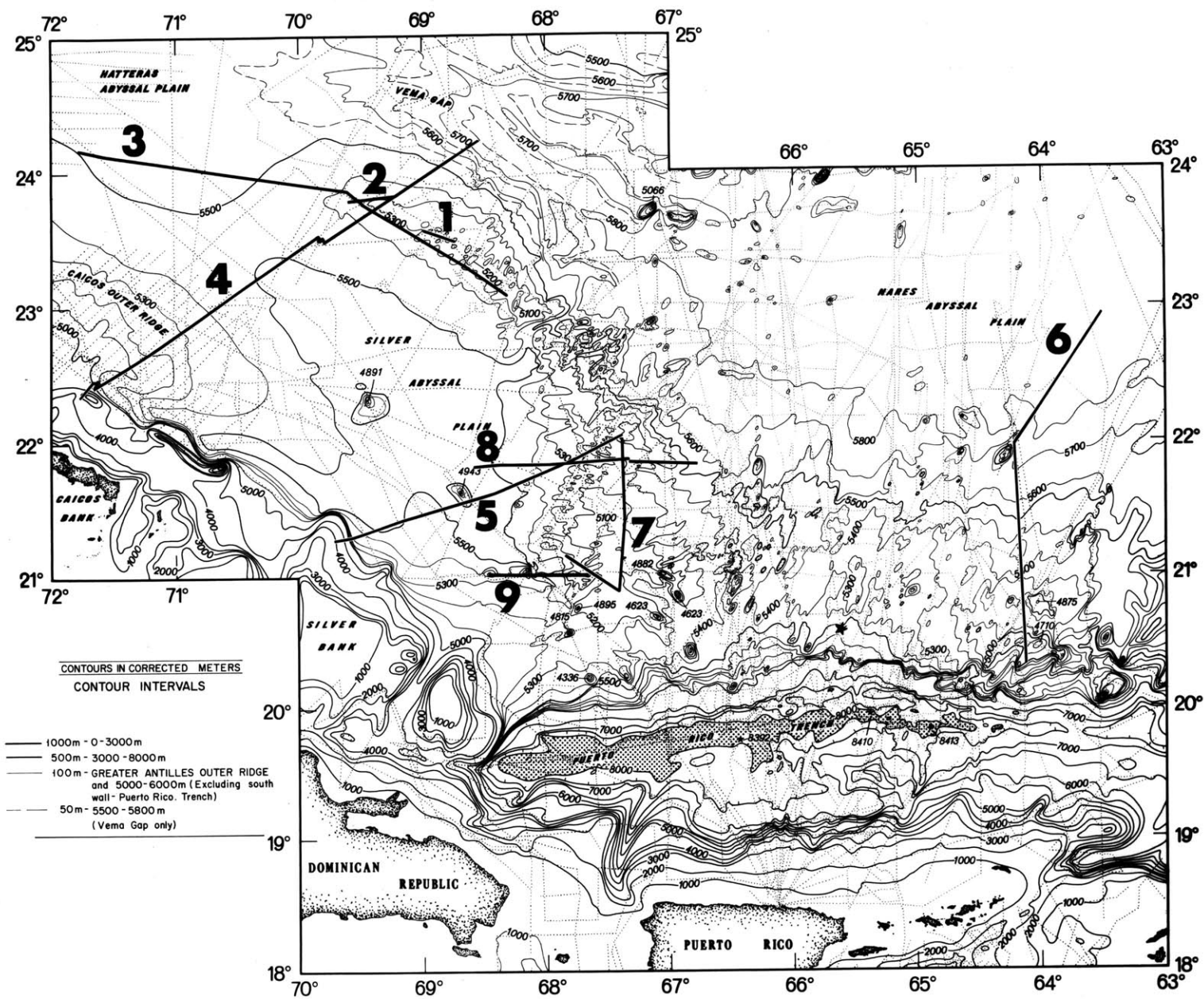
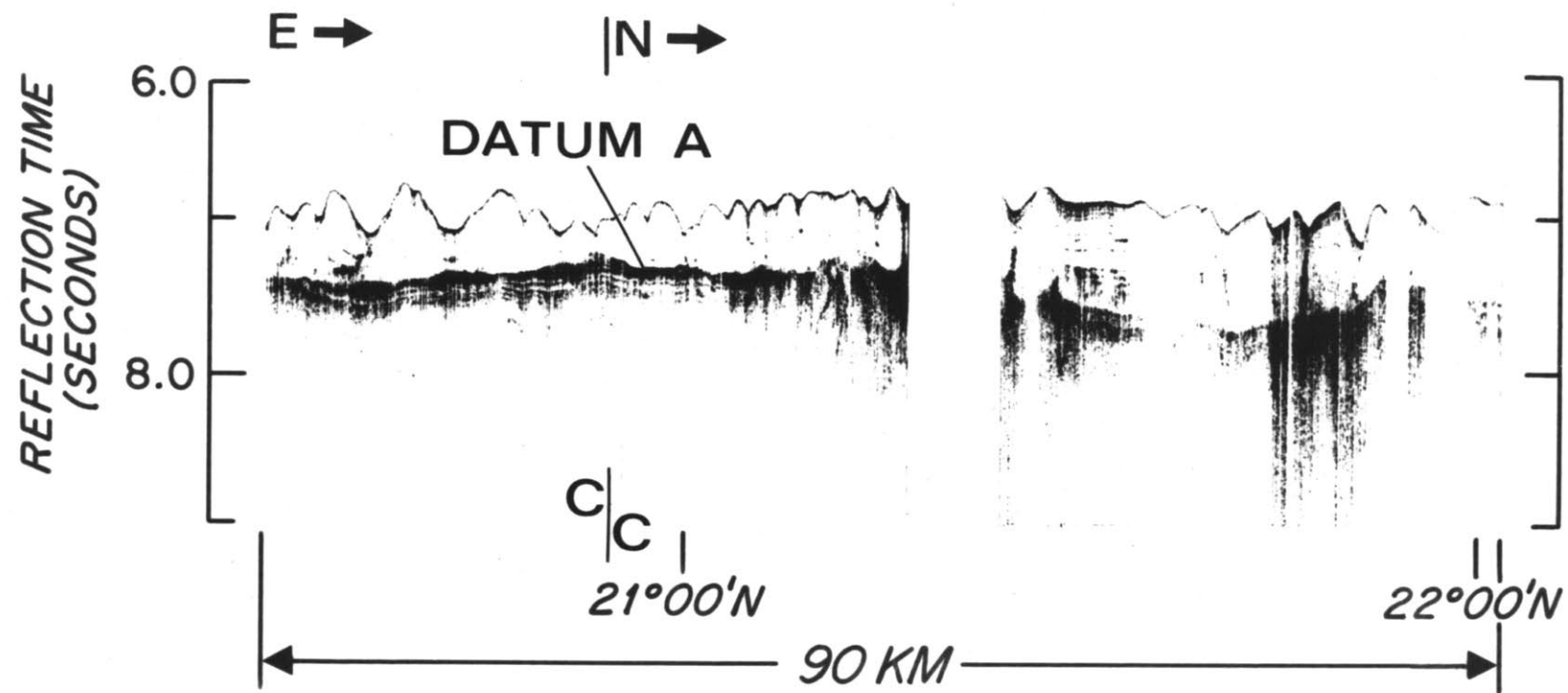


Figure 3.2. CONRAD 10 seismic reflection profile taken along the crest of the Greater Antilles Outer Ridge (Profile 7, Fig. 3.1). Note the upper, acoustically transparent layer and the stratified sediment beneath. Acoustic basement is poorly defined, with possible peaks interrupting the stratified layer at the right.



sequence corresponds to layered turbidity-current deposits. The stratified sequence overlies, and is often penetrated by, a deeper reflector that exhibits an irregular, sometimes broken, surface. No reflections are observed beneath the strong echo of this third unit, and it is therefore referred to as acoustic basement.

An observed increase in compressional wave velocity from 1.50 to 1.77 km/sec with depth in the upper, acoustically transparent layer, as determined by seismic refraction measurements, indicates that it becomes increasingly lithified with depth (Savit and others, 1964; Bunce and others, 1969). Velocities as high as 2.10 km/sec have been reported for the transparent layer (Bunce and Hersey, 1966), and a similar value was suggested by drilling through the base of the transparent layer at Site 28 of the Deep Sea Drilling Project (Bader and others, 1970; Fig. 3.2). The second or stratified unit is characterized by velocities of 3.7 to 4.5 km/sec (Savit and others, 1964; Bunce and Hersey, 1966) although velocities as low as 3.0 km/sec have been measured in certain areas west of 66°30'W long. (Northrop and Ransone, 1962; Savit and others, 1964). The unit referred to as acoustic basement has velocities of about 5.2 to 5.5 km/sec.

The geophysical studies indicate that the acoustically transparent layer blankets most of the Greater Antilles Outer Ridge, but it is absent on the adjacent abyssal plains;

the corresponding unit on the abyssal plains typically contains multiple reflective horizons which are thought to be stratified sediments emplaced by turbidity currents (Hersey, 1965). A thin (< 0.2 sec) transparent layer continues down the north slope of the Puerto Rico Trench in places and dips beneath the trench sediments (Bunce and Hersey, 1966; Chase and Hersey, 1968). Acoustically transparent sediments also occur on the two sills to the west of the Greater Antilles Outer Ridge and on the Caicos Outer Ridge (Fig. 3.3). The following discussion treats each of the above units in more detail.

ACOUSTIC BASEMENT

Acoustic basement under the eastern sector of the Greater Antilles Outer Ridge has velocities in the range 5.2 to 5.5 km/sec, suggesting that it is oceanic layer 2 (Raitt, 1963; Ludwig and others, 1970). It is extremely irregular in configuration, and in seismic reflection profiles it may dip to more than one-second reflection time beneath the sea floor. Acoustic basement also interrupts the overlying stratified and transparent sediment, occasionally rising more than 500 m above the surrounding sea floor to depths shallower than 4700 m (Figs. 3.1, 3.4). The irregularity appears more pronounced underneath the Greater Antilles Outer Ridge than under the Nares Abyssal Plain to the north, and, although there is a general increase in depth to acoustic basement north of the outer ridge, basement peaks

Figure 3.3. Map showing dominant sediment type and sediment thickness above Datum A and above the basement peaks interrupting Datum A. Thicknesses are in seconds reflection time. The southern limit of the study is marked by the Bahama Banks escarpment and the 7000 m contour on the north slope of the Puerto Rico Trench. Datum A (cross-hatched) crops out near the southern end of the Silver Abyssal Plain and in at least two places at the base of the Bahama Banks. The symbols at the lower left depict depths to basement peaks which interrupt Datum A. DSDP Site 28 is marked by a star, and control for mapping is shown by light dotted lines.

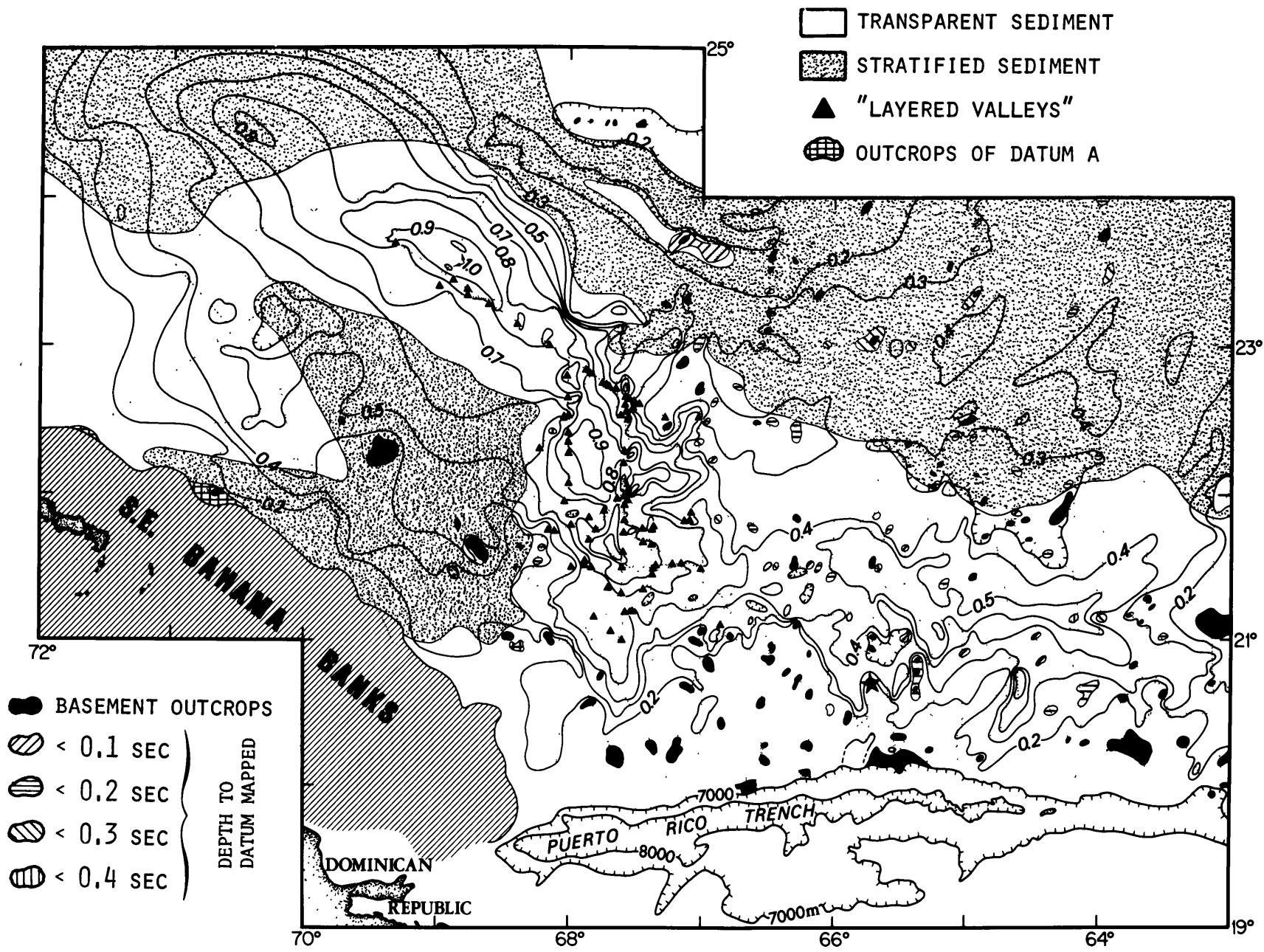
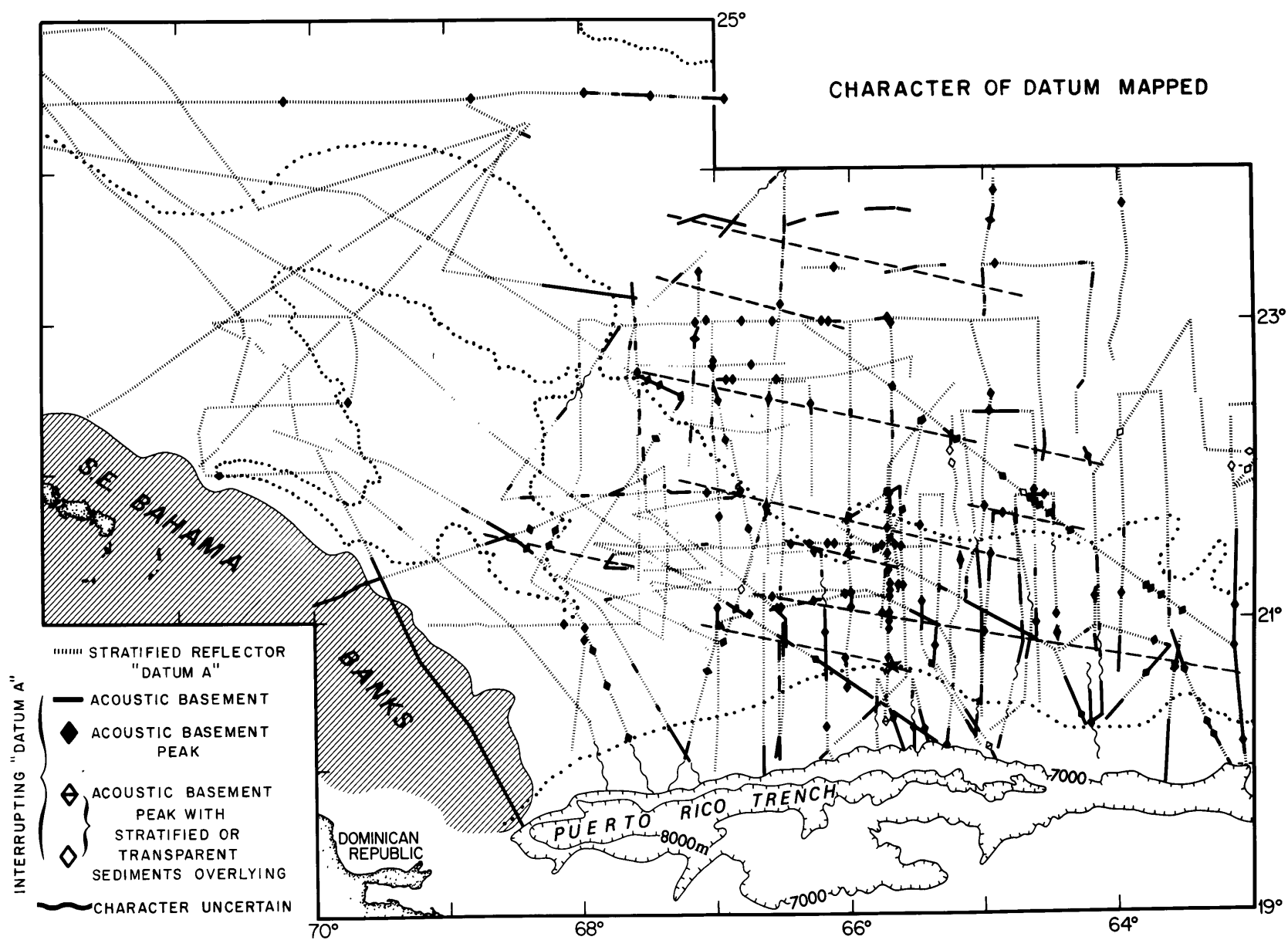


Figure 3.4. Map showing the distribution of Datum A and the basement peaks which interrupt it. The WNW/ESE-oriented, dashed lines indicate possible structural lineaments in the acoustic basement. See Figure 3.6 for an idealized representation of Datum A and the peaks which interrupt it. Note that basement interruptions of Datum A are restricted primarily to the eastern sector of the Greater Antilles Outer Ridge and to the Nares Abyssal Plain. The dotted lines roughly mark the 5500 m isobath, and the 7000 m contour along the north slope of the Puerto Rico Trench is the southern limit of mapping. DSDP Site 28 is marked by a star.



still locally break through the stratified abyssal-plain sediments. Acoustic basement thus forms a broad structural high under the eastern sector of the Greater Antilles Outer Ridge, parallel to the east-west trend of the Puerto Rico Trench.

There is also some indication of smaller scale, WNW-ESE trending, basement structural ridges within the outer ridge - abyssal plain province (Fig. 3.4). The lineations are poorly defined, but they agree closely with the overall tectonic fabric of the oceanic basement in this region (Johnson and Vogt, 1971).

Under the western sector of the Greater Antilles Outer Ridge, acoustic basement lies at such great depths (>1.5 seconds) that it is rarely observed.

Dredge hauls from near the level of the acoustic basement on the north slope of the Puerto Rico Trench have recovered basalt, serpentinite, chert and limestone. Bowin and others (1966) suggested that the 5.2 to 5.5 km/sec layer (layer 2) may be composed primarily of serpentinized peridotite with some altered basalt. However, Chase and Hersey (1968) felt that basalt flows, possibly interbedded with limestone and chert, compose the acoustic basement, and they concluded that the serpentinite came from the top of a deeper crustal layer of velocity 6.5 to 6.6 km/sec (the "oceanic layer" or layer 3). It seems reasonable that acoustic basement (layer 2) in this region is basaltic crust which originated at the Mid-Atlantic Ridge (Bunce and

others, 1973), and the upper portions probably contain subsequent local basalt flows interbedded with consolidated sedimentary rocks.

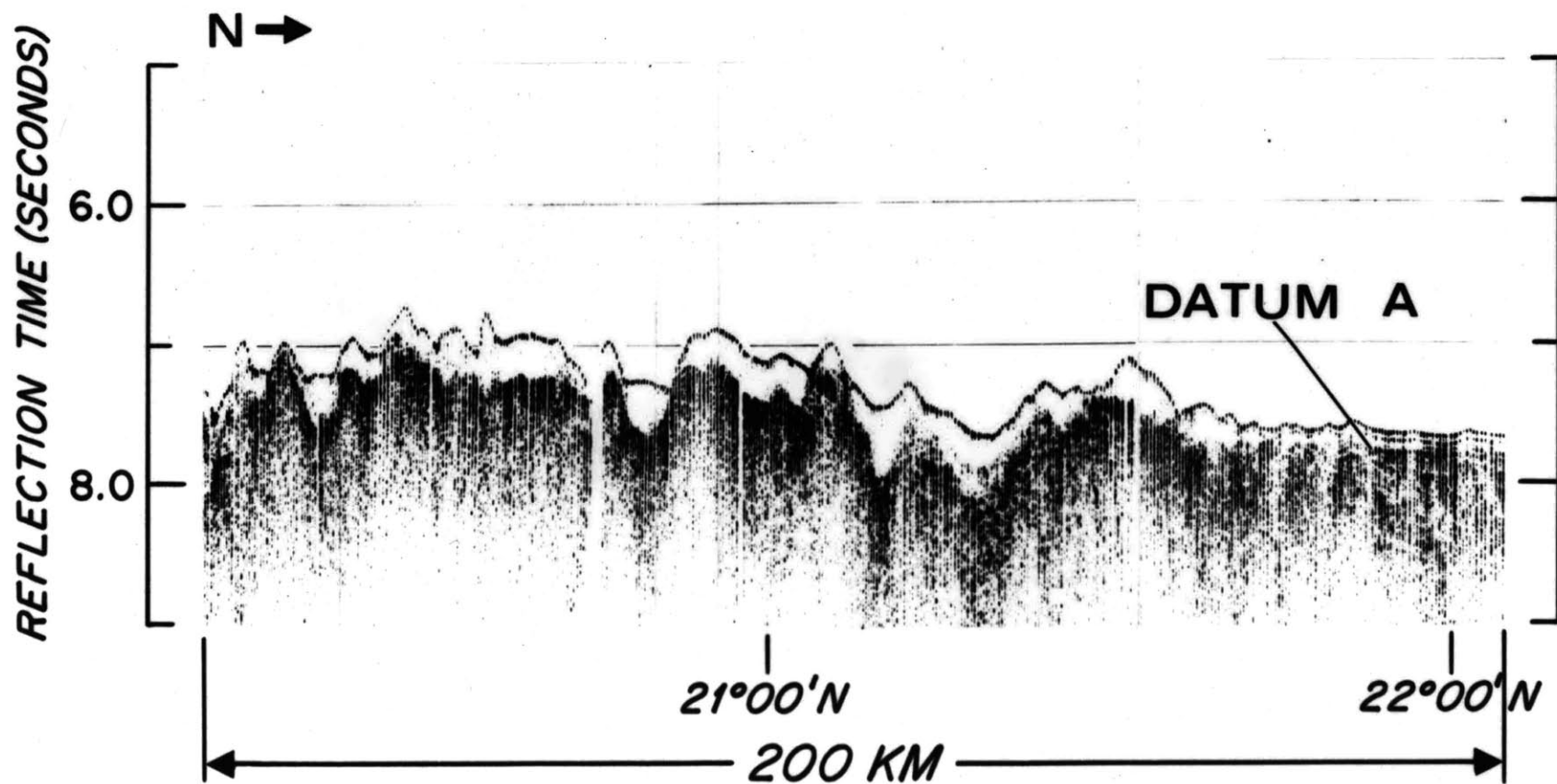
Certain limits can be placed on the age of acoustic basement and the "oceanic layer" under the eastern sector of the Greater Antilles Outer Ridge. The oldest sedimentary rocks recovered from the north slope of the Puerto Rico Trench are middle Cenomanian (about 100 m.y.) in age (Todd and Low, 1964), and they probably originated from near the top of acoustic basement (layer 2) or from the base of the overlying stratified layer. Extrapolation of data from magnetic anomalies and JOIDES borehole results (Pitman and Talwani, 1972) into this area suggests a crustal age of 110-130 m.y.. Thus the sea floor in this area was probably first formed no earlier than the early Cretaceous.

THE STRATIFIED LAYER

The acoustically stratified sediment directly overlying acoustic basement and forming flat-lying ponds between basement peaks under the Greater Antilles Outer Ridge is referred to hereafter as the stratified layer; it has compressional wave velocities of about 3.0 to 4.5 km/sec.

A distinctive reflector observed in the stratified layer and here referred to as Datum A is ubiquitous in the area studied, except under portions of the Greater Antilles Outer Ridge east of 63°W long. (Figs. 3.4-3.6). Datum A marks the top of the stratified layer under the eastern

Figure 3.5. CONRAD 8 seismic reflection profile from 20°13'N lat. to 22°04'N lat. along 62°52'W long. On this far eastern sector of the Greater Antilles Outer Ridge, Datum A and the stratified layer are usually absent, and the transparent layer lies directly on acoustic basement. However, Datum A is observed under the flanking Nares Abyssal Plain (right).



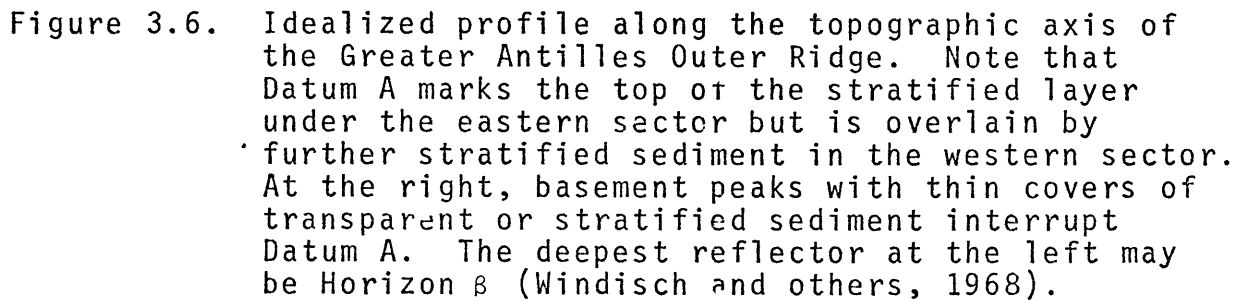
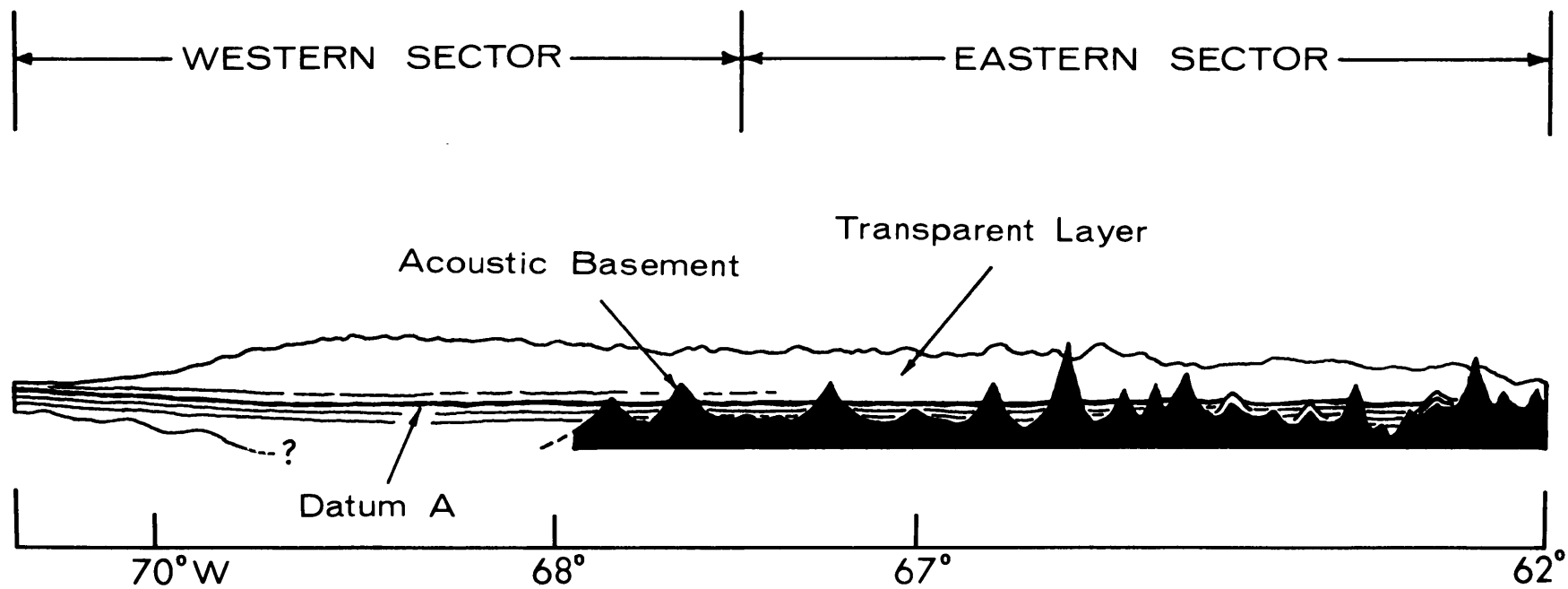


Figure 3.6. Idealized profile along the topographic axis of the Greater Antilles Outer Ridge. Note that Datum A marks the top of the stratified layer under the eastern sector but is overlain by further stratified sediment in the western sector. At the right, basement peaks with thin covers of transparent or stratified sediment interrupt Datum A. The deepest reflector at the left may be Horizon β (Windisch and others, 1968).



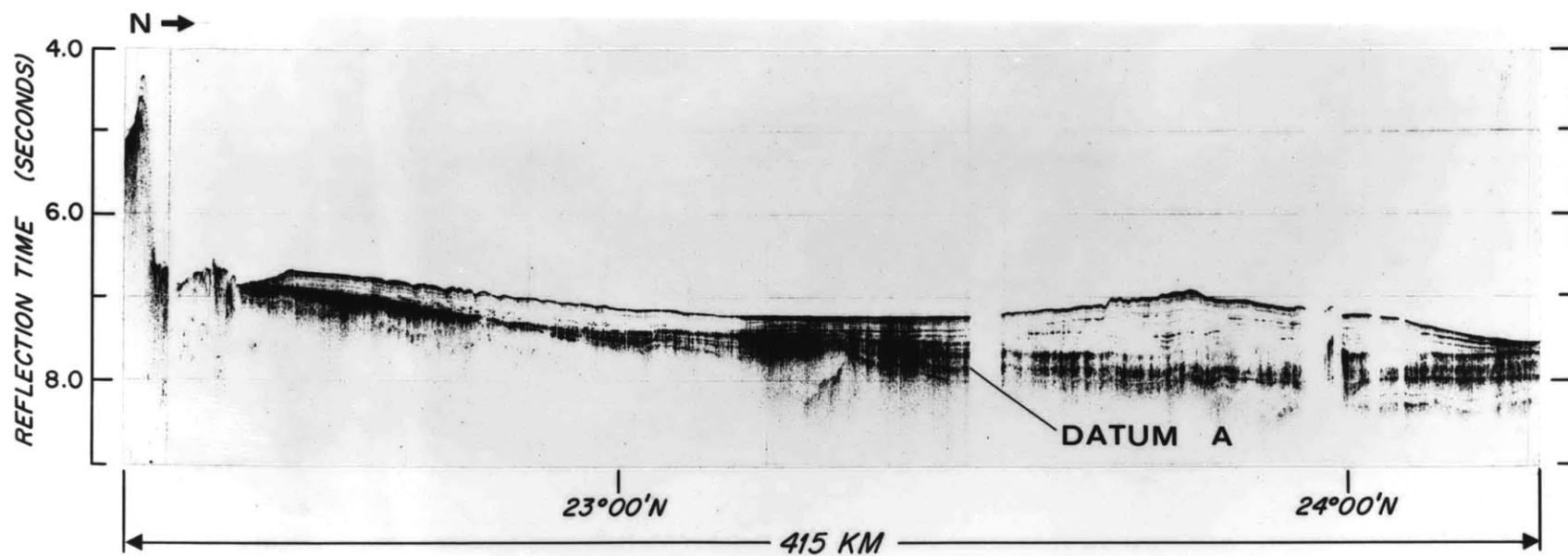
sector of the outer ridge, but it is commonly overlain by additional stratified sediments to the west (Fig. 3.6). Under the Greater Antilles Outer Ridge it is generally well defined and readily traced, although it becomes indistinct beneath the ridge axis in some profiles over the northwest section. In Vema Gap Datum A is strongly distorted, but in other areas it is relatively smooth.

The Woods Hole seismic profiles in several instances fail to define Datum A clearly under the outer ridge, particularly on the north-south lines. In these instances the reflector could be traced as a weak echo 0.05 to 0.20 sec above the stratified sequence.

In virtually all instances where profile tracks crossed, correlation of Datum A in the profiles was within 0.1 sec. Exceptions occurred in areas where rapidly changing basement topography and navigation uncertainties made exact correlation difficult.

Datum A resembles the sequence of reflectors referred to as Horizon A in the western North Atlantic (Ewing and others, 1966; Ewing and others, 1970). At the locations where it has been sampled, Datum A is of early to middle Eocene age (see below), as is Horizon A in certain parts of the Atlantic (Ewing and others, 1970). However, Datum A often overlies a deeper sequence of reflectors (Fig. 3.7) which could just as easily constitute Horizon A, and for this reason Datum A is treated separately from Horizon A.

Figure 3.7. CONRAD 10 seismic reflection profile from the Bahama Banks across the Caicos Outer Ridge and Greater Antilles Outer Ridge to Vema Gap (Profile 4, Fig. 3.1). Note that reflectors occur both above and below Datum A under the Greater Antilles Outer Ridge and that reflectors appear to rise and terminate in an angular unconformity under the Caicos Outer Ridge. Datum A appears to crop out at the base of the Bahama Banks.



Datum A is frequently interrupted by acoustic basement east of 68°W long. under the Nares Abyssal Plain and the Greater Antilles Outer Ridge, but the stratified layer forms a thick sequence over acoustic basement under most of the western sector of the outer ridge (Figs. 3.4, 3.6, 3.7).

The thickness of the stratified layer is quite variable under the eastern outer ridge, ranging from < 0.1 km to more than 1 km in places. From the crest of the eastern sector Datum A slopes gently north under the Nares Abyssal Plain and sharply to the south down the north slope of the Puerto Rico Trench; where it is frequently broken by fault blocks or is completely absent. Thicknesses of the stratified layer (below Datum A) are generally about the same under the eastern sector of the outer ridge and the Nares Abyssal Plain to the north.

The stratified layer undoubtedly crops out on the north slope of the Puerto Rico Trench. The cherts, consolidated mudstones, and limestones dredged on the north slope (Bowin and others, 1966; Chase and Hersey, 1968) may come from this layer. Core data from DSDP Site 28 (Bader and others, 1970) on the north slope indicate that middle Eocene siliceous limestone and banded cherty layers, which are probably from the top of the stratified layer (Datum A), were encountered about 175 m beneath the sea floor. The sediments below this depth consist of variegated lutites and silty lutites, claystones, chalk, and microfossil oozes.

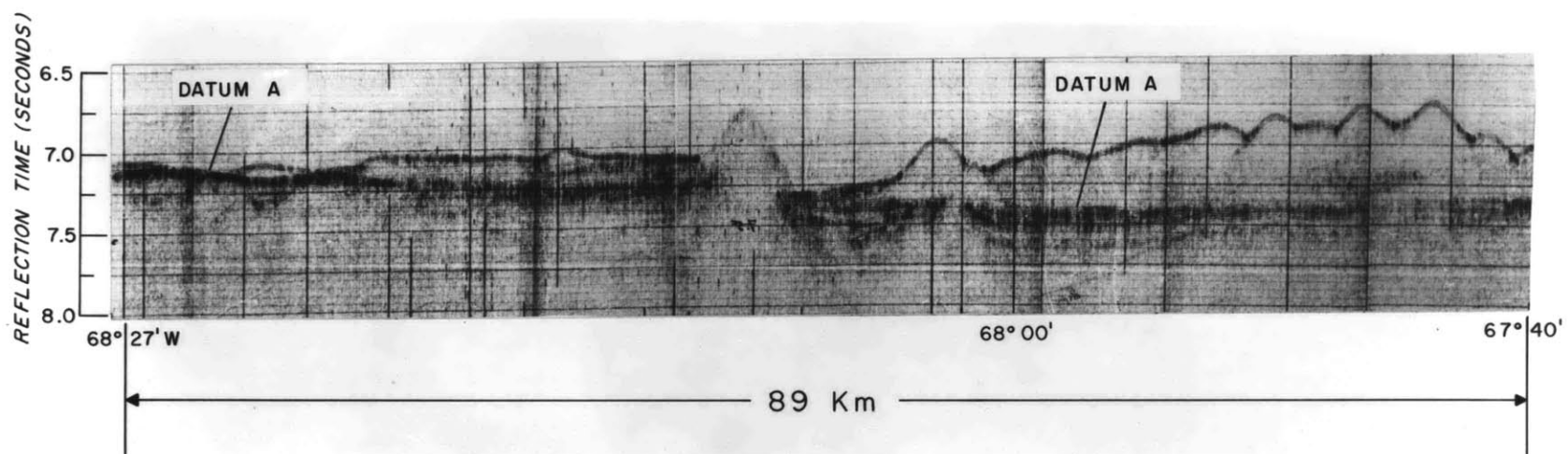
Drilling continued to 404 m but failed to reach acoustic basement, bottoming in Cretaceous (probably Upper Cretaceous) sediment. The Cenomanian limestones (Todd and Low, 1964) dredged from the north slope most likely came from near the base of the stratified layer.

Datum A is an important acoustic marker which divides two vastly different acoustic regimes under the eastern outer ridge: i.e., the stratified layer and the overlying acoustically transparent sediment. A piston core (RC 16-30; 21°00.3'N lat., 68°23.1'W long.) was obtained from the Datum A outcrop near the southern end of the Silver Abyssal Plain (Figs. 3.3, 3.8) to confirm the middle Eocene age suggested by very incomplete core recovery at DSDP Site 28. The core retrieved interbedded white marls and brown lutites of early to middle Eocene age at 870-962 cm beneath the sea floor. A reflection profile across this outcrop (Fig. 3.8) indicates that the surface of Datum A may have been eroded away, so it is possible that the core sampled sediment slightly below the datum and within the upper stratified layer. However, the available evidence strongly indicates a middle Eocene age for Datum A.

THE TRANSPARENT LAYER

The distribution of the post-middle Eocene transparent layer and stratified sediment was determined by constructing an isopach map of sediment thickness (in seconds reflection time) above Datum A (Fig. 3.3). The values on the map are

Figure 3.8. CHAIN 34 seismic reflection profile near the southern end of the Silver Abyssal Plain and extending onto the western sector of the Greater Antilles Outer Ridge (Profile 9, Fig. 3.1). The top of the stratified layer (Datum A) breaks the sea floor at the left, and a piston core taken from this outcrop (RC 16-30) is early to middle Eocene in age.



approximately equal to sediment thickness in kilometers if an average sound velocity of 2.0 km/sec is assumed. Although available data indicate that Datum A is of middle Eocene age, there is the real possibility that the reflector is not a time-line. If this is true, bias in the interpretation of post-middle Eocene sediment thickness would be expected. However, the pattern of sediment distribution that emerges is well defined, and significant departures of Datum A from a common time-line would be required to alter radically the following interpretations.

Except where basement peaks interrupt it, the surface of the transparent layer forms the sea floor over the Greater Antilles Outer Ridge. In general, this surface is not conformable to deeper reflectors, so it is unlikely that the transparent layer represents deposition by normal pelagic draping of sediment over an irregular sea floor.

The thickness of the transparent layer along the north slope of the Puerto Rico Trench is highly variable, but virtually everywhere it is thinner than 0.2 sec reflection time (Fig. 3.3). Its irregular distribution probably is due to slumping and faulting along the slope.

The maximum thickness of the transparent layer over the eastern sector of the outer ridge is about 0.5 sec reflection time. The axis of thickest sediments runs east-west near 21°15'N lat., and it is displaced about 60 km north of the topographic crest of the eastern outer ridge. The trans-

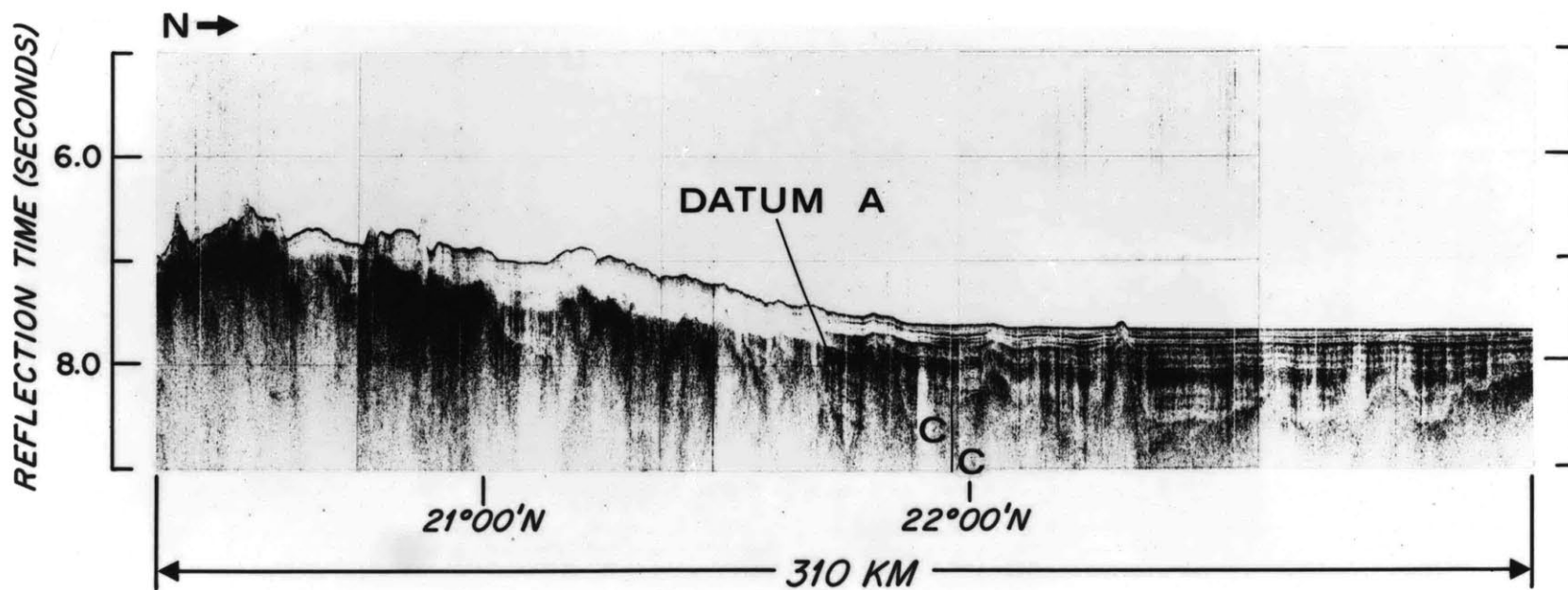
parent layer thins toward the east, rarely exceeding 0.2 seconds east of 63°W long. Basement peaks commonly interrupt the transparent layer, especially along the south slope of the outer ridge.

On the western sector of the Greater Antilles Outer Ridge the axis of thickest transparent sediments lies directly beneath the topographic crest of the outer ridge, and thick stratified sediments (up to 0.8 sec) continue northwest under the Hatteras Abyssal Plain beyond any surface expression of the outer ridge.

The sediments above Datum A gradually thin to the southwest under the Silver Abyssal Plain and Caicos Outer Ridge. Sediment cover is very thin along the base of the Bahama Banks, and Datum A crops out there in at least two places, as well as near the southern edge of the Silver Abyssal Plain (Figs. 3.3, 3.7, 3.8).

Some sediments of the transparent layer on the Greater Antilles Outer Ridge are thought to extend under the reflective layers of the Nares Abyssal Plain (Ewing and Ewing, 1962; Ewing and others, 1968) and therefore to predate the deposition of the abyssal-plain sediments. However, the profiles examined in this study show that the transparent layer interfingers with the sediments of the Nares as well as the Hatteras and Silver Abyssal Plains (Figs. 3.5, 3.7, 3.9, 3.10), indicating contemporaneous deposition in all provinces. The stratified sediments above Datum A which extend up to the

Figure 3.9. CONRAD 10 seismic reflection profile (Profile 6, Fig. 3.1) across the Nares Abyssal Plain and Greater Antilles Outer Ridge, showing the inter-fingering of abyssal-plain reflectors with the sediments of the transparent layer. Note the very thin transparent layer at the top of the north slope of the Puerto Rico trench (far left).



sea floor are observed only in the abyssal-plain provinces.

Although the transparent layer normally exhibits no internal reflectors in seismic reflection profiles, discrete segments of reflective sediments, termed layered valleys, do appear (Figs. 3.10, 3.11, 3.12). They probably result from small turbidity currents generated by slumping of sediment from nearby slopes, with subsequent deposition of graded material in depressions of the outer ridge (Chase and others, 1966; Bunce and others, 1973). These features are restricted entirely to the western sector of the Greater Antilles Outer Ridge (Fig. 3.3), suggesting that this area is characterized by rapid sedimentation and consequent slope instability.

In certain instances where the characteristics of the recording system were so adapted, some seismic profiles show layering within the transparent layer that is conformable with neither the sea floor nor the underlying stronger reflectors. The pattern of reflectors often suggests migration of sediment swells during the process of deposition (Fig. 3.13). Ewing and others (1971) have inferred that similar features in the Argentine Basin have been produced by abyssal currents.

The apparent migratory pattern of the sediment swells, their orientation at right angles to the sinuous axis of the outer ridge, and the relatively undisturbed attitude of the underlying stratified layer argue against compressional deformation as an agent in forming the swells.

Figure 3.10. Seismic reflection profile made on VEMA cruise 22 from the Hatteras Abyssal Plain onto the northwest section of the Greater Antilles Outer Ridge (Profile 3, Fig. 3.1). Note the inter-fingering of reflectors under the abyssal plain with the sediments of the transparent layer. Layered valleys occur as discrete reflector sequences within the transparent layer. The continuity of reflectors at the western end of the outer ridge indicates a history of net deposition rather than erosion (see Chapter VIII).

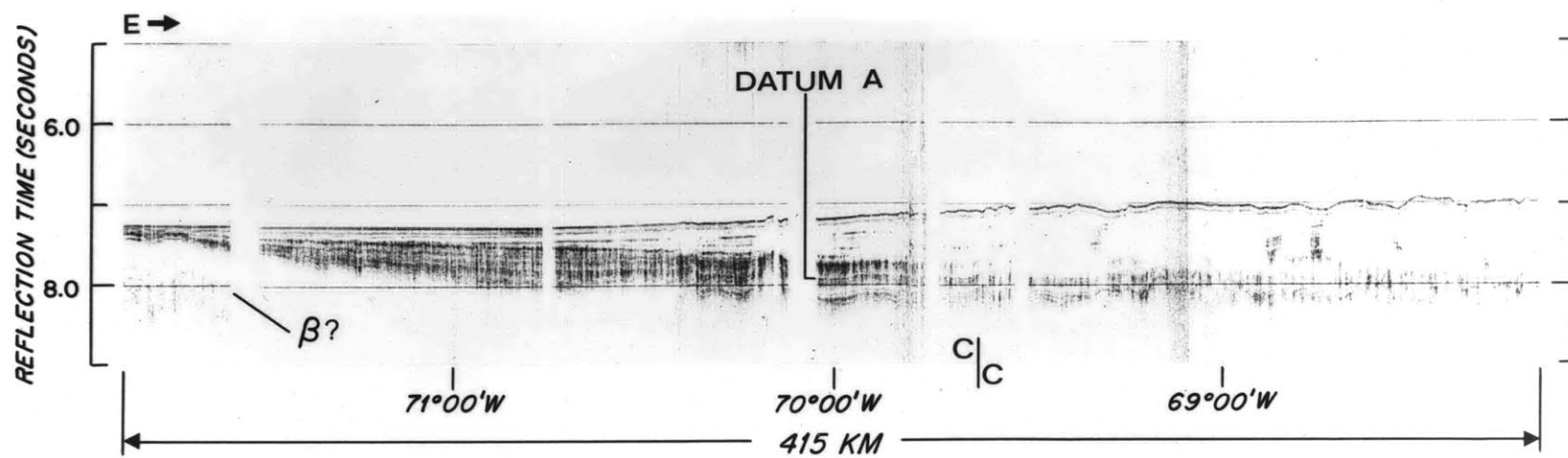


Figure 3.11. CONRAD 10 seismic reflection profile (Profile 5, Fig. 3.1) across the Silver Abyssal Plain and Greater Antilles Outer Ridge. Note the transparent sediment deposited against the west side of the seamount (arrow) and the sediment swells and layered valleys in the transparent layer on the outer ridge.

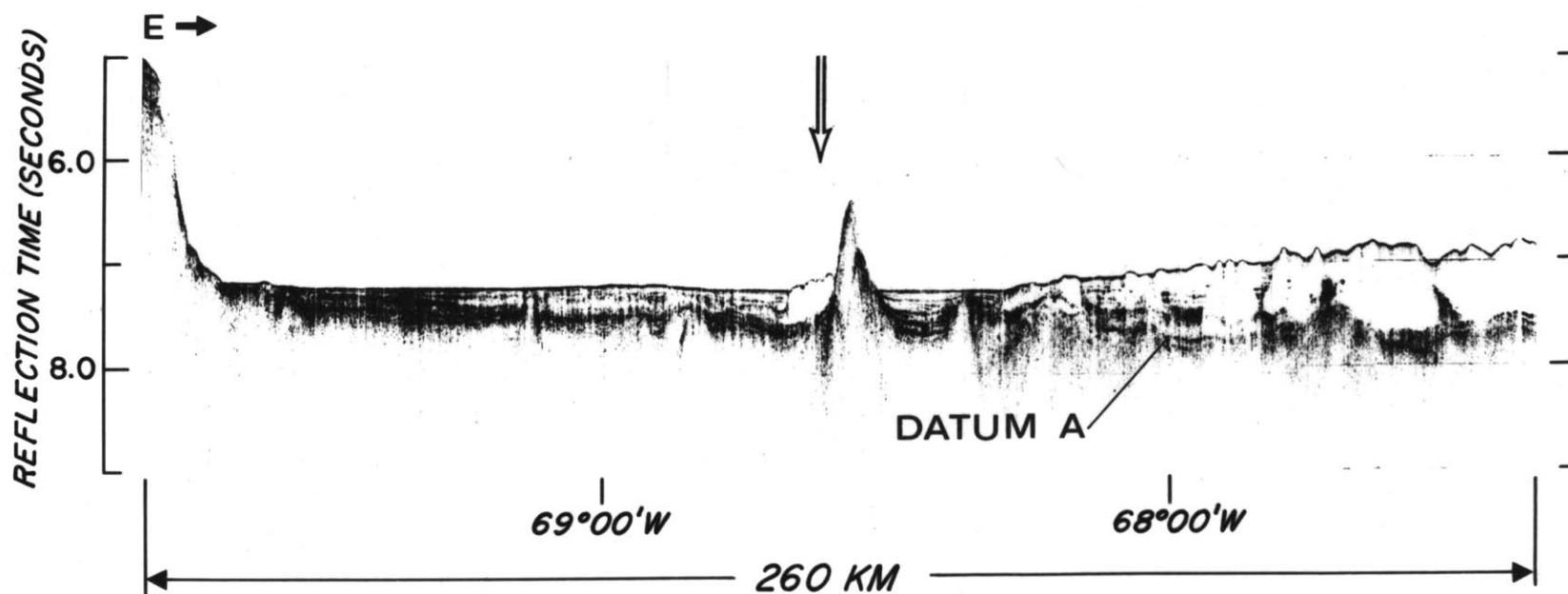


Figure 3.12. Echo-sounding profile (12 kHz), centered on 23°32'N lat., 68°48'W long., illustrating slumping from the flank of a steep swell into an adjacent valley. Small turbidity currents are probably associated with the slumping, and they may be responsible for formation of the layered valleys.

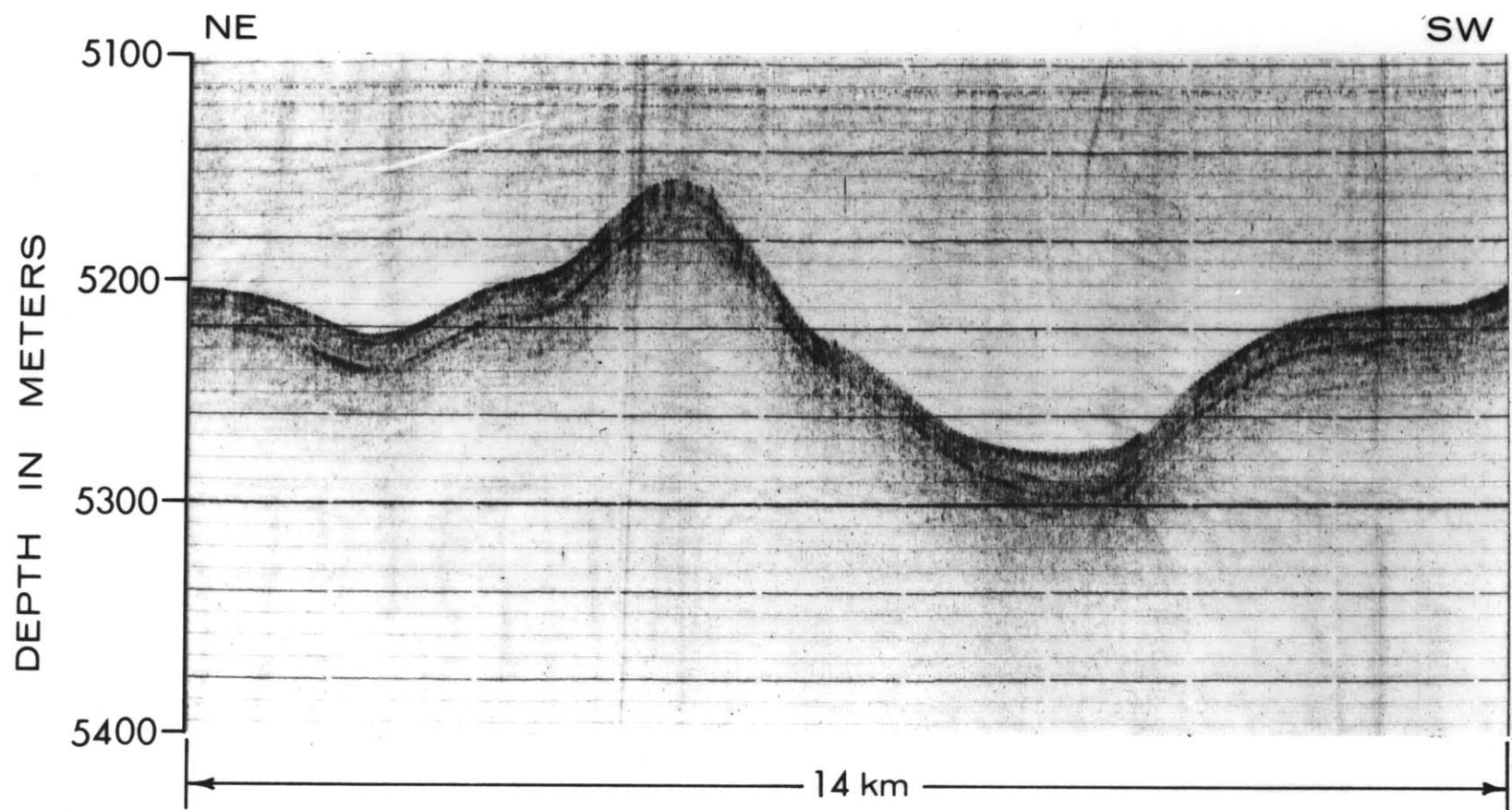
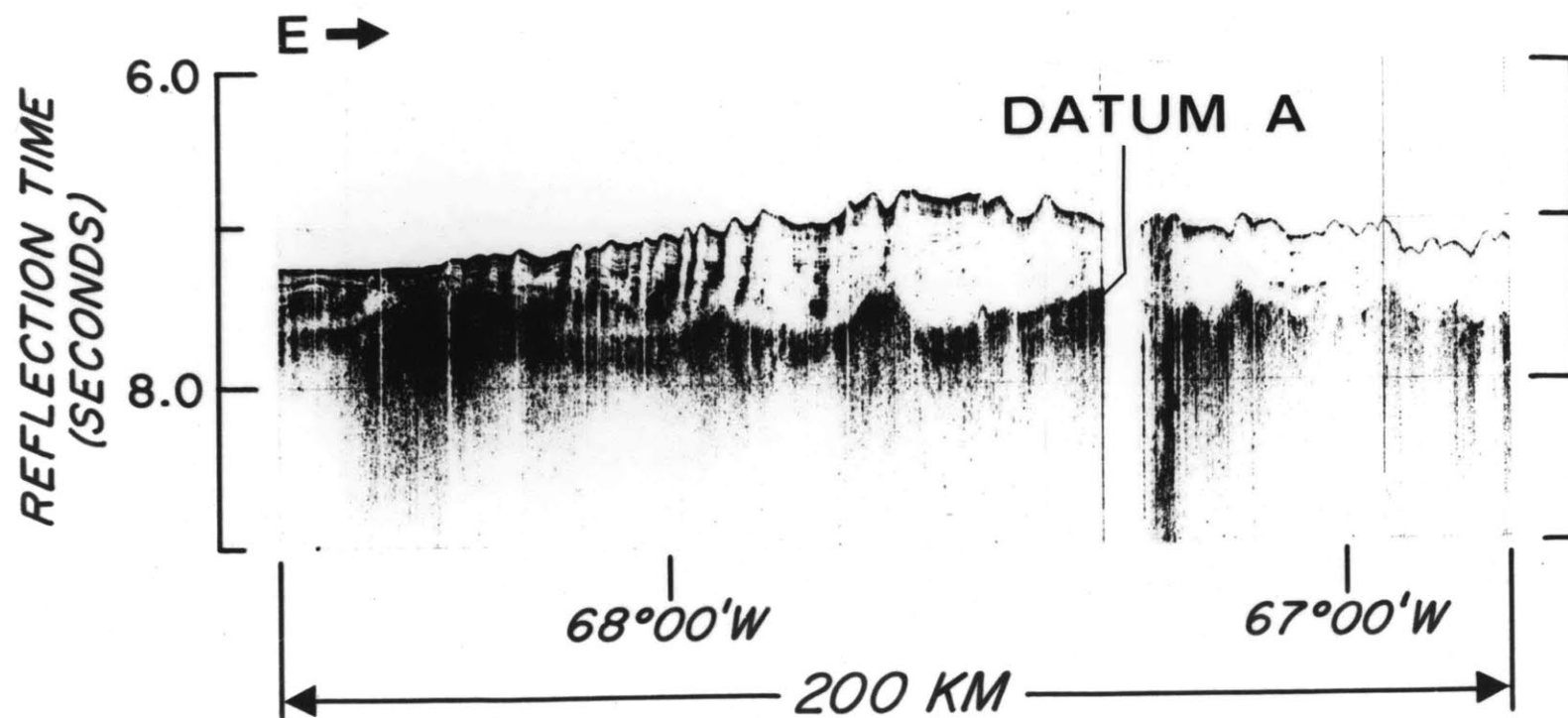


Figure 3.13. CONRAD 10 seismic reflection profile (Profile 8, Fig. 3.1) across the Greater Antilles Outer Ridge showing the migration of sediment swells during the evolution of transparent layer deposition.



The transparent layer represents sediment deposited since middle Eocene time, and its total volume is roughly $6 \times 10^4 \text{ km}^3$. Although sediment recovered from within this unit at Site 28 could not be dated, piston cores from the crest of the Greater Antilles Outer Ridge contain thick sequences of Pleistocene and Holocene sediment, demonstrating continued rapid deposition of the fine-grained, acoustically transparent material to the present. Inferences concerning modern and ancient depositional conditions are presented in later chapters.

CHAPTER IV

THE SEDIMENTS

GENERAL LITHOLOGY

Sediments on the Greater Antilles Outer Ridge typically consist of texturally homogeneous, terrigenous, abyssal brown, gray, and reddish lutites which exhibit little or no stratification, although contacts between zones of different color can be quite distinct (Fig. 4.1). Distinct layers of coarser sediment are rare; where present, these normally thin layers contain relatively high concentrations of carbonate, ash or manganese micronodules. Carbonate is enriched in discrete zones, but it is seldom greater than 30% of the total sediment. Burrow mottling by benthic organisms is very common throughout the cores and is especially noticeable at the base of the carbonate-enriched zones, where carbonate has been reworked into the adjacent, barren lutite. Manganese micronodules, rarely exceeding 1-2 mm in size, normally are scattered in the lutite but sometimes are enriched in certain zones. Very fine particulate manganese oxides commonly create gray-black, weakly laminated zones within the lutite. Layers of altered ash are infrequently observed (Fig. 4.1). Data on all cores used in this study are included in Appendix I.

Grain size of the sediment from the Greater Antilles Outer Ridge is quite uniform (Fig. 4.2) and consists of an

Figure 4.1. . General lithology of cores taken from the
Greater Antilles Outer Ridge. See Appendix I
and Figure 5.1 for locations.

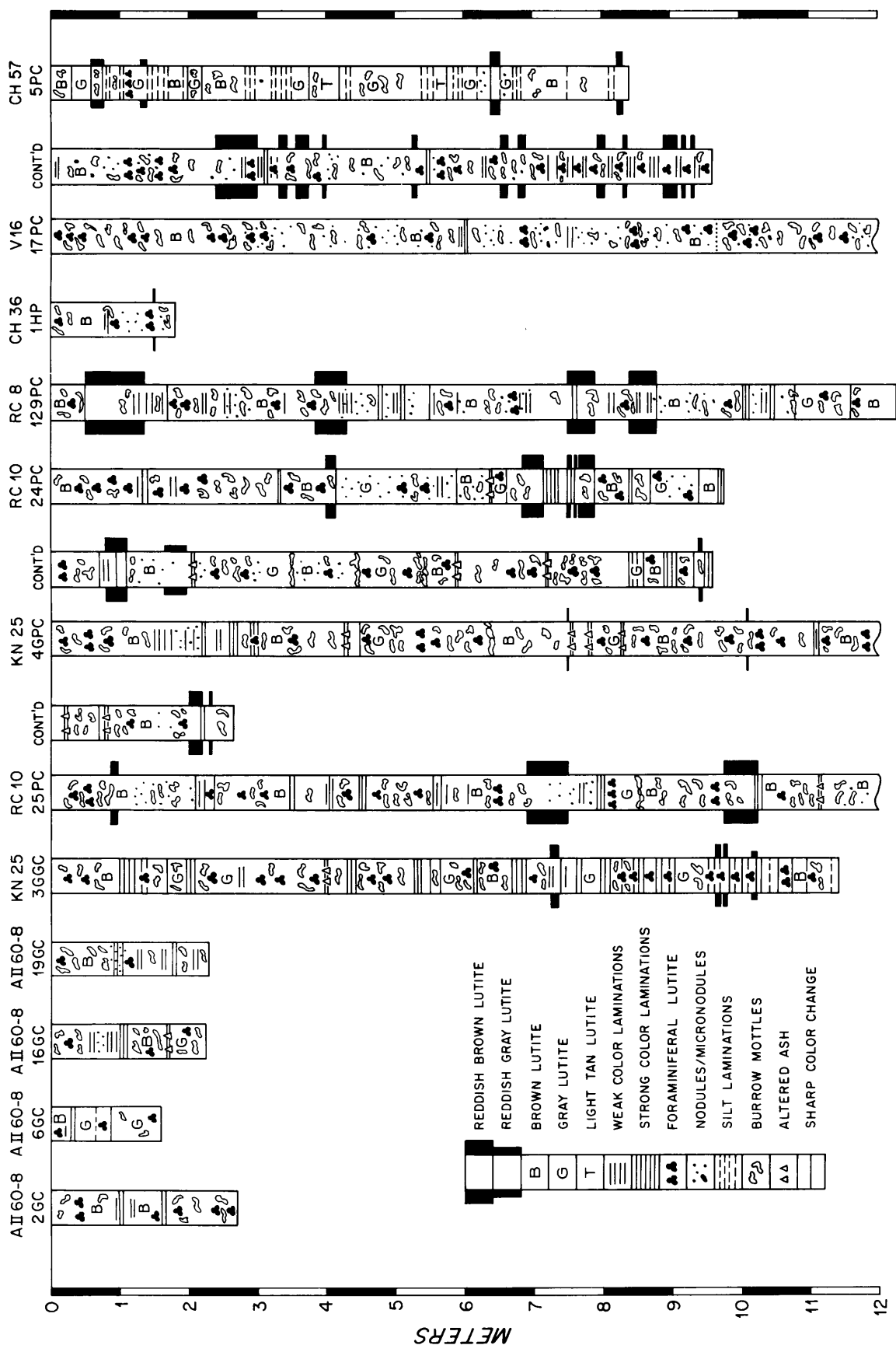
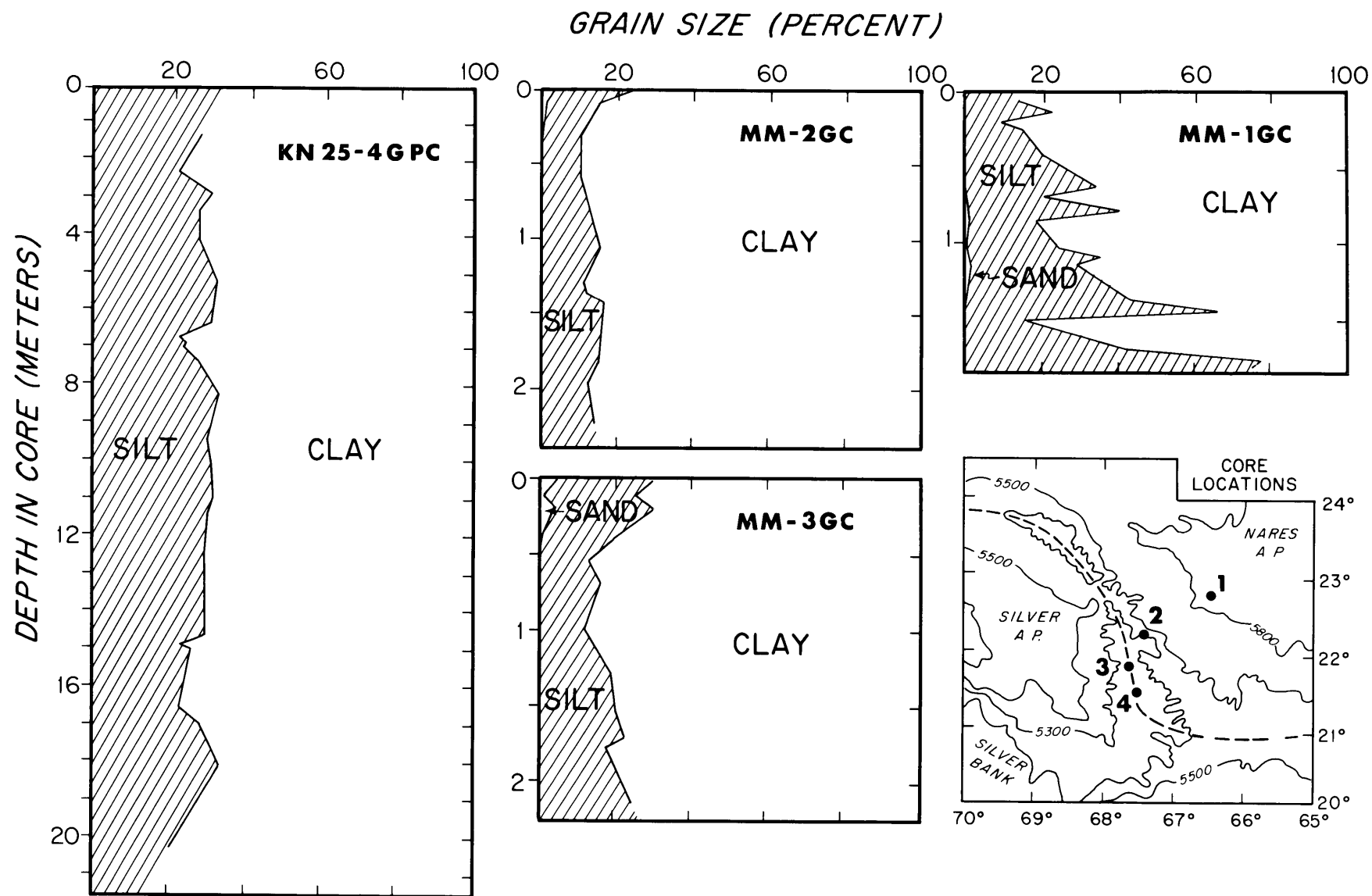


Figure 4.2. Grain-size distribution (deflocculated samples) in four cores from the Greater Antilles Outer Ridge and Nares Abyssal Plain. The sand in cores from the outer ridge is composed of foraminiferal tests. Core locations are shown by corresponding numbers on the simplified bathymetric map at lower right.



average of 80% lutite ($< 2 \mu\text{m}$) and 20% silt ($2\text{--}62 \mu\text{m}$). The only sand-size material ($> 62 \mu\text{m}$) normally present consists (in order of decreasing abundance) of: foraminiferal tests, manganese micronodules, fish teeth, siliceous spicules, and very rarely, radiolarian and diatom tests. The fine size of the sediments precludes detection of obvious current-produced primary structures.

Organic carbon is strongly enriched in the outer ridge sediment in comparison with abyssal lutites in other areas of similar depth. Organic carbon constitutes about one-half to two percent of the sediment (Fig. 4.3), whereas values less than one-half percent are normally encountered in abyssal oceanic areas (Lisitzin, 1972). This enrichment is more typical of continental margin sediments and thus may suggest a continental source for the detritus. Possible fragments of Sargassum weed observed in bottom photographs may also contribute organic carbon to the bottom sediment.

Enrichment of organic carbon in the sediment may also be demonstrated by another phenomenon. Bottom photographs taken over the Greater Antilles Outer Ridge (see Appendix II) show an abundance of benthic activity (Fig. 4.4) in the form of tracks, trails, and burrows; organisms themselves were frequently photographed (pennatulids, echinoids, asteroids, ophiuroids, polychaete (?) worms, sponges, and occasional holothurians). In 512 bottom photographs taken at 33 stations on the western sector of the outer ridge, the density of animals photographed varies from 0.4 to 3.2 organisms per

Figure 4.3. Organic carbon in two cores from the Greater Antilles Outer Ridge and one core from the Nares Abyssal Plain. Determinations were made by combustion at 650°C (P.Hatcher, written comm., 1973) using a combination of the methods of Konrad and others (1970) and Justin and Tefft (1966).

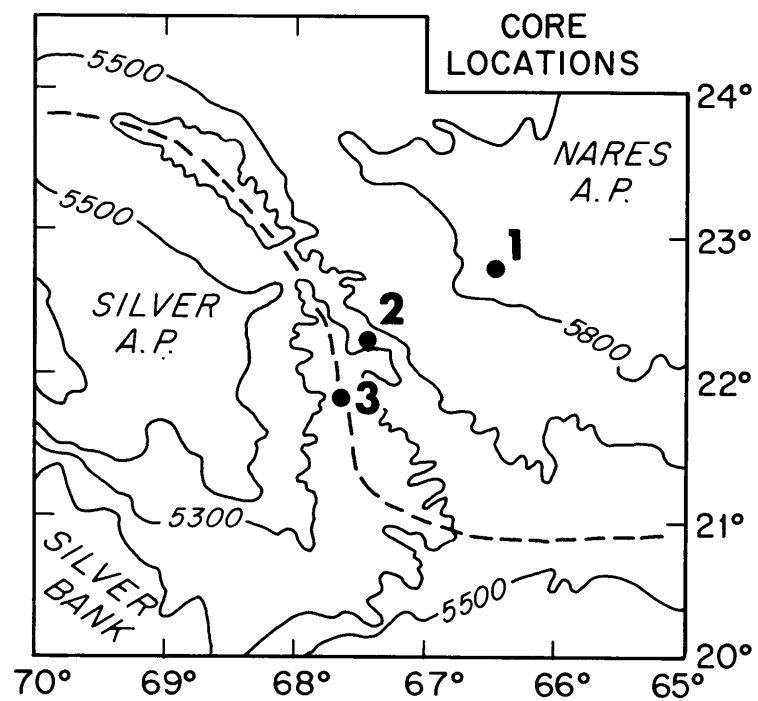
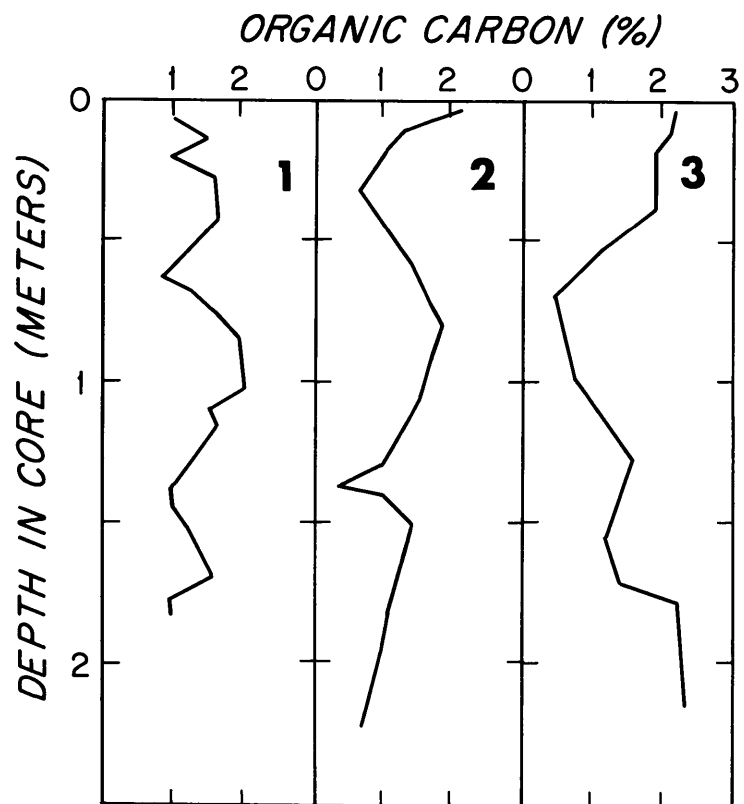
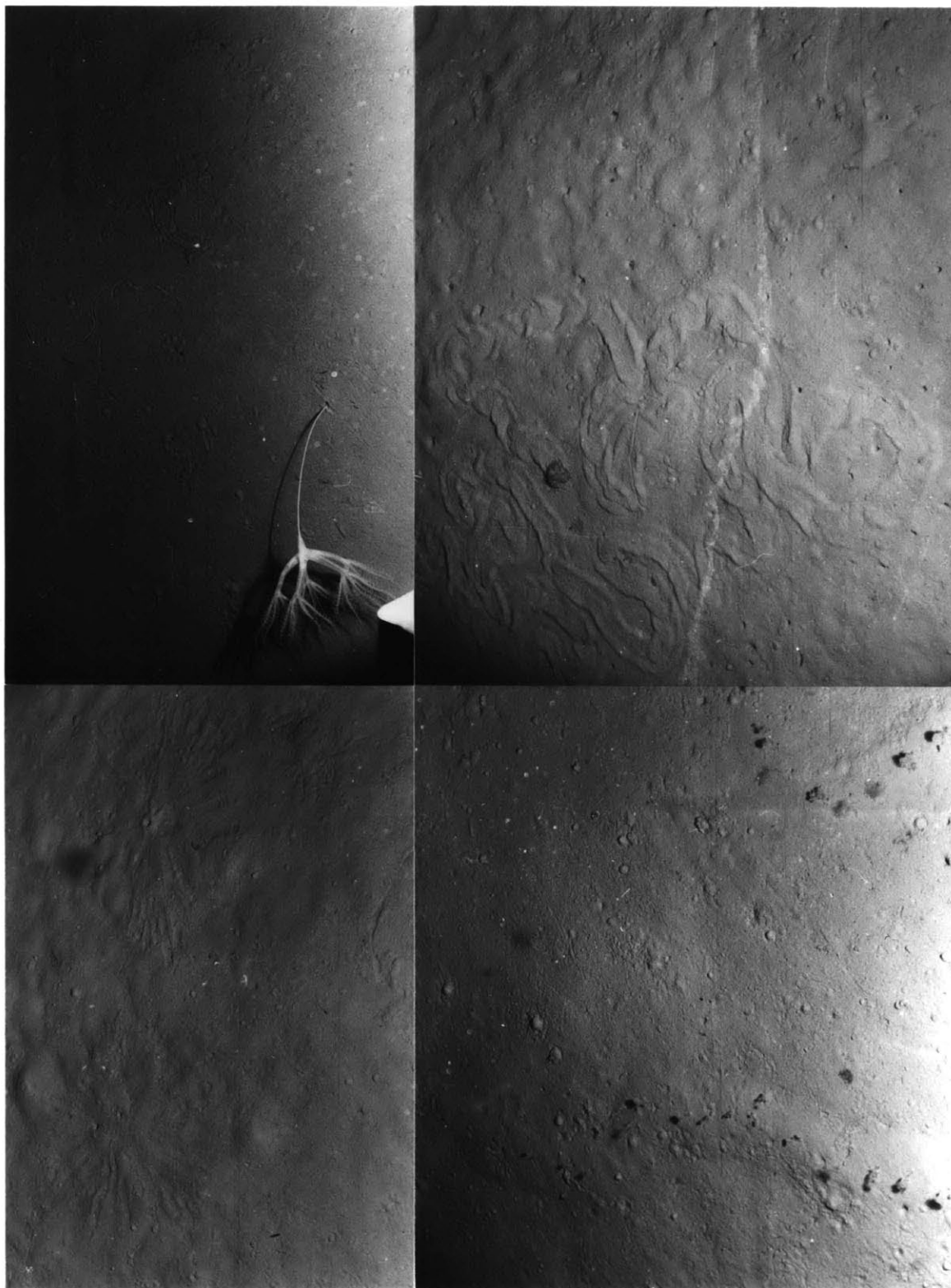


Figure 4.4. Bottom photographs taken on the flanks of the Greater Antilles Outer Ridge showing the abundance of benthic activity in the region.
UL - Spoke burrows, worm burrows, and mounds; KN25, Sta. K6, 5483 m. UR - Pennatulid bending in northwesterly current, worm burrows, plow marks; Camera frame is at lower left; AII60-8, Sta. K11, 5499 m. LL - Worms (?) ejecting sediment from burrows along obscure echinoid (?) trails; worm burrows, spoke burrows, plow marks; AII60-8, Sta. K12, 5400 m. LR - Echinoid feeding in sediment, worm burrows; AII60-8, Sta. K17, 5712 m. See Appendix II for photograph locations and additional descriptions. Each photograph covers an area of approximately 1.5 to 2.0 m².

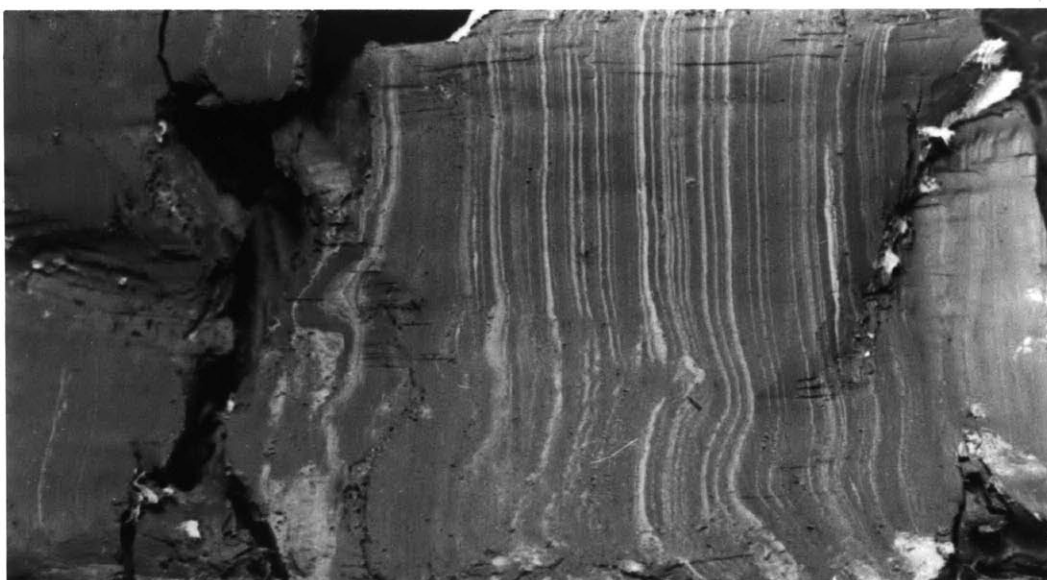
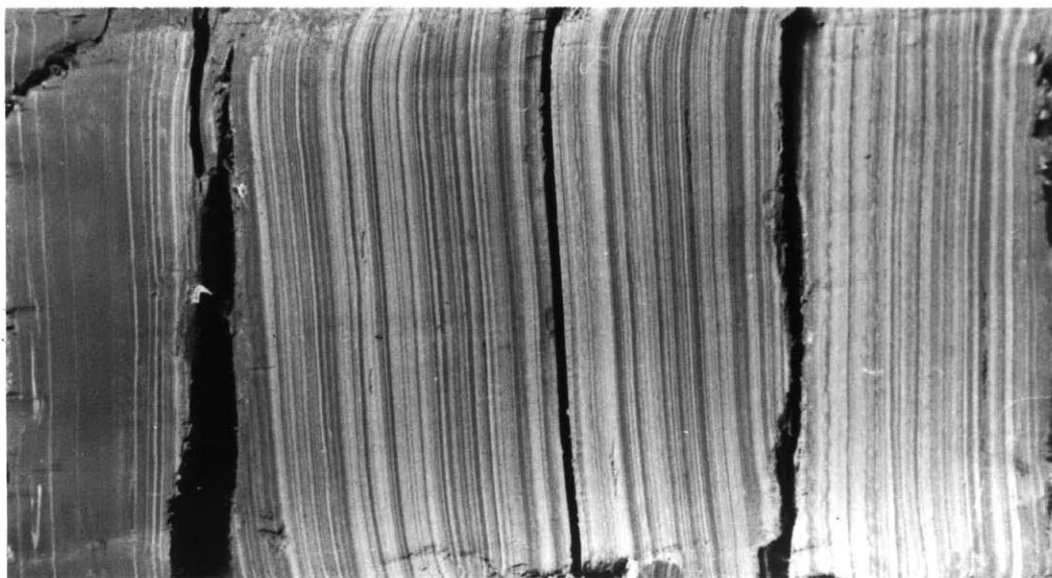


10 m², with an average value of 1.3 organisms per 10 m². The abundance of organisms at these depths and below a water mass of low productivity (southern Sargasso Sea) is very unusual (Rowe, 1971); expected animal densities are probably less than 0.2 organisms per 10 m² (Rowe and Menzies, 1969). Significant benthic activity is also confirmed by the abundance of burrow mottling in the cores (Fig. 4.1). The variety and intensity of benthic activity suggests that the high organic carbon in the sediment may create unusually rich feeding grounds for the organisms.

Sediment cores from the Silver and Nares Abyssal Plains show the typical alternation of pelagic and turbidite sequences normally encountered beneath abyssal plains (Ericson and others, 1961). This is most strongly demonstrated in the grain-size distribution (Fig. 4.2) where silt may constitute 80% of the sediment in a turbidite sequence on the Nares Abyssal Plain. The quantity of organic carbon is similar to that on the Greater Antilles Outer Ridge.

The Nares Abyssal Plain differs from other abyssal plains in the North Atlantic in that it is isolated from direct downslope sedimentation from continental margin sources; Vema Gap is the main tributary through which sediment is funneled to this area. The isolation of the Nares Abyssal Plain probably results in deposition of thin, distal turbidite sequences on its surface. This is indicated by the virtual absence of sand-sized material (Fig. 4.2) and by the thick sequences of fine silt and lutite laminae (Fig. 4.5).

Figure 4.5. Distal turbidite sequences in MT. MITCHELL core 1GC from the southern edge of the Nares Abyssal Plain: Left, 139-151 cm; right 172-184 cm. Each such sequence of fine-grained, finely laminated sediments may represent distal deposition from dozens of turbidity-current events. Scale: 1 division = 1 mm.

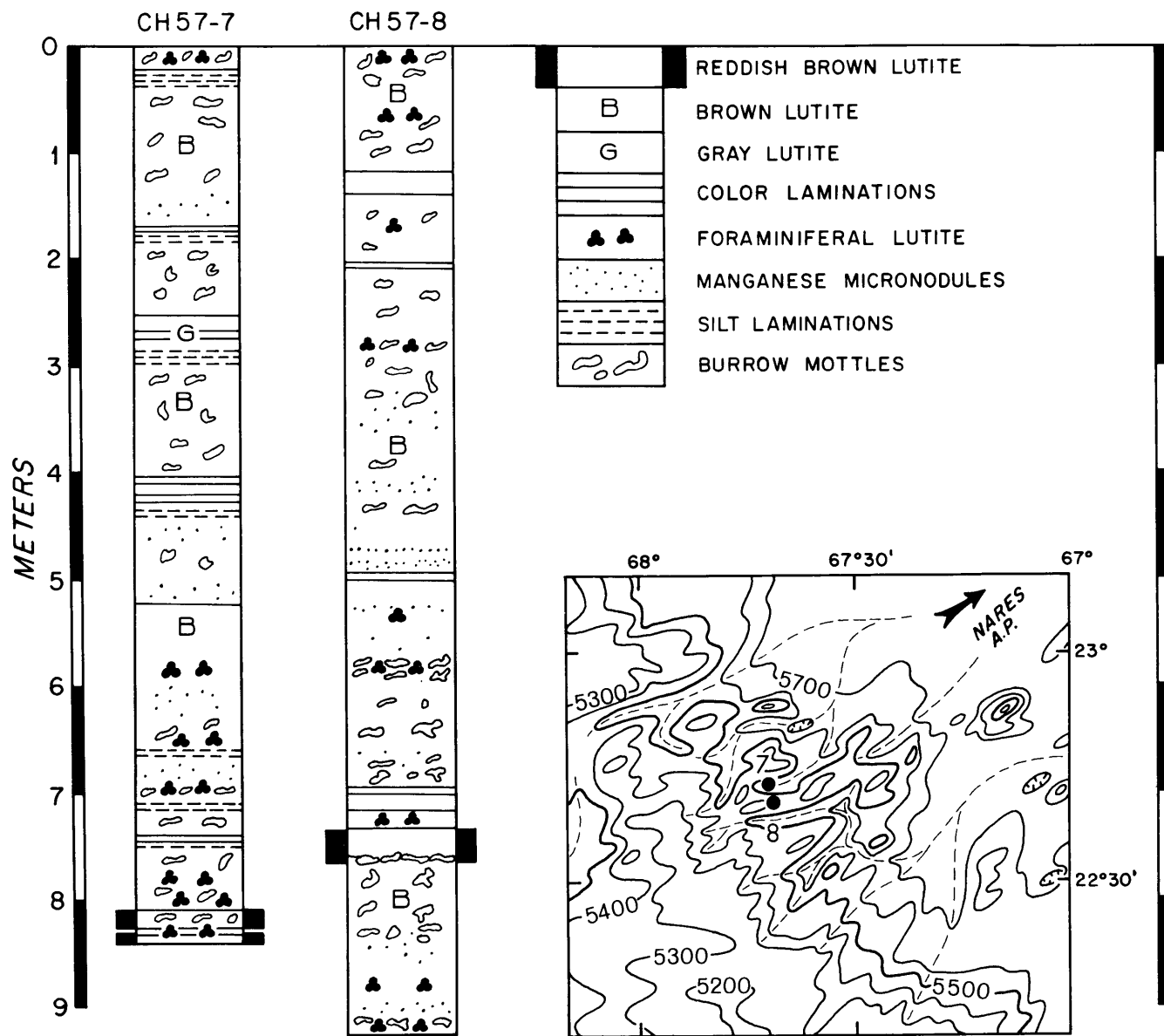


The laminated zones and overlying pelagic sequences are interpreted as facies (d) and (e), respectively, in the Bouma turbidite sequence (Bouma, 1962). Distal turbidites are characterized by the absence of facies (a) - graded bedding, (b) - sand/lutite laminae, and (c) - current-bedded sequences, since the high flow regime and coarse material do not reach the remote area of distal deposition (Bouma and Hollister, 1973).

On the Greater Antilles Outer Ridge, sequences of alternating lutite and micaceous silt laminae 1-2 mm thick occasionally occur in flat-lying ponds (layered valleys) within sediments of the transparent layer. They probably result from localized slumping and turbidity currents which may form mini-abyssal plains similar to those found in ponds on the Mid-Atlantic Ridge (Fig. 3.12; Hersey, 1965; Chase and others, 1966). The turbidite sequences are usually less than 10 cm thick, and they occur exclusively in topographic depressions in the outer ridge. The remaining core material consists of variegated lutites similar to other outer ridge sediment (Fig. 4.6).

Ten cores taken from the south flank of the eastern Greater Antilles Outer Ridge (north slope of the Puerto Rico Trench) and one core from the southwestern flank near the Silver Abyssal Plain contain uniform unfossiliferous lutites which are dominantly altered ash with rare zeolites. Glass shards in varying states of devitrification are also abundant.

Figure 4.6. General lithology of cores taken from a layered valley and adjacent sediment swell, showing inferred turbidite sequences which may result from localized slumping and turbidity currents. The bathymetric map of the layered valley area shows core locations and axes of the valleys (dashed lines) extending toward the Nares Abyssal Plain. Depths are in corrected meters.



THE CARBONATES

Foraminiferal tests generally constitute more than 90 percent of the carbonate in the cores from the Greater Antilles Outer Ridge, and consequently there is a strong correlation between foraminiferal abundance determined in visual core descriptions and the carbonate content (Fig. 4.7). Microscopic examination of smear slides shows that the non-foraminiferal carbonate consists mostly of nannoplankton remains with very small amounts of carbonate detritus which may be transported from shallower areas such as the Bahama Banks. The paucity and very fine size ($< 5 \mu\text{m}$) of this material make identification difficult, but coralline-algal fragments and dolomite rhombs have tentatively been identified.

Since the carbonate consists dominantly of foraminiferal tests, the cyclicity of carbonate content in the cored sediment (Figs. 4.7, 4.8) may be caused by any of four factors: 1) dilution by terrigenous, carbonate-free sediment, 2) current transportation of Foraminifera, 3) variations in carbonate dissolution, or 4) variations in zooplankton productivity of the overlying surface water.

Any effect of dilution by terrigenous sediment is largely ruled out by data on the observed rates of accumulation (see Chapter V); radiocarbon dates of the upper portions of cores indicate that average sedimentation rates are generally lower in the low-carbonate zones than in the high-carbonate zones. It is also unlikely that abyssal

Figure 4.7. Graph of carbonate factors for core KN25-4GPC. The paleotemperature curve of Emiliani (1971) is on a linear time scale, but the curves of core parameters represent depths in the core, and they are not adjusted to a time scale. The curve of relative surface productivity is derived from the carbonate and dissolution curves, using the assumptions that foraminiferal tests constitute 100% of the carbonate and that they were transported to the sediment by vertical settling with little or no horizontal transportation. The zonation (left) is based on the abundance of the Globorotalia menardii complex (see Chapter V).

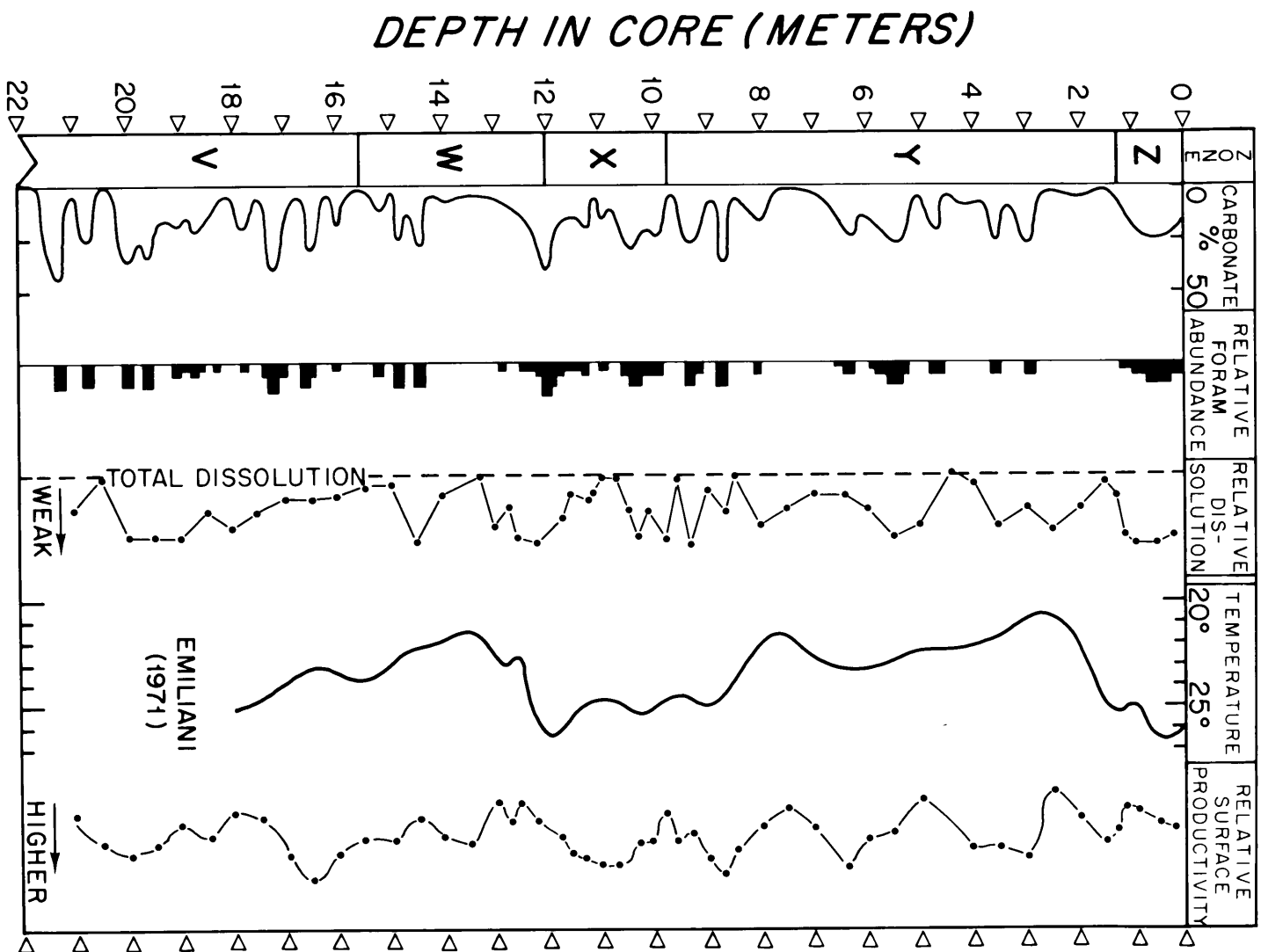
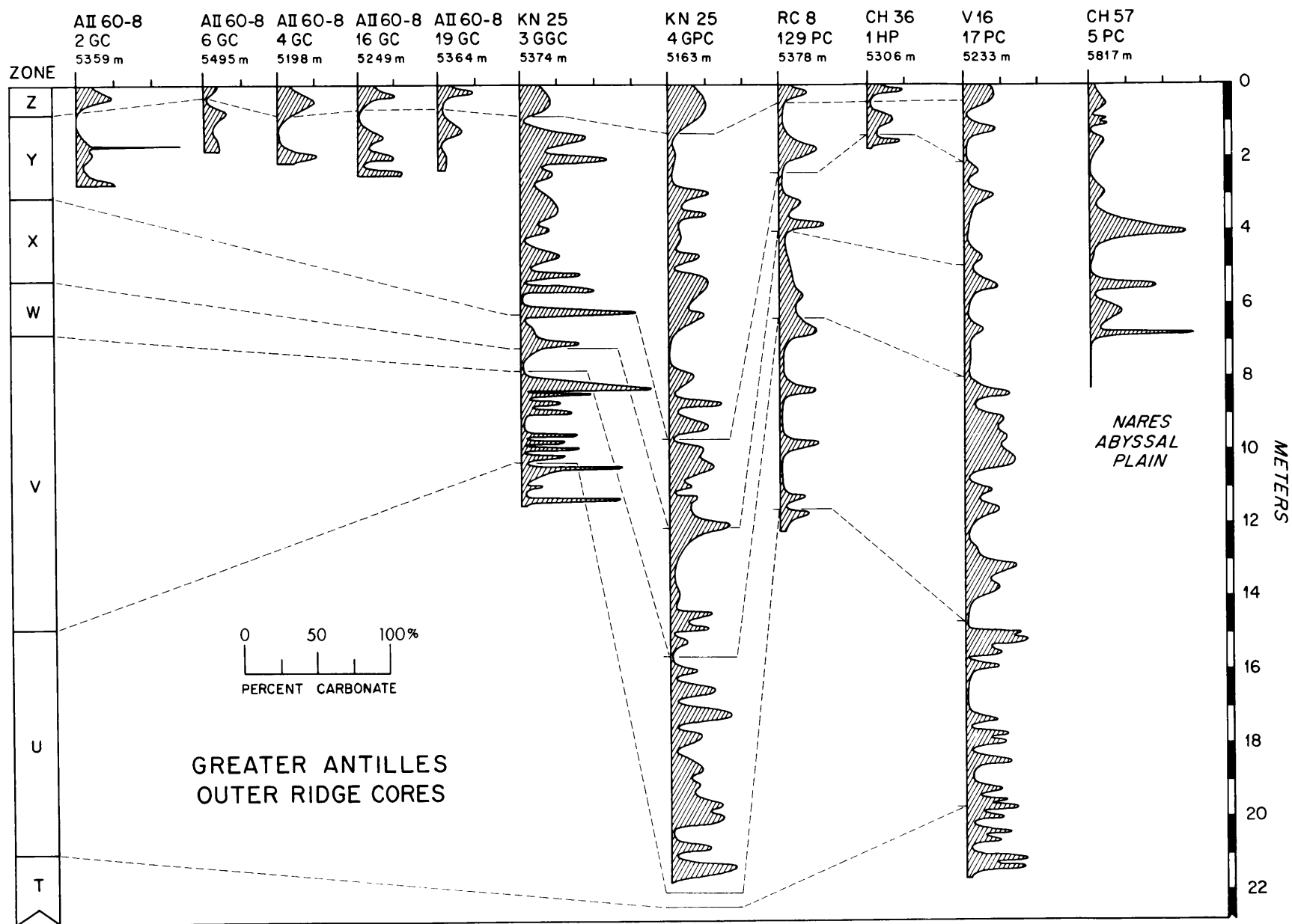


Figure 4.8. Curves of carbonate versus depth in eleven cores from the Greater Antilles Outer Ridge and Nares Abyssal Plain. The cyclicity is produced largely by a combination of decreasing depth of the lysocline (i.e. dissolution) and variations in surface productivity (see Fig. 4.7). The overall core-recovery ratio for the gravity core KN25-3GGC is 0.445. However, rapid carbonate variations together with visual evidence of compaction and incomplete coring indicate that core recovery was much less in the lower third of the core. KN25-GGC3 is the only core studied which contains strong carbonate peaks that are related to rich nanoplankton remains in thin layers. The zonation (left) is based on the abundance of the Globorotalia menardii complex (see Chapter V).



currents have transported many Foraminifera into or out of the region of the Greater Antilles Outer Ridge. Judging from the grain-size distribution of the non-carbonate fraction of outer ridge sediments, abyssal currents in this region are competent to carry and deposit only lutite and fine silt-size sediment; however, the hydrodynamic grain size of the Foraminifera in sediment from the outer ridge, determined from settling velocities, is in the coarse-silt and fine-sand range.

In the region just southeast of this area, Berger (1968) found that the lysocline (level of maximum increase in carbonate solution) closely matches the transition between Antarctic Bottom Water (AABW) and North Atlantic Deep Water (NADW). If a similar relationship exists over the Greater Antilles Outer Ridge, the present lysocline lies near 5000 m, or about 200-300 m above the crest of the outer ridge. This solution effect and the present low plankton production in the overlying Sargasso Sea (Be' and others, 1971) combine to give carbonate concentrations of 8-18% in the surficial sediments of the outer ridge (5100-5300 m depth) and less than 5% in those from the much deeper Nares Abyssal Plain (Fig. 4.8).

The effect of factors 3) and 4) above was examined by assuming that foraminiferal tests do constitute 100% of the carbonate fraction, and the cyclicity in carbonate content was analyzed by examining dissolution effects in the $> 62 \mu\text{m}$

fraction of the foraminiferal tests. A relative scale of weak to strong (or total) dissolution was used, based on visible corrosion and fragmentation of tests and on the abundance of easily corroded species (Berger, 1968). The resulting graph (Fig. 4.7) shows a reasonable (but not perfect) correlation between carbonate percentage and strength of dissolution. Both, in turn, tend to correlate in some aspects with the generalized paleotemperature curve of Emiliani (1971), with lower carbonate associated with cooler climates. If the lysocline is indeed coincident with the AABW-NADW transition, the dissolution curve indicates additional pulses of increased AABW production (elevated lysocline) beyond those associated with the three distinct cool peaks in the paleotemperature curve.

The relative surface productivity can be crudely derived from the carbonate and dissolution curves (i.e. low carbonate plus weak dissolution = low productivity, high carbonate plus strong dissolution = highest productivity, and so on), except where total dissolution prevents an evaluation. The resulting curve (Fig. 4.7) indicates that surface productivity has indeed been variable and that present production is moderate to low, relative to past production.

The observed cyclicity of carbonate in sediment from the Greater Antilles Outer Ridge therefore has resulted from variations both in surface productivity and in dissolution. Although cool climates tend to correlate with

increased dissolution (elevated lysocline), there are also numerous additional dissolution events which may represent pulses of Antarctic Bottom Water entering the western North Atlantic basin.

MINERALOGY

Methods

X-ray mineral determinations were made on the lutite ($< 2 \mu\text{m}$) and silt ($2-52 \mu\text{m}$) fractions of sediment samples from the Greater Antilles Outer Ridge and vicinity. The sand-size fraction, which never exceeded about 2% of the sample, was included in the silt analysis.

All samples were treated with 1:4 acetic acid to remove carbonate, dispersed in a weak sodium hexameta-phosphate solution, and centrifuged repeatedly to separate the less than $2 \mu\text{m}$ and greater than $2 \mu\text{m}$ fractions. The lutite fractions were vacuum-sedimented onto silver filters, thus providing an oriented aggregate to enhance basal lattice reflections while minimizing size fractionation due to settling. Samples were x-rayed (at $2^\circ 2\theta/\text{min}$, using Cu $K\alpha$ radiation and a curved-crystal monochromator) after each of three treatments: 1) removal of carbonate (referred to as the untreated sample), 2) vapor glycolation at 70°C for at least 4 hours, and 3) heat treatment at 400°C for at least one-half hour. Carbonate-free silts were x-rayed in random-powder mounts.

Diffractograms of the lutite fractions indicated that montmorillonite, mixed-layer montmorillonite-illite, illite, chlorite, and kaolinite constitute nearly 100 percent of the minerals in all samples. For purposes of this discussion, material which expands to a 17 \AA (001) peak upon glycolation is referred to as montmorillonite, although it also may include some interstratified illite layers (Reynolds and Hower, 1970). Clay which collapses to a 10 \AA (002) peak at 400°C is a combination of montmorillonite and mixed-layer montmorillonite-illite. Minerals showing a basal sequence $10, 5, 3.3, 2.5 \text{ \AA}$ that is affected by neither glycolation nor a 400°C heat treatment are identified as illite.

Assuming that these minerals represent the total sample, semiquantitative estimates of composition were made (Table 4.1) using the following peaks and weighting factors (Hathaway, 1972a): 1) the increase in intensity (peak area) of the 10 \AA peak of the sample when heated to 400°C above the intensity of the 10 \AA peak of the glycolated sample is assigned to montmorillonite plus mixed-layer montmorillonite-illite, 2) the intensity of the 10 \AA peak in the glycolated sample is assigned to illite, 3) one-half the intensity of the 7 \AA peak in the untreated sample is assigned to chlorite plus kaolinite, and 4) the relative contribution of chlorite and kaolinite to the 7 \AA peak is determined from the total peak area of each in the 3.5 \AA chlorite-kaolinite doublet, using the method of Biscaye (1964). Sample compositions were also calculated according to the method of Biscaye (1965) using

TABLE 4.1. MINERALOGY OF THE < 2 μ m SIZE FRACTION

Core No.	Sample Depth (cm)	$^{\circ}$ N Lat.	$^{\circ}$ W Long.	Composition(1) M:I:C:K	Composition(2) M:I:C:K	V/P(3)	Horn- blende(4)
Greater Antilles Outer Ridge							
AI160-8:2GC	2	23 $^{\circ}$ 49.0'	69 $^{\circ}$ 31.8'	46:39:10:5	17:60:15:8	.49	x
AI160-8:2GC	224	"	"	49:37:10:4	11:66:17:6	.37	x
AI160-8:6GC	14	23 $^{\circ}$ 10.5'	69 $^{\circ}$ 18.0'	36:44:12:8	12:61:16:11	.48	x
AI160-8:16GC	26	23 $^{\circ}$ 27.9'	68 $^{\circ}$ 33.8'	31:48:13:8	17:57:16:10	.48	x
AI160-8:16GC	86	"	"	31:50:14:5	11:63:18:8	.42	x
AI160-8:19GC	37	22 $^{\circ}$ 44.0'	67 $^{\circ}$ 53.7'	31:49:12:8	11:64:15:10	.50	x
AI160-8:19GC	153	"	"	41:43:11:5	17:60:16:7	.55	x
CH57:7PC	817	22 $^{\circ}$ 42.3'	67 $^{\circ}$ 42.2'	18:60:13:9	13:63:14:10	.33	-
KN25-1:3GGC	689	22 $^{\circ}$ 15.0'	67 $^{\circ}$ 57.5'	41:43:10:6	17:60:14:9	.47	x
KN25-1:4GPC	200	21 $^{\circ}$ 30.0'	67 $^{\circ}$ 31.0'	43:42:9:6	14:64:13:9	.39	x
KN25-1:4GPC	548	"	"	42:44:10:4	14:66:14:6	.37	x
KN25-1:4GPC	1272	"	"	46:39:8:7	11:65:13:11	.45	-
KN25-1:4GPC	1790	"	"	67:23:6:4	26:53:12:9	.55	-
KN25-1:4GPC	2020	"	"	54:35:8:3	16:64:14:6	.47	x
A282:12HF	10	20 $^{\circ}$ 22.0'	67 $^{\circ}$ 22.0'	35:47:11:7	11:64:15:10	.47	x
RC8:129PC	26	21 $^{\circ}$ 21.0'	66 $^{\circ}$ 08.0'	34:48:11:7	11:64:15:10	.42	x
CH36:1HP	8	21 $^{\circ}$ 08.4'	65 $^{\circ}$ 02.5'	38:44:9:9	15:60:13:12	.43	x
V16:17PC	12	20 $^{\circ}$ 52.5'	64 $^{\circ}$ 04.0'	35:45:12:8	13:61:16:10	.46	-
Puerto Rico Trench							
RC8:128PC	10	19 $^{\circ}$ 28.0'	65 $^{\circ}$ 25.7'	51:30:9:10	29:44:12:15	.40	-
CH57:1PC	11	20 $^{\circ}$ 14.2'	65 $^{\circ}$ 21.5'	40:40:9:11	21:53:11:15	.60	x
A172:14PC	10	19 $^{\circ}$ 54.0'	64 $^{\circ}$ 48.0'	47:33:10:10	24:48:13:15	.46	-
RC8:135PC	10	18 $^{\circ}$ 55.0'	62 $^{\circ}$ 13.5'	50:31:8:11	28:45:12:15	.45	-

TABLE 4.1. MINERALOGY OF THE < 2 μ m SIZE FRACTION (Cont'd.)

Core No.	Sample Depth (cm)	$^{\circ}$ N Lat.	$^{\circ}$ W Long.	Composition ⁽¹⁾ M:I:C:K	Composition ⁽²⁾ M:I:C:K	V/P ⁽³⁾	Horn- blende ⁽⁴⁾
Puerto Rico Trench (Con't.)							
CH57:12PC	190	20°11.4'	67°38.6'	70:12:0:18	44:22:0:34	.56	-
CH57:12PC	265	"	"	90:4:0:6	69:12:0:19	.63	-
Caicos Outer Ridge - Silver Bank Apron							
KN25-6:1GC	18	22°48.0'	71°30.0'	33:47:12:8	14:60:15:11	.58	x
AI160-8:24KC	7	20°38.5'	68°25.0'	34:46:12:8	16:59:15:10	.52	x
Vema Gap - Nares Abyssal Plain							
AI160-8:13GC	71	23°54.1'	68°04.7'	48:37:9:6	9:65:16:10	.46	x
CH57:5PC	650	22°40.7'	66°29.6'	34:47:12:7	11:63:17:9	.41	x
V7:23PC	13	23°28.0'	65°56.0'	35:48:11:6	7:68:16:9	.32	-
A172:17PC	10	22°46.0'	63°58.5'	36:46:11:7	12:64:15:9	.31	x
Bermuda Rise							
A282:18HF	12	27°05.0'	67°56.0'	69:18:5:8	40:35:9:16	.68	-
A282:15HF	10	25°29.0'	64°34.0'	55:31:7:7	18:56:13:13	.37	-
A282:23HF	10	30°27.0'	67°58.0'	51:35:7:7	15:60:13:12	.48	x

(1) Mineralogical composition computed using the method of Hathaway (1972a).

(2) Mineralogical composition computed using the method of Biscaye (1965).

(3) V/P is the "crystallinity ratio" employed by Biscaye (1965) for montmorillonite.

(4) x indicates at least a trace of hornblende is present.

the following peaks and weighting factors: 1) the area of the 17 Å peak of the glycolated sample is assigned to montmorillonite, 2) four times the area of the 10 Å peak of the glycolated sample is assigned to illite, 3) twice the area of the 7 Å peak in the untreated sample is assigned to chlorite plus kaolinite, and 4) the contribution of chlorite and kaolinite is determined as above. Some of the mixed-layer material produces a 17 Å peak upon glycolation and is thus defined as montmorillonite. However, this method does not detect any mixed-layer material that does not expand to 17 Å.

All clay-mineral diffraction patterns were recorded on magnetic tape, processed in a computer program developed by J.C. Hathaway, and peak intensities from the printout were used to calculate mineral abundances. The area of the 17 Å glycolated peak (montmorillonite) was determined graphically because of the inaccuracy of the computer baseline at low 2θ angles. Calculations based on graphic methods and those based on intensities from the computer printout gave virtually identical results for all other peaks.

Random-powder silt patterns were also recorded on magnetic tape and processed by the same computer program.

Results

Mineralogy determinations by Biscaye (1965) and Hathaway (1972a) demonstrated that the northern portion of the North Atlantic Basin and the northern continental margin

of North America have clay-mineral assemblages resulting dominantly from mechanical weathering; thus they are dominated by the clay minerals chlorite and illite. Below the latitude of Cape Hatteras, however, the sediments tend to be enriched in kaolinite and montmorillonite, reflecting sources in regions of tropical weathering.

If abyssal currents are transporting sediments from the continental margin of North America into the region of the Greater Antilles Outer Ridge, the mineralogy of the outer ridge sediments should reflect a northern provenance. This concept is strikingly supported by a tongue-like extension of chlorite-enriched sediments which lies beneath the axis of the Western Boundary Undercurrent and extends south along the Bahama Banks into the region of the Greater Antilles Outer Ridge (Figs. 4.9 and 4.10). A northern assemblage of clay minerals on the Greater Antilles Outer Ridge is evident when mineral compositions are determined by either the method of Biscaye (1965) or that of Hathaway (1972a). Hornblende, which is common in the northern assemblage, is also observed consistently in sediments of the area influenced by the Western Boundary Undercurrent (i.e. the Caicos Outer Ridge - Bahama Banks Apron and the Greater Antilles Outer Ridge). Hornblende is seldom observed in the Puerto Rico Trench or on the Bermuda Rise, where the Western Boundary Undercurrent has not deposited sediment (Table 4.1, 4.2).

Figure 4.9. Chlorite abundances (weighted peak-area percentage) in sediment samples from the western North Atlantic, showing the tongue of chlorite-enriched sediment which the Western Boundary Undercurrent has transported south along the margin of the basin as far as the Greater Antilles Outer Ridge. Compositions were calculated using the peaks and weighting factors of Biscaye (1965).

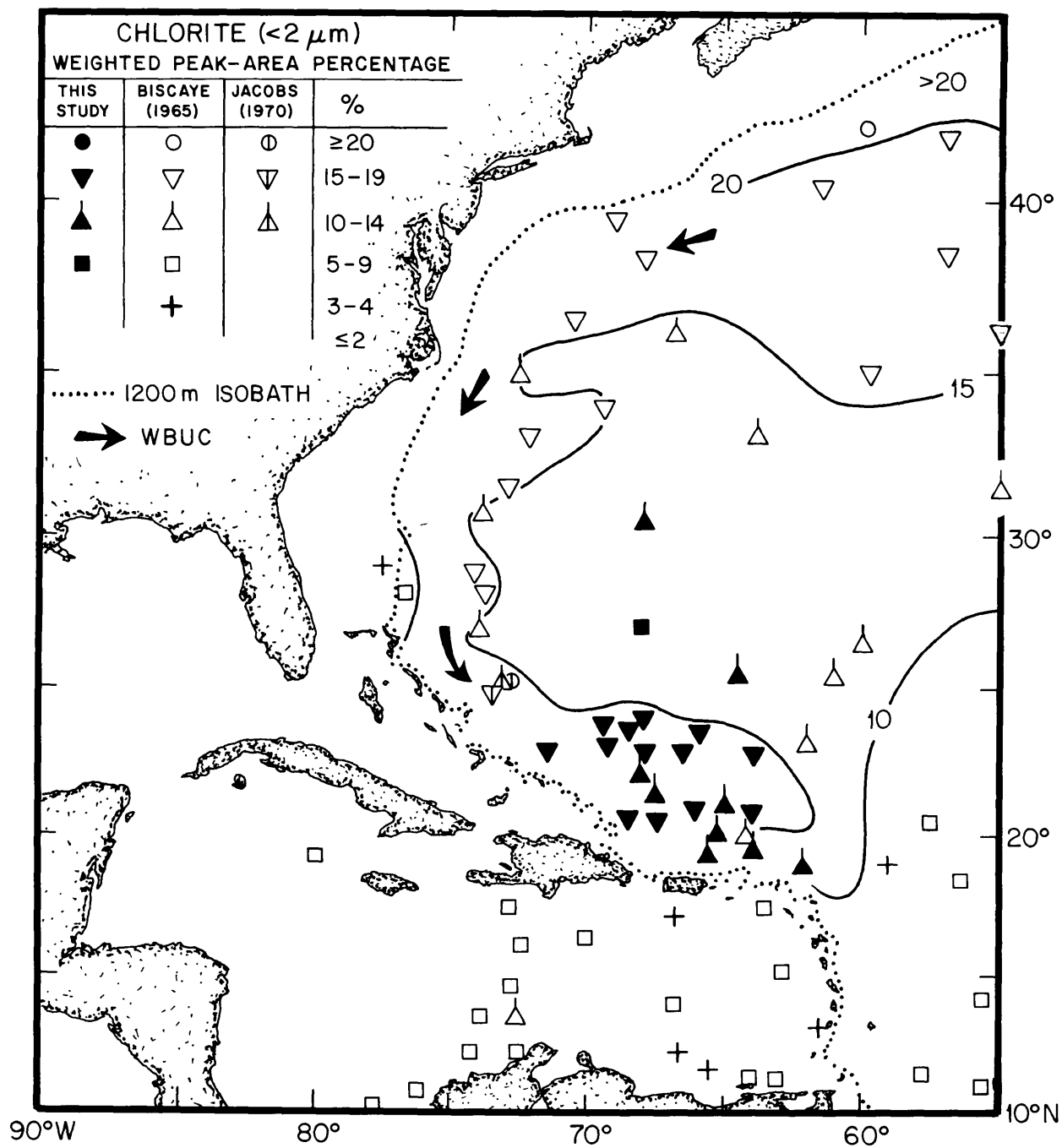
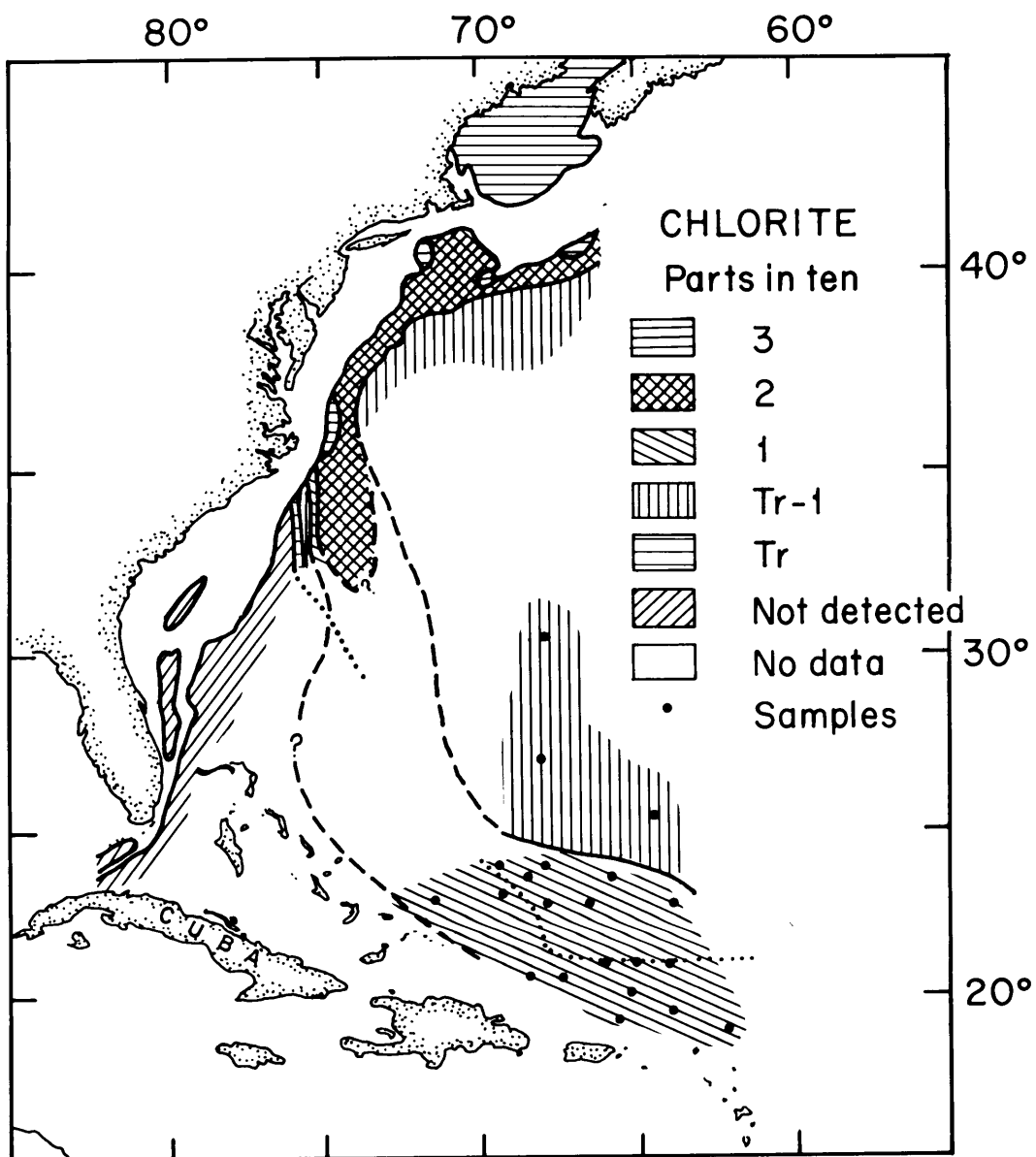


Figure 4.10. Chlorite abundances (weighted peak area, parts per ten) in sediment samples from the continental margin (Hathaway, 1972a) and Greater Antilles Outer Ridge, determined using the peaks and weighting factors of Hathaway. The dotted lines show the axes of the Blake Outer Ridge and the Greater Antilles Outer Ridge, and sample locations are shown by dots.



Obviously, dilution of the northern assemblage of minerals should be expected, since much of the sediment appears to have been transported more than 2500 km to the Greater Antilles Outer Ridge. This dilution by minerals other than illite and chlorite may explain why chlorite on the outer ridge is at the lower end of the spectrum for chlorite abundances in a northern assemblage (Figs. 4.9, 4.10).

There is no other source for the chlorite-enriched sediment on the Greater Antilles Outer Ridge (Fig. 4.9), nor is the assemblage found outside the areas influenced by the Western Boundary Undercurrent. The Antarctic Bottom Water which flows into the Puerto Rico Trench and onto the Nares Abyssal Plain from the south appears to carry a very small amount of sediment in suspension (Eittreim and Ewing, 1972), and the suspended material probably consists of a tropical mineral assemblage of kaolinite and montmorillonite derived from South America.

It has been suggested that chlorite may form in the marine environment by alteration of other continentally derived material (Griffin and Ingram, 1955; Powers, 1957), but the importance of this mechanism is doubtful. Hathaway (1972b) demonstrated that chlorite is more abundant in younger sediments at DSDP Site 105 on the continental rise, so it is unlikely that prolonged exposure to marine conditions had caused diagenetic chlorite formation. The close correlation between continental chlorite sources and marine chlorite

abundances (Biscaye, 1965; Rateev and others, 1966) strongly suggests a detrital origin for chlorite in the deep sea.

The effect of glacial/interglacial changes in sediment source and/or competence of currents which transport the sediment might be expected to appear in the sediments. Zimmerman (1972), for example, found consistent differences in the clay mineralogy of Holocene (montmorillonite-amphibole rich) and Pleistocene (montmorillonite-amphibole poor) facies beneath the Western Boundary Undercurrent on the New England continental rise. However, cores from the Greater Antilles Outer Ridge show no systematic differences in mineralogy between glacial and interglacial sediments (Cores AII60-8:GC2, GC16, GC19; Table 4.1). It is likely that mineral-dilution effects during the presumed long transport of the sediment damp out subtle mineralogical variations.

The samples from the north slope of the Puerto Rico Trench (CH57, core 12, 190 and 265 cm; Table 4.1) are typical of the sediments found there. Most of the sediment cored on the north slope is lithologically similar to the sample at 190 cm in core CH57-12 and probably has a similar composition. The sequences of altered ash in these cores would have a composition like the sample at 265 cm. It is likely that the ashes were deposited during the Pliocene-Pleistocene volcanism in the Antilles (Weyl, 1968) or at an even earlier time (see Chapter V).

The mineralogical composition of the silt fraction of sediments in the vicinity of the Greater Antilles Outer Ridge is generally similar in all samples analyzed; however, silt samples from the Bermuda Rise are different from the outer ridge silts in that they contain no hornblende (Table 4.2). Illite, relative to kaolinite plus chlorite, tends to be depleted in the silt fraction when compared to the lutite fraction.

The average composition of the silt fraction in sediment from the Greater Antilles Outer Ridge is 36% quartz, 21% plagioclase, 42% layer silicates, and < 1% hornblende. Using the assumption that the silt fraction constitutes an average of 20% of the total sediment, the bulk composition of the sediment is 7% quartz, 4% plagioclase, 89% layer silicates, and a trace of hornblende.

OTHER SEDIMENT TRACERS

Two other sediment parameters were considered for their possible use in tracing sediment of a northern provenance southward to the Greater Antilles Outer Ridge. The first of these is the reddish lutite derived from the Permian - Carboniferous red-bed area of the Canadian Maritime Provinces (Hollister, 1967; Zimmerman, 1972) and distributed southward along the continental rise at least to the Blake-Bahama Outer Ridge by the Western Boundary Undercurrent (Needham and others, 1969). This tracer is of limited use because the lutite colors become diluted to the south, and only reddish-

TABLE 4.2. MINERALOGY OF THE 2-62 μ m SIZE FRACTION

Core No.	Sample Depth (cm)	Quartz %	Plagio-clase %	Layer Silicates %	Dolomite %	Horn-blende %	Illite Kaol. + Chl. (Silt)	Illite Kaol. + Chl. (Clay)	Other
Greater Antilles Outer Ridge									
AII60-8:2GC	2	37	22	39	0	TR	2.22	2.60	2% Gibbsite (?)
AII60-8:16GC	26	44	26	30	0	TR	1.88	2.28	. .
AII60-8:19GC	37	35	20	45	0	TR	1.81	2.45	TR Siderite
KN25-1:4GPC	200	38	23	38	0	1	1.90	2.80	. .
RC8:129PC	26	44	16	40	0	TR	2.31	2.67	. .
CH36:1HP	8	26	18	56	0	0	1.44	2.44	. .
V16:17PC	12	28	19	53	0	TR	1.90	2.25	. .
Caicos Outer Ridge - Silver Bank Apron									
KN25-6:1GC	18	47	23	27	2	1	2.79	2.35	. .
AII60-8:24KC	7	48	28	23	0	1	2.44	2.30	. .
Bermuda Rise									
A282:15HF	10	38	23	39	0	0	1.92	2.21	. .
A282:18HF	12	37	18	45	0	0	1.99	1.38	. .
A282:23HF	10	43	22	30	5	0	1.82	2.50	. .
Nares Abyssal Plain									
A172:17PC	10	44	23	32	0	1	2.25	2.56	TR Siderite

gray lutites persist near the Blake-Bahama Outer Ridge (Fig. 15 of Hollister and Heezen, 1972). The reddish-gray and reddish-brown lutites in cores from the Greater Antilles Outer Ridge (Figs. 4.1, 4.5) may represent a further extension of this color/sediment dispersal pattern, although the validity of this observation is uncertain.

Samples from three cores on the Greater Antilles Outer Ridge (AII60-8:16GC, 50-53 cm; AII60-8:6GC, 16-19 cm; and KN25:4GPC, 33-40 cm) were also examined for palynomorphs of northern affinity. Upper Carboniferous palynomorphs derived from the red-beds of the Canadian Maritime Provinces have been used to trace red-sediment dispersal to the south along the continental rise to the Blake-Bahama Outer Ridge (Needham and others, 1969; Habib, 1972). However, samples from the Greater Antilles Outer Ridge are dominated by pine pollen and fern spores, except for a few grains of subtropical affinity (D. Habib, 1973, written comm.), and no palynomorphs are observed which would be useful in determining sediment provenance. This situation is not altogether surprising when we consider the probable distance of sediment transport and the consequent dilution of sediment tracers.

In summary, sedimentary parameters of cores from the Greater Antilles Outer Ridge strongly suggest a sediment provenance along the northeastern continental margin of North America. Organic carbon is enriched in the cores (similar to continental margin sediments and unlike isolated

deep-sea areas), the sediment mineralogy indicates a northern provenance, and sediment colors agree with the observed dispersal pattern of red sediment by the Western Boundary Undercurrent. No evidence has been found to contradict a northern provenance for the sediment that comprises the Greater Antilles Outer Ridge.

CHAPTER V

CHRONOLOGY OF SEDIMENTATION

REGIONAL PATTERNS

The average rates of sedimentation for the provinces in the vicinity of the Greater Antilles Outer Ridge over approximately the past 45 million years can be estimated from the thickness of sediments above Datum A, which is inferred to be of middle Eocene age (Table 5.1) (see Chapter III). These rates are not absolute, since they probably include periods of erosion, nondeposition, and unusually rapid sedimentation. However, even rough accumulation rates can be used to place constraints on some sedimentation conditions. The two striking trends that appear are: 1) relatively high rates of deposition along the axis of the Greater Antilles Outer Ridge, and 2) low average rates (probably with long periods of nondeposition or erosion) along the southeast Bahama Banks and on the north slope of the Puerto Rico Trench. The relationship of these generalized observations to Pleistocene/Holocene sedimentation is discussed below.

GREATER ANTILLES OUTER RIDGE

Although two cores taken on the Greater Antilles Outer Ridge are more than 20 m long (KN25:4GPC - 21.59 m; V16:17PC - 21.70 m), neither these cores nor any of the other 23 outer ridge cores studied penetrated the

TABLE 5.1. AVERAGE RATES OF SEDIMENTATION
FOR THE GREATER ANTILLES OUTER RIDGE AND SURROUNDING
PROVINCES SINCE MIDDLE EOCENE TIME[†]

Province	Average Rate - (cm/1000 yr)*	
	Minimum	Maximum
Eastern Sector - Greater Antilles Outer Ridge	0.4	1.2
Western Sector - Greater Antilles Outer Ridge	1.4	2.0
Nares Abyssal Plain	0.3	0.8
Silver Abyssal Plain	0.4	1.0
Southern end of Hatteras Abyssal Plain	0.4	1.6
Caicos Outer Ridge - Bahama Banks Apron	0	1.0
North Slope of Puerto Rico Trench	0	0.4

[†] Based on the assumptions 1) that Datum A is a time line of middle Eocene age, and 2) the average compressional wave velocity for the sediments overlying Datum is 1.8 km/sec.

* No corrections have been made for compaction effects.

Pliocene/Pleistocene boundary. The bottoms of all cores contain the planktonic foraminiferans Globorotalia truncatulinoides, and Discoasteridae are absent; thus all sediment cores is assumed to be Pleistocene and Holocene in age (Ericson and others, 1964; Berggren and others, 1967).

The zonation of the Globorotalia menardii complex in these cores was studied to determine the rates of sediment accumulation on the Greater Antilles Outer Ridge. Ericson and Wollin (1968), Ruddiman (1971) and Kennett and Huddlestun (1972), among others, have utilized a semi-quantitative evaluation of the relative abundance of this taxonomic complex (G. menardii menardii, G. menardii tumida, and G. menardii flexuosa) as an indicator of alternating warm and cool intervals in tropical and subtropical areas during the Quaternary. A sequence of zones designated Q-Z in order of decreasing age represents these intervals, where Q, S, U, W and Y are cool zones in which G. menardii is rare or absent, and R, T, V, X and Z are warm zones with abundant G. menardii (Ericson and Wollin, 1968). This warm/cool zonation is supported by curves of oxygen-isotope variations down through the V zone (Ruddiman, 1971).

The > 175 μm fraction of Foraminifera from the cores was judged representative of climatic change at this latitude (Kennett and Huddlestun, 1972), and frequency counts of a microsplit of about 300 specimens from each sample were made to determine the abundance of G. menardii.

and thus the T-Z zonation (Fig. 5.1). Determination of exact zonal boundaries was difficult in some cores because total dissolution of foraminiferal tests prevented an evaluation of the abundance of G. menardii. In these few instances, a constant sedimentation rate was assumed (within the constraints imposed by samples of known G. menardii abundances), and boundaries were placed so that the relative proportion of each zone approximated its absolute time span (Ruddiman, 1971). The last appearance of G. menardii flexuosa was used as an indicator of the X zone (Kennett and Huddleston, 1972). However, it cannot always be used as such an indicator in this area, since it is not universally present in the X and older warm zones, and in one instance (Core CH57-8) it does not appear at all.

The zonation thus derived can be used to determine gross average sedimentation rates during the warm and cool intervals (Table 5.2). It is apparent that the highest sedimentation rates for the late Pleistocene and Holocene occur on the crest of the western sector of the Greater Antilles Outer Ridge, with lower rates on the far north flank and on the eastern sector. This pattern is expected, since the layered valleys (presumably associated with rapid sedimentation and consequent slumping) are confined entirely to the western sector of the outer ridge (see Fig. 3.3).

The time scale of Broecker and van Donk (1970) and Ericson and Wollin (1968) is used because it gives fairly consistent and uniform sedimentation rates for each of the

Figure 5.1. Percent abundance of the Globorotalia menardii complex in ten cores taken along the crest and north flank of the Greater Antilles Outer Ridge. These species are used to determine the T-Z zonation of the Pleistocene and Holocene sediments. The paleomagnetic stratigraphy of core KN25-4GPC (Denham, 1973) shows that the Blake event spans the entire X-zone in this core. The arrows show the last appearance of G. menardii flexuosa. Barren samples are indicated by open circles and are connected to other sample depths with dashed lines.

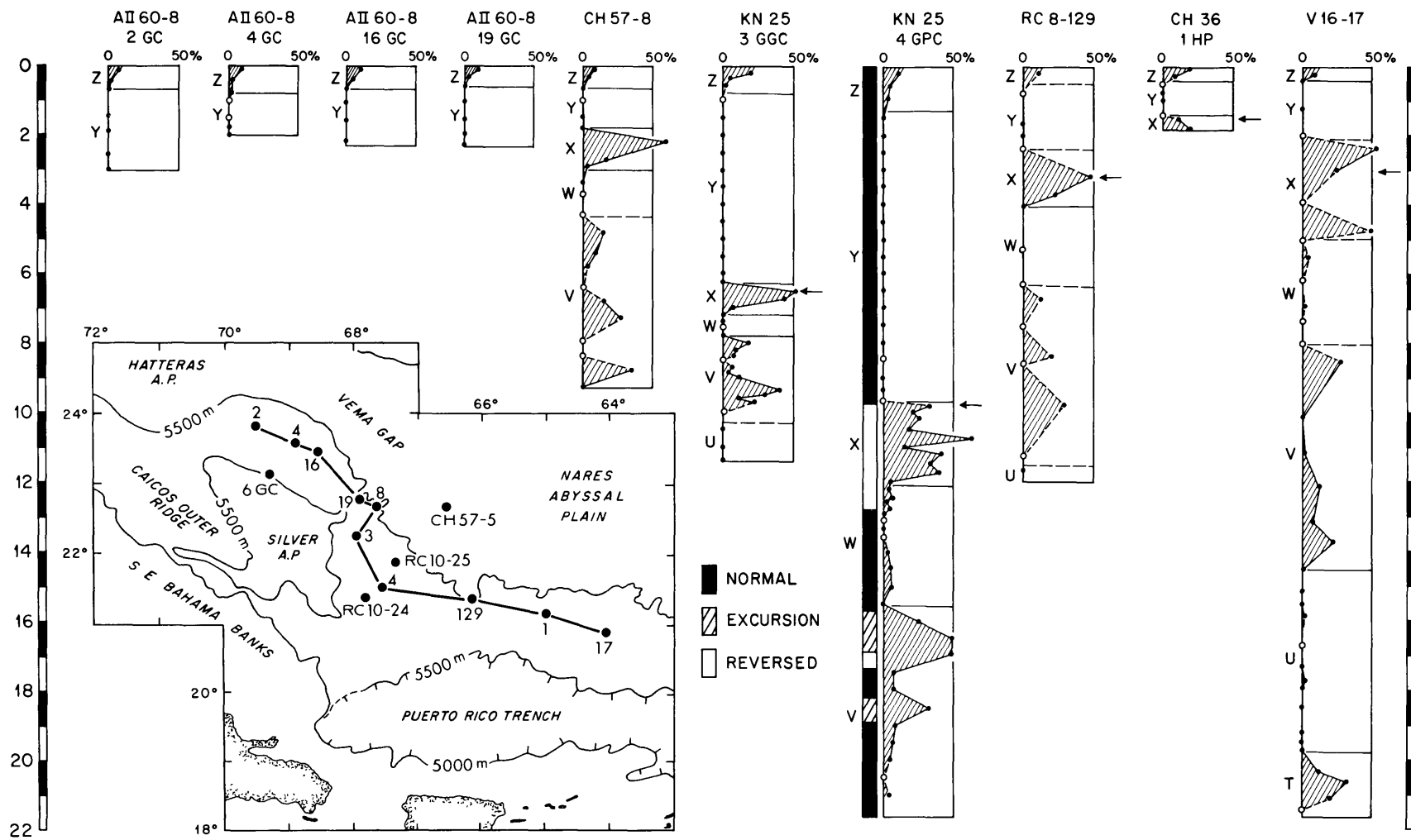


TABLE 5.2. AVERAGE RATES OF SEDIMENT ACCUMULATION
DURING WARM AND COOL PERIODS* (cm/1000 yr)

Core No.	Zone						
	Z	Y	X	W	V	U	T
Crest - Western Sector of Outer Ridge							
AII60-8:2GC	5.9	>3.2					
AII60-8:4GC	5.5	>2.2					
AII60-8:16GC	5.9	>2.6					
AII60-8:19GC	5.5	>2.6					
KN25:3GGC	7.3	8.5	1.8	1.6	1.1	>0.7	
KN25:4GPC	10.9	13.3	4.6	9.2	>2.3		
North Flank - Western Sector							
CH57:8PC	3.6	2.2	2.3	3.3	>2.1		
South Flank - Western Sector							
AII60-8:6GC	2.7	>2.2					
Crest and North Flank - Eastern Sector							
RC8:129PC	3.6	3.1	3.1	5.3	2.3		
CH36:1HP	3.6	1.6	>0.8				
V16:17PC	3.2	2.7	5.4	6.3	3.1	3.3	>0.5

* All values are uncorrected for core shortening and natural compaction. Based on the initiation of zones at the following times: Z - 11,000 yr, Y - 75,000 yr, X - 127,000 yr, W - 165,000 yr, V - 400,000 yr, U - 550,000 yr, and T - 920,000 yr (Ericson and Wollin, 1968; Broecker and van Donk, 1970).

W through Z zones in these cores. The time scale of Emiliani (1971) would yield much higher rates for the W and X than for the V and Z zones. This difference would be even more pronounced if sediment compaction effects were considered.

Two factors suggest that the X-zone in core KN25-4GPC is incomplete, possibly because of erosion at the beginning of the Y (glacial) zone: 1) unlike other cores, the average sedimentation rate in the X zone is much lower than in adjacent zones, and 2) the Blake event of reversed polarity (Fig. 5.1), assumed to have occurred about 110,000 years ago, spans the entire X-zone in this core, whereas the event normally covers less than 20% of the X-zone in other cores where it has been detected (Smith and Foster, 1969).

The rates determined for the X-zone and older sediments in core KN25-3GGC (< 1.8 cm/1000 yr) are also probably much lower than true rates; the very rapid changes in carbonate content (Fig. 4.7), along with a sharp decrease in moisture content and an increase in shear strength in the lower half of the core, may indicate compaction and incomplete core recovery, resulting in a very low core-recovery ratio (see Appendix IV).

Absolute rates of sediment accumulation were determined by radiocarbon dating of intervals in three cores (Table 5.3). There are several possible explanations for the relatively great radiocarbon age (5000 - 8000 years BP) of the

TABLE 5.3. RADIOCARBON DATES AND
CALCULATED SEDIMENTATION RATES

Sample No.	Core No.	Depth Interval (cm)	Date (yr B.P.)	Rate (cm/1000 yr)		Method
				(1)	(2)	
I-6958	AII60-8:6GC	0-8	8,205 \pm 160	9.2-10.2.....13.0-14.4	Total C
I-6959	AII60-8:6GC	64-71	14,770 \pm 200	9.2-10.2.....13.0-14.4	Total C
I-6779	AII60-8:4GC	9-17	5,000 \pm 105	9.3-11.1.....13.1-15.6	Carbonate
I-6780	AII60-8:4GC	38-42	7,665 \pm 120	9.3-11.1.....13.1-15.6	Carbonate
I-6957	AII60-8:4GC	186-191	26,500 \pm 660	7.6- 8.2.....10.7-11.5	Carbonate
I-6773	KN25:4GPC	4-10	5,190 \pm 110	19.5-24.7.....25.8-32.7	Carbonate
I-6778	KN25:4GPC	47-53	7,160 \pm 120	12.9-14.7.....17.1-19.5	Carbonate
I-6960	KN25:4GPC	95-102	11,200 \pm 155	Total C
I-6961	KN25:4GPC	304-310	> 40,000	< 7.3 < 9.7	Carbonate

(1) uncorrected for core shortening or compaction.

(2) corrected only for core shortening using the core recovery ratios 0.71 (AII60-8:6GC and 4GC) and 0.75 (KN25:4GPC), determined by the exterior mud line on the core barrel.

near-surface samples: 1) the wide sampling interval (6-8 cm) which includes older carbon, 2) the presence of older carbonate reworked from the Bahama Banks or older carbon carried in by currents, 3) carbonate formation in surface waters having a reduced C^{14}/C^{12} ratio relative to the atmosphere (Broecker and others, 1960), or 4) very low Recent sedimentation rates. The last explanation seems doubtful, since earlier interglacial periods (V and X, Table 5.2) show reasonably high sedimentation rates. Average sedimentation rates are derived by assuming that these factors have the same relative effect on each sample dated.

The radiocarbon dates suggest rapid sedimentation (10-30 cm/1000 yr) on the crest and extreme south flank of the western Greater Antilles Outer Ridge. Rates determined by this method are slightly higher than those determined from the microfossil zonation, but the difference may be accounted for by sediment compaction effects deeper in the cores, beyond the range datable by radiocarbon. The dates are in general agreement with an 11,000 yr B.P. age for the initiation of the Holocene warming trend.

Rapid sedimentation is also indicated by measurements of physical properties made on cores from the Greater Antilles Outer Ridge (see Appendix IV). Consolidation measurements demonstrate that the sediments are underconsolidated with respect to their depth of burial, whereas sediments from areas of less rapid sedimentation are normally

consolidated (A.J. Silva, pers. comm.). Moisture content in the sediment is generally high and saturated bulk densities are low in comparison to other abyssal oceanic areas, also suggesting rapid deposition.

At an average Pleistocene/Holocene sedimentation rate of 7 cm/1000 yr for the western sector of the Greater Antilles Outer Ridge and 3 cm/1000 yr for the eastern sector, approximately 126 m and 54 m of sediment have accumulated in these provinces, respectively, since the beginning of the Pleistocene. These rates and thicknesses constrain the average rates of middle Eocene to Pliocene sedimentation to values slightly less than those in Table 5.1.

From considerations of depth, remoteness, and sea-floor morphology, the rates of sediment accumulation (up to 30 cm/1000 yr) on the Greater Antilles Outer Ridge are more than an order of magnitude higher than expected, and only about 20% of the sediment can be attributed to carbonate deposition. Normally, a ridge isolated from downslope sedimentation and below the carbonate compensation depth would accumulate only pelagic sediment, probably at rates less than 0.5 cm/1000 years (Arrhenius, 1963). Thus the observed rapid sedimentation rates are strongly indicative of deposition of sediment from other than normal pelagic sources.

ABYSSAL PLAINS

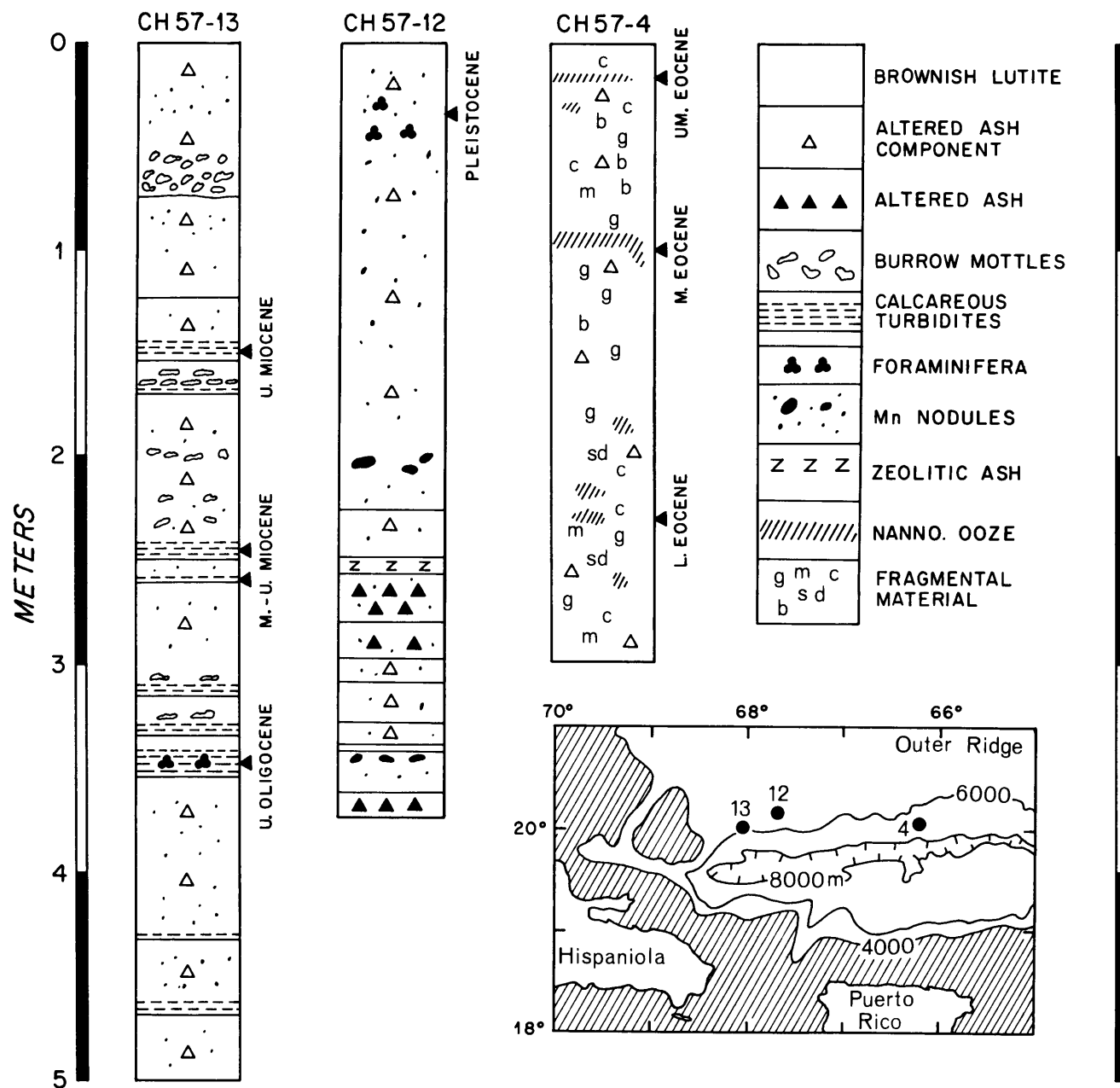
The great depth and consequent carbonate dissolution of

sediments on the Silver and Hatteras Abyssal Plains generally precludes age dating by radiocarbon or microfossil zonation. The cores obtained from these areas (Appendix I) do not penetrate the Pliocene-Pleistocene boundary, so only minimum sedimentation rates of 0.2 to 0.5 cm/1000 yr can be determined. Furthermore, sedimentation rates on the abyssal plains must be less than those on the outer ridge for the ridge to maintain its morphological expression on a crust of uniform age. On the Nares Abyssal Plain, Pleistocene/Holocene rates are therefore probably lower than the average 3 cm/1000 years determined in core CH57-8 deep on the north flank of the Greater Antilles Outer Ridge. The Silver Abyssal Plain is closer to a source area and therefore may have slightly higher rates for this time interval, although, for the same reasons noted above, the rates are probably less than the 2.7 cm/1000 yr determined on the south flank of the western outer ridge (Core AII60-8: 6GC; Table 5.2).

NORTH SLOPE - PUERTO RICO TRENCH

Of the ten cores examined from the north slope of the Puerto Rico Trench (south flank of the Greater Antilles Outer Ridge), only three have enough biogenic carbonate for dating (Fig. 5.2). The westernmost core, consisting of pelagic lutite and altered volcanic ash, is interrupted by numerous calcareous turbidites which probably originated from Navidad Bank. They range from late Oligocene to late Miocene

Figure 5.2. Ages and general lithology of the three datable cores from the north slope of the Puerto Rico Trench. Fragmental material from less than one cm to over 8 cm in size is scattered throughout core CH57-4. Symbols are G - clay galls; C - chert; S - serpentinite; M - very coarse-grained mafic rocks; D - dolomite; B - bedded siltstones and sandstones. Contour interval is 2000 m on the location map, and areas shallower than 4000 m are shaded.



in age, and the ash is probably associated with the Oligocene and Miocene volcanism in Haiti and the Dominican Republic, respectively (Weyl, 1968). The foraminiferal assemblage near the top of the next core to the east (CH57-12) includes G. truncatulinoides and G. menardii flexuosa, dating the sediment as X-zone (75,000 years) or older. The abundant altered ashes in the lower half of the core may be associated with late Pliocene and Pleistocene volcanism in Hispaniola (Schuchert, 1968). Core CH57-4, deep on the north slope of the Puerto Rico Trench, can be described as a breccia lutite of altered ash with layers and inclusions of chalky nannoplankton ooze. The obvious mixing of material at all depths (Fig. 5.2) indicates slumping, although the regular dated sequence of lower to upper-middle Eocene sediment argues against large-scale disruption. The Eocene geosynclinal volcanism in the Greater or Lesser Antilles (Weyl, 1968) may account for the ash in this core.

The ages of these cores suggest that sedimentation rates at the core locations have been extremely low (average < 1 mm/1000 yr) since Eocene time. The other cores from the north slope of the Puerto Rico Trench are lithologically similar to the three dated cores, in that they contain unfossiliferous mixtures of altered ash and pelagic lutite; thus all cores from the north slope are distinctly different from outer ridge cores, which contain only a few thin beds of altered ash. This suggests that the north slope of the

Puerto Rico Trench has received sediment only from occasional ash falls and from normal pelagic sedimentation in a depositional environment totally unlike that of the rapidly accumulating Greater Antilles Outer Ridge.

In order to fully understand the regional sedimentation and sediment dispersal patterns discussed thus far, it is necessary to evaluate the effect of the abyssal currents as an agent in moving and depositing sediment in this region. Recent sedimentation patterns may be closely linked to the present deep circulation pattern over the Greater Antilles Outer Ridge, and once this relationship is understood, earlier depositional patterns and the depositional history of the outer ridge can be deduced.

The following chapter deals with the modern pattern of abyssal circulation over the Greater Antilles Outer Ridge, and the development of earlier deep circulation patterns and their effect on sedimentation are discussed in Chapter VIII.

CHAPTER VI

ABYSSAL CIRCULATION⁽¹⁾

WATER MASSES

The two abyssal water masses above the Greater Antilles Outer Ridge that may affect sediment provenance and dispersal are the Antarctic Bottom Water (AABW) and the overlying North Atlantic Deep Water (NADW). These water mass terms are used in the sense of Wright and Worthington (1970), who defined NADW as water on the potential temperature/salinity (θ/S) diagram for the North Atlantic falling roughly between $1.8^{\circ}\theta$, $34.89^{\circ}/\text{oo}$ and $4.0^{\circ}\theta$, $35.00^{\circ}/\text{oo}$. AABW includes water that is both colder and fresher than NADW down to $0.5^{\circ}\theta$, $34.74^{\circ}/\text{oo}$. Unless otherwise specified, potential temperature in degrees centigrade, signified by θ , will be used throughout the text.

There is no sharp boundary between the NADW and AABW in the North Atlantic. Charts of salinity distribution on potential temperature surfaces (Worthington and Wright, 1970) demonstrate that AABW is affected by mixing with NADW down to at least $1.7^{\circ}\theta$. Between 1.0° and $1.6^{\circ}\theta$ there is only slight latitudinal change in the salinity of AABW at a given temperature, but there is an increase of more than $0.01^{\circ}/\text{oo}$ toward the north at 1.7° and $1.8^{\circ}\theta$. The salinity increase

(1) Portions of this chapter are included in Tucholke and others (1973).

must result from mixing with the overlying warmer and saltier NADW because there is no other adjacent source of salt. Below $1.8^{\circ}\theta$, the water of southern origin (AABW) and that of northern origin are geographically separated by more than 500 km.

The AABW just southeast of the Greater Antilles Outer Ridge is characterized by high silicate values (about $50-75 \mu\text{g-at/l}$), and the NADW by lower values (minimum about $15 \mu\text{g-at/l}$ at $4.0^{\circ}\theta$ up to about $50 \mu\text{g/l}$ at $1.8^{\circ}\theta$; Metcalf, 1969). Some mixing of the two water masses in that area is indicated by the uniform transition from low to high silicate values beneath the NADW.

EARLIER STUDIES OF CIRCULATION

Wüst (1933) recognized that the deepest water in the vicinity of the Greater Antilles Outer Ridge is AABW, and he postulated a general northwestward spreading of that water mass. Later dynamical calculations (Wüst, 1955, 1957) indicated that at 10°N most of the flow was concentrated toward the western side of the basin with speeds greater than 5 cm/sec. He inferred that this flow continued northwestward to include a branch of AABW on each side of the Greater Antilles Outer Ridge, flowing west and northwest at speeds close to 10 cm/sec (Wüst, 1964). Wright (1970) used IGY data to calculate a volume transport of northwestward-flowing AABW of about $1 \times 10^6 \text{m}^3/\text{sec}$ across the 50th meridian into the area of the Greater Antilles Outer Ridge.

The NADW overlying the AABW in the region of the Greater Antilles Outer Ridge was recognized to have a general northerly source (Worthington and Wright, 1970), although the details of NADW transfer to this region had not been worked out. The sloping isotherms in the IGY sections across the western North Atlantic at 24°N and 67°W (Fuglister, 1960, pls. 33 and 51) and the southerly persistence of low silicate NADW along the western margin of the North American basin (Fig. 2 of Metcalf, 1969) suggest a southerly extension of the Western Boundary Undercurrent (WBUC) into the region of the Greater Antilles Outer Ridge. The WBUC has generally been considered to consist of NADW. Hydrographic observations where direct current measurements were made in the WBUC (Swallow and Worthington, 1961; Volkmann, 1962; Barrett, 1965; Richardson and Knauss, 1971; Zimmerman, 1971; Worthington and Kawai, 1972) have shown potential temperatures warmer than 1.8°C and salinities greater than $34.890/_{\text{oo}}$. However, water as cold as 1.66°C and of salinity $34.860/_{\text{oo}}$ was reported deep on the flanks of the Blake-Bahama Outer Ridge as part of the WBUC (Amos, Gordon, and Schneider, 1971).

Few direct current measurements have been made on the Greater Antilles Outer Ridge. Bruce (1964) examined the flow between 19° and 23°N lat. at 66°W long. with closely spaced hydrographic observations, drogues and Swallow floats. His dynamic calculations, based on a reference level at 3800 m (the depth of the lower oxygen maximum) showed general

eastward flow of NADW between 1500 and 3800 m with variable flow at greater depths. A Swallow float at 5200 m in AABW over the crest of the eastern sector of the outer ridge went east at 4 cm/sec; one at 5500 m on the south flank, also in AABW, went north at 2 cm/sec; and a third at 4500 m in NADW on the north flank went 3 cm/sec northeast. More recently, an eight-hour near-bottom current measurement at 5500 m in AABW on the far eastern section of the outer ridge (20°47'N lat., 61°56'W long.) showed speeds up to 25 cm/sec to the southeast (Amos and Escowitz, 1971).

Clearly more data were needed to resolve the modern pattern of abyssal circulation. Therefore we initiated a program of long-term near-bottom current measurements, closely spaced hydrographic stations, and bottom photography on the Greater Antilles Outer Ridge early in 1971.

METHODS

Current Meters

The current meters used were modified Geodyne Model 850, magnetic tape-recording instruments (McCullough and Tupper, 1969), and they were set to sample currents every 30 minutes for periods up to six months. The meters were incorporated in a relatively short (< 220 m) mooring package with an anchor, a flotation package and an acoustically triggered release.

Current meters were set on the Greater Antilles Outer Ridge during two periods (Table 6.1). The first setting,

TABLE 6.1. SUMMARY OF CURRENT METER MOORINGS

Current Meter	Lat. °N	Long. °W	Depth (m)	Height Above Bottom (m)	Recording Period	Comments
A(upper)	22°48.2'	66°28.8'	5616	200	71-I-21 to 71-V-23 (122 days)	Good Record
A(lower)	22°48.2'	66°28.8'	5801	15	71-I-21 to 71-V-23 (122 days)	Good Record
B(upper)	22°14.6'	67°18.3'	5201	200	71-I-22 to 71-IV-20 (88 days)	33 days lost due to tape slippage
B(lower)	22°14.6'	67°18.3'	5386	15	71-I-22 to 71-V-23 (121 days)	Good Record
C	21°16.0'	68°01.0'	5309	15	71-I-24 to 71-V-22 (118 days)	Rotor stuck, direction only
D	23°21.7'	69°08.6'	5352	100	71-XI-19 to 72-V-05 (169 days)	Good Record
E	23°48.2'	68°38.1'	5290	100	71-XI-21 to 72-V-04 (166 days)	Good Record
F	23°45.1'	69°36.8'	5276	100	71-XI-21 to 72-V-04	Channels over- written, no data

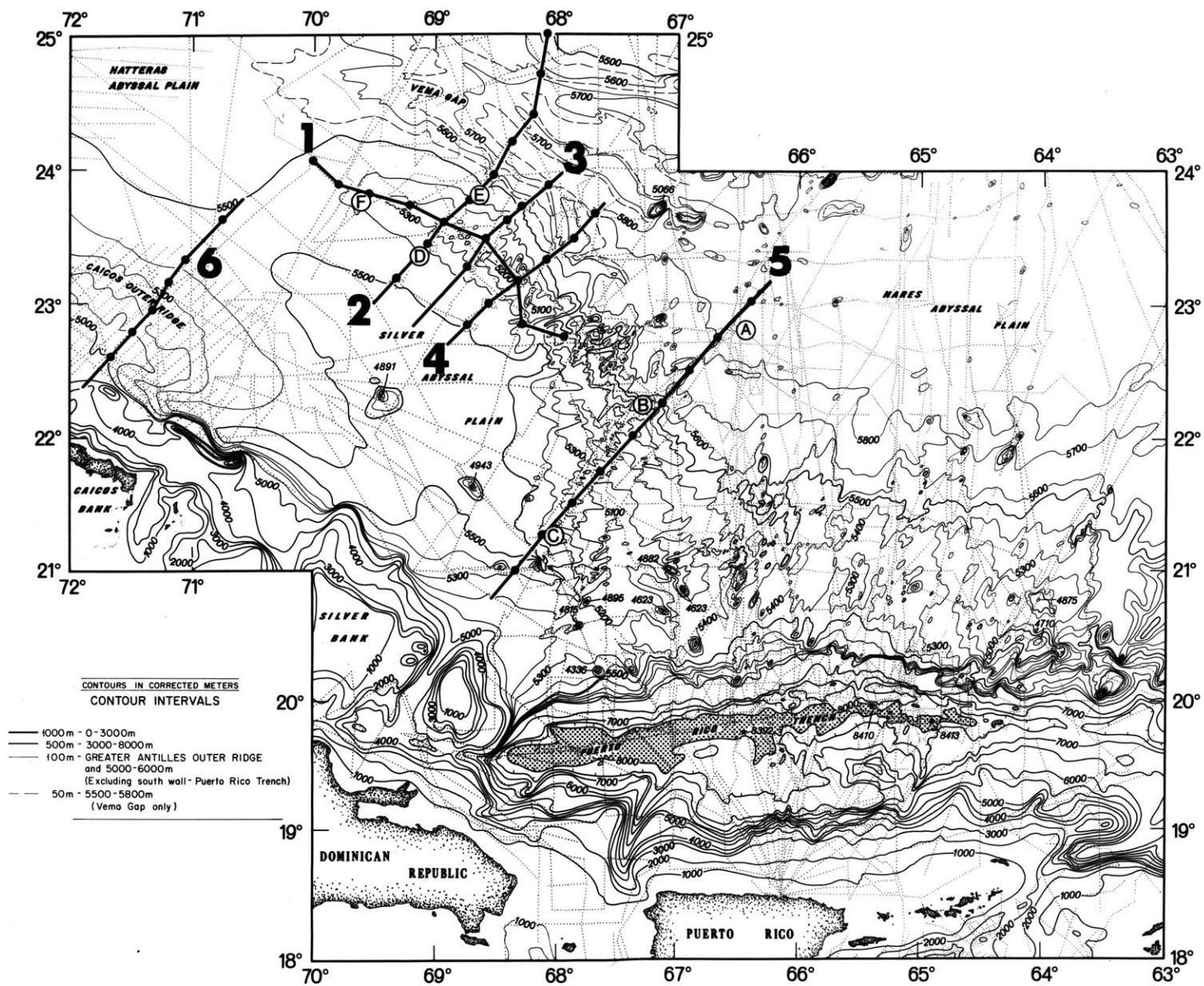
which recorded currents for about four months, incorporated five current meters in three moorings. The moorings on the southern edge of the Nares Abyssal Plain and north flank of the Greater Antilles Outer Ridge (A and B respectively, Fig. 6.1) included two current meters, at 15 and 200 m off the bottom, to determine variability of currents with depth. The third mooring (C) contained only a single current meter.

Since the records from the deep and shallow instruments were nearly identical in the first setting of current meters, the second setting was made with one current meter per mooring, at 100 m above the bottom. The meters were set for about six months near a common depth of 5300 m, with one at the northwest tip of the outer ridge and one each on the north and south flanks (D,E,F, Fig. 6.1), in an attempt to monitor the clockwise flow around the end of the outer ridge indicated by the hydrography and the bottom photographs.

Hydrographic Stations

Hydrographic data from depths greater than 3500 meters were collected at 57 stations during five cruises made since early 1971 (Fig. 6.1). Four deep stations were made in January, 1971, from MSS MT. MITCHELL, and in February a section of deep stations was made from R/V KNORR along the current meter line from 23° to 21°N lat. In August, 1971, we made 23 stations combining bottom photography and water sampling from R/V ATLANTIS II over the northwestern section of the outer ridge. KNORR made additional stations with

Figure 6.1. Bathymetric map of the Greater Antilles Outer Ridge and vicinity showing positions of hydrographic stations and the locations of hydrographic sections (Fig. 6.2). Letters indicate current-meter positions (see Table 6.1). Current-meter moorings A to C were bracketed by Section 5 (KNORR, February, 1971) and moorings D to F by pairs of hydrographic stations (KNORR, February, 1972).



bottom photographs in February, 1972, which extended one of the ATLANTIS II sections to the north across Vema Gap, and bracketed the second setting of current meters, which was placed in November, 1971. A section from the southeast Bahama Banks across the Caicos Outer Ridge toward the northwest tip of the Greater Antilles Outer Ridge was made from KNORR in May, 1972.

Each hydrographic cast contained 12-14 Nansen bottles, with six bottles in the bottom 200 m. Salinities were determined on board by conductivity measurement, and silicate analyses were run during the two 1972 KNORR cruises. Temperatures are considered good to $\pm 0.01^\circ\text{C}$.

Bottom Photography

A bottom-triggered camera was used in place of the standard lead weight on most hydrographic casts, and oriented bottom photographs were taken at 39 stations. Direction and relative speed of currents were deduced from the photographs by three methods: 1) Attached benthic organisms bending in the flow, 2) dispersal of mud clouds stirred up by the camera, and 3) current lineations, scour marks, and ripples in the sediment. Current directions determined by the first two methods, although consistent with the observed flow pattern, are at best only momentary indicators of currents and have even greater limitations than short-term current-meter records. However, persistent unidirectional flows are necessary to create the observed ripples and lineations in

the fine-grained sediment of the Greater Antilles Outer Ridge, and such features are not easily erased by short-term fluctuations in currents, unless the fluctuations are particularly strong (Hollister and Heezen, 1972). However, the current-meter measurements indicate that variations from the mean flow direction on the outer ridge are always associated with lower speeds. The current directions obtained from sedimentary features in the bottom photographs were therefore considered to be, and later proved to be, reliable indicators of the mean flow in this region.

RESULTS

Hydrography

Plots of potential temperature against salinity for all the observations except those on the ATLANTIS II cruise showed more than 90 percent within the envelope of one standard deviation ($\pm .003^{\circ}/\text{oo}$ to $.006^{\circ}/\text{oo}$ below $2.5^{\circ}\theta$) from the deep θ/S curve of Worthington and Metcalf (1961) for the western North Atlantic. The ATLANTIS II observations averaged $.006^{\circ}/\text{oo}$ fresher than the curve, with slightly more scatter than the other plots. Plots of silicate measured on the 1972 KNORR cruises show a tighter fit for potential temperature vs. silicate than for either potential temperature vs. salinity or silicate vs. salinity, suggesting that the salinity measurements are the least precise of the three.

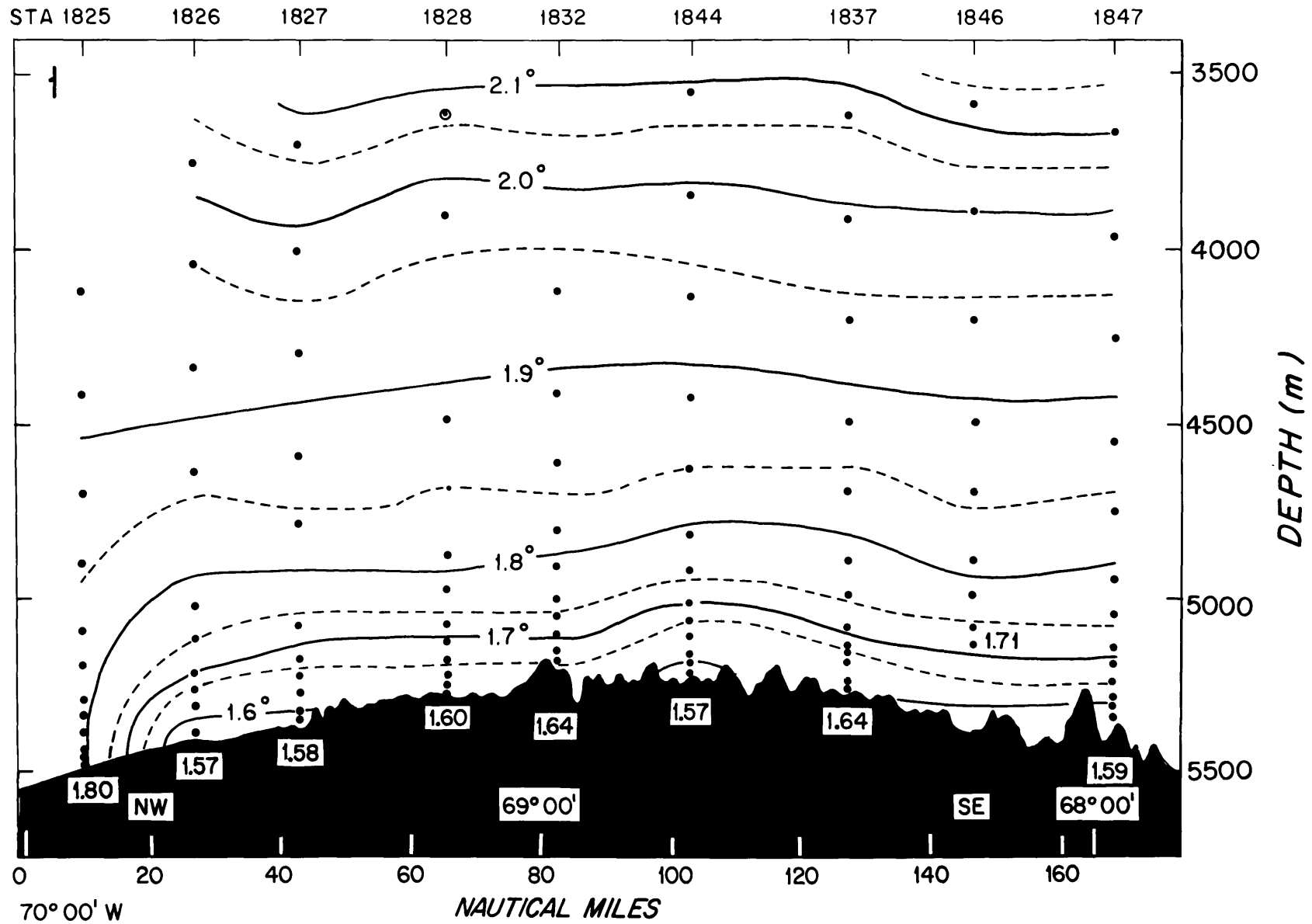
Several important features were observed in the hydrography (Fig. 6.2). On all sections the water below 5000 m is 1.8°C or colder, and fresher than $34.892^{\circ}/\text{oo}$. Except for one station discussed below, the water immediately above the sea floor is colder than 1.7°C (most of it colder than 1.6°C) and fresher than $34.875^{\circ}/\text{oo}$. Water with these characteristics (AABW) must ultimately be derived from the south (Worthington and Wright, 1970). The isotherms on all six sections follow the bottom topography, indicating clockwise circulation around topographic highs and counterclockwise flow around depressions if an intermediate reference level is used.

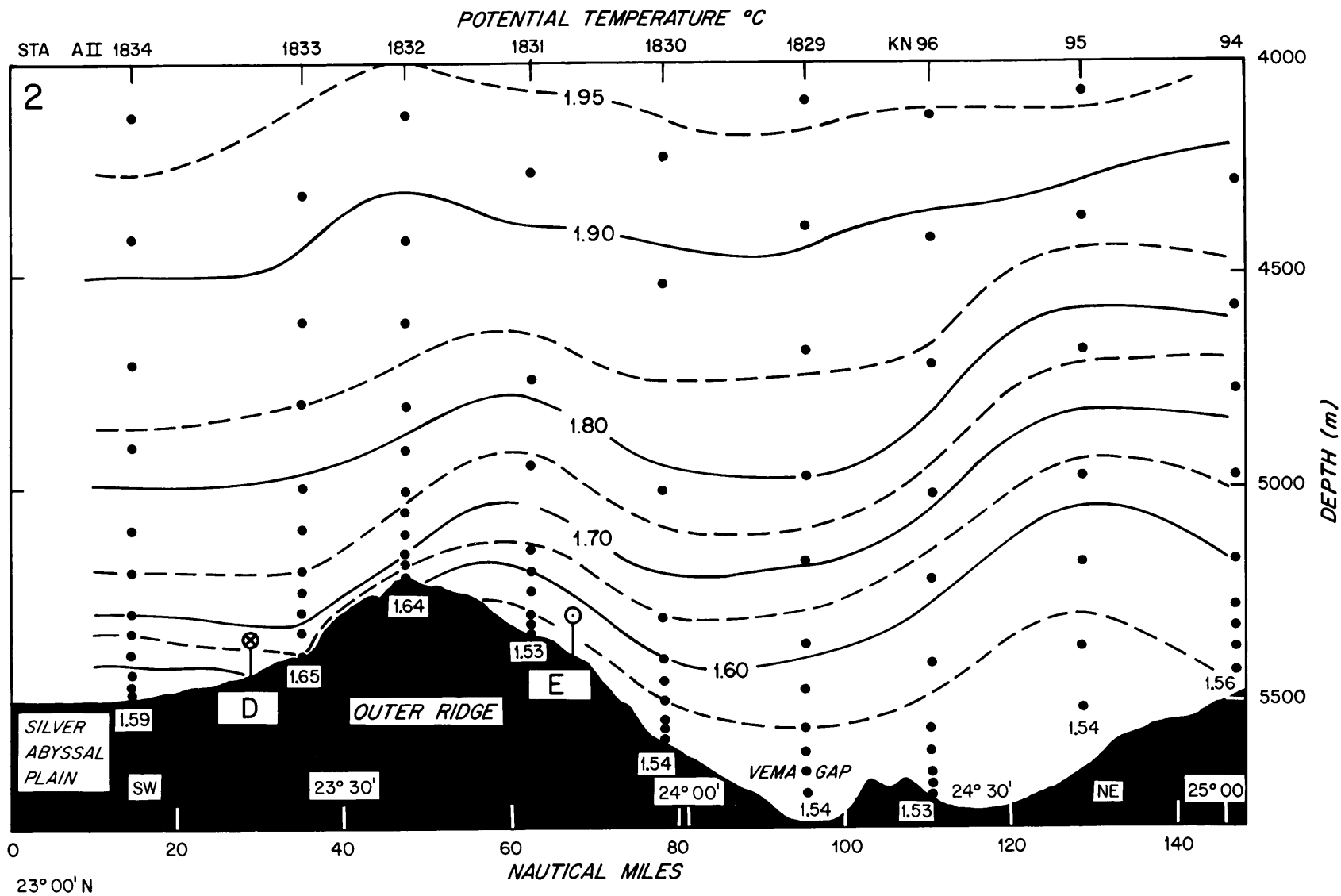
This isotherm structure is also apparent in an extensive region surrounding the Greater Antilles Outer Ridge (Fig. 6.3). Two major potential-temperature regimes occur, divided by the 21°N parallel. In the northern regime the potential temperature distribution is consistent with that shown in the hydrographic sections (Fig. 6.2). The colder water near the edges of the basins indicates northwestward flow south of the Bermuda Rise, general southward flow along the Blake-Bahama Outer Ridge and Bahama Banks, clockwise circulation around the northwest end of the Greater Antilles Outer Ridge, and eastward flow along the north flank of the outer ridge. South of 21°N there is warmer water along the southern and western edge of the Puerto Rico Trench, suggesting a broad flow of AABW westward into the trench. The flow appears to

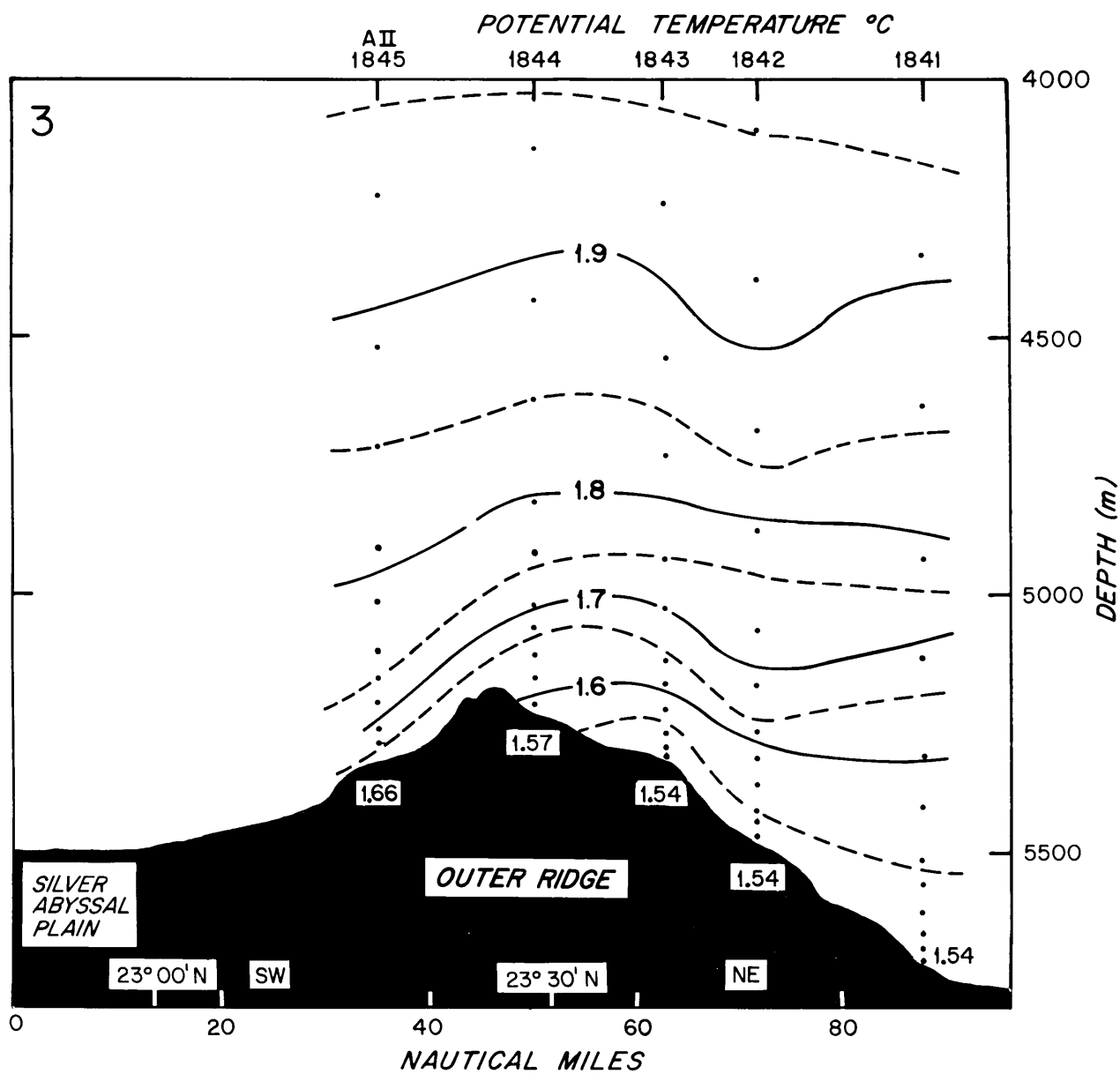
Figure 6.2. Potential-temperature sections (see Fig. 6.1 for locations). Salinity profiles are not shown because of their close resemblance to those for potential temperature. Section 1: along the crest of the Greater Antilles Outer Ridge; made by ATLANTIS II, Aug. 3-12, 1971. Section 2: across the Greater Antilles Outer Ridge by ATLANTIS II, Aug. 5-7, 1971; extended northward across Vema Gap by KNORR, February 10-11, 1972; current-meter positions and directions of mean flow are shown. Section 3: across the Greater Antilles Outer Ridge, by ATLANTIS II, Aug. 9-11, 1971. Section 4: across the Greater Antilles Outer Ridge, by ATLANTIS II Aug. 7-9, 1971. Section 5: across the Greater Antilles Outer Ridge by KNORR February 18-19, 1971; current-meter positions are indicated. Section 6: across the Caicos Outer Ridge, by KNORR, May 2-3, 1972.

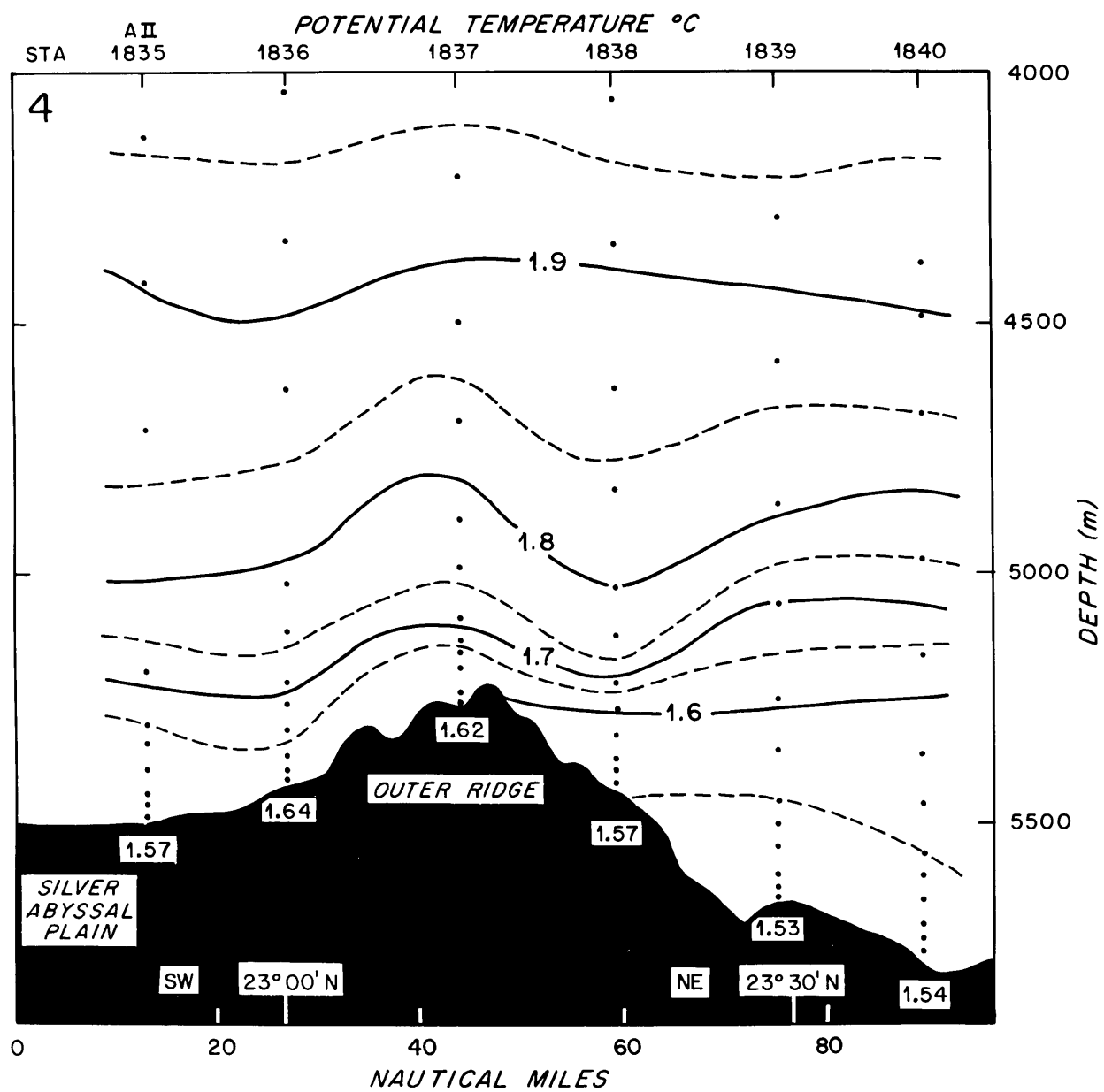
POTENTIAL TEMPERATURE °C

AII









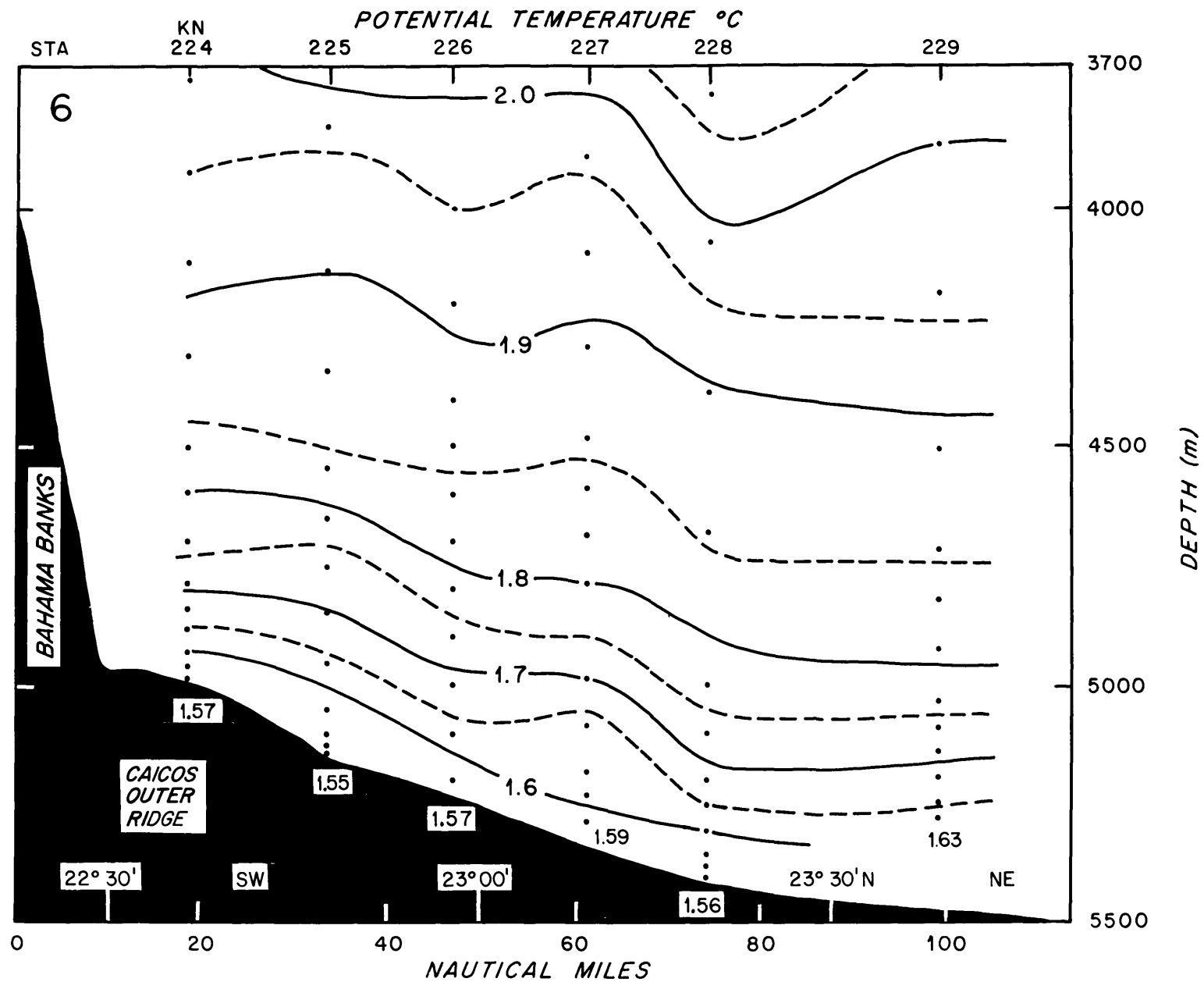
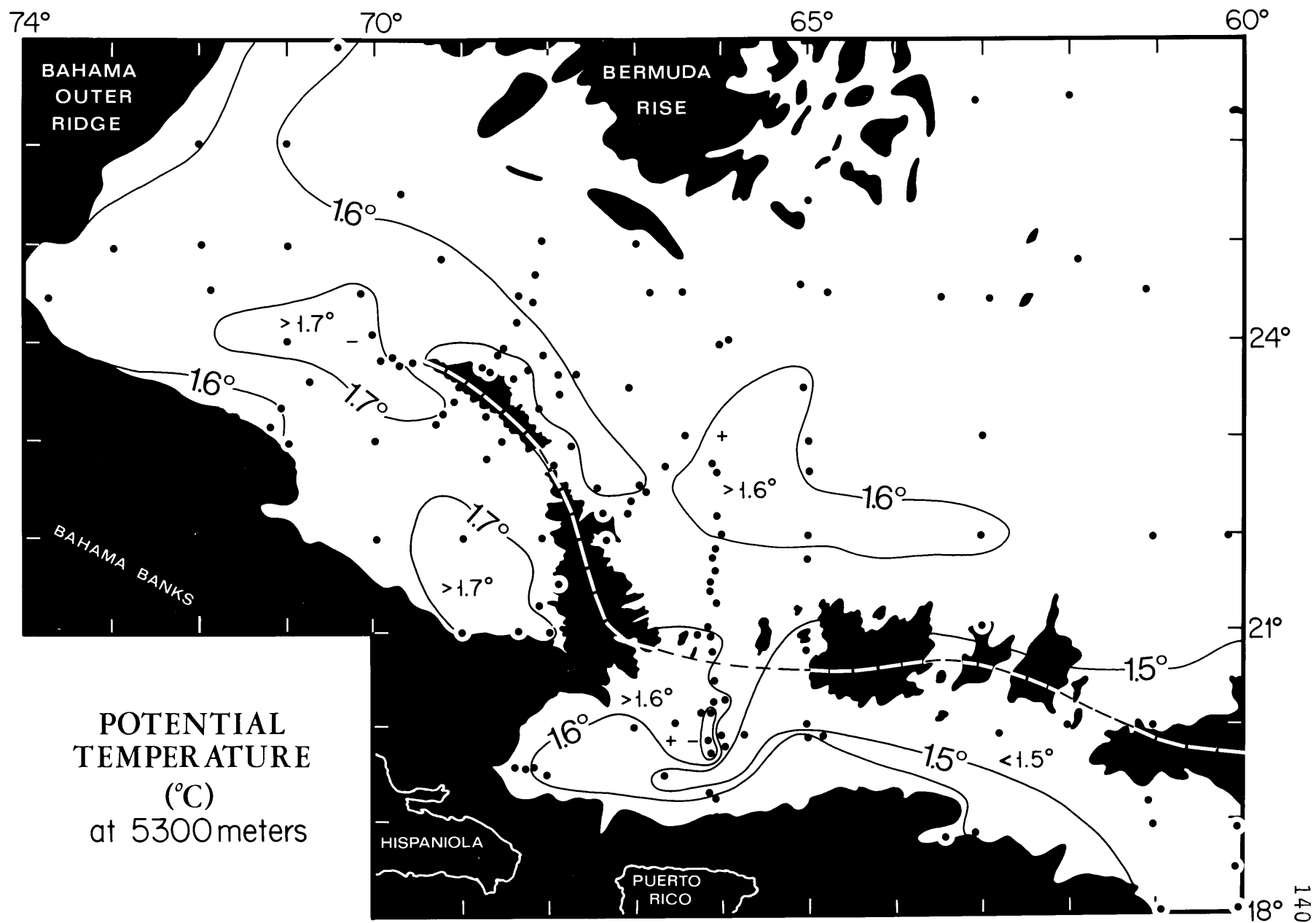


Figure 6.3. Potential temperature at 5300 m for an extensive area surrounding the Greater Antilles Outer Ridge. Plus and minus signs indicate points outside the range of the contour interval by more than 0.01°C . Station positions are shown by dots. The data, compiled from the files of Woods Hole Oceanographic Institution and the National Oceanographic Data Center, cover 23 years from 1949 to our cruises in 1971 and 1972. The axis of the Greater Antilles Outer Ridge is indicated by a dashed line, and black areas are shallower than 5300 m.



turn north in the western part of the trench, and some water may pass across gaps in the Greater Antilles Outer Ridge east of 65°W to become part of the eastward flow on the north flank. Some flow of warmer water from the Silver Abyssal Plain southeast across the outer ridge sill at 21°N lat., 68°W long. is also indicated.

Over the western sector of the Greater Antilles Outer Ridge the coldest water on the four transverse profiles (Fig. 6.2) is 1.52 to 1.54°C , and it lies exclusively north of the crest at depths greater than 5200 m. This water may have an eastern source north of the outer ridge. However, water this cold is found in the Puerto Rico Trench, and it may move to the north across depressions in the outer ridge east of 65°W .

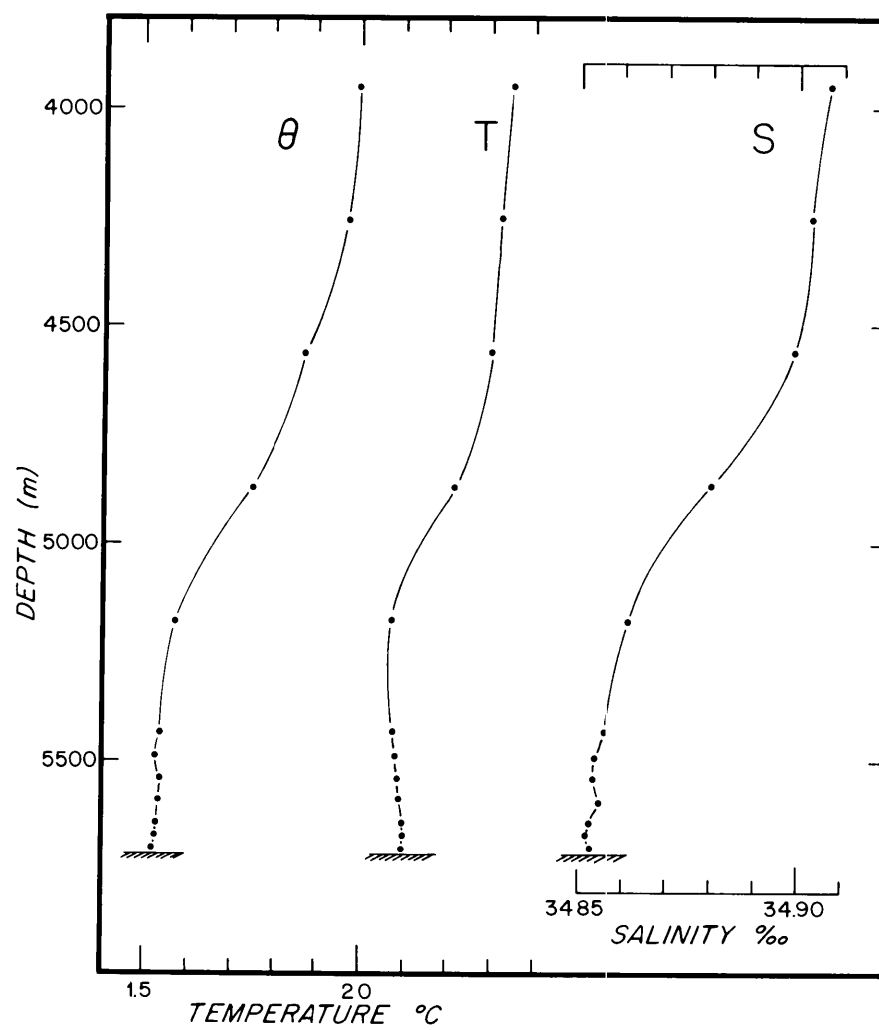
One station (AII Sta. 1825) at the northwest tip of the Greater Antilles Outer Ridge was unique in that the potential temperature never dropped below 1.80°C (Section 1, Fig. 6.2). All five temperature readings in the bottom 150 m were 1.80°C , and the salinities ranged from $34.884^{\circ}/\text{oo}$ to $34.886^{\circ}/\text{oo}$. Although these salinities are $.004$ to $.006^{\circ}/\text{oo}$ fresher than Worthington and Metcalf's (1961) curve, they are in close agreement with the other ATLANTIS II observations. Consistent thermometric depths from four unprotected thermometers in the bottom 400 m eliminate any possibility that the deep part of the cast tripped improperly, and the calculated depth for the deepest thermometer was 8 m above the sea floor at 5496 m.

At Station 1826, twenty-two km to the southeast, the bottom temperature was 1.57°C at 5415 m. The warmest bottom temperature observed on any other station was 1.65°C at 5389 m (ATLANTIS II Sta. 1833). Although we were not able to repeat Station 1825, earlier observations near this station include anomalously warm temperatures (in the area warmer than 1.7°C west of the outer ridge, Fig. 6.3) but none as warm as 1.8°C .

The isotherms and isohalines are spaced more closely between 1.6°C and 1.8°C than above and below this interval (Fig. 6.4) on every station except the anomalously warm station ATLANTIS II 1825. A nearly isothermal bottom layer colder than 1.6°C was observed on all stations except a few made in water shallower than 5400 m, where the gradient persisted to the bottom. The layer of increased gradient begins at $1.81 \pm .06^{\circ}\text{C}$ at a depth of 4840 ± 250 m, and it ends at $1.58 \pm .04^{\circ}\text{C}$ at 5290 ± 150 m. The potential temperature gradient above the layer is $0.20 \pm .03^{\circ}\text{C}/\text{km}$, and below the layer it is 0 to $0.20^{\circ}\text{C}/\text{km}$. Within the layer it averages $0.55^{\circ}\text{C}/\text{km}$ with a range from 0.33 to $1.29^{\circ}\text{C}/\text{km}$. The variation within the layer may result in part from the wide bottle spacing (up to 200 m) near the top of the layer. Since the adiabatic gradient at these depths and temperatures is about $0.13^{\circ}\text{C}/\text{km}$, the observed temperatures above and below the layer are very nearly isothermal.

This type of structure is observed in the southwestern North Atlantic wherever deep stations are made with close

Figure 6.4. Traces of potential temperature, in situ temperature, and salinity vs. depth for KNORR Sta. 55 (22°44.5'N lat., 66°40.8'W long.), illustrating the transition layer observed in the deep water over the Greater Antilles Outer Ridge. Note that in situ temperature is nearly isothermal above and below the transition layer.

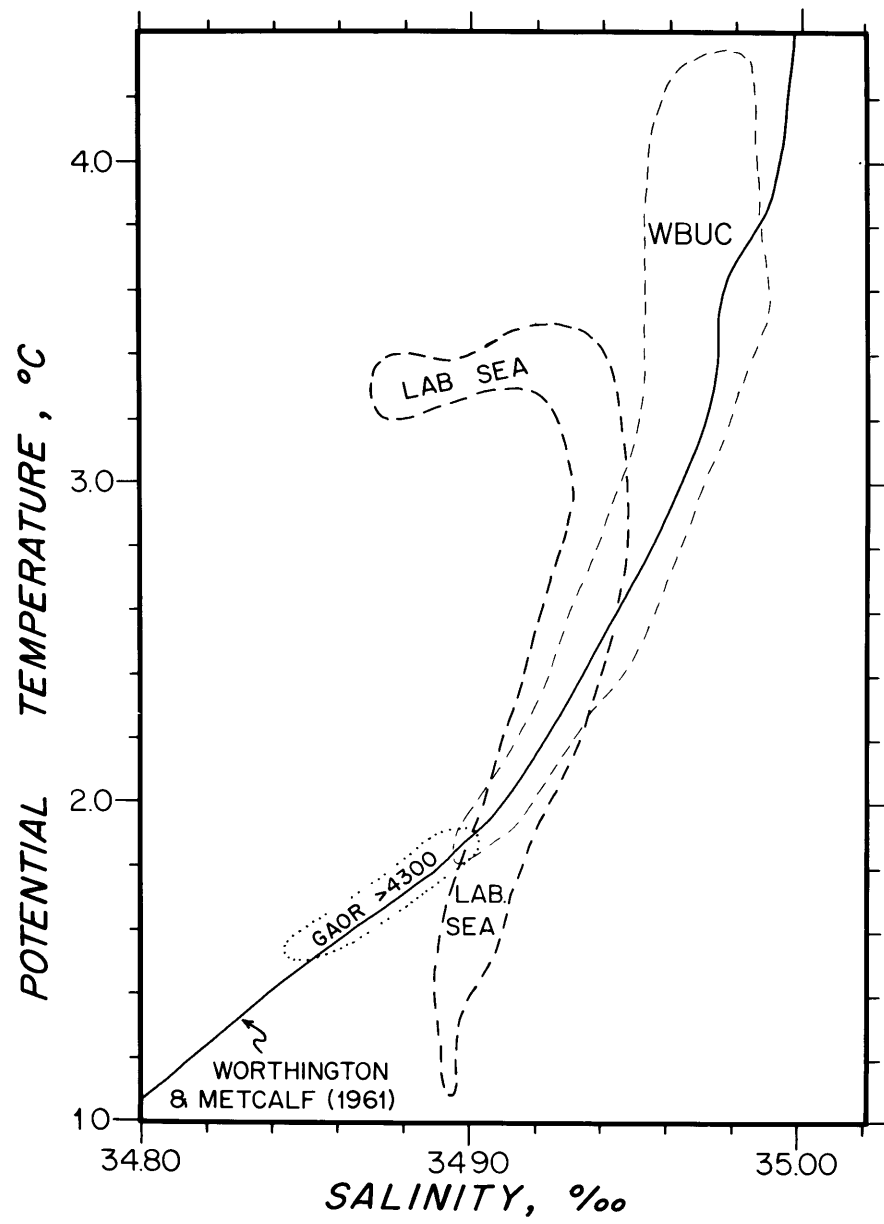


bottle spacing. An example is the IGY temperature section at 8°N (Fuglister, 1960, p. 29). The region of increased gradient is considered to be the transition between AABW and the overlying NADW. As mentioned earlier, it is in this temperature interval that marked indications of increased salinity first appear in AABW as it penetrates toward the north.

Recent STD (salinity/temperature/depth) observations (Amos, Gordon, and Schneider, 1971) indicate that the transition may be more abrupt than the Nansen bottles show. Their STD traces recorded changes of 0.02 to $0.04^{\circ}\theta$ occurring over intervals of less than 20 m at about $1.8^{\circ}\theta$, but they argue that the gradient layer is not a transition between AABW and NADW because some influence of AABW can be found at shallower depths. Although the AABW and NADW may influence each other outside the 1.6° to $1.8^{\circ}\theta$ interval in this part of the ocean, the influence is probably too small to discern with existing techniques, and the waters above and below the transition region should be considered as two distinct water masses.

The θ/S envelope of all the hydrographic observations deeper than 4300 m lies on the curve of Worthington and Metcalf (1961) for the western North Atlantic. Although generally colder and fresher, it overlaps the envelope of θ/S values associated with the Western Boundary Undercurrent up to $1.93^{\circ}\theta$ (Fig. 6.5).

Figure 6.5. Diagram of potential temperature vs. salinity for water flowing south along the western margin of the North Atlantic basin. The envelope labelled Labrador Sea encloses observations in the deep counterclockwise gyre in the Labrador Sea (Swallow and Worthington, 1969). The flow is considered to be a continuation of the Norwegian Sea overflow (Worthington, 1969) with some contribution of fresher and warmer Labrador Sea water. The envelope labelled WBUC encloses only those points in the Western Boundary Undercurrent where simultaneous hydrographic observations and direct current measurements have been made (Swallow and Worthington, 1961; Volkmann, 1962; Barrett, 1965; Richardson and Knauss, 1971; Worthington and Kawai, 1972). It would extend down the Worthington-Metcalf curve to about $1.66^\circ\theta$ if the data from Amos, Gordon, and Schneider (1971) were included. The third envelope, marked GAOR (Greater Antilles Outer Ridge), represents all the observations made deeper than 4300 m in this investigation.



The silicate values plotted against potential temperature fall very nearly on a straight line ($\pm 2 \mu\text{g-at/l}$) from 1.90°C , $34 \mu\text{g-at/l}$, to 1.55°C , $59 \mu\text{g-at/l}$ (Fig. 6.6). Below 1.75°C the values are identical to the plot of Metcalf (1969) for the western Atlantic between the Equator and about 10°N , an indication that the AABW over the Greater Antilles Outer Ridge is not strongly affected by mixing below about 1.7°C . Silicate values from water warmer than 1.75°C over the outer ridge form a tighter curve with lower mean values than Metcalf's curve.

Dynamic Calculations

The geostrophic method (Lafond, 1951) was used to calculate volume transports through all six sections (Table 6.2) and between six pairs of stations bracketing the current meters. Additional calculations between the end stations of the sections were made to determine total transports into and out of the region. Since the region is characterized by active currents, the reference surface is probably neither level nor fixed in time. Calculations were made for two different reference levels, at 4300 m and 4700 m, to determine representative flow around the Greater Antilles Outer Ridge.

The shallower depth is at the level of both minimum horizontal and minimum vertical density gradients and is thus a level of minimum shear. However, it is not a level of zero shear since indications of the deeper temperature

Figure 6.6. Silicate ($\mu\text{g-atoms/liter}$) versus potential temperature for hydrographic stations on the Greater Antilles Outer Ridge (KNORR 25, leg 1) and Caicos Outer Ridge (KNORR 25, leg 6).

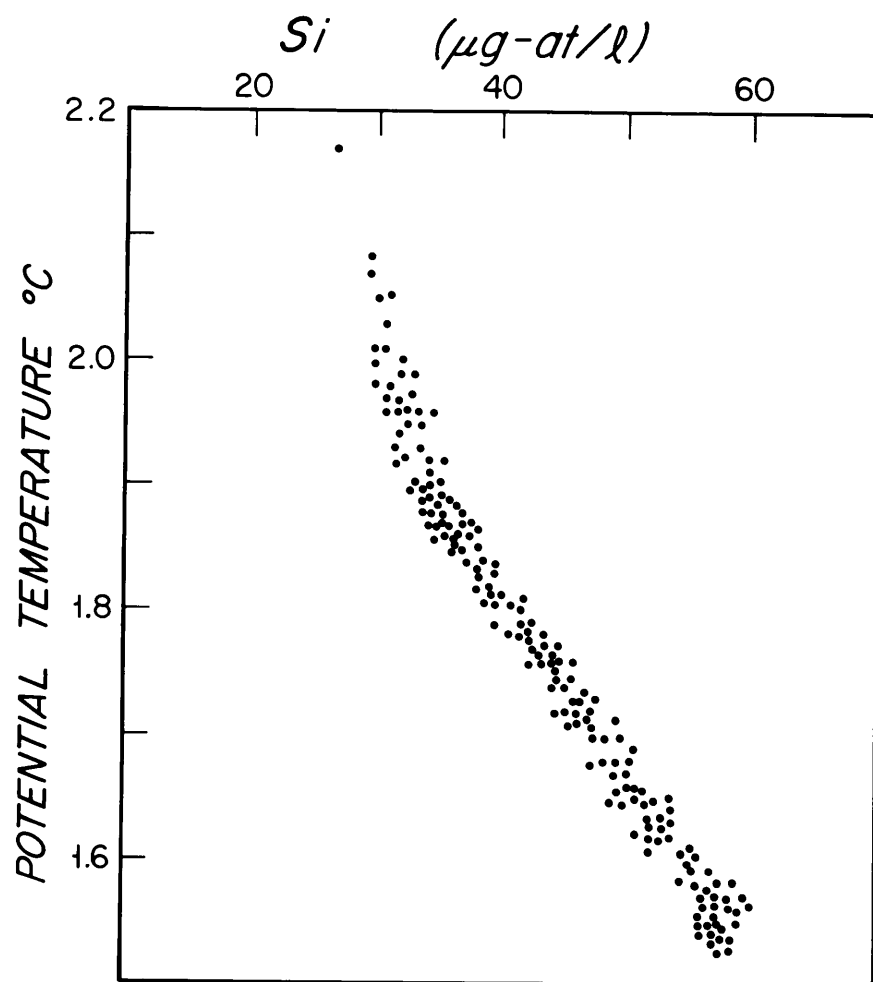


TABLE 6.2. CALCULATED VOLUME TRANSPORTS
FOR REFERENCE LEVELS AT 4300 m and 4700 m

Section	4300 m		4700 m	
	T*	Direction	T*	Direction
Section 1 (Crest)				
NW (AII 1825-1832)	0.7	NE	0.6	NE
Middle (AII 1832-1837) [†]	0	-	0	-
SE (AII 1837-KN59) [†]	0.5	NE	0.3	NE
Section 2				
Vema Gap (KN94-AII 1829)	1.6	W	1.2	W
N of Ridge (AII 1829-1832)	0.2	SE	0.2	SE
S of Ridge (AII 1832-1834)	0.2	NW	0.1	NW
Section 3				
N of Ridge (AII 1841-1844)	0.4	SE	0.2	SE
S of Ridge (AII 1844-1845)	0.1	NW	0.1	NW
Section 4				
N of Ridge (AII 1837-1840) [†]	0.7	SE	0.3	SE
S of Ridge (AII 1835-1837) [†]	0.1	SE	0.1	SE
Section 5				
N of Ridge (KN54-59)	0.5	SE	0.4	SE
S of Ridge (KN59-62)	0.3	NW	0.3	NW
Section 6				
Caicos Outer Ridge (KN224-229)	1.2	SE	0.7	SE

* Transport values are $\times 10^6 \text{ m}^3/\text{sec}$ and are rounded to nearest $0.1 \times 10^6 \text{ m}^3/\text{sec}$.

[†] Calculations for Station 1837 were made with observed temperatures, but salinity values were taken from the mean θ/S curve for the cruise. See text for explanation.

structure persist at and above 4300 m. The potential temperature at 4300 m is $1.91 \pm 0.04^\circ\text{C}$ and the salinity is $34.899 \pm .006^\circ/\text{oo}$, clearly within the NADW, which is generally considered to be moving slowly southward, but near its lower limits according to Wright and Worthington (1970).

At 4700 m the potential temperature is $1.84 \pm .04^\circ\text{C}$ and the salinity is $34.891 \pm .007^\circ/\text{oo}$, close to the defined boundary between NADW and AABW. Wright (1970) used a reference level at about $34.89^\circ/\text{oo}$ to calculate the transport of AABW in the western basin of the Atlantic Ocean. In the region of the Greater Antilles Outer Ridge, however, there is some evidence that the NADW and AABW are moving in the same direction, and there may be no motionless level between them. Using the deeper reference surface does not substantially affect the pattern of circulation below that level. The volume transports are reduced by amounts up to 40 percent, but the directions are not changed except where the transport is negligible. With either reference level there is a reversal of flow in the shallower water because of the upward persistence of the temperature structure, and the reversal is smaller with the shallower level. Uncertainties inherent in the method of dynamic calculations and those introduced by possible measurement errors are such that there is little reason to refine the calculation by using a reference level of varying depth.

Clearly the circulation pattern around the Greater Antilles Outer Ridge would be the same with any reasonable

reference level above the crest of the ridge. If the 4700 m surface is used, the flow represents AABW only; with the 4300 m surface, it includes NADW up to a temperature of about 1.93°C .

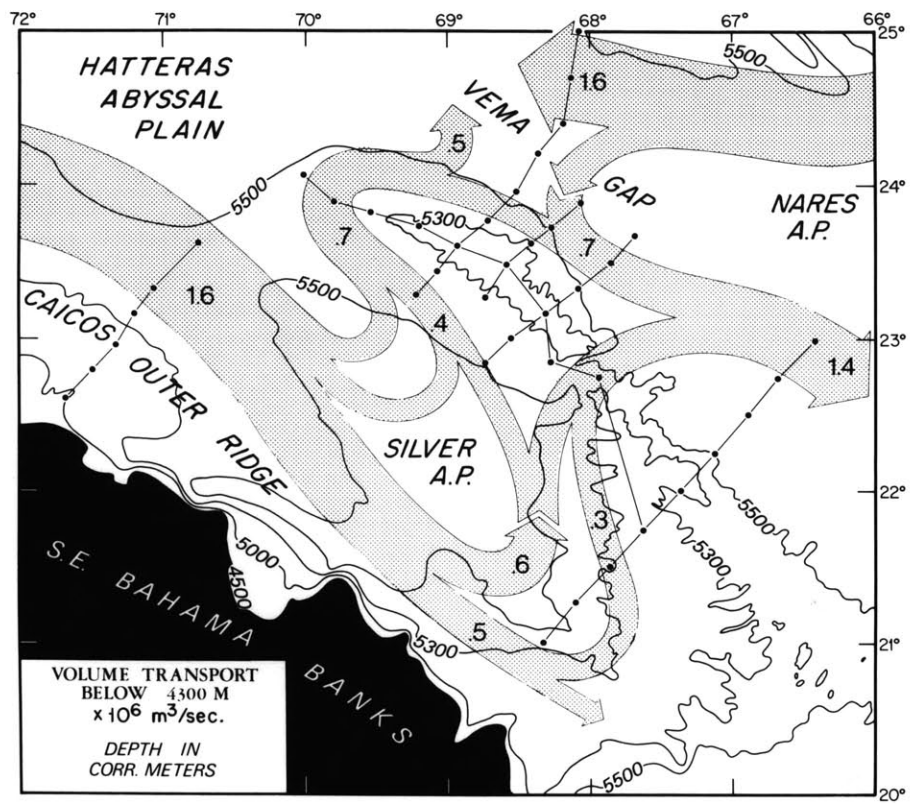
The calculations involving ATLANTIS II Station 1837 in section 4 across the crest of the Greater Antilles Outer Ridge (Fig. 6.2) were made with salinities taken from the mean σ_t/S curve for the region because salinity observations at 4693 m and 4891 m were anomalously fresh by about $0.03^{\circ}/\text{oo}$. No other observations departed more than $0.01^{\circ}/\text{oo}$ from the mean curve. Using the observed salinities would have created a counterclockwise circulation around Station 1837 of about $0.3 \times 10^6 \text{ m}^3/\text{sec}$ but would not have affected the other transport values.

A circulation pattern for the region based on the values in Table 6.2 and on the calculations between the end stations using the 4300 m reference level shows the following (Fig. 6.7):

- 1) A flow composed largely of Antarctic Bottom Water westward through the northern section of the Vema Gap.

- 2) A southeasterly flow of approximately the same magnitude, composed of AABW and NADW, along the Caicos Outer Ridge, most of which turns northward and then northwestward following the general trend of the bathymetric contours. This flow is considered to be the southern extension of the Western Boundary Undercurrent. Since Section 6 is not closed off to the Bahama Banks (Fig. 6.2), it is possible that a

Figure 6.7. Current pattern and volume transports based on dynamic calculations with a reference level at 4300 m. Transport units are $\times 10^6 \text{m}^3/\text{sec}$. Widths of arrows are approximately proportional to volume transports. Consequently, the arrows do not show the precise location of flow, which may include part, or all, of a given section. The black area is shallower than 4500 m.



substantial flow not indicated in these calculations may pass southeast through this gap and over the sill at 21°N lat., 68°W long. to the south slope of the Puerto Rico Trench. This seems especially plausible since the calculated volume transport through the Caicos Outer Ridge section is only $1.6 \times 10^6 \text{ m}^3/\text{sec}$. The calculated volume transport of the Western Boundary Undercurrent around the Blake-Bahama Outer Ridge to the northwest is an order of magnitude greater (Amos, Gordon, and Schneider, 1971), although a much shallower reference surface (about 2500 m) was used for their calculations.

3) Clockwise flow of AABW and NADW around the northwest tip of the Greater Antilles Outer Ridge, again following the bathymetric contours, and a southeasterly flow along the north flank of the outer ridge.

This simple picture is complicated by flow to the north across a depression in the western Greater Antilles Outer Ridge at 23°N lat., and by connections between the northwest flow through Vema Gap and the southeast flow along the north flank of the outer ridge.

Direct Current Measurements

The first series of current meters was set across the Greater Antilles Outer Ridge in January 1971 for approximately four months (Table 6.1). The pair of current meters moored on the southern edge of the Nares Abyssal Plain (A in Fig. 6.1, Table 6.1) recorded currents generally to the WNW at

speeds of 2 cm/sec (the stall speed of the rotor) to 12 cm/sec for the first two months of the recording period (Figs. 6.8, 6.9). The flow then shifted to the south for about three weeks with speeds less than 7 cm/sec before turning to the southeast at about the same speeds. The two current meters, separated by a vertical distance of 185 meters, showed virtually identical patterns of current direction and speed. The major speed discrepancy, from February 7-27, resulted from the rotor sticking on the lower current meter. The southeasterly current was faster at the deeper meter during the last part of the recording period.

A second pair of current meters, also at 15 m and 200 m from the bottom (B in Fig. 6.1, Table 6.1), was moored a day after the first pair, on the north flank of the Greater Antilles Outer Ridge (Figs. 6.9, 6.10). Both records show ESE currents at speeds 2 to 10 cm/sec for the first 5 weeks although the deeper meter recorded higher average speeds. A 360° counterclockwise shift in flow with greatly diminished current speeds occurred during the next two months. The shallow meter failed in mid-April, but the deep one continued until recovery on May 23, recording an ENE current up to 9 cm/sec. As in the northern mooring, similar changes in direction were recorded simultaneously by both meters, but speed differences were slightly more pronounced, with the lower current meter generally recording higher speeds.

The observed current pattern can be explained by two

Figure 6.8. Progressive vector diagrams of currents recorded on the south edge of the Nares Abyssal Plain (A in Fig. 6.1). The diagrams are constructed by vector addition of successive velocity measurements, creating a simulated trajectory for a parcel of water initially located at the current-meter site. Crosses mark one-day intervals. The major speed discrepancy, February 7-27, resulted from the rotor sticking on the lower current meter.

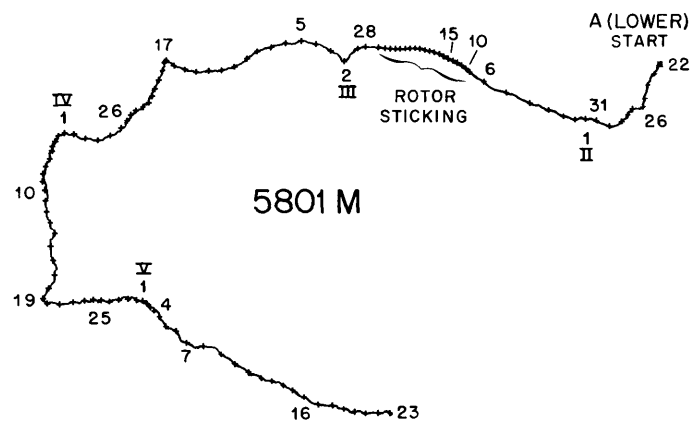
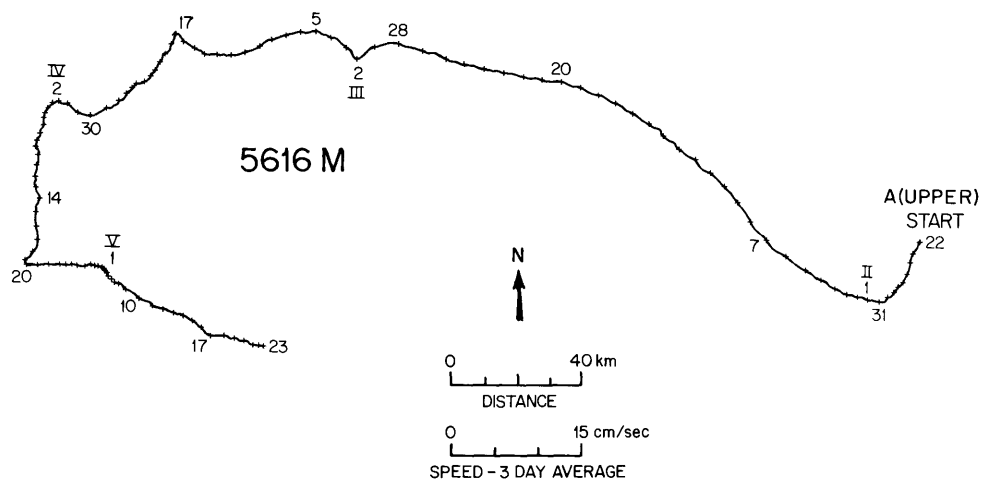


Figure 6.9. Polar histograms of currents recorded at the deep meters of moorings A and B and at moorings D and E (see Fig. 6.1). Each point represents the tip of a vector of current speed averaged over a one-hour interval. The dark circle (2 cm/sec) marks the stall velocity of the current-meter rotor. Speeds are in cm/sec.

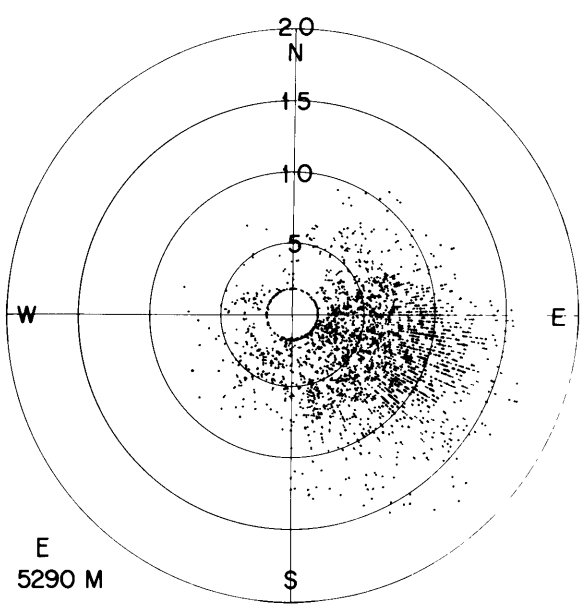
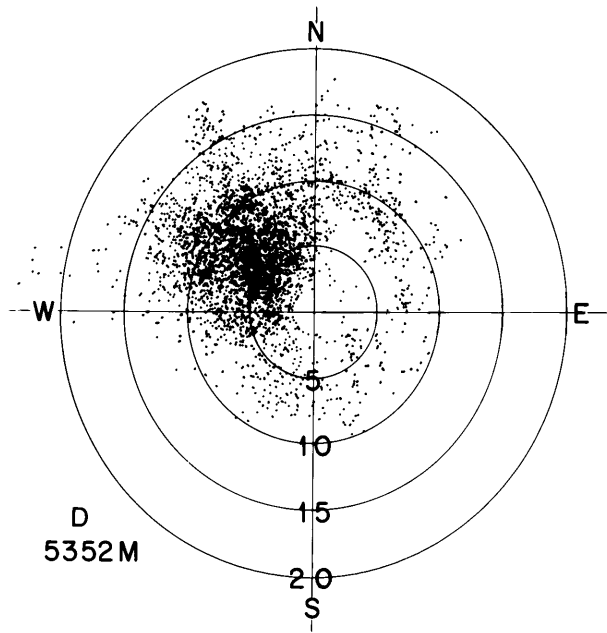
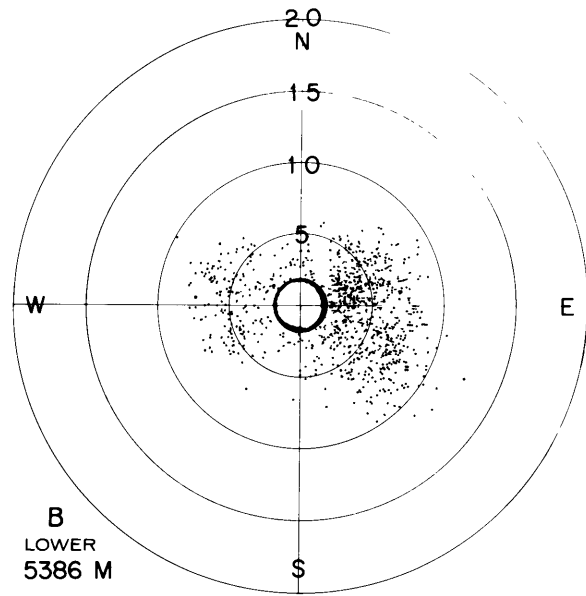
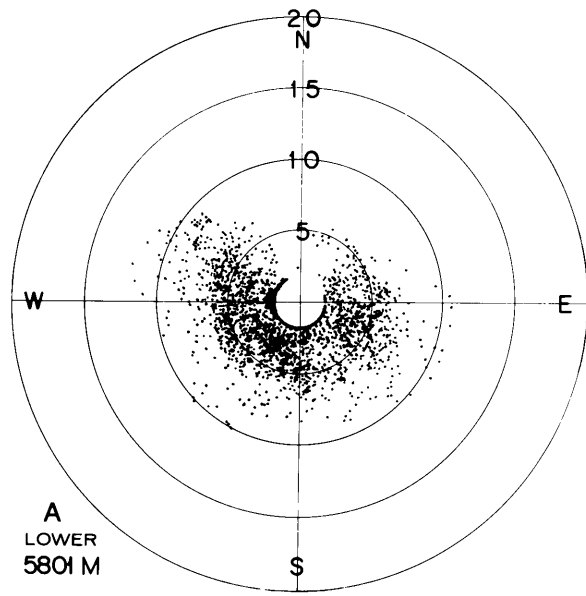
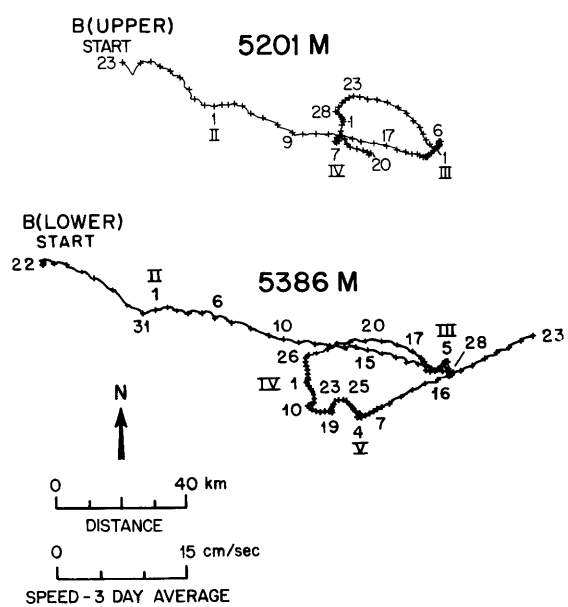


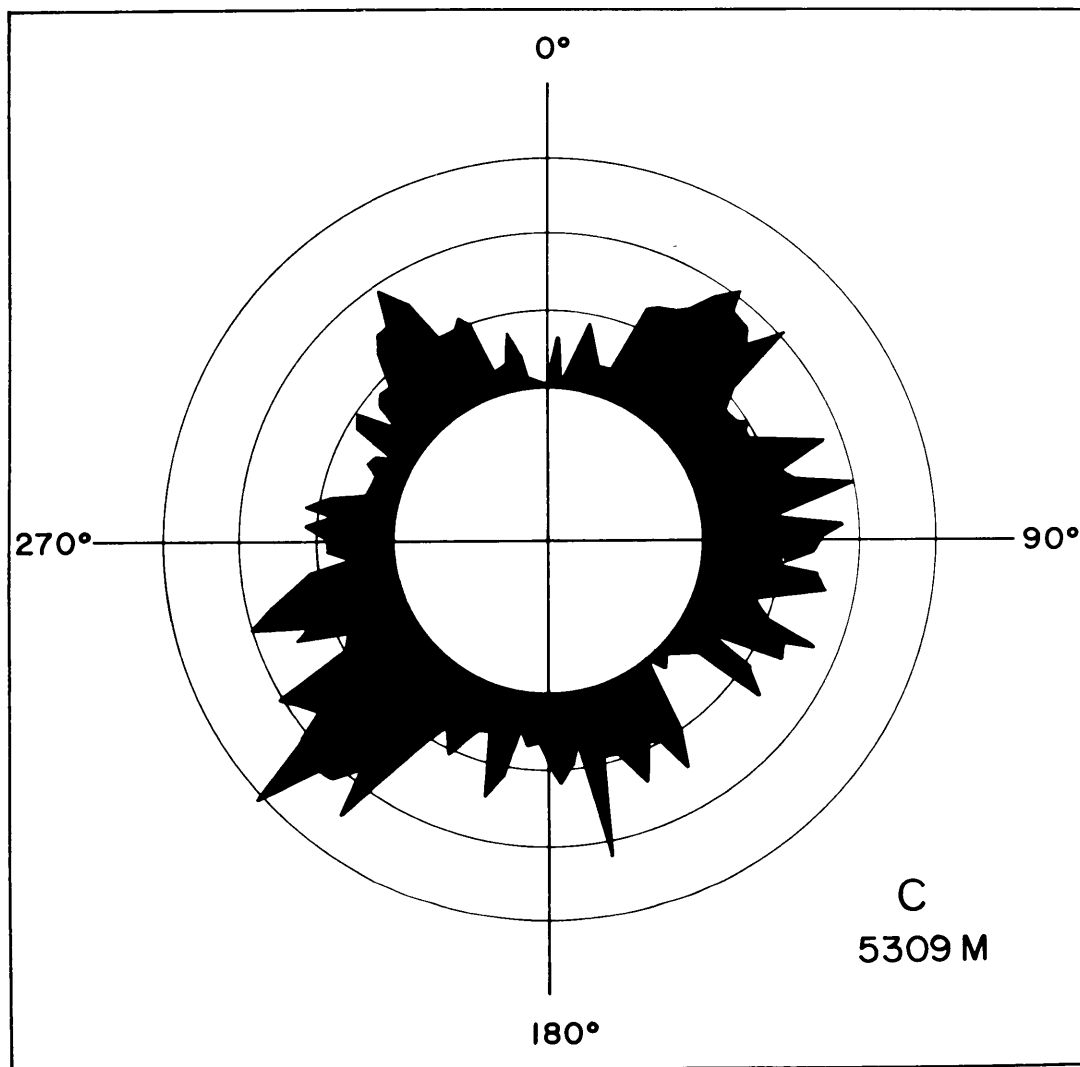
Figure 6.10. Progressive vector diagrams for currents recorded on the north flank of the Greater Antilles Outer Ridge (point B, Fig. 6.1). Crosses mark one-day intervals.



broad opposing flows, one to the WNW over the Nares Abyssal Plain and one to the ESE along the northern flank of the Greater Antilles Outer Ridge, with a boundary between the flows which shifts periodically in a N-S direction. This concept is supported by a time lag between shifts in current direction recorded at the two moorings. For example, the NW flow recorded at the northern mooring from 31 January to 17 March is not observed at the southern mooring until the beginning of March. The subsequent easterly flow beginning about 10 April at the southern mooring is recorded at the northern mooring about 20 April. This pattern agrees with a southerly shift of opposing flows to a point where both moorings are in the region of the westerly flow (first week in March), followed by a northerly shift until both moorings are within the easterly flow (third week in April). The lesser variations in the records may be due to interactions between the flows.

A third mooring, consisting of a single current meter (C in Fig. 6.1, Table 6.1), was set 15 m from the bottom on the western flank of the Greater Antilles Outer Ridge near the southern end of the Silver Abyssal Plain. Unfortunately, the rotor failed and only directions were recorded. A direction histogram for this meter (Fig. 6.11) shows no preferred flow orientation. The topographic constriction at the southeastern end of the Silver Abyssal Plain may form a cul-de-sac creating weak and variable currents.

Figure 6.11. Polar histogram of current direction (number of measurements vs. azimuth) for current meter C. For location see Fig. 6.1.



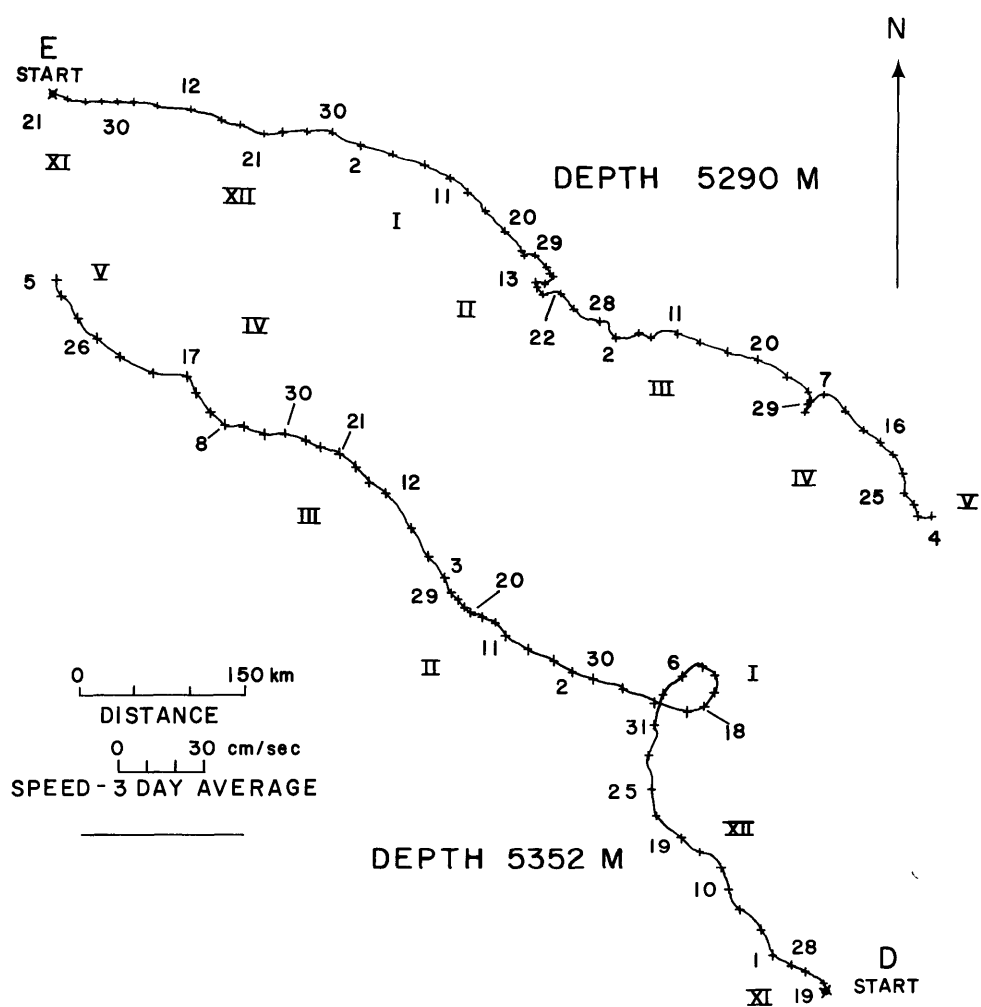
In November, 1971, a second series of three current meters was set on the western sector of the Greater Antilles Outer Ridge near a common depth of 5300 m: one at the northwest end and one each on the north and south flanks (Fig. 6.1, Table 6.1). A fourth current meter which was planned on the Caicos Outer Ridge was not set because the acoustic release functioned improperly in pre-mooring tests. A six-month record was obtained from the instruments on the flanks but the one at the northwest end of the Greater Antilles Outer Ridge malfunctioned and no useful data were obtained.

Current meter E, moored at 5290 m on the north flank of the Greater Antilles Outer Ridge, showed nearly unidirectional flow to the ESE parallel to the bathymetric contours over the entire recording period (166 days) (Fig. 6.12). Speeds, averaged over one-hour intervals, ranged from 2 to 17 cm/sec (Fig. 6.9); the maximum three-day average speed was 13 cm/sec. Speeds greater than 10 cm/sec were uniformly to the east and southeast.

Current meter D, at 5352 m on the south flank, showed a nearly unidirectional current to the northwest for 169 days, also parallel to the bathymetric contours (Fig. 6.12). Current speeds were similar to those observed on the north flank, although the higher speeds were generally directed to the north and northwest (Fig. 6.9). The maximum three-day-average speed was 15 cm/sec.

Two small-scale variations occur in each of the six-month

Figure 6.12. Progressive vector diagrams for current meter D on the south flank of the Greater Antilles Outer Ridge and E on the north flank, Nov. 19, 1971 to May 4, 1972 (Fig. 6.1). Crosses mark three-day intervals.



progressive vector diagrams (Fig. 6.12). On the southern mooring, the first is a clockwise loop from 1-21 January and the second is a sharp drop in speed with no change in direction over the interval 17-29 February. On the north flank, sharp changes in speed and direction occur at 7-19 February and 26 March - 7 April. Thus variations are observed in the northern record 4 1/2 and 5 1/2 weeks after variations of similar duration in the southern record. Five weeks is the approximate time necessary to transport a parcel of water from the location of the southern mooring around the northwest end of the Greater Antilles Outer Ridge to the northern mooring at the average current speeds observed, suggesting that the flow variations observed in the southern mooring may have been transmitted "downstream" to the northern mooring.

These last two current-meter records clearly support the concept of topographic control of deep oceanic flow in this region, and the arguments frequently raised against the significance of short-term current-meter measurements are difficult to apply to these measurements, which show nearly unidirectional currents for six months. If the observed currents are part of a cyclic phenomenon, the period of the fluctuation must be greater than one year.

The dynamic calculations for hydrographic stations bracketing the current meters agree with recorded directions except in one case. The dynamic topography between KNORR stations 54 and 55 (Section 5, Fig. 6.2) is not reflected in

the flow recorded at current meter mooring A, where recorded velocities were about 6 cm/sec to the west, and calculated velocities were 1-2 cm/sec southeast. A reference surface at the bottom would have given closer agreement in this case. A very different situation occurred in the case of current meter E, which was bracketed by a pair of stations on 12 February 1972. Dynamic calculations indicated a flow to the west at 5 cm/sec which matched the current-meter record, even though the westerly flow was only a transient of six-day duration superimposed on a long-term southeasterly current (see Fig. 6.12).

Recorded speeds at the other two moorings (B and D) were double the calculated values, implying a reference level above 3500 m, where our shallowest observations were made. The highest speed calculated from hydrographic data was 6 cm/sec to the northeast between ATLANTIS II Stas. 1825 and 1826 at the northwest tip of the ridge (Section 1, Fig. 6.2), where the current meter (F) that failed was located.

Current Evidence from Bottom Photographs

More than 800 oriented bottom photographs were taken on the Greater Antilles Outer Ridge to determine current effects on the sediment, the nature of the sea-floor microrelief, and to observe the activity of benthic organisms (see Chapter IV and Appendix II). The photographs show evidence of currents similar to that recorded by the current meters, of a contour-following flow moving clockwise around the outer ridge

(Fig. 6.13). The strongest currents were on the tip of the northwestern section of the outer ridge, where the sea floor was strongly smoothed, and on the north flank of the northwestern section, where ripples had developed in the fine-grained sediment (Fig. 6.14). Moderate currents were observed on the south flank, and evidence of weak to moderate currents appeared across the central section of the outer ridge. Indications of northwest currents of moderate speed were observed in the northern portion of Vema Gap, in agreement with the hydrographic data. Evidence of a SSE flow at the single station just north of Silver Bank indicates that the shallower water may cross the ridge sill there and then flow south and east along the south slope of the Puerto Rico Trench.

SUMMARY

The flow of deep and bottom water determined by hydrocasts, current-meter measurements, and bottom photography on the Greater Antilles Outer Ridge can be accounted for, with minor variations, by a circulation pattern similar to that shown in Fig. 6.7. These measurements are current indicators representative of periods ranging from seconds up to 23 years (the time span of hydrographic measurements used in Fig. 6.3), and they show the following pattern:

- 1) There is westward flow of AABW as cold as 1.52°C across the Nares Abyssal Plain and through the northern portion of Vema Gap. The magnitude of the flow through

Figure 6.13. Directions and relative intensities of bottom currents on the Greater Antilles Outer Ridge determined from bottom photographs. Strong currents, >10 cm/sec; moderate currents, 5-10 cm/sec; weak currents, < 5 cm/sec.

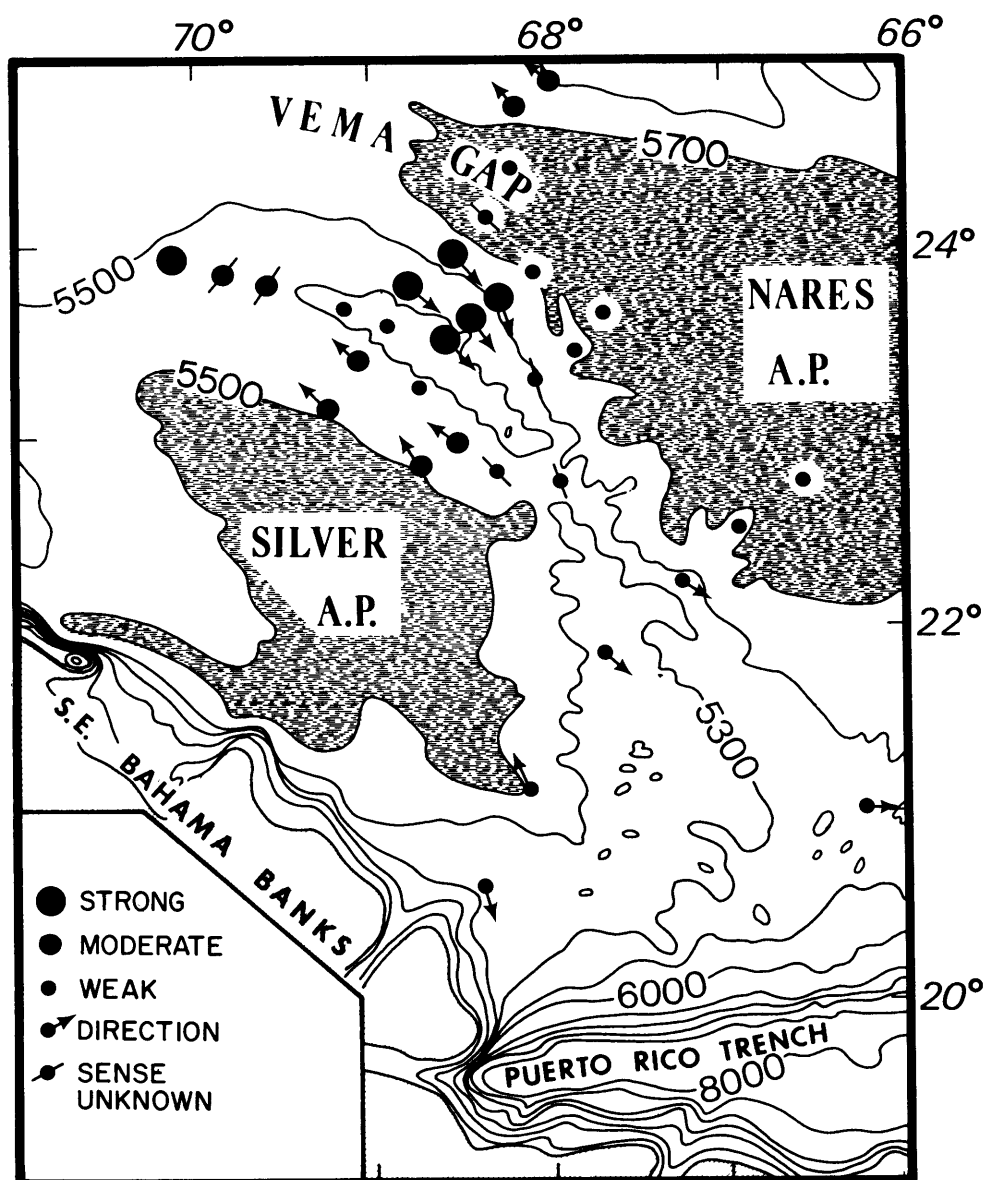


Figure 6.14. Bottom photograph taken at ATLANTIS II 60 Sta. K20A at 5197 m depth. The current lineations, ripples, and bending pennatulid all indicate a strong current to the southeast. Note the debris deposited on the lee side of the ripples. The area photographed is roughly three square meters.



Section 2 (Figs. 6.1, 6.7) is about $1.6 \times 10^6 \text{ m}^3/\text{sec}$.

2) A return flow of the same magnitude, and of only slightly warmer water (the Western Boundary Undercurrent), moves southward along the Blake-Bahama Outer Ridge and to the southeast along the Caicos Outer Ridge. Both AABW and NADW are included in this flow.

3) This return flow swings north and then northwest, following the bathymetric contours around the Silver Abyssal Plain, and then curves toward the northeast around the tip of the Greater Antilles Outer Ridge before continuing toward the southeast along the north flank of the outer ridge. A smaller amount of water moves northward through a saddle in the outer ridge at 23°N lat., 68°W long. and rejoins the southeastward flow north of the outer ridge. A third, smaller branch crosses the outer ridge sill at 21°N lat., 68°W long. and flows into the Puerto Rico Trench.

4) A broad flow of cold AABW enters the Puerto Rico Trench from the east. The shallower portion of this water mass apparently flows northward through depressions in the Greater Antilles Outer Ridge east of 66°W and then eastward along the north flank of the ridge.

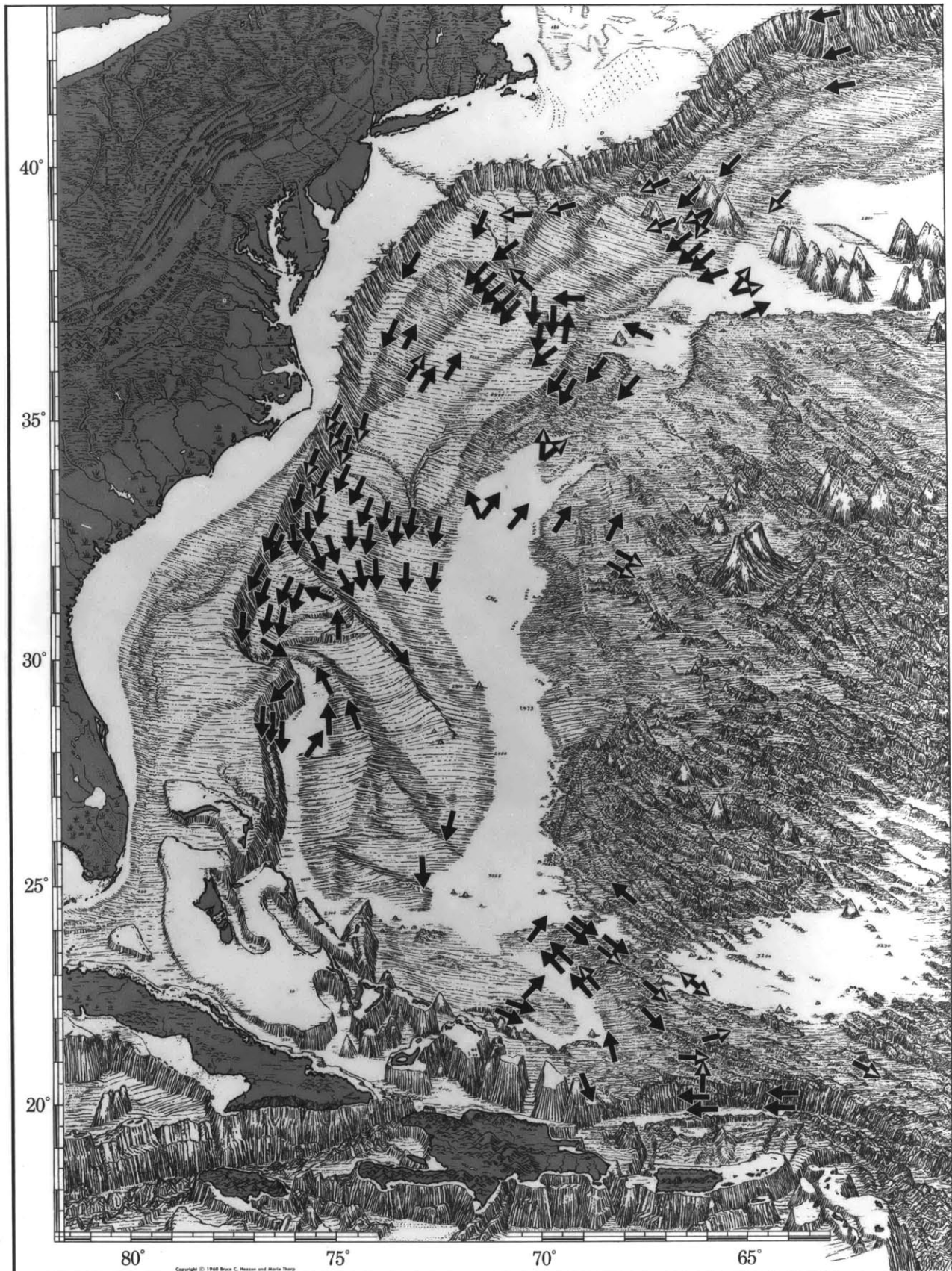
5) The boundary between the "new" AABW flowing westward across the Nares Abyssal Plain and through Vema Gap and the "older" AABW flowing eastward along the north flank of the ridge is probably neither distinct nor stationary. It appears to shift laterally (N-S) across the boundary between the Nares Abyssal Plain and the north flank of the

Greater Antilles Outer Ridge, and there is almost surely some exchange of water between the two main flows. The marked similarity between the upper and lower current meter records at A and B suggest that the boundary between the flows is nearly vertical.

6) In areas of marked topography, such as the Bahama Banks and the flanks of the Greater Antilles Outer Ridge, the topography clearly controls the pattern of abyssal circulation.

The broad pattern of abyssal circulation in the western North Atlantic has begun to emerge from evidence of direct current measurements, bottom photography, dynamic calculations, and analysis of sediment tracers during the past 15 years (Fig. 6.15). These measurements indicate that the Western Boundary Undercurrent, composed dominantly of NADW north of Cape Hatteras, flows south along the continental rise parallel to the bathymetric contours. AABW, entering the system via the Vema Gap/southern Bermuda Rise, flows around the Hatteras Abyssal Plain and joins the NADW near the latitude of Cape Hatteras to become the deeper portion of the WBUC. This picture is supported by the dynamic calculations of Amos, Gordon, and Schneider (1971), showing a contour-following flow around the Blake-Bahama Outer Ridge which includes about $2 \times 10^6 \text{ m}^3/\text{sec}$ of AABW. In addition, the Bermuda-Elbow Cay hydrographic section made by ATLANTIS in 1955 shows a narrow band of intense southeast flow along the eastern flank of the Blake Outer Ridge and a broader, weaker

Figure 6.15. Summary of direct current measurements (white center arrows) and photographic indications of bottom currents in the western North Atlantic Ocean. Compiled from data in the Woods Hole bottom-photograph library and Buoy Group data files, and from Amos and Escowitz (1971), Bruce (1964), S. Eittreim (pers. communication), Ewing and Mouzo (1968), Heezen, Hollister, and Ruddiman (1966), and the summary by Hollister and Heezen (1972). The base map is a portion of the Physiographic Diagram of the North Atlantic Ocean, published by the Geological Society of America, Boulder, Colorado, copyright 1968, Bruce C. Heezen and Marie Tharp; reproduced by permission.



northwest flow along the west flank of the Bermuda Rise, both containing AABW.

The present observations extend the southerly flow of the Western Boundary Undercurrent into the region of the Greater Antilles Outer Ridge and indicate additional contributions of colder AABW in the deep southwestern basin of the western North Atlantic Ocean. The added easterly flowing AABW comprises the bottom water circulating around the Greater Antilles Outer Ridge, and it lies immediately beneath the warmer water flowing in from the lower continental rise further north.

The transport of sediment from the northern continental margin of North America to the Greater Antilles Outer Ridge by this current system is considered in the following chapter, and the implications of its effect on the history of sedimentation on the Greater Antilles Outer Ridge are considered in Chapter VIII.

CHAPTER VII

SUSPENDED PARTICULATE MATTER

INTRODUCTION

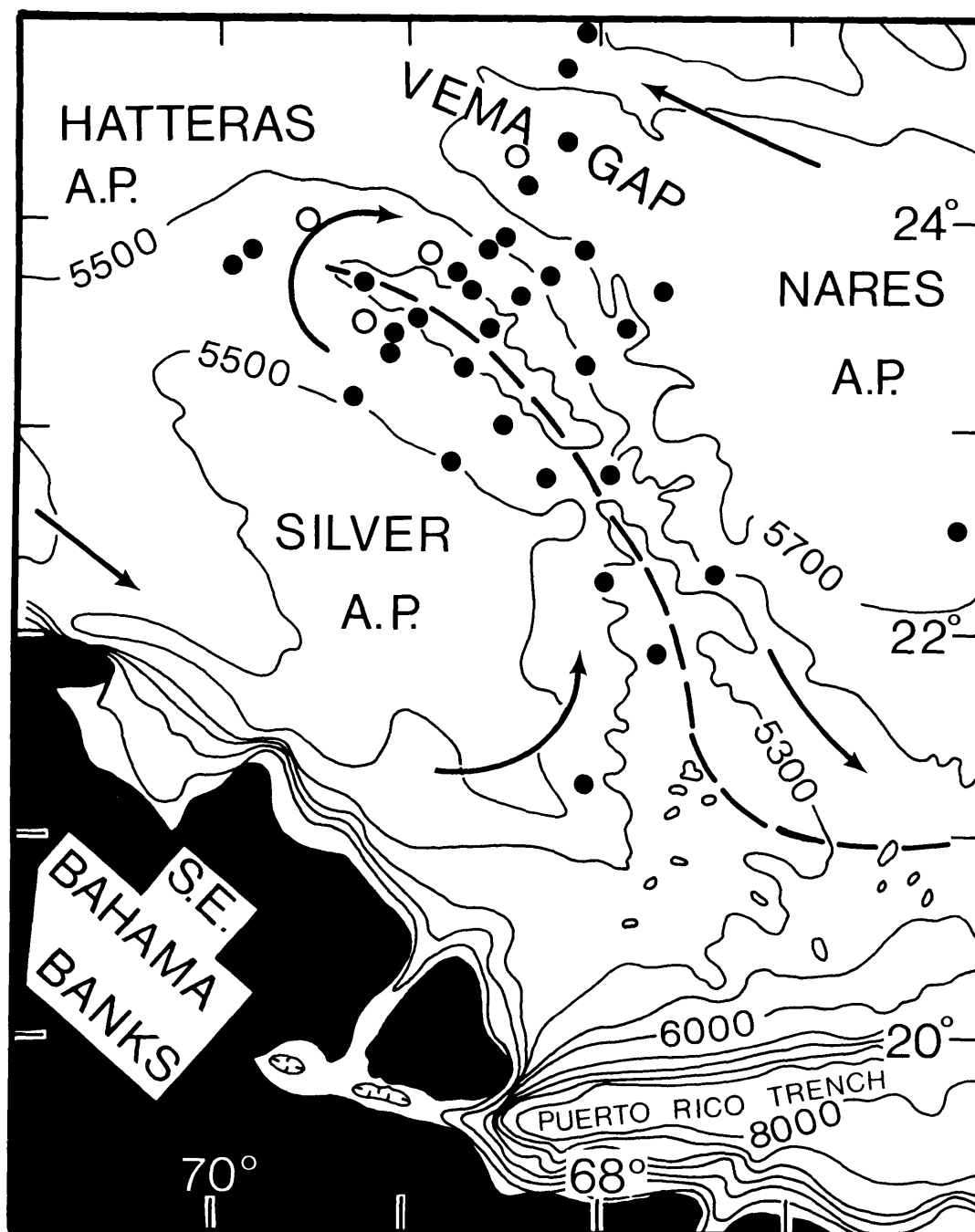
The evidence presented thus far has dealt with patterns of sea-floor morphology, bottom-sediment distribution, and abyssal circulation on the Greater Antilles Outer Ridge. The following discussion is devoted to an examination of the sediment carried in suspension in the deep currents and its relationship to these patterns.

Concentrations of suspended particulate matter were determined on 101 water samples from 32 stations over the Greater Antilles Outer Ridge (Fig. 7.1). Five additional samples were collected directly on silver filters (0.45 μm pore size) for x-ray analysis. Samples were collected primarily from depths of 4580 to 5730 m in the North Atlantic Deep Water and Antarctic Bottom Water (see Appendix III).

METHODS

Water samples were taken in 30 liter Niskin bottles spaced between 12 to 14 Nansen bottles in the bottom 350 m of hydrographic casts, thus allowing accurate determination of the θ/S relationship of the water sampled. Each water sample was filtered on shipboard under 14 pounds nitrogen pressure through preweighed pairs of Millepore filters (0.45 μm pore size) or through a single preweighed Nuclepore

Figure 7.1. Locations of suspended-particulate-matter samples (dots), and locations of nephelometer profiles illustrated in Figure 7.2 (circles, from Eittreim and Ewing, 1972): clockwise from top - C11-196; C11-195; C11-194; C11-197. Arrows show schematically the flow of the Western Boundary Undercurrent around the Greater Antilles Outer Ridge and the flow of AABW through Vema Gap. The dashed line marks the axis of the Greater Antilles Outer Ridge.



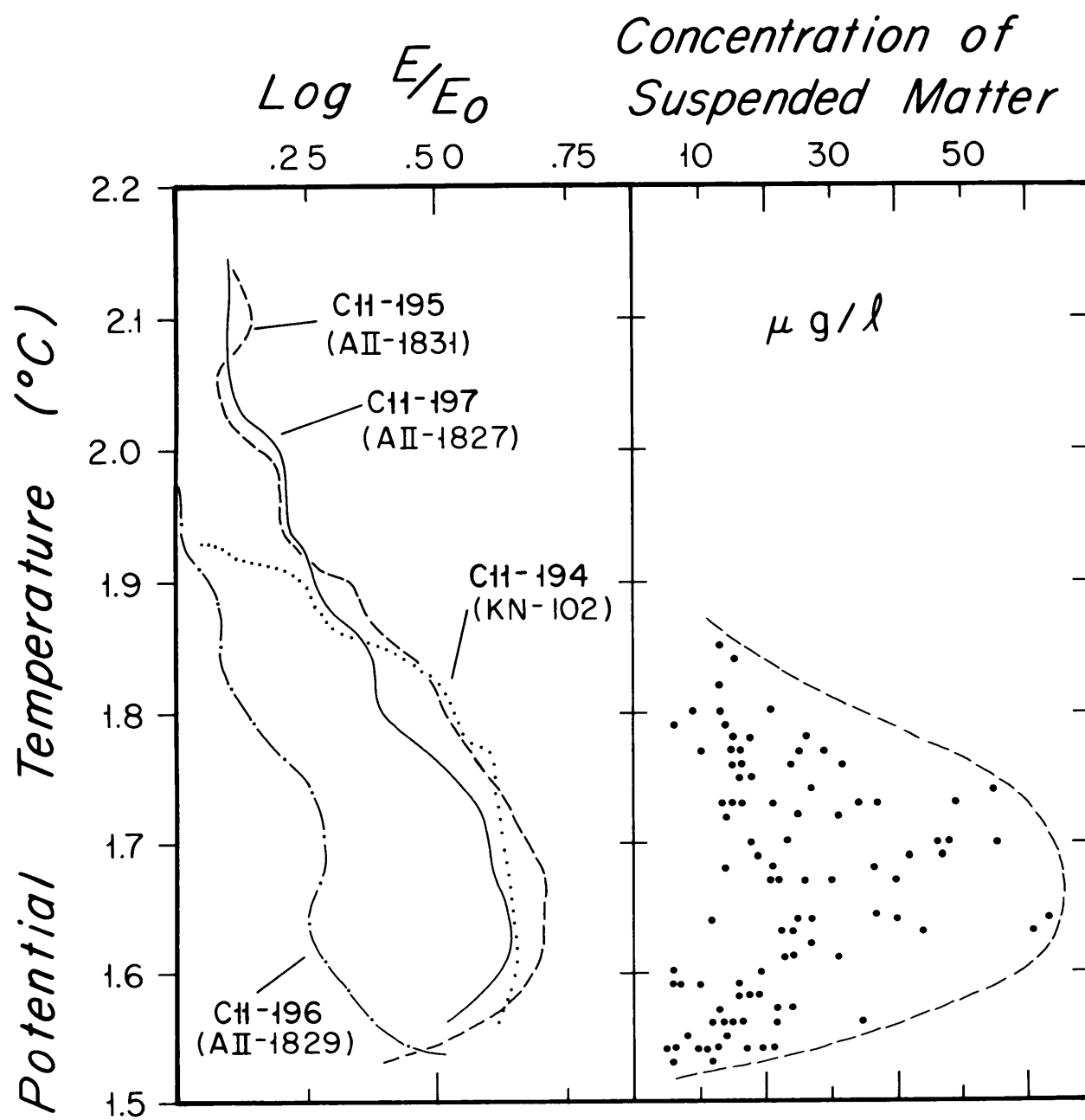
filter (0.50 μm pore size). After filtration, filters were rinsed five times with distilled water to remove salts. The samples were air dried and weighed in the shore laboratory after they had equilibrated with the laboratory atmosphere. The precision of the procedure is 50 μg for total suspended matter (Spencer and Sachs, 1970). Weights of total suspended matter collected per sample ranged from 120 to 1650 μg .

CONCENTRATION AND DISTRIBUTION

The particulate matter concentrations ranged from 6 to 63 μg per liter of sea water; all values greater than 40 $\mu\text{g/liter}$ were restricted to the depth range 5050-5400 m, and concentrations dropped abruptly above and below these depths. Since all samples were collected in standard hydrocasts, the concentrations can be plotted accurately against potential temperature (Fig. 7.2), thus relating suspended matter to the water mass which is transporting it. The average concentrations for discrete potential temperature intervals are: 1.51 to 1.60° - 15 $\mu\text{g/liter}$ (34 samples), 1.61 to 1.70° - 31 $\mu\text{g/liter}$ (29 samples), 1.71 to 1.80° - 22 $\mu\text{g/liter}$ (32 samples), and 1.81 to 1.90° - 14 $\mu\text{g/liter}$ (3 samples). Samples taken at individual stations seldom showed a regular pattern of increasing or decreasing concentrations toward the sea floor.

The overall circulation pattern responsible for transporting suspended matter to the Greater Antilles Outer Ridge

Figure 7.2. Light-scattering profiles (Eittreim and Ewing, 1972) and suspended-matter concentrations plotted against potential temperature. The potential-temperature curves used to plot the light-scattering profiles are from hydrographic casts (shown in parentheses) taken within 22 km of the nephelometer stations. Profile C11-196 was made in Vema Gap; the other profiles are from the Greater Antilles Outer Ridge. See Figure 7.1 for locations. In the light-scattering profiles, values of film exposure (E) are normalized to the exposure in the clearest water (E_0) (Eittreim and Ewing, 1972).



has been discussed. As pointed out by Eittreim and others (1969) and Eittreim and Ewing (1972), the nepheloid layer north of Cape Hatteras is deep and intense, while it is more diffuse and spans a broader depth range to the south. In their detailed discussion of light-scattering observations in the western North Atlantic, Eittreim and Ewing point out that, among the several sediment inputs to the nepheloid layer north of Cape Hatteras (Western Boundary Undercurrent "load" from north, hemipelagic, pelagic, atmospheric, sea-floor erosion, and turbidity currents), turbidity currents are probably most important. Small, episodic turbidity currents originating in the numerous submarine canyons north of Cape Hatteras would maintain the intense light-scattering observed in the nepheloid layer there, while the layer would be considerably weaker to the south, where there are few submarine canyons to contribute sediment. This effect is illustrated in Figure 7.3 where several of Eittreim's profiles are related to the transporting water mass by plotting light scattering against potential temperature.

The extent of mixing of NADW and AABW has also been discussed previously (Chapter VI). However, since the water masses lie along the same θ/S curve, which is very nearly a straight line below $2.0^\circ\theta$, one cannot use the classical methods to determine the degree of mixing. One indication that mixing is not strong is that the coldest water returning from the north along the Caicos Outer Ridge (Section 6,

Figure 7.3. Light-scattering profiles (Eittreim and Ewing, 1972) plotted against potential temperature for areas affected by the Western Boundary Undercurrent. Note that water colder than about 1.7°C is found only in the southern basin and that near-bottom light scattering is much less intense for this temperature than the scattering in warmer bottom water to the north. The potential-temperature curves used to plot the light-scattering profiles are from hydrographic casts (shown in parentheses) taken within 45 km of the nephelometer stations, except for the Caicos Outer Ridge profiles which are compared with hydrographic stations 120 km "upstream". Profile V22-2 has no sensitometer control and units are in optical density of the film (Eittreim and Ewing, 1972).

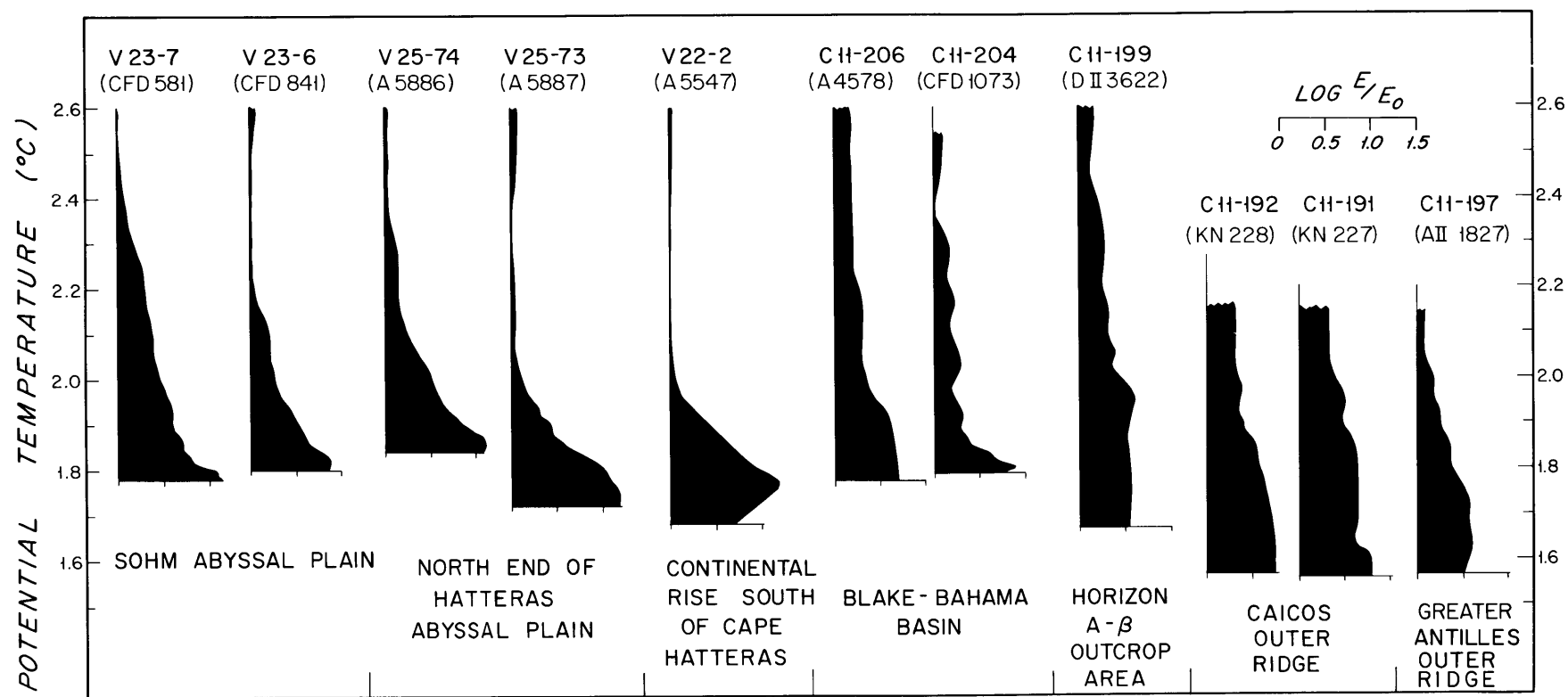


Fig. 6.2) is only about 0.05°C warmer than that entering the basin through the Vema Gap, with no change in either the θ/S or Si/θ relationships.

If mixing between NADW and AABW is not important in the southern extension of the Western Boundary Undercurrent, there are two ways in which AABW can serve to transport sediment from the continental rise southward to the Greater Antilles Outer Ridge. First, the AABW itself may erode sediment in its southward flow along the base of the lower continental rise. The geostrophic calculations of Amos, Gordon, and Schneider (1971), based on a reference level of 2500 m, show current speeds greater than 25 cm/sec in water colder than $1.7^{\circ}\theta$ on the Blake-Bahama Outer Ridge. These speeds are sufficient to transport fine-grained debris (see Fig. 3 of Hollister and Heezen, 1972), and, since sediments on the Blake-Bahama Outer Ridge and continental rise are not as uniformly fine-grained as sediments on the Greater Antilles Outer Ridge, the currents may also erode the sediments along the continental margin. Occasional higher speeds would almost certainly cause erosion (Partheniades, 1962; Southard and others, 1971; Zimmerman, 1971). Erosional patterns have been detected in seismic profiles and by deep-sea drilling on the Blake-Bahama Outer Ridge (Hollister and others, 1972) and in 3.5-kHz profiles further north on the continental rise south of New England (R. Young, pers. comm.). However, any

extensive erosion on the lower continental rise south of Cape Hatteras at the present time should cause strong light scattering near the bottom, and this is not observed (Fig. 7.3).

Alternatively, sediment entrained upstream by the NADW may settle into the underlying AABW as the Western Boundary Undercurrent flows south along the continental rise. This is supported by the observation of a deepening and weakening nepheloid layer toward the south in the western North Atlantic (Fig. 7.3).

The latter mechanism probably provides the best explanation for the transportation of terrigenous sediment to the Greater Antilles Outer Ridge at the present time. However, the evidence of earlier erosion on the Blake-Bahama Outer Ridge and lower continental rise indicates that large amounts of sediment may have been resuspended and entrained by the Western Boundary Undercurrent in the past.

If either of the above mechanisms is operative, "new" AABW flowing westward through Vema Gap should be relatively free of suspended matter, while the return flow (Western Boundary Undercurrent) should be transporting a larger suspended load. Nephelometer profiles (Figs. 7.1, 7.2) in fact show that light scattering is much lower in Vema Gap (Eittrheim and Ewing, 1972), and suspended matter concentrations of the 14 samples from Vema Gap average only

12 $\mu\text{g/liter}$, compared with an average of 31 $\mu\text{g/liter}$ in the return flow around the Greater Antilles Outer Ridge.

There is a good correlation between average suspended matter concentrations and intensity of light scattering (Fig. 7.2). Although low concentrations occur over the entire range of potential temperatures, minimum values are somewhat higher in the region of maximum light scattering. Local temporal variations probably occur in the amount of sediment in the nepheloid layer (Biscaye and Eittreim, 1973; Eittreim and others, 1973) and in the abyssal circulation (Tucholke and others, 1973), so the random sampling results in scattered concentrations, the whole of which are representative of average conditions. The uniformity of the nephelometer traces compared with the variability of individual samples suggests that short vertical concentration gradients or "patchiness" in the water column may have been sampled, but were not detected in the light scattering profiles, which have a vertical depth resolution of only 20 m (Eittreim and Ewing, 1972). However, it also appears likely that many of the low concentrations in filtered samples may be due to passage of some of the very fine detritus through the 0.45 to 0.50 μm pores in the filters (see discussion below).

GRAIN SIZE AND GENERAL COMPOSITION

Both suspended particulate matter and bottom-sediment samples were examined with a scanning electron microscope

(SEM) to determine composition, grain fabric, and size distribution (Figs. 7.4, 7.5). Most grains in the suspended matter samples are flat platelets oriented parallel to the viewing plane; therefore the vertical axis is normally shorter than the other two axes, and the shorter of the two axes in the horizontal plane was judged representative of particle size. Particles on the filters range in size from about 0.2 μm to greater than 30 μm , although the larger particles are much less frequent. Flocculated aggregates of particles are seldom observed in low concentration samples, but are more common (10-30% by area) in the samples of higher concentration (Fig. 7.5). Because it is not known whether the filtration process destroys or even creates floccules, and because bottom-sediment grain-size determinations were made on unflocculated samples in dispersant solution, all grain-size determinations on floccules were made on individual particles to facilitate comparison between suspended and bottom sediment. The less than 2 μm fraction of suspended matter averages less than 15 percent of the samples by volume, and the mean grain size (by volume) ranges roughly from 2.7 to 4.1 μm . The average particle size of suspended matter samples is thus somewhat greater than that of the underlying sediment. The difficulty encountered in identifying and counting particles less than about 0.3 μm in size may bias these results.

Figure 7.4. Scanning electron micrograph of suspended-matter sample #271 from 5169 m depth (left) and of a smear of bottom sediment from the top of core KN25-4GPC (right). The biogenic fraction includes the coccoliths *E. huxleyi* (with radiating spines) and *G. oceanica* (perforated disc). A diatom fragment is at right center in the suspended-matter sample. Note the dusting of very fine grains ($< 0.45 \mu\text{m}$) in the bottom-sediment sample. Scale bar = $5 \mu\text{m}$.

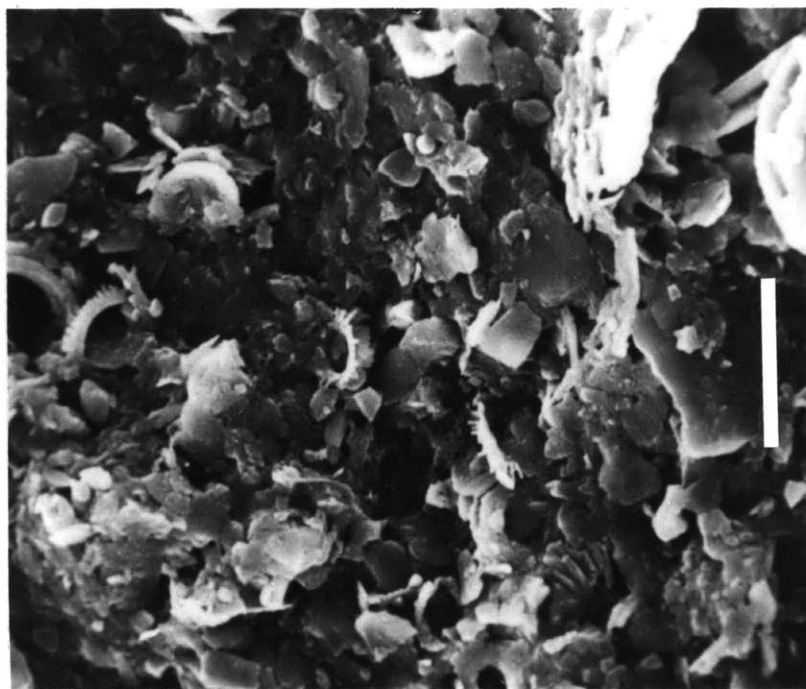
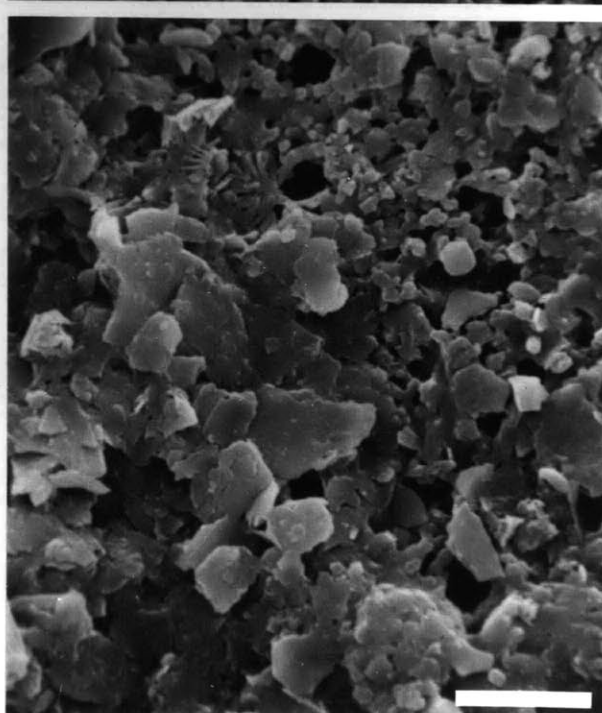
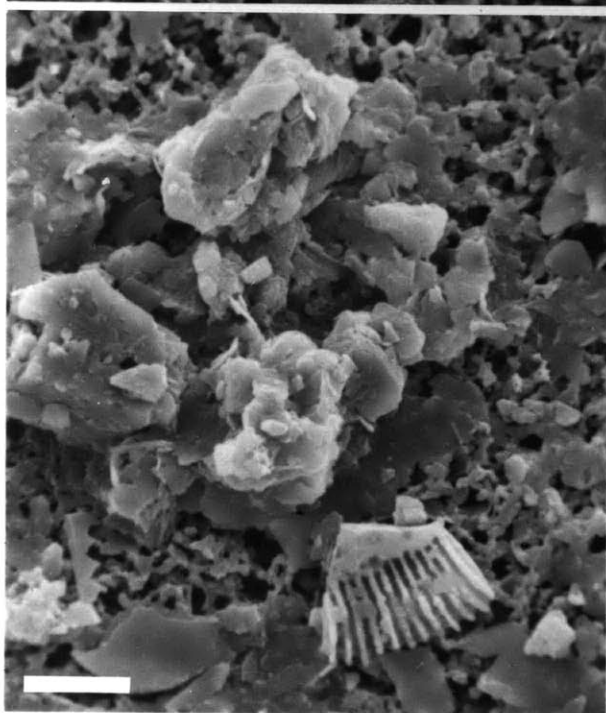
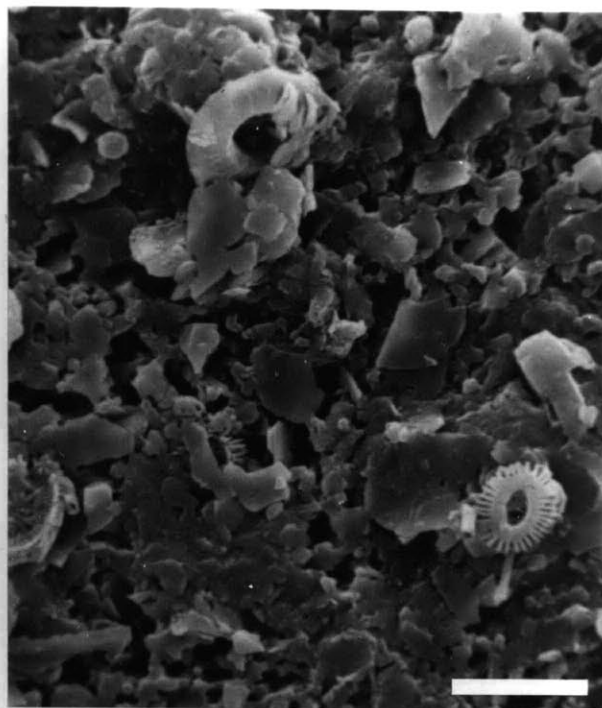
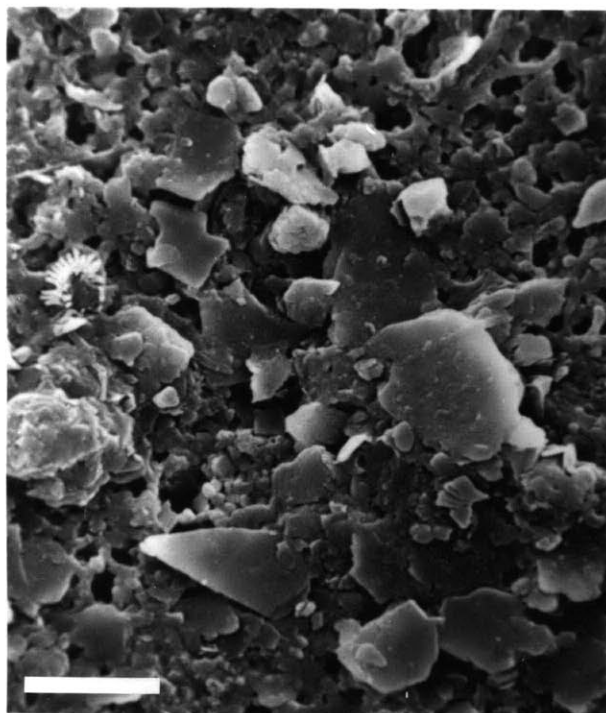


Figure 7.5. Scanning electron micrographs of suspended-matter samples taken over the Greater Antilles Outer Ridge. UL: Sample 245, 5355 m, north flank of northwest outer ridge. UR: Sample 257, 5145 m, south flank of northwest outer ridge. LL: Sample 269, 5375 m, south flank of northwest outer ridge. LR: Sample 311, 5266 m, near crest of western outer ridge. Note the flat clay-mineral platelets, floccules, and biogenic remains. The sponge-like background is the surface of the Millepore filter. Scale bars = 5 μ m.



The less than 2 μm (lutite) fraction of all suspended matter samples taken over the Greater Antilles Outer Ridge is composed almost entirely of clay-mineral platelets. Feldspar, quartz, and fragments of calcareous nannoplankton and biogenous silica constitute less than 5 percent of this fraction.

In the silt fraction (2-62 μm) about 30-50 percent of the sample is layer silicates. Kaolinite is infrequently recognized as fragments of hexagonal plates, but the other clay minerals cannot be differentiated. Quartz and plagioclase feldspar are common, constituting 30 percent of the sample in some instances. The calcareous nannoplankton are mostly Gephyrocapsa oceanica and Emiliana huxleyi, and their abundance is quite variable but may range up to 10 percent by area. Foraminifera are very rarely observed.

Samples taken from Vema Gap have consistently less biogenous material and less total suspended matter than those taken over the Greater Antilles Outer Ridge, and flocculated aggregates appear more commonly.

The bottom sediment examined with the SEM is visually similar in composition to that of the suspended matter. However, the bottom material appears to contain a larger proportion of material finer than about 0.4 μm (Fig. 7.4). It is entirely possible that a substantial amount of suspended matter smaller than 0.4 μm was not trapped on the filters,

thus accounting for this grain size discrepancy and possibly explaining the abundance of low concentration samples (Fig. 7.2).

When all factors are considered, the physical characteristics of the suspended particulate matter and the bottom sediment are quite similar.

MINERALOGY

Methods

The limiting factor in determining mineralogy of suspended matter is the small sample size, and it is important to consider whether semiquantitative x-ray diffraction analysis of such small samples will yield the same results as that of the same samples in larger quantities. Jacobs and Ewing (1965) recognized that the quality of x-ray diffraction spectra could be limited by the very minute quantity of material available in suspended-matter studies. The work of Jonas and Oliver (1967) further suggested that quantitative relationships may be affected when very small samples are analyzed. They found that montmorillonite appears to have an effective crystallite thickness of one unit cell and a width of 20-30 unit cells. In a pure montmorillonite suspension, stacking of these crystallites provides layer overlap and allows face-to-face bonding with such crystallographic regularity that 00 λ x-ray diffraction occurs much as if the lattice were a single crystal.

In a sample where additional clay minerals characterized by booklet crystallites are present, one would expect that the booklets would inhibit the formation of a regular lattice of montmorillonite crystallites in the oriented aggregate used for x-ray diffraction analysis. The effect of this disruption is probably similar in samples at any concentration. Of greater importance is the possibility that at low sample concentrations, insufficient montmorillonite is present to develop a regular lattice capable of well-developed Bragg diffraction.

A second problem in analyzing samples of suspended matter is that the quantities are so small that size fractionation usually cannot be performed. This places unfortunate limitations on the determination of sample composition, in that particle size can have significant effects on the analysis. X-ray analysis of very fine particles may not yield distinct diffraction maxima, in effect causing extreme broadening of certain peaks (Jacobs and Ewing, 1965). The expansion properties of micas are also determined by particle size (Jonas and Roberson, 1960), an important consideration when samples are treated by glycolation.

An experiment was conducted to determine if a relationship exists between apparent variations in mineralogy and the concentration of the sample analyzed. Multiple x-ray analyses of the carbonate-free, $< 2 \mu\text{m}$ fraction of a

single bottom-sediment sample (Core KN25-4GPC, 548 cm) with high montmorillonite and mixed-layer mineral content were made, using different sample concentrations on each silver filter. Concentrations of samples on ten filters ranged from 0.025 mg/cm^2 to 6.4 mg/cm^2 , and they were checked by weighing similar aliquots filtered onto preweighed Nuclepore filters ($0.4 \text{ }\mu\text{m}$ pore size). The effect of particle size on the analysis of each sample was assumed to be uniform since all aliquots were taken from the same dispersed sediment sample. Instrument conditions and x-ray procedures are described in Chapter IV.

Fairly consistent mineralogical compositions were observed at sample concentrations greater than about 1.6 mg/cm^2 ($7.28 \text{ }\mu\text{m}$ sample thickness; Table 7.1) using the peaks and weighting factors of either Hathaway (1972a) or Biscaye (1965). At lower sample concentrations, however, there is a marked decrease in the calculated abundance of montmorillonite and montmorillonite + mixed-layer material, with a corresponding increase of illite. No basal reflections are recorded in the x-ray diffraction pattern below concentrations of about 0.1 mg/cm^2 ($0.22 \text{ }\mu\text{m}$ thickness).

The abundance of kaolinite and chlorite is quite uniform when determined by either method of calculation where basal reflections (peaks) are well enough developed to facilitate comparison. The exception is that these two minerals appear to increase slightly in abundance at high

TABLE 7.1. CALCULATED CLAY MINERAL COMPOSITION
VERSUS SAMPLE CONCENTRATION

Sample Concentration on Filter (mg/cm ²)	ML:I:C:K ⁽¹⁾	M:I:C:K ⁽²⁾
0.025	ND:ND:ND:ND	ND:ND:ND:ND
0.05	ND:ND:ND:ND	ND:ND:ND:ND
0.10	ND:P:P:P	ND:P:P:P
0.15	5:82:9:4	0:86:10:4
0.20	9:77:10:4	0:84:11:5
0.40	15:73:8:4	7:80:9:4
0.81	20:65:10:5	13:71:11:5
1.61	39:48:9:4	15:66:13:6
3.22	41:44:10:5	14:64:15:7
6.45	40:45:10:5	16:63:15:6

ND = not detected, P = present

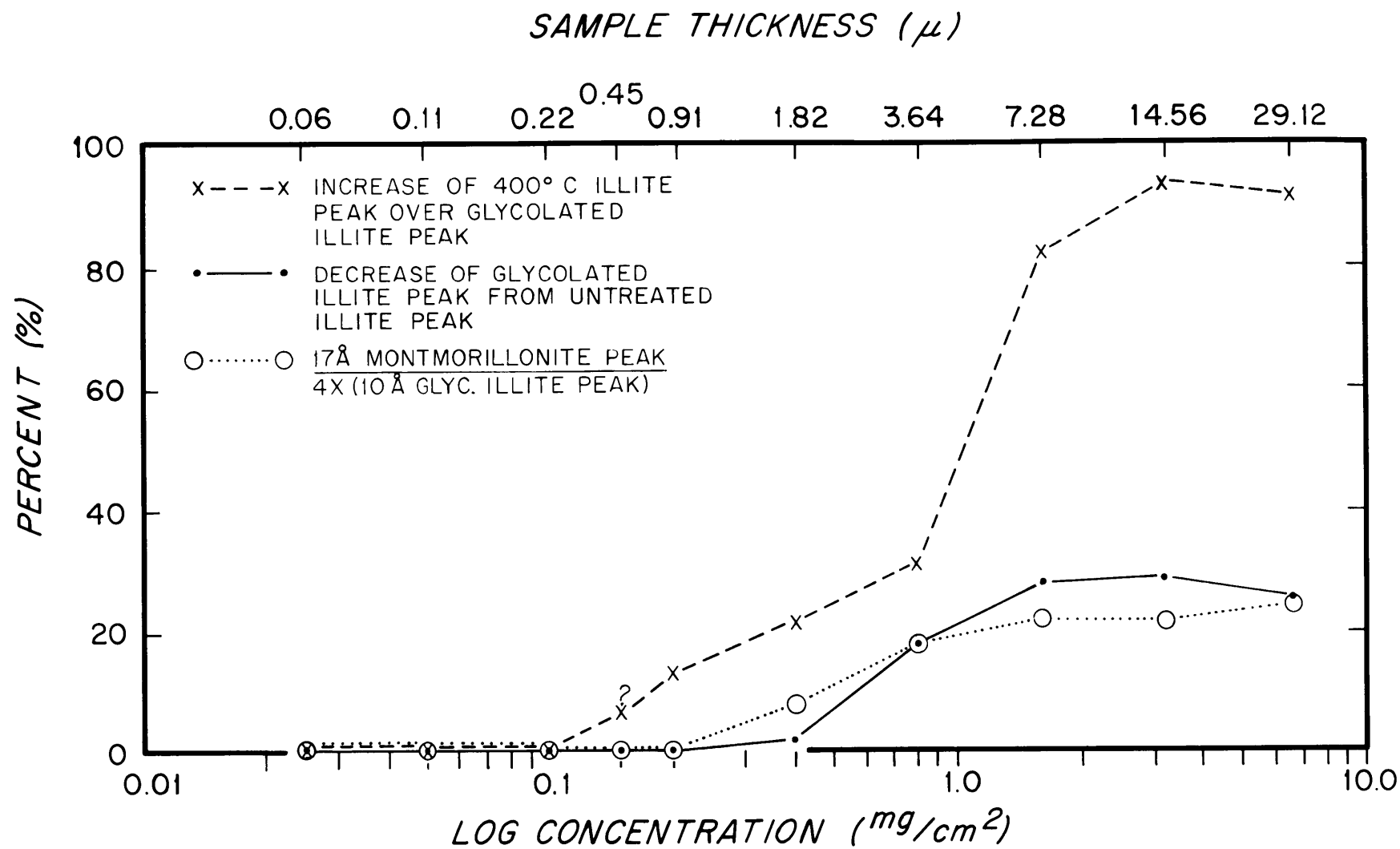
- (1) Calculated according to the method used by Hathaway (1972a); see text for explanation. ML = montmorillonite plus mixed-layer illite-montmorillonite, I = illite, C = chlorite, K = kaolinite.
- (2) Calculated using peak areas and weighting factors of Biscaye (1965). M = montmorillonite, I = illite, C = chlorite, K = kaolinite.

concentrations when the weighting factors of Biscaye (1965) are used. This can be related to increased detection of montmorillonite and its shift to 17 Å upon glycolation of the high-concentration samples, resulting in a loss of intensity in the 10 Å illite peak of the glycolated samples (Fig. 7.6). The consequent increase in the calculated abundance of kaolinite-chlorite (compared at 1:2 with the 10 Å illite peak) is greater than that of montmorillonite (compared at 1:4 with the illite peak).

It is apparent that consistent, high-intensity 00 ℓ reflections from the montmorillonite lattice are recorded only when this mineral is analyzed at relatively high concentrations. At lower concentrations the lattice formed by particle-upon-particle deposition of the thin crystallites is apparently too small to create fully developed constructive and destructive interference of basal reflections. Thus, for sediment with this particular grain-size distribution and mineralogy, a sample thickness comparable to about 5×10^2 unit cells of montmorillonite is needed for fully developed Bragg diffraction.

Obviously, the graph illustrated (Fig. 7.6) cannot be used for direct comparison with other samples of widely ranging mineralogical composition and grain-size distribution. For example, samples with a higher true montmorillonite content will probably yield consistent semiquantitative estimates of composition at lower concentrations. The important point is that calculated mineral abundances

Figure 7.6. Relationship between peak areas on x-ray diffractograms and sample concentrations on silver filters for aliquots of the same sediment sample. In each sample, the increase in intensity (measured as peak area) of the 10 Å peak on heating the sample to 400°C over the intensity of the 10 Å peak in the glycolated sample is caused by collapse of montmorillonite and mixed-layer montmorillonite-illite. The increase is compared directly with the intensity of the 10 Å peak of the glycolated sample to determine the abundance of these minerals. Increased detection of montmorillonite and mixed-layer montmorillonite-illite at the higher sample concentrations is indicated by 1) greater increase of intensity of the 10 Å peak in the sample heated to 400°C over the intensity of the 10 Å peak (illite) in the glycolated sample (dashed line), 2) larger decrease of intensity of the 10 Å peak in the glycolated sample from the intensity of the 10 Å peak in the untreated sample due to expansion of mixed-layer montmorillonite-illite away from 10 Å (solid line), and 3) increase of the 17 Å montmorillonite peak area in the glycolated sample relative to that of the 10 Å (illite) peak in the glycolated sample (dotted line). Sample thicknesses (top) are based on an assumed sample density of 2.20 g/cm³.



cannot always be accepted at face value when low sample concentrations, such as those of suspended matter, are used.

The five suspended-matter samples collected directly on silver filters on shipboard were x-rayed under the same conditions as the bottom-sediment samples (see Chapter IV) in order to make mineralogical comparisons with the bottom sediment and to determine whether the suspended matter may be a source for sediment on the Greater Antilles Outer Ridge. These samples were not treated before analysis because of the minute quantities collected. However, results of the SEM studies indicate that the effects of organic aggregates and amorphous silica on the analyses should be minimal. Calculations of composition (Table 7.2) were made using the peaks and weighting factors of Hathaway (1972a). The calculations were based on the assumption that the entire suspended-matter sample was composed of layer silicates. While not true in the strictest sense (i.e. the SEM studies indicate that quartz, plagioclase, and biogenic tests may constitute up to 15% of the sample, the assumption is justified because the quartz and feldspar peaks are virtually unidentifiable in the x-ray diffractogram.

Results

Chlorite and kaolinite constitute about 2 parts in 10 of the suspended matter (Table 7.2), as they do in the $< 2 \mu\text{m}$ fraction of the underlying sediment (Table 4.1).

TABLE 7.2. MINERALOGY OF SUSPENDED MATTER SAMPLES

Sample	Lat. °N	Long. °W	Depth (m)	M:I:C:K*
KN25-SF1	23°52.6'	68°35.1'	5340	ND:P:P:P†
KN25-SF2	23°43.5'	68°41.5'	5766	ND:75:18:7
KN25-SF3	23°24.0'	69°06.1'	5232	6:73:19:2
KN25-SF4	23°48.0'	69°56.0'	5326	8:72:16:4
KN25-SF5	22°25.4'	67°56.9'	5124	ND:78:18:4

* M = montmorillonite plus mixed-layer minerals, I = illite, C = chlorite, K = kaolinite. Calculated using the peak areas and weighting factors of Hathaway (1972a).

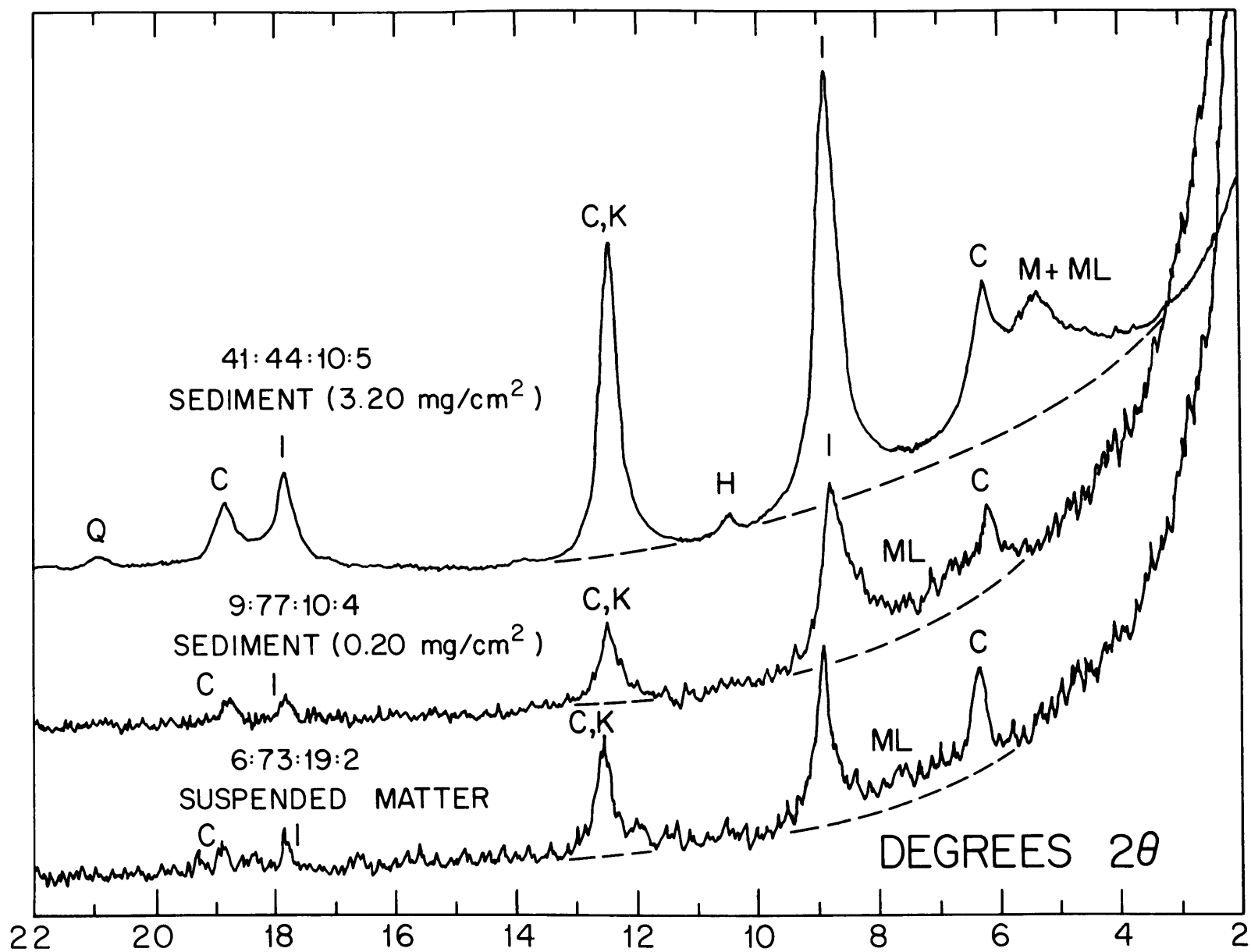
† ND = not detected, P = present, but with peaks too ill-defined for semi-quantitative calculations.

The apparent enrichment of chlorite in the suspended matter is probably due to the uncertainty involved in resolving the contribution of chlorite to the small 3.5 Å doublet in the diffractogram of these low-concentration samples.

The major mineralogical difference between suspended and bottom sediment from the Greater Antilles Outer Ridge is in the relative abundances of illite and montmorillonite plus mixed-layer minerals. The maximum concentration of suspended matter recovered on any Millepore or Nuclepore filter was about .172 mg/cm²; although the residue concentration on the silver filters could not be determined, it almost certainly falls below this value and thus is in the range where montmorillonite and mixed-layer montmorillonite-illite are not fully detected (Fig. 7.6). The effect is strikingly illustrated by a comparison of the diffractogram of a glycolated suspended-matter sample to that of a low and a high concentration, glycolated, bottom-sediment sample (Fig. 7.7).

It is conceivable that the suspended-matter samples are actually, rather than apparently, depleted in montmorillonite. However, in view of the arguments outlined concerning the montmorillonite-depletion effect, it is assumed that the mineralogy of the suspended matter and subjacent bottom sediment are quite similar, if not identical. This assertion, together with evidence of the depositional regime presented in the next section, argues

Figure 7.7. X-ray diffractograms of glycolated samples. The top two traces are aliquots of the same bottom sediment sample (KN25-4GPC, 548 cm) x-rayed at different concentrations (in parentheses) on the silver filters, and the bottom trace is from a suspended matter sample (KN25-SF3). Note that montmorillonite plus mixed-layer montmorillonite-illite is not detected as a 17 Å peak in either the suspended matter or dilute sediment sample, but it is readily detected at higher concentrations (top). Hornblende and quartz detected in the concentrated sample are not seen in the dilute sample. The bottom two traces were recorded at the same range ($10^2 \times 5$) and the top trace at a greatly increased range ($10^3 \times 5$). Numbers represent the calculated composition (using the method of Hathaway, 1972a) in the order, montmorillonite + mixed-layer montmorillonite-illite: illite: chlorite: kaolinite. Letters are Q - quartz, C - chlorite, I - illite, K - kaolinite, H - hornblende, M - montmorillonite, ML - mixed-layer montmorillonite-illite.



in favor of the concept that the suspended particulate matter is a source for the sediment on the Greater Antilles Outer Ridge. The suspended matter, much as the bottom sediment, is enriched in chlorite and thus appears to have a northern provenance.

THE DEPOSITIONAL CONDITIONS

The current regime over the Greater Antilles Outer Ridge that has allowed the observed deposition of suspended sediment cannot yet be fully correlated with theoretical and empirical data because 1) the behavior of fine-grained cohesive sediments in salt water cannot be mathematically modelled, and 2) the small amount of empirical data from salt-water flume experiments are not sufficient to fully resolve the problem.

The few empirical data that are available indicate that lutite ($< 2 \mu\text{m}$) will be deposited from salt-water flows at velocities less than about 10 cm/sec. Einstein and Krone (1962) found that a 0.1 g/l suspension of San Francisco Bay mud, which was only partially lutite and was enriched in organic material, was all slowly deposited at velocities below 7 cm/sec. Kuenen (1965), using higher concentrations of lutite-silt mixtures in a circular salt-water flume, found that all the sediment settled out at current velocities of less than 10 cm/sec. Partheniades (1962) used San Francisco Bay mud and determined that rapid deposition of lutite occurred at velocities below about

14 cm/sec.

The rate of deposition of lutite is undoubtedly related to grain size, mineralogy, percent organic material, flocculation effects, salinity, and temperature, as well as the velocity, turbulence, and shear within the flow, and it is therefore difficult to relate the results of these experiments to actual abyssal environments; salt-water flume experiments simulating the deep-sea environment are undoubtedly needed to resolve the problem. However, in view of the existing experimental data and data collected in the deep sea (Hollister and Heezen, 1972) it seems reasonable to predict that there will be net deposition of suspended sediment at speeds less than about 10 cm/sec.

The bulk of current speeds recorded on the Greater Antilles Outer Ridge thus fall in the range necessary for lutite deposition (see Fig. 6.9). The zone of shear between the opposing currents on the north and south flanks of the western Greater Antilles Outer Ridge is probably characterized by even lower current speeds.

If abyssal currents are transporting sediment to this region, the greater thickness of acoustically transparent sediments and higher rates of accumulation on the western sector of the Greater Antilles Outer Ridge, compared to the eastern sector, suggest that suspended sediment is preferentially deposited in the western sector. This contention is supported to some extent by a nephelometer profile (C11-3)

on the north flank of the far eastern outer ridge (Eittreim and Ewing, 1972) which shows greatly reduced light scattering in the nepheloid layer. However, it is possible that some of the easterly flow along the north flank has not reached this longitude, but has escaped to the south through intervening depressions in the outer ridge.

The zone of current shear which shifts N-S across the boundary between the north flank of the eastern Greater Antilles Outer Ridge and the Nares Abyssal Plain is also probably associated with preferential deposition, but rates of accumulation there would be reduced since the Western Boundary Undercurrent has already lost much of its suspended load when it reaches that area; the westerly-flowing AABW also contains very little suspended matter.

There is probably little erosion of the fine-grained cohesive sediment on the Greater Antilles Outer Ridge at present, since maximum current speeds are only 15-20 cm/sec. Southard and others (1971) found that velocities of 15-20 cm/sec were necessary for incipient erosion of calcareous ooze of less than 30 percent lutite when the water content of the sediment approximated that found in the deep sea. Postma (1967, Fig. 1) noted that velocities greater than 30 cm/sec would probably be necessary to erode sediment with a water content and grain size similar to those on the outer ridge.

Any extensive erosion on the Greater Antilles Outer Ridge should be detected by a strong near-bottom nepheloid layer, but this is not observed (Fig. 7.2). Furthermore, there is no evidence in high-frequency sub-bottom profiles taken over the outer ridge for the small-scale lensing or unconformities that erosion would create (Fig. 2.1). Although transient current speeds may infrequently become high enough to erode the outer ridge sediment, the average current speeds observed are low enough that most of the material thus entrained is probably redeposited very quickly, and the area must be characterized as largely depositional.

The activity of benthic organisms on the Greater Antilles Outer Ridge may also resuspend sediment (see Fig. 4.4), but the intensity of resuspension and the character of the re-worked detritus are uncertain. Therefore it is not possible at present to evaluate the significance of this mechanism.

DISCUSSION

The volume of transparent sediments above Datum A on the Greater Antilles Outer Ridge is roughly $6 \times 10^4 \text{ km}^3$, and the mass approximately $1.2 \times 10^{20} \text{ g}$ at an average sediment density of 2.0 g/cm^3 . Using the present water-volume transport of $1.6 \times 10^6 \text{ m}^3/\text{sec}$ and a suspended matter concentration of $50 \text{ } \mu\text{g/l}$, approximately $1.2 \times 10^{20} \text{ grams}$ of sediment could have been transported into the region of the Greater Antilles Outer Ridge since middle Eocene time (the assumed age of Datum A). These rough calculations indicate

that enough suspended matter has been transported into the region to account for the volume of the transparent layer if all the suspended matter were deposited, but it is unlikely that total deposition ever occurred. The discrepancy is partially resolved when foraminiferal tests, composing perhaps 20% of the bottom sediment, are considered. However, it seems likely that either water volume transports or suspended matter concentrations were higher at times during the geologic evolution of the Greater Antilles Outer Ridge than they are now. Pulses of increased AABW flow into the area (see Chapter IV), for example, may have contributed substantial amounts of sediment to the Greater Antilles Outer Ridge in the past.

In summary, suspended sediment transported to the Greater Antilles Outer Ridge by the Western Boundary Undercurrent is both a likely and a reasonable source of sediment for the transparent layer. Grain size, composition, total volume of sediments, and current regimes are all in reasonable agreement with the requirements of a model of current-controlled deposition.

CHAPTER VIII

THE GEOLOGICAL EVOLUTION OF THE GREATER ANTILLES OUTER RIDGE

PREVIOUS THEORIES

Earlier concepts concerning the formation of the transparent layer which comprises most of the Greater Antilles Outer Ridge have relied on interpretations of seismic profiles. Ewing and others (1968) felt that the transparent layer must predate the deposition of Nares Abyssal Plain sediments because portions of the layer dip beneath the stratified sediments of the Nares Abyssal Plain, and they offered two possible explanations: 1) filling of a long depression with lutites, followed by later elevation of the sediment body, or 2) formation of the transparent layer as the extreme outer end of the Blake-Bahama ridge system, with later separation by erosion at the southern end of the Hatteras Abyssal Plain. Bunce and Hersey (1966) observed a thin layer of transparent sediments dipping beneath the Puerto Rico Trench Abyssal Plain and suggested that the layer was the remnant of a Puerto Rico continental rise predating formation of the trench. Savit and others (1964) speculated that sediment erosion and/or transportation processes might be active in regulating the configuration of the transparent layer, but they made no comment on the timing or methods of formation.

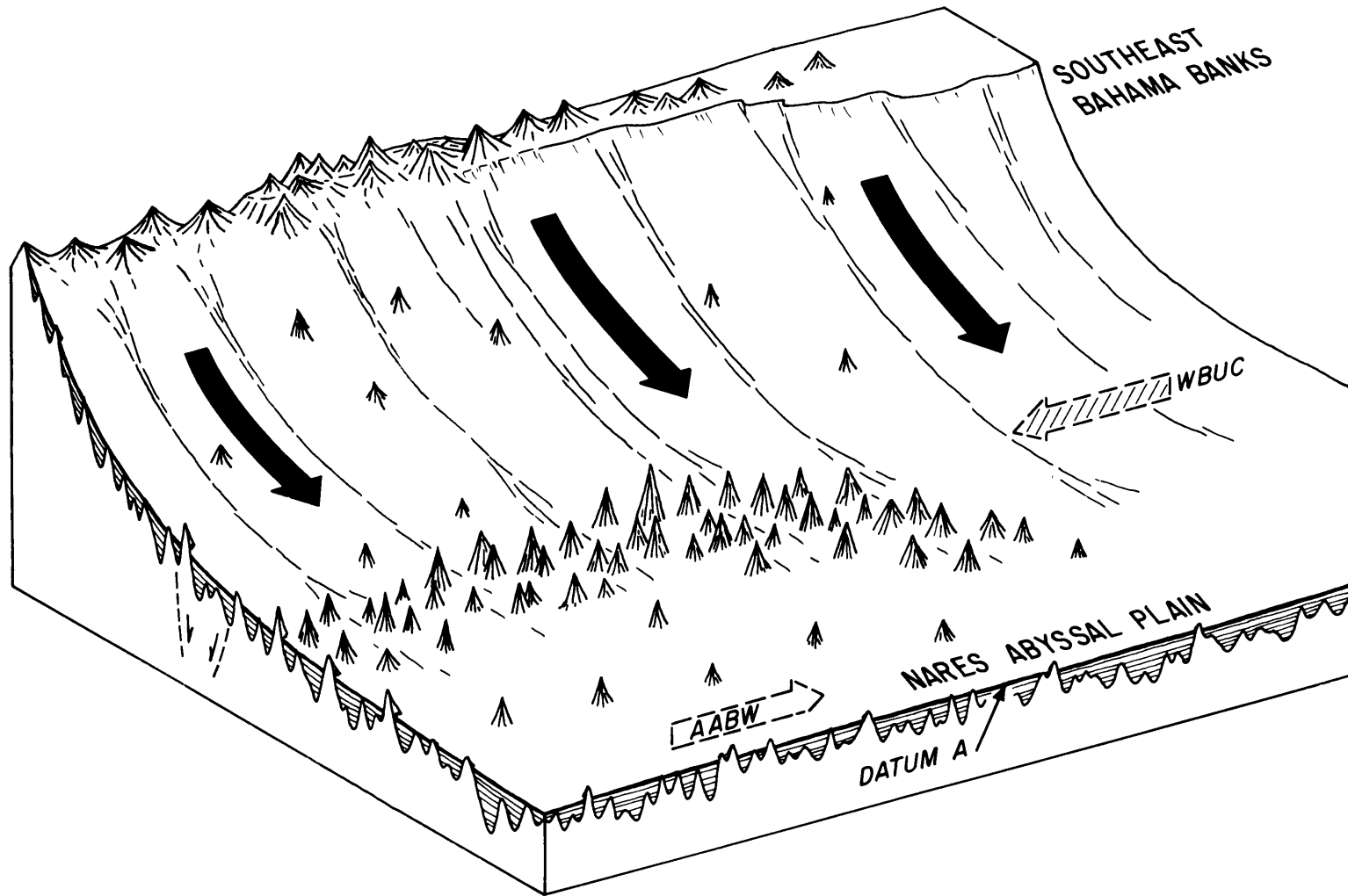
The following pages describe a model based on a synthesis of the data outlined in earlier chapters of this work combined with information from the published literature. Several factors must be considered in interpreting the history of sedimentation in this area: 1) the probable sedimentary processes before formation of the Puerto Rico Trench, 2) the effect of formation of the trench on these processes, 3) the time of initiation and the effect of geologically significant deep-current activity in the basin of the western North Atlantic Ocean, and 4) the subsequent sedimentary environment. An attempt is made here to resolve all conflicting interpretations into a single unified evolutionary sequence. The following discussion will describe the formation of the Greater Antilles Outer Ridge from middle Cretaceous time to the present.

MIDDLE CRETACEOUS TO MIDDLE EOCENE

The oceanic basement under the Greater Antilles Outer Ridge was probably formed during the early to middle Cretaceous, and the Puerto Rico Trench had not yet formed (Fig. 8.1). The distribution of basement peaks which now penetrate Datum A (Fig. 3.4) suggests that a rugged, ridge-like elevation occupied the location of the present eastern Greater Antilles Outer Ridge and possibly also the area of the present Puerto Rico Trench. Uchupi and others (1971) suggested that the southeastern Bahama Banks, lying on the same trend as this basement rise, may have formed atop a

Figure 8.1. Schematic sketch of sedimentation conditions during the early to middle Eocene. The Puerto Rico Trench had not yet formed and detritus shed from the Greater Antilles (black arrows) formed a sequence of stratified sediments which covered and ponded between peaks of the basement ridge presently beneath the Greater Antilles Outer Ridge. The abyssal flow of the Western Boundary Undercurrent (shaded arrow) and Antarctic Bottom Water (open arrow) may have been initiated near this time.

EARLY TO MIDDLE EOCENE



series of ridges associated with an early east-west transform fault. If so, the basement structures under the Greater Antilles Outer Ridge may represent a younger extension of this fault zone.

During late Cretaceous time the rugged sea floor received pyroclastic sediments from the Greater Antilles, which were experiencing extensive geosynclinal volcanism (Weyl, 1968; Monroe, 1968). Some of the siltstones, claystones, cherts, and limestones dredged from the north slope of the present Puerto Rico Trench probably also were derived from the Greater Antilles, and they may have been interbedded with flows of tholeiitic magma (Chase and Hersey, 1968). The Cenomanian limestones dredged from the north slope were probably deposited at depths greater than 3000 m (Todd and Low, 1964); their nonclastic texture indicates that they may have been deposited on an elevated area which was not influenced by the downslope sedimentation.

Core data from DSDP Site 28 on the north slope of the Puerto Rico Trench indicate that the deposition of interbedded layers of chert, limestone, siltstone, lutite, and microfossil ooze apparently continued under similar conditions, but without the basalt flows, until middle Eocene time, thus forming the present stratified layer. Pyroclastic debris was furnished by early to middle Eocene volcanism in the Greater Antilles (Mattson and Pessagno, 1971). It is likely that the acoustic stratification of the pre-middle Eocene sediment is due to interbedding of these

sediment types and to layering formed by downslope sediment movement and turbidity currents, similar to the layering found on modern continental rises and abyssal plains.

The absence of the stratified layer under the Greater Antilles Outer Ridge east of about 63°W long. (Figs. 3.4, 3.5) indicates either that there was no source of land-derived material to the south or that an intervening deep (possibly a precursor of the Puerto Rico Trench) was present to cut off the supply of sediment from the Greater Antilles.

MIDDLE TO LATE EOCENE

The middle Eocene Datum A is the top of the stratified layer under the eastern Greater Antilles Outer Ridge, and it marks a distinct change from acoustically stratified to acoustically transparent sediment. It is suggested here that this acoustic dissimilarity also represents a change in depositional conditions and that Datum A marks the final stage of downslope sedimentation on the eastern sector of the Greater Antilles Outer Ridge. The formation of the Puerto Rico Trench may have proceeded far enough at this time to form a chasm along the southern portion of the eastern outer ridge, and it trapped sediments which were shed from the present region of Puerto Rico and the Virgin Islands (Fig. 8.2) (Tucholke and others, 1972). This timing for the formation of the Puerto Rico Trench is in general agreement with independent geologic evidence from Puerto Rico which dates initial trench formation as late

Eocene to Oligocene (Monroe, 1968).

If the stratified layer was deposited before the Puerto Rico Trench formed, its present flat layering indicates that the tectonic movement associated with trench formation was localized in the immediate area of the trench. There is some indication that normal faulting may have disturbed the stratified unit in a few places under the Greater Antilles Outer Ridge, much as it has on the north wall of the trench (Chase and Hersey, 1968), but this effect is not pronounced. Although the gentle northward slope of Datum A under the eastern Greater Antilles Outer Ridge may indicate that the sea floor was elevated there while the Puerto Rico Trench was forming, the slope may also represent the original attitude of the layering. Seismic profiles over the far eastern outer ridge show Datum A under the Nares Abyssal Plain but not under the Greater Antilles Outer Ridge (Fig. 3.5), suggesting that the basement ridge under the outer ridge was an elevated feature even before the Puerto Rico Trench formed. The possibility of transcurrent faulting associated with formation of the Puerto Rico Trench is largely eliminated by the presence of unbroken, northwest-southeast trending magnetic lineations across its present north slope (Griscom and Geddes, 1966).

Although the formation of the Puerto Rico Trench undoubtedly had a significant effect on mechanisms of sediment deposition on the Greater Antilles Outer Ridge,

there are also other factors which must be considered. The abyssal circulation of the North Atlantic probably was initiated sometime between Paleocene and middle Eocene time, when Greenland and Scandinavia separated far enough to allow cold dense water to invade the North Atlantic Basin from the Norwegian Sea (Jones and others, 1970; Berggren and Hollister, 1972; Ewing and Hollister, 1972). The introduction of this cold water mass probably correlates with the initiation of the Western Boundary Undercurrent, and we could expect that the WBUC was transporting sediment from the continental margin of North America to the Greater Antilles Outer Ridge by early to middle Eocene time. Furthermore, if Layer A in the South Atlantic is synchronous with Horizon A in the North Atlantic, as proposed by Le Pichon and others (1971), then the sequence of seismic reflectors recorded in Vema Channel in the South Atlantic suggests that Antarctic Bottom Water must also have entered the western North Atlantic basin about this time (Fig. 8.2). These abyssal-circulation/sedimentation events, together with the cessation of downslope sedimentation to the Greater Antilles Outer Ridge from Puerto Rico, are suggested here as the cause for the acoustic and compositional changes which are marked by Datum A.

The effect of these events on source areas for the sediment composing the Greater Antilles Outer Ridge is evident in data on sediment composition from DSDP Site 28

Figure 8.2. Synthesis of sea-floor morphology and sedimentation conditions in middle to late Eocene time. By this time, the Puerto Rico Trench had developed enough to cut off downslope sedimentation to the eastern sector of the Greater Antilles Outer Ridge, but turbidity currents continued to feed sediment to the Nares Abyssal Plain and the area of the present western ridge-sector. Antarctic Bottom Water was flowing westward into the North American Basin, and the Western Boundary Undercurrent was depositing the basal unit of the transparent layer.

MIDDLE TO LATE EOCENE

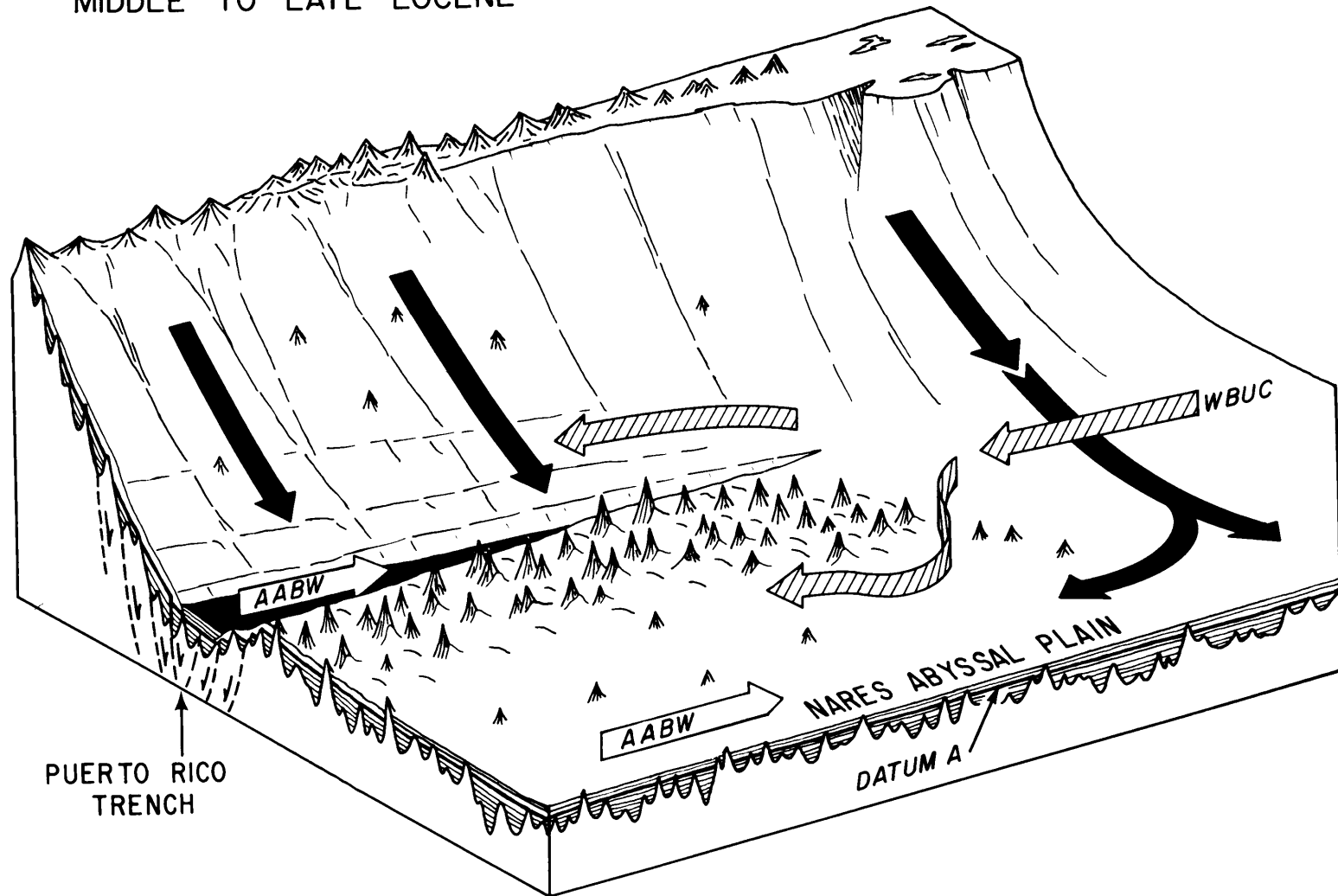


(Table 8.1). The interbedded silts and silty lutites below Datum A are enriched in carbonate, montmorillonite, and clinoptilolite, and thus form an assemblage which may have been derived largely from the volcanic ashes and carbonate banks of the Greater Antilles. In the overlying transparent layer, however, these components are rare, and they are replaced by a northern assemblage of minerals (quartz, mica, chlorite and plagioclase), which suggests current transportation of sediment. The low carbonate content of the homogeneous lutites in the transparent layer may also reflect increased dissolution by the cold abyssal currents.

As the juvenile Western Boundary Undercurrent encountered the elevated basement ridge structure which is presently under the eastern Greater Antilles Outer Ridge, and as it interacted with the AABW entering from the south, fine-grained sediments probably were deposited to form the earliest unit of the transparent layer (Fig. 8.2). This type of deposition was ubiquitous over the eastern sector of the Greater Antilles Outer Ridge, the north slope of the incipient Puerto Rico Trench, and the northern continental slope of Puerto Rico (south slope of the trench). It is proposed here that the sediment cover deposited by currents on the north slope of the Puerto Rico Trench during middle to late Eocene time represents the thin transparent layer which presently extends beneath the sediments of the Puerto Trench Abyssal Plain (Fig. 8.2) (Bunce and Hersey, 1966;

TABLE 8.1. COMPARISON OF SEDIMENT COMPOSITION ABOVE AND
BELOW DATUM A AT SITE 28*

Unit	Organic Carbon %	Carbonate %	Quartz %	Mica %	Chlorite %	Mont. %	Plagio. %	Clinop. %
Transparent Layer, Core 2, 68-77 m	0.0	1.4	34.8	15.8	23.1	0.0	21.1	0.0
Stratified Layer, Core 3, 170-178 m	0.3	27.8	6.3	0.0	7.9	28.8	0.2	7.8

* Figures are average compositions for Core 2, Sections 2-4, and Core 3, Sections 2-6.
Data are from Pimm (1970) and Rex and Murray (1970).

Chase and Hersey, 1968). The thin transparent layer observed in some places beneath the stratified sediments on the south slope of the Puerto Rico Trench (Ewing and others, 1968) may also have been deposited at this time, but most of the homogeneous sediment deposited there has probably been masked by downslope sediment movement or has itself slumped into the trench. Most of the transparent sediment deposited in the trench would be masked in a similar way.

Meanwhile, downslope sediment movement and turbidity currents from the area of the present southeastern Bahama Banks continued to deposit flat-lying, stratified sediments above Datum A in the region where the western Greater Antilles Outer Ridge now lies (Figs. 3.6, 3.7, 8.2). Although it is impossible to assess the extent of current deposition of lutite along the base of the Bahama Banks during this period, the lutite which was deposited there probably was eroded by turbidity currents and redeposited in the flat-lying sediments above Datum A under the present western Greater Antilles Outer Ridge. The restriction of these post-Datum A turbidites to the western ridge sector suggests that they may correlate with the 3.0 km/sec layer presently found under portions of the western Greater Antilles Outer Ridge (see Northrop and Ransone, 1962; Savit and others, 1964). Isolated pockets of current-deposited lutite, such as the one on the western side of the seamount in the Silver Abyssal Plain (Fig. 3.11), apparently formed despite the turbidity-current activity. The location and

configuration of this pocket of acoustically transparent sediment suggests that it is a foredrift deposited by the Western Boundary Undercurrent.

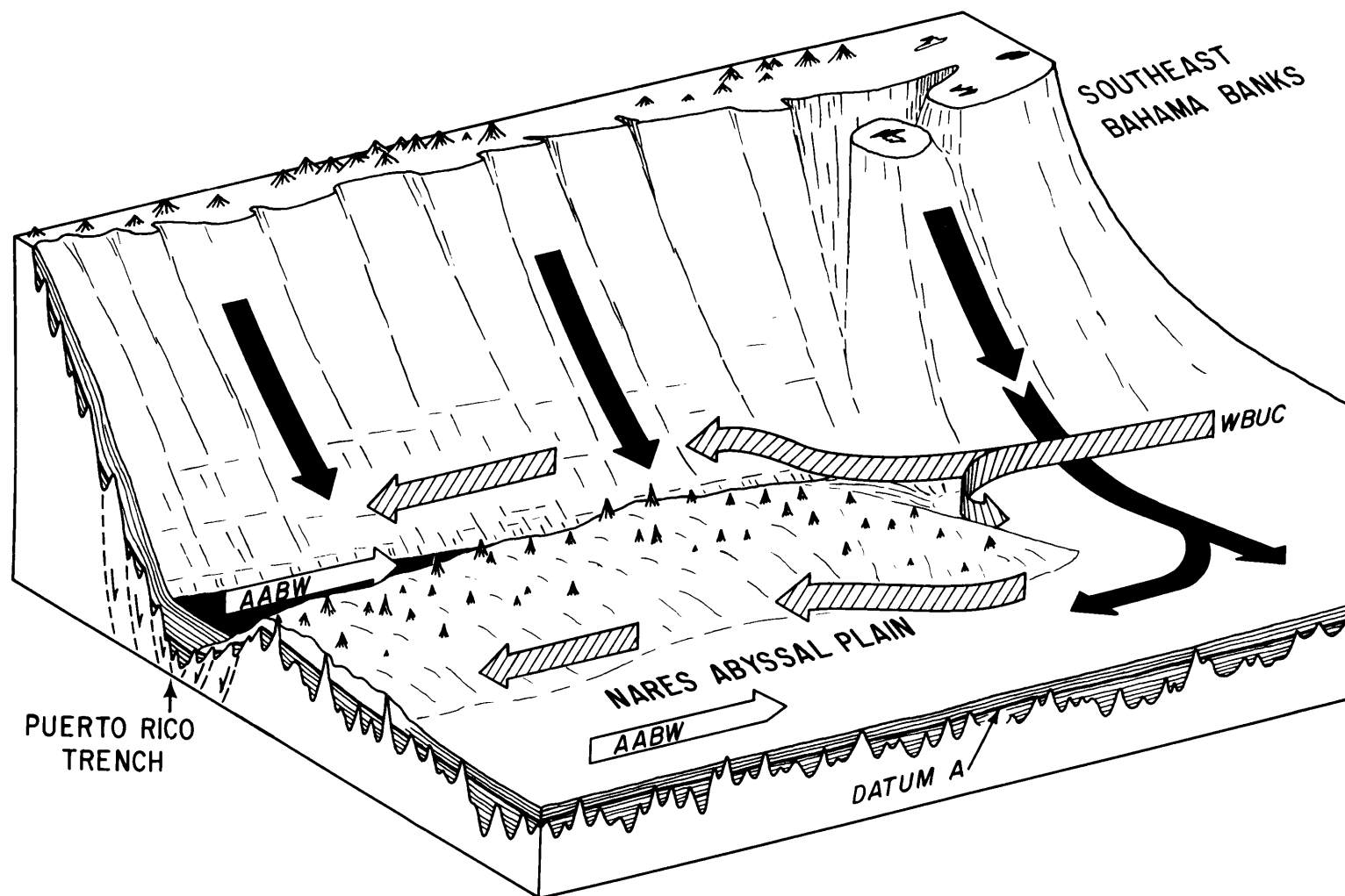
The Nares Abyssal Plain continued to receive sediments from turbidity currents, but the source area was now the Bahama Banks rather than the Puerto Rico-Virgin Islands platform (Fig. 8.2).

LATE EOCENE TO MIOCENE

As the Puerto Rico Trench continued to deepen and as the eastern Greater Antilles Outer Ridge was further constructed by current-controlled deposition, the resulting topography probably split the Western Boundary Undercurrent into two branches (Fig. 8.3), thereby isolating the north slope of the Puerto Rico Trench from current-controlled sedimentation. Since that time, probably only thin accumulations of pelagic sediment and ashes from episodic volcanic activity in the Greater Antilles have been deposited on the north slope. This is largely substantiated by the cores recovered from the north slope, which contain mostly altered ash and pelagic lutite of probable early and middle Tertiary age (see Chapter V). Furthermore, the high compressional-wave velocity which drilling at DSDP Site 28 indicated for the transparent layer on the north slope (> 2.1 km/sec) may reflect the relatively great age (and thus the advanced compaction) of this unit.

Figure 8.3. Schematic diagram of sedimentation on the Greater Antilles Outer Ridge in the late Oligocene. A substantial portion of the transparent layer was deposited on the eastern Greater Antilles Outer Ridge by late Oligocene time, interfingering with the abyssal plain deposits. Deposition rates had dropped sharply on the north slope of the Puerto Rico Trench as it became isolated from current-controlled deposition, and stratified sediments in the Puerto Rico Trench Abyssal Plain lapped onto the transparent layer there.

LATE OLIGOCENE



Downslope sedimentation covered the lutites deposited on the south slope of the Puerto Rico Trench, and the stratified sediments in the trench continued to lap onto the basal transparent layer on the north slope. Stratified sediments were deposited on the Nares Abyssal Plain contemporaneously with the transparent layer on the eastern Greater Antilles Outer Ridge, but at a lesser rate, resulting in an interfingering of the two units, with the transparent layer gradually overlapping the edge of the stratified sediments (Fig. 3.9). Maximum rates of sediment accumulation, and consequently the thickest sections of transparent sediment, were beneath the WBUC flowing along the north flank of the eastern Greater Antilles Outer Ridge.

The exact timing of formation of the northwestern extension of the Greater Antilles Outer Ridge is uncertain. Although the morphology of the eastern sector of the outer ridge might have diverted the northern limb of the Western Boundary Undercurrent to some extent (Fig. 8.3), it is doubtful that it turned the current far enough to create a northwest-trending depositional axis. However, the initiation of this depositional event may be estimated from other evidence.

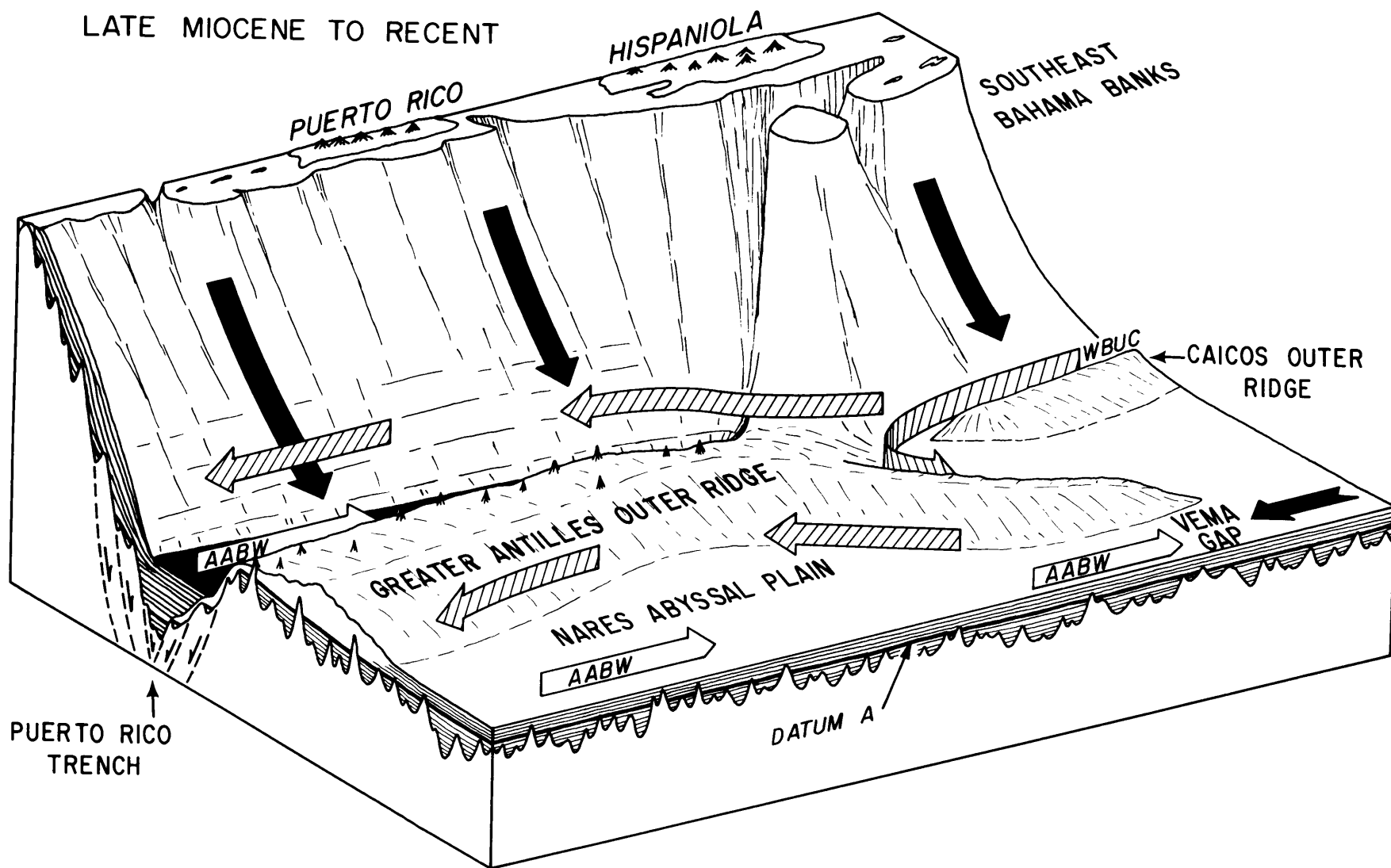
Recent results of deep-sea drilling off Antarctica (Hayes and others, 1973) suggest that Antarctic glaciation intensified in middle to late Miocene time. This event may have caused increased production of AABW, thus creating an

increased flow of AABW westward across the Nares Abyssal Plain into the North American Basin. If this flow was strong enough to divert the Western Boundary Undercurrent, it could have initiated deposition of the western Greater Antilles Outer Ridge out over flat-lying sediments (Figs. 3.7, 3.10, 8.4). Once the surface expression of the western sector of the outer ridge was established, abyssal currents would probably continue to follow the bathymetric contours and produce further construction of the outer ridge, much as we observe at the present time.

An independent, although very uncertain, estimate of the time of initial formation of the western Greater Antilles Outer Ridge can be derived from the 600 m thickness of transparent sediment above the uppermost, flat-lying reflector (Fig. 3.7). Assuming an average compressional wave velocity of 1.8 km/sec and assuming an average sedimentation rate of 5 cm/1000 yr (see Chapter V), the reflector would be about 12 m.y., or late middle Miocene in age.

During the period of increased AABW flow, the AABW input also may have intensified the Western Boundary Undercurrent, possibly causing the erosional conditions which created the angular unconformity under the Caicos Outer Ridge (Fig. 3.7) and left the base of the Bahama escarpment with a very thin sediment cover (Figs. 3.3, 3.7). The attitude of the reflectors in Figure 3.7 suggests that

Figure 8.4. Sketch showing the development of the Greater Antilles Outer Ridge from the late Miocene to the Recent. The western sector of the Greater Antilles Outer Ridge was probably built out over flat-lying sediments in middle to late Miocene time. Deposition of the Caicos Outer Ridge began shortly thereafter, and increased deposition occurred on the western Greater Antilles Outer Ridge, a condition which has persisted to the present.



sediment was being eroded in the region of the Caicos Outer Ridge at the same time that deposition was initiated on the western Greater Antilles Outer Ridge. The thin sediment cover on the sill south of the Silver Abyssal Plain may also be a result of erosion or nondeposition by the Western Boundary Undercurrent. Very slow deposition or erosion is indicated by the presence of the Datum A outcrop (Fig. 3.3) and the Oligocene/Miocene core (CH57-13) recovered from this area (see Chapter V).

A decrease in current velocities shortly after this time may have been responsible for sediment deposition on the Caicos Outer Ridge and increased sedimentation on the weakly developed western section of the Greater Antilles Outer Ridge. Golovchenko and others (1973) found that the Bahama Outer Ridge to the northwest began to develop above a late Miocene turbidite sequence, and they attribute its formation to deposition caused by decreased current velocities. Rapid sedimentation (19 cm/1000 yr) also occurred on the Blake Outer Ridge during the late Miocene (Ewing and Hollister, 1972), and the source of the sediment was the northeastern continental margin of North America (Habib, 1972).

The time of initial formation of the Caicos Outer Ridge, the Bahama Outer Ridge, and the western sector of the Greater Antilles Outer Ridge is roughly the same, and it is suggested here that all three features resulted from

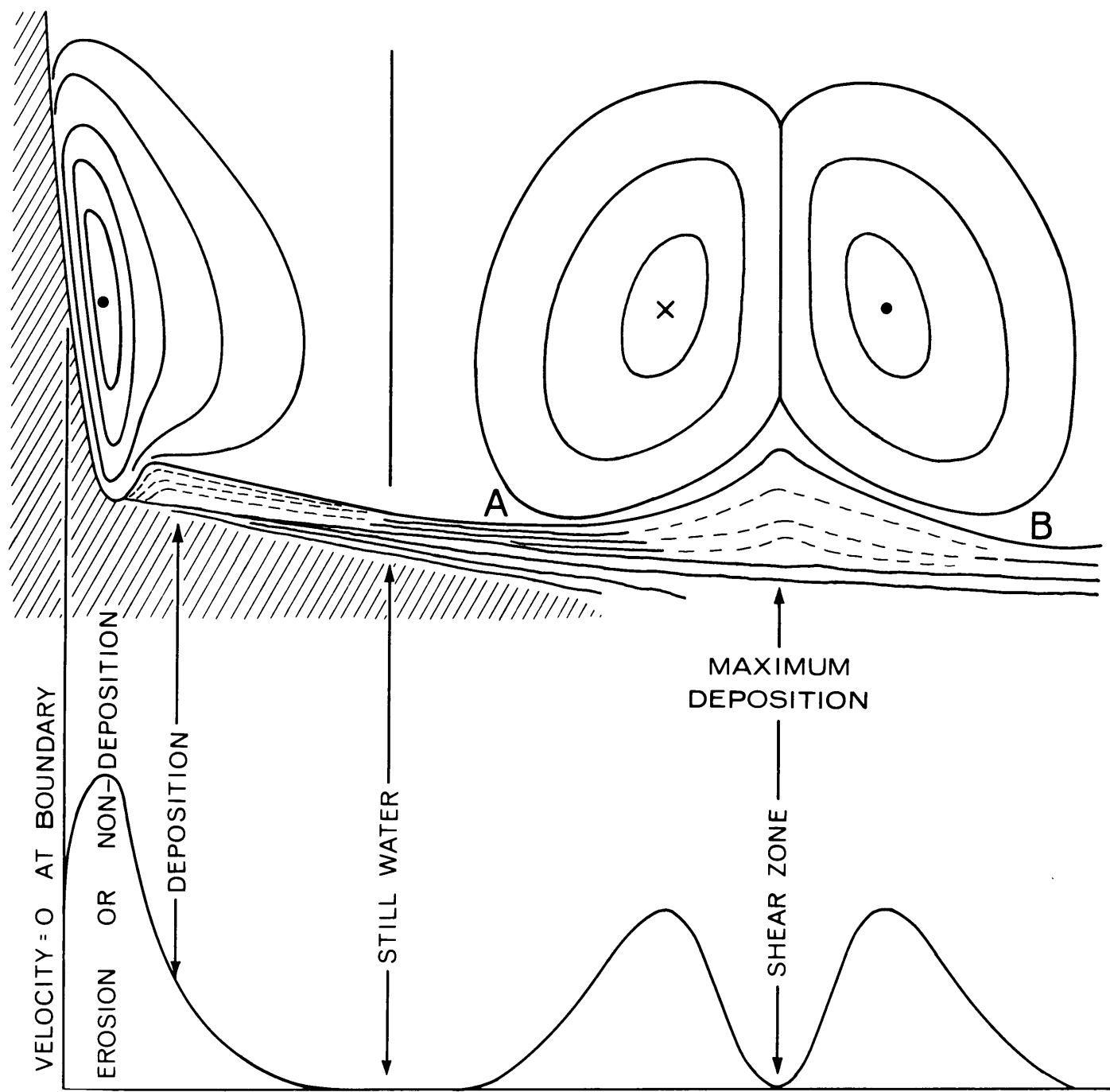
the same event of current-controlled sedimentation.

PLIOCENE TO RECENT

Since its initial development, the northwest trend of the western sector of the Greater Antilles Outer Ridge has apparently controlled the flow of the Western Boundary Undercurrent, and the outer ridge has continued to grow both upward and to the northwest through preferential deposition from the zone of current shear above its crest (Fig. 8.5). The configuration of seismic reflectors resolved within the transparent layer of the western Greater Antilles Outer Ridge and in the stratified sediments of the flanking abyssal plains (Fig. 3.10) demonstrates that the outer ridge has formed by preferential deposition rather than by erosion of a pre-existing sediment body. During the development of the Greater Antilles Outer Ridge, the zone of most rapid sediment accumulation has shifted toward the west, and it is now centered on the western sector of the outer ridge, although the eastern sector still accumulates sediment at a rate of several cm per thousand years.

At the present time, part of the Western Boundary Undercurrent probably still continues southeast toward Puerto Rico with high enough velocity to inhibit deposition on the sill near 21°N lat., 68°W long. Similarly, rapid currents along the Bahama escarpment probably prevent much deposition above the unconformity created by Miocene erosion (Figs. 3.7, 8.5). The definition of reflectors in the southern edge of

Figure 8.5. Idealized representation of the modern bottom-flow regime and erosional/depositional conditions across the Caicos Outer Ridge (left) and Greater Antilles Outer ridge (right) (compare with Fig. 3.7). Dots represent currents flowing toward the reader; x's are currents flowing away. Maximum deposition occurs in places where current speeds drop far enough that the currents are not competent to carry their suspended load. For similar models, see Davies and Laughton (1972).



the Caicos Outer Ridge is sufficient on the full-scale profile to show that the absence of sediment at the base of the Bahama Banks is due to nondeposition rather than erosion.

Where the current decreases in intensity away from the steep slope of the Bahama Banks and interacts with the "still" water to the north, deposition is rapid and has formed the Caicos Outer Ridge (Fig. 8.5). The zone of interaction or shear between the opposing sediment-laden currents on the north and south flanks of the western Greater Antilles Outer Ridge is also associated with very rapid deposition of sediment.

It is puzzling that depositional ridges have not formed in the zones where these currents interact with water over the Silver Abyssal Plain and central Vema Gap (points A and B in Fig. 8.5). Deposition of turbidites in Vema Gap and on the Silver Abyssal Plain, especially during the Pleistocene, may have been sufficient to cover or eradicate any small ridges formed by the contour-following flow. It is equally likely that the flow boundaries at A and B shift frequently in a N-S direction, much as the WBUC-AABW boundary over the Nares Abyssal Plain shifts, so that thin lutite layers rather than distinct ridges are formed. Where the flow is more constrained by topography, i.e. against the Bahama Banks and on the Greater Antilles Outer Ridge, the depositional axis is more stable.

The sediment swells or dunes which form the present surface of the Greater Antilles Outer Ridge, and which also

formed earlier depositional surfaces (Fig. 3.13), are most reasonably explained by current activity. There is no strongly pronounced pattern in the configuration of the swells, and we cannot rule out the possibility that periodic erosion has modified their structure. However, current speeds higher than those on the outer ridge at present (2-18 cm/sec) would probably be required to erode this fine-grained, cohesive sediment. Also, the probable shifts in current boundaries and in the shear zone between flows may obscure or prevent formation of a regular pattern of dunes. In addition, the nature of the fine-grained sediment itself may not be conducive to formation of a series of regular dunelike features.

COMPARISON WITH OTHER DEPOSITIONAL RIDGES

Some similarities between the Greater Antilles Outer Ridge and other depositional ridges in the North and South Atlantic Oceans have been noted; this section briefly describes the similarities and dissimilarities of the depositional ridges affected by the Western Boundary Undercurrent, which is here considered to extend from the Norwegian Sea overflow at least as far south as the Greater Antilles Outer Ridge.

As might be expected, the greatest dissimilarities among depositional ridges in the North Atlantic are in sediment composition, since sediment sources as well as patterns and intensities of bottom circulation vary greatly.

Detailed compositional comparisons are beyond the scope of this discussion, and the reader is referred to Hollister and others (1972) and Laughton and others (1972) for descriptions of sediments composing the Blake-Bahama Outer Ridge, Gardar Ridge, and other depositional ridges in the northernmost Atlantic. However, it is noteworthy that organic carbon is enriched in the sediments of the Blake-Bahama Outer Ridge, where values as high as 1.3% have been reported, although most values are less than 1.0% (Boyce, 1972). The even greater values of organic carbon encountered in sediments from the Greater Antilles Outer Ridge may indicate that a large amount of very fine carbonaceous material is transported beyond the continental rise at least as far as the Greater Antilles Outer Ridge.

All of the depositional ridges in the North Atlantic appear to share certain characteristics which can be identified in seismic reflection profiles (Davies and Laughton, 1972).

1) The sediments composing the ridges are relatively transparent (acoustically). This transparency is most pronounced in seismic profiles taken over the Greater Antilles Outer Ridge, while other ridges such as the Gardar, Feni, Eirik, and Blake-Bahama ridges have weak to moderate internal reflectors (Jones and others, 1970; Davies and Laughton, 1972; Ewing and Hollister, 1972). The difference is probably related to the fine grain-size and

homogeneity of the sediments on the Greater Antilles Outer Ridge; the other depositional ridges often contain weakly bedded lutite, silt, and occasionally sand.

2) The sediments are seldom conformable to deeper strong reflectors, but are deposited in piles and ridges where current velocities fall below those necessary to transport the particular grain-size of sediment being carried (Fig. 8.5).

3) The upper surface of the depositional ridges commonly exhibits regular to irregular sediment swells. The swells observed on the Greater Antilles Outer Ridge have been discussed, and striking examples also occur on the Blake-Bahama Outer Ridge (Markl and others, 1970), and on other ridges in the northern North Atlantic (Davies and Laughton, 1972).

4) Marginal channels or moats are frequently developed where the sediment body encounters basement highs, and the sediments may thin or dip toward the obstacle. This characteristic is seldom observed on the Greater Antilles Outer Ridge, the best examples being shown in Figures 3.8 and 3.9, and in Plate 4 of Bunce and Hersey (1966).

Another common characteristic of these depositional ridges is their high rate of sediment accumulation (several cm to tens of cm per thousand years). While rates of accumulation can be roughly estimated by tracing reflectors of known age in some seismic reflection profiles, they

normally must be determined by coring or drilling.

Finally, the age of the depositional ridges must be considered. The evidence presently available from deep-sea drilling and interpretation of seismic profiles suggests that the depositional ridges in the northern North Atlantic and Labrador Sea probably began to form in Paleocene time or later (Davies and Laughton, 1972; Jones and others, 1970). The Blake-Bahama Outer Ridge has developed above Horizon A and thus probably began to form in the early Tertiary (Ewing and Hollister, 1972); the Greater Antilles Outer Ridge is interpreted to be sediment deposited since middle Eocene time. The available evidence therefore indicates that the construction of sedimentary ridges by the Western Boundary Undercurrent began in Paleocene to Eocene time.

SUGGESTIONS FOR FUTURE WORK

Although considerable data have been collected and studied to reconstruct the history of sedimentation and abyssal circulation in the region of the Greater Antilles Outer Ridge, there are several lines of inquiry that would help clarify the hypotheses outlined in this manuscript.

1) North Slope - Puerto Rico Trench:

Although this region is covered largely by barren abyssal lutites, long piston cores taken in areas shallower than about 5500 meters might contain enough biogenous carbonate to date the sediment and test the low post-Eocene sedimentation rates postulated here.

2) South Slope - Puerto Rico Trench:

Deep hydrographic sections extending north from Puerto Rico are needed to delineate the possible flow of the Western Boundary Undercurrent in this area. Similar sections are also needed north of the Bahama Banks between Cat Gap and the Caicos Outer Ridge. Study of cores taken from the south slope of the Puerto Rico Trench may also reveal current-produced primary structures related to the flow of the WBUC.

3) Eastern Sector - Greater Antilles Outer Ridge:

A carefully chosen and continuously cored deep-sea drill hole near the crest of the outer ridge could fully establish a) the depositional history of the transparent layer, b) similar information for Datum A and the underlying stratified layer, and c) the composition and probable age of acoustic basement.

4) Western Sector - Greater Antilles Outer Ridge:

Deep-sea drilling on the southern flank of this sector could establish the time of ridge formation, the presence or absence of the 3.0 km/sec layer, the age of Datum A, and the history of downslope sedimentation from the Bahama Banks.

REFERENCES CITED

- Amos, A.F. and E.C. Escowitz (1971) Abyssal water circulation and spreading of Antarctic Bottom Water in the western North Atlantic: *Trans. Am. Geophys. Union*, v. 52, p. 241-242.
- Amos, A.F., A.L. Gordon and E.D. Schneider (1971) Water masses and circulation patterns in the region of the Blake-Bahama Outer Ridge: *Deep-Sea Res.*, v. 18, p. 145-166.
- Arrhenius, G. (1963) Pelagic sediments: *in* Hill, M.N. (ed.), *The Sea*, Interscience Publ., New York, v. 3, p. 655-727.
- Bader, R.G., R.D. Gerard, W.E. Benson, H.M. Bolli, W.W. Hay, W.T. Rothwell, Jr., M.H. Ruef, W.R. Riedel and F.L. Sayles (1970) Site 28: *in* Bader, R.G. and others, *Initial Reports of the Deep Sea Drilling Project, U.S. Gov't. Printing Office, Washington*, v. 4, p. 125-143.
- Barrett, J.R., Jr. (1965) Subsurface currents off Cape Hatteras: *Deep-Sea Res.*, v. 12, p. 173-184.
- Beal, A.W.H., J.M. Forns and O.A. Roels (1971) Plankton abundance in the North Atlantic Ocean: *in* Costlow, J.D. (ed.), *Fertility of the Sea*, Gordon and Breach, New York, v. 1, p. 17-50.
- Berger, W.H. (1968) Planktonic Foraminifera: selective solution and paleoclimatic interpretation: *Deep-Sea Res.*, v. 15, p. 31-43.
- Berggren, W.A., J.D. Phillips, A. Bertels and D. Wall (1967) Late Pliocene-Pleistocene stratigraphy in deep sea cores from the south-central North Atlantic: *Nature*, v. 216, p. 253-254.
- Berggren, W.A. and C.D. Hollister (1972) Biostratigraphy and circulation history of the North Atlantic: *in* Hay, W.W. (ed.), *Geological History of Oceans*, Soc. Econ. Paleontologists and Mineralogists Spec. Paper (in press).
- Biscaye, P.E. (1964) Distinction between kaolinite and chlorite in Recent sediments by x-ray diffraction: *Am. Mineralogist*, v. 49, p. 1281-1289.
- Biscaye, P.E. (1965) Mineralogy and sedimentation of Recent deep-sea clay in the Atlantic Ocean and adjacent seas and oceans: *Geol. Soc. America Bull.*, v. 76, p. 803-832.

- Biscaye, P.E. and S.L. Eittreim (1973) Short-term variability of bottom boundary layer phenomena: North American Basin: Trans. Am. Geophys. Union, v. 54, p. 321.
- Bouma, A.H. (1962) Sedimentology of some flysch deposits, Elsevier Publ. Co., New York, 168 pp.
- Bouma, A.H. and C.D. Hollister (1973) Deep ocean basin sedimentation: in Turbidites and deep-water sedimentation, short course, Pacific Section SEPM, p. 79-118.
- Bowin, C.O., A.J. Nalwalk and J.B. Hersey (1966) Serpentinized peridotite from the north wall of the Puerto Rico Trench: Geol. Soc. America Bull., v. 77, p. 257-270.
- Boyce, R.E. (1972) Carbon and carbonate analyses, Leg 11: in Hollister, C.D., Ewing, J.I. and others, Initial Reports of the Deep Sea Drilling Project, U.S. Gov't. Printing Office, Washington, v. 11, p. 1059-1071.
- Broecker, W.S., R. Gerard, M. Ewing and B.C. Heezen (1960) Natural radiocarbon in the Atlantic Ocean: Jour. Geophys. Res., v. 65, p. 2903-2931.
- Broecker, W.S. and J. van Donk (1970) Insolation changes, ice volumes, and the O^{18} record in deep-sea cores: Reviews Geophys. and Space Physics, v. 8, p. 169-198.
- Bruce, J.G. (1964) Deep current measurements north of Puerto Rico: Woods Hole Oceanogr. Inst. Ref. #64-34, 26 pp. (unpublished manuscript).
- Buchan, S., F. Dewes, D.M. McCann and D.T. Smith (1967) Measurements of the acoustic and geotechnical properties of marine sediment cores: in Richards, A.F. (ed.), Marine Geotechnique, Univ. of Illinois Press, Chicago, p. 65-92.
- Bunce, E.T. and D.A. Fahlquist (1962) Geophysical investigation of the Puerto Rico Trench and Outer Ridge: Jour. Geophys. Res., v. 67, p. 3955-3972.
- Bunce, E.T. and J.B. Hersey (1966) Continuous seismic profiles of the Outer Ridge and Nares Basin north of Puerto Rico: Geol. Soc. America Bull., v. 77, p. 803-812.
- Bunce, E.T., D.A. Fahlquist and J.W. Clough (1969) Seismic refraction and reflection measurements - Puerto Rico outer ridge: Jour. Geophys. Res., v. 74, p. 3082-3094.

- Bunce, E.T., J.D. Phillips and R.L. Chase (1973) Geophysical study of the Antilles Outer Ridge, the Puerto Rico Trench, and the northeast margin of the Caribbean Sea: Am. Assoc. Petroleum Geologists Bull., v. 57 (in press).
- Chase, R.L., E.T. Bunce, S.T. Knott and F.B. Wooding (1966) Partly filled submarine valleys of the Outer Ridge north of Puerto Rico (abstract): Geol. Soc. America Abs. with Programs, Ann. Mtg. 1966, p. 37-38.
- Chase, R.L. and J.B. Hersey (1968) Geology of the north slope of the Puerto Rico Trench: Deep-Sea Res., v. 15, p. 297-317.
- Davies, T.A. and A.S. Laughton (1972) Sedimentary processes in the North Atlantic: in Laughton, A.S., Berggren, W.A. and others, Initial Reports of the Deep Sea Drilling Project, U.S. Gov't. Printing Office, Washington, v. 12, p. 905-934.
- Denham, C.R. (1973) Giant core reversed polarity event 10^5 years B.P.: Trans. Am. Geophys. Union, v. 54, p. 255.
- Einstein, H.A. and R.B. Krone (1962) Experiments to determine modes of cohesive sediment transport in salt water: Jour. Geophys. Res., v. 67, p. 1451-1461.
- Eittrheim, S.L., M. Ewing and E.M. Thorndike (1969) Suspended matter along the continental margin of the North American Basin: Deep-Sea Res., v. 16, p. 613-624.
- Eittrheim, S.L. and M. Ewing (1972) Suspended particulate matter in the deep waters of the North American Basin: in Gordon, A.L. (ed.), Studies in Physical Oceanography, Gordon and Breach, New York, v. 2, p. 123-167.
- Eittrheim, S.L., P.E. Biscaye and A.F. Amos (1973) Time variations in the nepheloid layer of the North American Basin: Trans. Am. Geophys. Union, v. 54, p. 321.
- Emery, K.O., E. Uchupi, J.D. Phillips, C.O. Bowin, E.T. Bunce and S.T. Knott (1970) Continental rise off eastern North America: Am. Assoc. Petroleum Geologists Bull., v. 54, p. 44-108.
- Emiliani, C. (1971) The last interglacial: paleotemperatures and chronology: Science, v. 171, p. 571-573.
- Ericson, D.B., M. Ewing and B.C. Heezen (1952) Turbidity currents and sediments in the North Atlantic: Am. Assoc. Petroleum Geologists Bull., v. 36, p. 489-511.

- Ericson, D.B., M. Ewing, G. Wollin and B.C. Heezen (1961) Atlantic deep-sea sediment cores: Geol. Soc. America Bull., v. 72, p. 193-286.
- Ericson, D.B., M. Ewing and G. Wollin (1964) The Pleistocene epoch in deep-sea sediments: Science, v. 146, p. 723-732.
- Ericson, D.B. and G. Wollin (1968) Pleistocene climates and chronology in deep-sea sediments: Science, v. 162, p. 1227-1234.
- Ewing, J.I. and M. Ewing (1962) Reflection profiling in and around the Puerto Rico Trench: Jour. Geophys. Res., v. 67, p. 4729-4739.
- Ewing, J.I., J.L. Worzel, M. Ewing and C. Windisch (1966) Ages of Horizon A and the oldest Atlantic sediments: Science, v. 154, p. 1125-1132.
- Ewing, J.I., C. Windisch and M. Ewing (1970) Correlation of Horizon A with Joides bore-hole results: Jour. Geophys. Res., v. 75, p. 5645-5653.
- Ewing, J.I. and C.D. Hollister (1972) Regional aspects of deep sea drilling in the western North Atlantic: in Hollister, C.D., Ewing, J.I., and others, Initial Reports of the Deep Sea Drilling Project, U.S. Gov't. Printing Office, Washington, v. 11, p. 951-973.
- Ewing, M., A. Lonardi and J.I. Ewing (1968) The sediments and topography of the Puerto Rico Trench and Outer Ridge: Trans. Fourth Caribbean Geol. Conf., Trinidad, 1965, p. 325-334.
- Ewing, M. and F. Mouzo (1968) Ocean bottom photographs in the area of the oldest known outcrops, North Atlantic Ocean: Proc. Nat. Acad. Sci., v. 61, p. 787-793.
- Ewing, M., S. Eittreim, M. Truchan and J.I. Ewing (1969) Sediment distribution in the Indian Ocean: Deep-Sea Res., v. 16, p. 231-248.
- Ewing, M., S.L. Eittreim, J.I. Ewing and X. Le Pichon (1971) Sediment transport and distribution in the Argentine Basin. 3. Nepheloid layer and processes of sedimentation: in Ahrens, L.H., and others (eds.), Physics and Chemistry of the Earth, Pergamon Press, New York, v. 8, p. 3-28.
- Frassetto, R. and J. Northrop (1957) Virgin Islands bathymetric survey: Deep-Sea Res., v. 4, p. 138-146.

- Fuglister, F.C. (1960) Atlantic Ocean Atlas of temperature and salinity profiles and data from the International Geophysical Year of 1957-1958: Woods Hole Oceanogr. Inst. Atlas Series, v. 1, 209 pp.
- Golovchenko, X., R.E. Sheridan and J.I. Ewing (1973) Late Cenozoic history of sedimentation in the Blake-Bahama Basin: Trans. Am. Geophys. Union, v. 54, p. 336.
- Griffin, G.M. and R.L. Ingram (1955) Clay minerals of the Neuse River estuary: Jour. Sed. Petrology, v. 25, p. 194-200.
- Griscom, A. and W.H. Geddes (1966) Island-arc structure interpreted from aeromagnetic data near Puerto Rico and the Virgin Islands: Geol. Soc. America Bull., v. 77, p. 153-162.
- Habib, D. (1972) Dinoflagellate stratigraphy Leg 11, Deep Sea Drilling Project: in Hollister, C.D., J.I. Ewing and others: Initial Reports of the Deep Sea Drilling Project, U.S. Gov't. Printing Office, Washington, v. 11, p. 367-425.
- Hamilton, E.L. (1970) Sound velocity and related properties of marine sediments, North Pacific: Jour. Geophys. Res., v. 75, p. 4423-4446.
- Hathaway, J.C. (1972a) Regional clay mineral facies in estuaries and continental margin of the United States east coast: Geol. Soc. America Mem. 133, p. 293-316.
- Hathaway, J.C. (1972b) X-ray mineralogical studies - Leg 11, Part 2: in Hollister, C.D., J.I. Ewing and others, Initial Reports of the Deep Sea Drilling Project, U.S. Gov't. Printing Office, Washington, v. 11, p. 772-789.
- Hayes, D.E., L.A. Frakes, P. Barrett, D.A. Burns, P. Chen, A.B. Ford, A.G. Kaneps, E.M. Kemp, D.W. McCollum, D.J.W. Piper, R.E. Wall and P.N. Webb (1973) Leg 28 deep-sea drilling in the southern ocean: Geotimes, (June), p. 19-24.
- Heezen, B.C. and H.W. Menard (1963) Topography of the deep-sea floor: in Hill, M.N. (ed.), The Sea, Interscience Publ., New York, v. 3, p. 233-280.
- Heezen, B.C., C.D. Hollister and W.F. Ruddiman (1966) Shaping of the continental rise by deep geostrophic contour currents: Science, v. 152, p. 502-508.
- Heezen, B.C. and C.D. Hollister (1971) The Face of the Deep, Oxford University Press, New York, 659 pp.

- Hersey, J.B. (1965) Sediment ponding in the deep sea: Geol. Soc. America Bull., v. 76, p. 1251-1260.
- Hollister, C.D. (1967) Sediment distribution and deep circulation in the western North Atlantic: unpublished Ph.D. Dissertation, Columbia University, New York.
- Hollister, C.D. and B.C. Heezen (1972) Geological effects of ocean bottom currents: western North Atlantic: in Gordon, A.L. (ed.), Studies in Physical Oceanography, Gordon and Breach, New York, v. 2, p. 37-66.
- Hollister, C.D., J.I. Ewing, D. Habib, J.C. Hathaway, Y. Lancelot, H. Luterbacher, F.J. Paulus, C.W. Poag, J.A. Wilcoxon and P. Worstell (1972) Sites 102-103-104-Blake-Bahama Outer Ridge (northern end): in Hollister, C.D., J.I. Ewing and others, Initial Reports of the Deep Sea Drilling Project, U.S. Gov't. Printing Office, Washington, v. 11, p. 135-218.
- Hoskins, H. (1967) Seismic reflection observations on the Atlantic continental shelf, slope, and rise southeast of New England: Jour. Geology, v. 75, p. 598-611.
- Jacobs, M.B. and M. Ewing (1965) Mineralogy of particulate matter suspended in sea water: Science, v. 149, p. 179-180.
- Jacobs, M.B. (1970) Clay mineral investigations of Cretaceous and Quaternary deep sea sediments of the North American Basin: Jour. Sed. Petrology, v. 40, p. 864-868.
- Johnson, G.L. and P.R. Vogt (1971) Morphology of the Bermuda Rise: Deep-Sea Res., v. 18, p. 605-617.
- Jonas, E.C. and H.E. Roberson (1960) Particle size as a factor influencing expansion of the three-layer clay minerals: Am. Mineralogist, v. 45, p. 828-838.
- Jonas, E.C. and R.M. Oliver (1967) Size and shape of montmorillonite crystallites: Clays and Clay Minerals, Proc. 15th Clay Minerals Conf., Pergamon Press, New York, p. 27-33.
- Jones, E.J.W., M. Ewing, J.I. Ewing and S.L. Eittreim (1970) Influences of Norwegian Sea overflow water on sedimentation in the northern North Atlantic and Labrador Sea: Jour. Geophys. Res., v. 75, p. 1655-1680.
- Justin, G.M. and M.L. Tefft (1966) Improved accuracy of rapid micro carbon and hydrogen method by modified combustion-absorption techniques: Microchemical Jour., v. 10, p. 236-243.

- Kennett, J.P. and P. Huddleston (1972) Late Pleistocene paleoclimatology, foraminiferal biostratigraphy and tephrochronology, western Gulf of Mexico: *Quaternary Res.*, v. 2, p. 38-69.
- Konrad, J.G., G. Chesters and D.R. Keeney (1970) Determination of organic- and carbonate-carbon in freshwater lake sediments by a microcombustion procedure: *Jour. Thermal Anal.*, v. 2, p. 199-208.
- Kuenen, Ph.H. (1965) Experiments in connection with turbidity currents and clay suspensions: in Whittard, W.F. and R. Bradshaw (eds.), *Submarine Geology and Geophysics*, Colston Papers, v. 17, p. 47-71.
- Lafond, E.C. (1951) Processing oceanographic data: U.S. Navy Hydrographic Office Publ. 614, 114 pp.
- Laughton, A.S., W.A. Berggren, R.N. Benson, T.A. Davies, U. Franz, L.F. Musich, K. Perch-Nielsen, A.S. Ruffman, J.E. van Hinte and R.B. Whitmarsh (1972) Initial Reports of the Deep Sea Drilling Project, U.S. Gov't. Printing Office, Washington, v. 12, 1243 pp.
- Le Pichon, X., S.L. Eittreim and W.J. Ludwig (1971) Sediment transport and distribution in the Argentine Basin. 1. Antarctic Bottom Current passage through the Falkland Fracture Zone: in Ahrens, L.H., and others (eds.), *Physics and Chemistry of the Earth*, Pergamon Press, New York, v. 8, p. 3-28.
- Lisitzin, A.P. (1972) Sedimentation in the World Ocean: *Soc. Economic Paleontologists and Mineralogists Spec. Publ.* 17, 218 pp.
- Ludwig, W.J., J.E. Nafe and C.L. Drake (1970) Seismic refraction: in Maxwell, A.E. (ed.), *The Sea*, Wiley-Interscience, New York, v. 4, p. 53-84.
- Markl, R.G., G.M. Bryan and J.I. Ewing (1970) Structure of the Blake-Bahama Outer Ridge: *Jour. Geophys. Res.*, v. 75, p. 4539-4555.
- Matthews, D.J. (1939) Tables of the velocity of sound in pure water and sea water for use in echo sounding and echo ranging: Admiralty Hydrographic Dept., London, 52 p.
- Mattson, P.H. and E.A. Pessagno, Jr. (1971) Caribbean Eocene volcanism and the extent of Horizon A: *Science*, v. 174, p. 138-139.

- McCullough, J.R. and G.H. Tupper (1969) Summary of current meter operations in 1968. Woods Hole Oceanogr. Inst. Ref. #69-14, 25 pp. (unpublished manuscript).
- Metcalf, W.G. (1969) Dissolved silicate in the deep North Atlantic: Deep-Sea Res., Suppl. to v. 16, p. 139-145.
- Monroe, W.H. (1968) The age of the Puerto Rico Trench: Geol. Soc. America Bull., v. 79, p. 487-494.
- Needham, H.D., D. Habib and B.C. Heezen (1969) Upper Carboniferous palynomorphs as a tracer of red sediment dispersal patterns in the northwest Atlantic: Jour. Geology, v. 77, p. 113-120.
- Northrop, J. and M. Ransone (1962) Some seismic profiles near the western end of the Puerto Rico Trench: Jour. Gen. Physiology, v. 45, p. 243-251.
- Partheniades, E. (1962) A study of erosion and deposition of cohesive soils in salt water: unpublished Ph.D. Dissertation, University of California, Berkeley.
- Pimm, A.C. (1970) Carbon carbonate results, Leg 4: in Bader, R.G. and others, Initial Reports of the Deep Sea Drilling Project, U.S. Gov't. Printing Office, Washington, v. 4, p. 307-314.
- Pitman, W.C., III and M. Talwani (1972) Sea-floor spreading in the North Atlantic: Geol. Soc. America Bull., v. 83, p. 619-646.
- Postma, H. (1967) Sediment transport and sedimentation in the estuarine environment: in Lauff, G.H. (ed.), Estuaries, American Assoc. for the Advancement of Science, Washington, p. 158-179.
- Powers, M.C. (1957) Adjustment of land-derived clays to the marine environment: Jour. Sed. Petrology, v. 27, p. 355-372.
- Raith, R.W. (1963) The crustal rocks: in Hill, M.N. (ed.), The Sea, Interscience Publ., New York, v. 3, p. 85-102.
- Rateev, M.A., Z.N. Gorbunova, A.P. Lisitzin and G.I. Nosov (1966) Climatic distribution zonality of clay minerals in sediments of the World Ocean (in Russian): Litol. i Polez. Iskopy., no. 3.
- Rex, R.W. and B. Murray (1970) X-ray mineralogy studies, Leg 4: in Bader, R.G. and others, Initial Reports of the Deep Sea Drilling Project, U.S. Gov't. Printing Office, Washington, v. 4, p. 325-369.

- Reynolds, R.C. and J.. Hower (1970) The nature of interlayering in mixed-layer illite-montmorillonites: *Clays and Clay Min.*, v. 18, p. 25-36.
- Richards, A.F. (1962) Investigations of deep-sea sediment cores, II. Mass physical properties: U.S. Navy Hydrographic Office Technical Report 106, 146 pp.
- Richardson, P.L. and J.A. Knauss (1971) Gulf stream and Western Boundary Undercurrent observation at Cape Hatteras: *Deep-Sea Res.*, v. 18, p. 1089-1110.
- Rowe, G.T. and R.J. Menzies (1969) Zonation of large benthic invertebrates in the deep-sea off the Carolinas: *Deep-Sea Res.*, v. 16, p. 531-537.
- Rowe, G.T. (1971) Benthic biomass and surface productivity: in Costlow, J.D. (ed.), *Fertility of the Sea*, Gordon and Breach, New York, v. 2, p. 441-454.
- Ruddiman, W.F. (1971) Pleistocene sedimentation in the equatorial Atlantic: stratigraphy and faunal paleoclimatology: *Geol. Soc. America Bull.*, v. 82, p. 283-302.
- Ryther, J.H. and D.W. Menzel (1960) The seasonal and geographic range of primary production in the western Sargasso Sea: *Deep-Sea Res.*, v. 6, p. 235-238.
- Savit, C.H., W.A. Knox, D.M. Blue and L. Paitson (1964) Reflection and velocity profiles at the Outer Ridge, Puerto Rico: *Jour. Geophys. Res.*, v. 69, p. 701-719.
- Schneider, E.D. and B.C. Heezen (1966) Sediments of the Caicos Outer Ridge, the Bahamas: *Geol. Soc. America Bull.*, v. 77, p. 1381-1398.
- Schuchert, C. (1968) *Historical Geology of the Antillean-Caribbean Region*, Hafner Publ. Co., New York, 811 pp.
- Smith, J.D. and J.H. Foster (1969) Geomagnetic reversal in Brunhes normal polarity epoch: *Science*, v. 163, p. 565-567.
- Southard, J.B., R.A. Young and C.D. Hollister (1971) Experimental erosion of calcareous ooze: *Jour. Geophys. Res.*, v. 76, p. 5903-5909.
- Spencer, D.W. and P.L. Sachs (1970) Some aspects of the distribution, chemistry, and mineralogy of suspended matter in the Gulf of Maine: *Marine Geol.*, v. 9, p. 117-136.

- Swallow, J.C. and L.V. Worthington (1961) An observation of a deep counter-current in the western North Atlantic: Deep-Sea Res., v. 8, p. 1-19.
- Swallow, J.C. and L.V. Worthington (1969) Deep currents in the Labrador Sea: Deep-Sea Res., v. 16, p. 77-84.
- Todd, R. and D. Low (1964) Cenomanian (Cretaceous) Foraminifera from the Puerto Rico Trench: Deep-Sea Res., v. 11, p. 395-414.
- Tolstoy, I. (1951) Submarine topography in the North Atlantic: Geol. Soc. America Bull., v. 62, p. 441-450.
- Tucholke, B.E. and C.D. Hollister (1970) Deposition and composition of acoustically transparent deep-sea sediments (Greater Antilles Outer Ridge) (abstract): Geol. Soc. America Abs. with Programs, v. 2, p. 710.
- Tucholke, B.E., C.D. Hollister and J.I. Ewing (1972) Deep circulation and sedimentation north of Puerto Rico (abstract): Geol. Soc. America Abs. with Programs, v. 4, p. 693.
- Tucholke, B.E., W.R. Wright and C.D. Hollister (1973) Abyssal circulation over the Greater Antilles Outer Ridge: Deep-Sea Res., v. 20 (in press).
- Uchupi, E., J.D. Milliman, B.P. Luyendyk, C.O. Bowin and K.O. Emery (1971) Structure and origin of southeastern Bahamas: Am. Assoc. Petroleum Geologists Bull., v. 55, 687-704.
- Volkman, G.H. (1962) Deep current observations in the western North Atlantic: Deep-Sea Res., v. 9, p. 493-500.
- Weyl, R. (1968) Volcanoes and volcanic rocks in Central America and the West Indies: Trans. Fourth Caribbean Geol. Conf., Trinidad, 1965, p. 357-360.
- Windisch, C.C., R.J. Leyden, J.L. Worzel, T. Saito and J.I. Ewing (1968) Investigation of Horizon Beta: Science, v. 162, p. 1473-1479.
- Worthington, L.V. and W.G. Metcalf (1961) The relationship between potential temperature and salinity in deep Atlantic water: Rapp. Proc. - v. Comb. int. Explor. Mer., v. 149, p. 122-128.
- Worthington, L.V. (1969) The Norwegian Sea as a Mediterranean basin: Deep-Sea Res., v. 16, p. 77-84.

- Worthington, L.V. and W.R. Wright (1970) North Atlantic Ocean atlas of potential temperature and salinity in the deep water including temperature, salinity, and oxygen profiles from the ERIKA DAN cruise of 1962: Woods Hole Oceanogr. Inst. Atlas Series, v. 2, 58 pl., 28 pp.
- Worthington, L.V. and H. Kawai (1972) Comparison between deep sections across the Kuroshio and the Florida Current and Gulf Stream: in Stommel, H. and K. Yoshida (eds.), Kuroshio: Its Physical Aspects, Univ. of Tokyo Press, Tokyo, p. 371-385.
- Wright, W.R. (1970) Northward transport of Antarctic Bottom Water in the Western Atlantic Ocean: Deep-Sea Res., v. 17, p. 367-371.
- Wright, W.R. and L.V. Worthington (1970) The water masses of the North Atlantic Ocean: a volumetric census of temperature and salinity: Ser. Atlas Marine Environ., Am. Geogr. Society Folio 19.
- Wüst, G. (1933) Schichtung und Zirkulation des Atlantischen Ozeans: Das Bodenwasser und die Gliederung der Atlantischen Tiefsee: Wiss. Ergebn. dt. atlant. Exped. 'Meteor' 1925-1927, v. 6, p. 1-107.
- Wüst, G. (1955) Stromgeschwindigkeiten im Tiefen- und Bodenwasser des Atlantischen Ozeans auf Grund dynamischer Berechnung der Meteor- Profile der Deutschen Atlantischen Expedition 1925/27: Deep-Sea Res., Suppl. to v. 3, p. 373-397.
- Wüst, G. (1957) Stromgeschwindigkeiten und Strommengen in den Tiefen des Atlantischen Ozeans: Wiss. Ergebn. dt. atlant. Exped. 'Meteor' 1925-1927, v.6, p. 261-420.
- Wüst, G. (1964) Stratification and circulation in the Antillean-Caribbean basins. Part I. Spreading and mixing of the water types with an oceanographic atlas: VEMA Res. Series, Columbia Univ. Press, v. 2, 201 pp.
- Zimmerman, H.B. (1971) Bottom currents on the New England continental rise: Jour. Geophys. Res., v. 76, p. 5865-5876.
- Zimmerman, H.B. (1972) Sediments of the New England continental rise: Geol. Soc. America Bull., v. 83, p. 3709-3724.

APPENDIX I SEDIMENT CORES

Cores from the geological sample collections at Woods Hole Oceanographic Institution and Lamont-Doherty Geological Observatory, as well as cores obtained on four cruises to the Greater Antilles Outer Ridge, were studied (Table A1.1). The cores were taken from the research vessels ATLANTIS (A), ATLANTIS II (AII), CHAIN (CH), KNORR (KN), MT. MITCHELL (MM), ROBERT CONRAD (RC), and VEMA (V). All AII60 cores were obtained on leg 8. Cores KN25-3GGC and KN25-4GPC were taken on leg 1 and core KN25-1GC on leg 6 of KNORR cruise 25. Core types are: PC - standard piston core, HF and HP - heat-flow cores, GC - open-barrel gravity core, KC - cumulative camera-core, GGC - giant gravity-core, and GPC - giant piston-core.

Physiographic locations are: PRT - Puerto Rico Trench, NAP - Nares Abyssal Plain, SAP - Silver Abyssal Plain, VGAP - Vema Gap, GAOR - Greater Antilles Outer Ridge, SILL - sill between Greater Antilles Outer Ridge and Silver/Navidad Banks, BDAR - Bermuda Rise, NSLP - north slope of Puerto Rico Trench, COR - Caicos Outer Ridge, DTMA - Datum A outcrop at southern end of Silver Abyssal Plain. All depths are in corrected meters.

Core recovery ratios are based on the length of core obtained versus the mud line on the exterior of the core barrel (i.e. penetration), and they give a rough

approximation of the amount of shortening that each core has undergone during the coring process. Unfortunately, the exterior mud-line is not always a reliable indicator of total core-barrel penetration because some mud may be washed off during recovery, so the figures can only be considered as maximum ratios of core recovery.

TABLE A1.1. DATA ON CORES STUDIED

Core No.	Lat. °N	Long. °W	Physiographic Location	Depth (m)	Length (m)	Core Recovery Ratio	Age at Bottom of Core
A172-14PC	19°54.0'	64°48.0'	PRT	7132	3.00	..	Pleistocene
A172-17PC	22°46.0'	63°58.5'	NAP	5612	3.78
A282-10HF	23°37.5'	67°53.0'	VGAP	5641	1.60	..	Pleistocene
A282-11HF	21°47.5'	68°49.0'	SA	5513	1.85
A282-12HF	20°22.0'	67°22.0'	SILL	5427	1.55	..	Pleistocene
A282-13HF	21°53.8'	66°37.0'	GAOR	5641	1.80	..	Pleistocene
A282-14HF	23°40.5'	65°36.0'	NAP	5771	2.43
A282-15HF	25°29.0'	64°34.0'	BDAR	5691	2.40
A282-18HF	27°05.0'	67°56.0'	BDAR	5188	2.20
A282-23HF	30°27.0'	67°58.0'	BDAR	5182	1.30	0.88	..
AII60-1GC	24°01.2'	70°01.0'	GAOR	5492	0.15	..	Pleistocene
AII60-2GC	23°49.0'	69°31.8'	GAOR	5359	2.71	0.81	Pleistocene
AII60-3GC	24°08.3'	68°20.3'	VGAP	5762	0.28	0.38	Pleistocene
AII60-4GC	23°35.0'	68°54.0'	GAOR	5198	2.01	~0.63	Pleistocene
AII60-5GC	23°24.4'	69°02.7'	GAOR	5362	2.31	~0.72	Pleistocene
AII60-6GC	23°10.5'	69°18.0'	GAOR	5495	1.60	0.71	Pleistocene
AII60-7GC	22°51.4'	68°45.6'	GAOR	5499	1.84	~0.76	Pleistocene
AII60-8GC	23°00.0'	68°32.0'	GAOR	5400	2.27	0.65	Pleistocene
AII60-9GC	23°09.9'	68°20.5'	GAOR	5294	2.87	0.85	Pleistocene
AII60-10GC	23°19.8'	68°05.6'	GAOR	5437	1.49	~0.49	Pleistocene
AII60-11GC	23°28.7'	67°52.0'	GAOR	5637	2.62	~0.86	Pleistocene
AII60-13GC	23°54.1'	68°04.7'	VGAP	5718	1.89	0.79	Pleistocene
AII60-15GC	23°36.0'	68°23.2'	GAOR	5379	1.45	~0.66	Pleistocene
AII60-16GC	23°27.9'	68°33.8'	GAOR	5249	2.23	0.67	Pleistocene
AII60-17GC	23°14.7'	68°42.4'	GAOR	5333	0.55	..	Pleistocene
AII60-18GC	22°51.1'	68°13.3'	GAOR	5284	1.33	0.36	Pleistocene
AII60-19GC	22°44.0'	67°53.7'	GAOR	5364	2.26	0.62	Pleistocene

TABLE A1.1. DATA ON CORES STUDIED (Cont'd.)

Core No.	Lat. °N	Long. °W	Physiographic Location	Depth (m)	Length (m)	Core Recovery Ratio	Age at Bottom of Core
AI160-24KC	20°38.5'	68°25.0'	SILL	5157	1.09	..	Pleistocene
CH19-3PC	20°15.0'	66°33.3'	NSLP	5784	5.12
CH36-1HP	21°08.4'	65°02.5'	GAOR	5306	1.73	..	Pleistocene
CH57-1PC	20°14.2'	65°21.5'	NSLP	6154	5.81
CH57-2PC	20°05.3'	64°35.7'	NSLP	5804	4.64	0.87	..
CH57-3PC	20°06.3'	65°01.2'	NSLP	6160	5.47
CH57-4PC	20°03.3'	66°09.0'	NSLP	6619	2.98	~0.89	Early Eocene
CH57-5PC	22°40.7'	66°29.6'	NAP	5817	8.41	0.86	Pleistocene
CH57-6PC	22°28.0'	66°34.0'	GAOR	5612	8.78	~0.91	Pleistocene
CH57-7PC	22°42.3'	67°42.2'	GAOR	5530	8.95	0.83	Pleistocene
CH57-8PC	22°40.0'	67°41.0'	GAOR	5390	9.27	0.85	Pleistocene
CH57-9PC	20°00.0'	64°17.8'	NSLP	6414	8.08
CH57-10PC	20°06.2'	65°50.5'	NSLP	7074	6.04
CH57-11PC	19°56.0'	67°01.0'	NSLP	6907	6.11	~0.88	..
CH57-12PC	20°11.4'	67°38.6'	NSLP	5437	3.73
CH57-13PC	19°59.0'	68°02.1'	NSLP	5398	5.02	..	Late Oligocene
CH57-14PC	21°30.8'	68°13.7'	GAOR	5366	5.17
KN25-3GGC	22°15.0'	67°57.5'	GAOR	5374	11.39	0.44	Pleistocene
KN25-4GPC	21°30.0'	67°31.0'	GAOR	5163	21.59	0.76	Pleistocene
KN25-1GC	22°48.0'	71°30.0'	COR	5098	1.01	0.71	Pleistocene
MM-1GC	22°44.0'	66°28.0'	NAP	5817	1.86	~0.61	Pleistocene
MM-2GC	22°16.5'	67°26.2'	GAOR	5515	2.38	~0.69	Pleistocene
MM-3GC	21°51.3'	67°38.2'	GAOR	5194	2.27	~0.66	Pleistocene
RC8-128PC	19°28.0'	65°25.7'	PRT	5338	6.88
RC8-129PC	21°21.0'	66°08.0'	GAOR	5378	12.25	..	Pleistocene
RC8-135PC	18°55.0'	62°13.5'	PRT	~6270	7.90
RC10-24PC	21°21.0'	67°48.0'	GAOR	5139	9.75	..	Pleistocene

TABLE A1.1. DATA ON CORES STUDIED (Cont'd.)

Core No.	Lat. °N	Long. °W	Physiographic Location	Depth (m)	Length (m)	Core Recovery Ratio	Age at Bottom of Core
RC10-25PC	21°53.0'	67°20.5'	GAOR	5251	14.67	..	Pleistocene
RC16-30PC	21°00.3'	68°23.1'	DTMA	5398	9.62	..	E to M Eocene
V7-23PC	23°28.0'	65°56.0'	NAP	5832	6.55
V15-186PC	20°26.5'	67°40.0'	SILL	5286	7.65
V16-17PC	20°52.5'	64°04.0'	GAOR	5233	21.70*	..	Pleistocene
V22-17PC	22°48.0'	69°32.0'	GAOR	5339	7.77	..	Pleistocene

*Length corrected for flow-in over the interval 1480-1650 cm.

APPENDIX II BOTTOM PHOTOGRAPHS

Bottom photographs were examined to determine the microstructure of the sediment surface, the direction of bottom currents (see Chapter 6), and the type and activity of benthic organisms. Benthic activity and the effect of bottom currents is most pronounced on the Greater Antilles Outer Ridge, while currents are weak or absent and benthic activity is greatly reduced on the Nares Abyssal Plain and on the north slope of the Puerto Rico Trench. Unless otherwise noted in the photograph descriptions (Table A2.1), the microrelief is roughly 1-2 cm for tracks, trails, and current lineations, 2-5 cm for burrow mounds, and 4-6 cm for ripples.

The bottom photographs studied were taken from the following ships: ATLANTIS II (AII), CHAIN (CH), KNORR (KN), LONG LINES (LL), STANLEY ANGWIN (SA), and WILLEBROAD SNELLIUS (WS). Locations and depths (in corrected meters) are the mean values for each station. Stations with compass-oriented photographs are indicated by an asterisk (*). GAOR refers to the Greater Antilles Outer Ridge.

TABLE A2.1. BOTTOM PHOTOGRAPHS

Cruise	Station	Lat. °N	Long. °W	Depth (m)
AII 11	1	20°08.0'	65°05.0'	6375
	North slope of Puerto Rico Trench. Moderate to no current evidence. Bottom varies from soft, rippled mud with moderate tracks and trails to angular rock outcrops.			
AII 11	2	19°58.6'	65°10.9'	7116
	Lower north slope of Puerto Rico Trench. Soft muddy bottom with some tracks and trails. No current evidence.			
AII 60 Leg 8	K1	24°03.5'	70°00.5'	5492
	Northwest tip of GAOR. Flat, current-smoothed, mud bottom. Numerous small burrow mounds, occasional faint holothurian and echinoid tracks. Unoriented photos.			
AII 60 Leg 8	K2*	23°53.3'	69°48.2'	5417
	Flat to slightly hummocky, current smoothed mud bottom. Current lineations NE-SW. Small burrow mounds and echinoid trails. Northwest tip of GAOR.			
AII 60 Leg 8	K3*	23°49.0'	69°32.8'	5382
	Nearly flat, current-smoothed, mud bottom with NE-SW lineations from moderate currents. Few indications of benthic activity. Northwest tip of GAOR.			

TABLE A2.1. BOTTOM PHOTOGRAPHS (Cont'd.)

Cruise	Station	Lat. °N	Long. °W	Depth (m)
AII 60 Leg 8	K4*	23°43.7'	69°12.2'	5272
	Slightly hummocky, mud bottom with weak and variable currents. Occasional weak NE-SW lineations in mud. Partially obscured holothurian trails, small burrow mounds and few asteriods and pennatulids. Crest of northwest GAOR.			
AII 60 Leg 8	K5*	24°09.7'	68°21.2'	5763
	Flat to hummocky mud bottom with some weak-moderate NW-SE current lineations. Echinoid and holothurian trails, worm burrows, and spoke burrows all largely obscured by currents. Shrimp. Southern side of Vema Gap.			
AII 60 Leg 8	K5A*	24°12.0'	68°21.6'	5769
	Same as Station K5.			
AII60 Leg 8	K6*	23°56.6'	68°30.6'	5573
	Fairly flat mud bottom. Worm burrows, spoke burrows, holothurian and abundant echinoid trails partially obscured by moderate-strong SE current flow. Pennatulid bending SE in current. North flank of northwest GAOR.			
AII 60 Leg 8	K7*	23°46.0'	68°43.5'	5539
	Flat mud bottom lineated by moderate-strong SE current. Ophiuroids, asteriods, worm tubes and burrows, echinoid trails. Several mounds developing slip-face from current. Mud waves about 10 m long and 1 m high indicated in some photographs. North flank of northwest GAOR.			

TABLE A2.1. BOTTOM PHOTOGRAPHS (Cont'd.)

Cruise	Station	Lat. °N	Long. °W	Depth (m)
AII 60 Leg 8	K8*	23°35.6'	68°55.7'	5194
Soft, flat to slightly hummocky mud bottom. Worm tubes, burrows, spoke burrows, ophiuroids, pennatulid, few small plow marks. Very weak currents. Crest of northwest GAOR.				
AII 60 Leg 8	K9*	23°25.6'	69°04.5'	5398
Flat to slightly hummocky mud bottom. Spoke burrows, worm burrows, obscure holothurian and echinoid trails, fecal coil, ophiuroids. Moderate NW current shown by mud lineations. South flank of northwest GAOR.				
AII 60 Leg 8	K10*	23°11.0'	69°18.7'	5497
Nearly flat mud bottom, smoothed and lineated by moderate-strong NW current. Obscure spoke burrows and holothurian trails. Worm tubes and burrows, pennatulids, ophiuroid. South flank of northwest GAOR.				
AII 60 Leg 8	K11*	22°50.2'	68°43.8'	5499
Nearly flat mud bottom smoothed and lineated by moderate N to NW current. Worm burrows and tubes, spoke burrows, asteroid burrows, small plow marks, ophiuroid, pennatulid bending in NW current (see Fig. 4.4), shrimp. South flank of northwest GAOR.				
AII 60 Leg 8	K12*	22°59.8'	68°32.7'	5400
Mud bottom smoothed and slightly lineated by moderate NW current. Burrow mounds, few small plow marks, obscure echinoid trails, spoke burrows. Apparent worm burrows along old echinoid trails (Fig. 4.4). South flank of northwest GAOR.				

TABLE A2.1. BOTTOM PHOTOGRAPHS (Cont'd.)

Cruise	Station	Lat. °N	Long. °W	Depth (m)
AII 60 Leg 8	K13*	23°10.0'	68°19.3'	5241
	Very hummocky mud bottom with lineations indicating moderate N to NW current. Actinarian, sponges (?), pennatulid, worm tubes and burrows, spoke burrows, echinoid trails. Crest of northwest GAOR.			
AII 60 Leg 8	K14*	23°19.5'	68°05.5'	5424
	Fairly flat to hummocky mud bottom. Lineations and ripples indicate moderate current to SE. Possible mud waves of ~1 m amplitude indicated in some photos. Numerous worm burrows, small plow marks, spoke burrows. North flank of northwest GAOR.			
AII 60 Leg 8	K15*	23°28.8'	67°51.5'	5630
	Flat to hummocky mud bottom with some evidence for weak southerly currents. Possible mud waves 0.5 to 1 m high and 5-10 m long suggested in several photos. Numerous obscure to fresh echinoid trails, holothurian trails, worm burrows and tubes, spoke burrows, small plow marks. North flank of northwest GAOR.			
AII 60 Leg 8	K16*	23°39.7'	67°41.3'	5766
	Nearly flat mud bottom with obscure echinoid tracks and fresh worm burrows. Little current evidence, but a few weak NW-SE lineations. Southern side of Vema Gap.			

TABLE A2.1. BOTTOM PHOTOGRAPHS (Cont'd.)

Cruise	Station	Lat. °N	Long. °W	Depth (m)
AII 60 Leg 8	K17*	23°53.2'	68°03.4'	5712
Flat to rolling mud bottom with some lineations showing weak S to SE currents. Good indications of mud waves of spacing > 5 m and amplitude of 0.5 to 1 m. Asteroids, echinoids making trails (Fig. 4.4) small plow marks, worm burrows and mounds, spoke burrows, possible Sargassum weed on surface. Southern side of Vema Gap.				
AII 60 Leg 8	K18*	23°43.4'	68°16.6'	5452
Nearly flat mud bottom with strong current lineations to SSE. Spoke burrows, worm burrows and echinoid trails largely obscured by current lineations. North flank of northwest GAOR.				
AII 60 Leg 8	K19*	23°37.4'	68°24.6'	5379
Mud bottom with ripples and mounds a few cm in height. Ripples mostly developed when slip faces form on mounds in strong SE current. Spoke burrows, echinoid trails, worm burrows and tubes, small plow marks. North flank of northwest GAOR.				
AII 60 Leg 8	K20A*	23°29.4'	68°35.0'	5197
Nearly flat to well-rippled mud bottom (Fig. 6.13) beneath moderate to strong SE current. Worm burrows and tubes, large plow marks, pennatulids, spoke burrows, echinoid and holothurian trails. North flank of northwest GAOR.				

TABLE A2.1. BOTTOM PHOTOGRAPHS (Cont'd.)

Cruise	Station	Lat. °N	Long. °W	Depth (m)
AII 60 Leg 8	K21	23°15.7'	68°43.6'	5303
	Smoothed mud bottom with worm burrows, mounds and tubes. Possible moderate currents of unknown direction. Murky water. South flank of northwest GAOR.			
AII 60 Leg 8	K22*	22°51.5'	68°17.1'	5347
	Hummocky mud bottom with NW-SE lineations indicating weak to moderate current. Some very poorly developed ripples. Actinarian, tunicate, worm tubes and burrows, spoke burrows. South flank of northwest GAOR.			
AII 60 Leg 8	K23*	22°45.2'	67°55.8'	5409
	Flat to slightly hummocky mud bottom with weak NW-SE current lineations. Worm burrows, mounds, and tubes, obscure echinoid trails, small plow marks, spoke burrows, ophiuroid burrows. North flank of northwest GAOR.			
AII 60 Leg 8	K24*	22°51.7'	66°32.4'	5821
	Flat mud bottom with no current evidence. Obscure echinoid trails, worm burrows. Nares Abyssal Plain.			
AII 60 Leg 8	K25*	22°32.0'	66°55.0'	5635
	Flat mud bottom with no current evidence. Worm burrows, obscure fecal coils and echinoid trails, few small plow marks. Deep on north flank of GAOR.			

TABLE A2.1. BOTTOM PHOTOGRAPHS (Cont'd.)

Cruise	Station	Lat. °N	Long. °W	Depth (m)
AII 60 Leg 8	K26*	22°15.5'	67°21.1'	5458
	Nearly flat mud bottom with weak current lineations to SE. Spoke burrows, worm burrows, plow marks, fecal coils, holothurian trail, possible small manganese nodules. North flank of GAOR.			
AII 60 Leg 8	K27*	21°51.1'	67°40.9'	5207
	Nearly flat mud bottom with few mounds and weak SE current lineations. Worm burrows, spoke burrows, fecal coils, pennatulid bending to S in current. Crest of western GAOR.			
AII 60 Leg 8	K28*	21°07.3'	68°06.4'	5444
	Mud bottom with large (10-20 cm wide, 3-5 cm high) fossil lineations oriented generally NNE-SSW. Weak recent lineations to NNW. Holothurian trails, spoke burrows, worm burrows and tubes, small plow marks. Flank of GAOR near southern end of Silver Abyssal Plain.			
AII 60 Leg 8	K29*	20°38.5'	68°25.0'	5159
	Nearly flat mud bottom of slightly coarser texture with very weak lineations to the S and SE. Worm tubes and burrows, spoke burrows, ophiuroid, few mounds and small plow marks, small pennatulid. Apron at base of Navidad Bank.			
AII 60 Leg 8	K30*	20°13.0'	68°37.0'	4850
	Flat, coarse textured, mud bottom with lighter color where mud is disturbed by benthos. Spoke burrows, worm burrows and tubes, fecal coils, mounds, holothurian trails, plow marks, faint indications of weak southerly currents. Base of Navidad Bank.			

TABLE A2.1. BOTTOM PHOTOGRAPHS (Cont'd.)

Cruise	Station	Lat. °N	Long. °W	Depth (m)
CH 11	SC6	19°35.0'	66°28.0'	~7800
	Puerto Rico Trench. Soft mud bottom with mounds. No current evidence. Little benthic activity except for worm burrows and tubes.			
CH 11	8A	19°59.0'	66°30.0'	7259
	Lower north slope of Puerto Rico Trench. Blocky, angular rocks to sand-size material with no current evidence. Also muddy-sand bottom with moderate currents.			
CH 11	10*	20°54.0'	66°26.0'	5339
	Crest of eastern sector GAOR. Mud bottom covered with manganese nodules. Scour around nodules shows moderate current to east.			
CH 19	3*	20°07.0'	66°18.0'	5708
	North slope of Puerto Rico Trench. Worm burrows, rare spoke burrows and echinoid trails. No current evidence to evidence for weak westerly current. Coarse textured, nearly flat, mud bottom with a few talus piles.			
CH 19	5*	20°05.0'	66°04.0'	6966
	North slope Puerto Rico Trench. Nearly flat, muddy to granular bottom with occasional angular blocks. N-S sediment lineations may be current induced or be due to downslope sedimentation. Very little current evidence and little benthic activity except for occasional worm burrows.			

TABLE A2.1. BOTTOM PHOTOGRAPHS (Cont'd.)

Cruise	Station	Lat. °N	Long. °W	Depth (m)
CH 19	7*	20°08.0'	65°58.5'	6531
	North slope Puerto Rico Trench. Mud bottom to rock outcrops or blocks showing evidence of downslope sediment movement to SW. No current evidence. Worm burrows, fecal coils, holothurian and echinoid trails rare to moderate in abundance.			
CH 19	8*	20°01.5'	66°29.5'	6424
	North slope Puerto Rico Trench. Flat mud bottom strongly corrugated (1-2 cm height) by mostly old echinoid and holothurian trails and fresh worm burrows. No current evidence.			
CH 19	9*	20°00.0'	66°30.0'	6375
	North slope Puerto Rico Trench. Rock outcrops and angular blocks with thin sediment cover. No current evidence or benthic activity.			
CH 34	3	20°16.5'	65°46.2'	6393
	Soft, flat, mud bottom on north slope of Puerto Rico Trench. No current evidence. Some echinoid trails and worm burrows.			
CH 34	4	22°11.0'	66°24.5'	5727
	Deep on north flank of eastern sector of GAOR. Flat mud bottom weakly corrugated by numerous, mostly obscure, echinoid and holothurian trails. Large ophiuroids, scattered manganese nodules. Little current evidence.			

TABLE A2.1. BOTTOM PHOTOGRAPHS (Cont'd.)

Cruise	Station	Lat. °N	Long. °W	Depth (m)
CH 36	CD1	21°30.0'	66°30.0'	5480
	North flank of GAOR. Nearly flat mud bottom, smoothed by weak to moderate currents of unknown direction. Worm burrows, spoke burrows, obscure trails.			
CH 57	15-1	20°09.0'	65°12.0'	6550
	Soft, muddy bottom on north slope of Puerto Rico Trench. No current evidence. Very murky, poor quality photos.			
CH 75	2*	19°29.5'	60°46.5'	5296
	Far eastern end of GAOR. Soft mud bottom with manganese nodules 4-7 cm in diameter on surface. Currents and benthic activity not determinable.			
KN 25	K1*	25°01.5'	68°03.5'	5519
	North side of Vema Gap. Fairly flat, current smoothed, mud bottom with few lineations showing weak to moderate NW currents. Numerous worm burrows, fewer spoke burrows, plow marks and echinoid trails.			
KN 25	K2*	24°42.2'	68°08.0'	5689
	North side of Vema Gap. Flat mud bottom smoothed by weak to moderate N to NW currents. Echinoid trails, worm burrows, plow marks, spoke burrows. Unidentified floating holothurian.			

TABLE A2.1. BOTTOM PHOTOGRAPHS (Cont'd.)

Cruise	Station	Lat. °N	Long. °W	Depth (m)
KN25	K3*	24°23.8'	68°11.4'	5737
	Central Vema Gap. Flat mud bottom with current lineations oriented E-W to SE-NW. Fresh worm burrows, spoke burrows. Mostly obscure plow marks and echinoid trails.			
KN 25	K4*	23°45.2'	69°40.8'	5390
	Northwest tip of GAOR. Current smoothed mud bottom indicating N to NW current. Worm burrows, few spoke burrows and plow marks, actinarian.			
KN 25	K5*	23°48.5'	69°54.5'	5411
	Northwest tip of GAOR. Flat mud bottom strongly smoothed by northerly currents. Burrow mounds (occasionally with slip face developing), worm tubes and burrows, holothurian trails, plow marks, pennatulids, tunicate.			
KN 25	K6*	23°52.6'	68°35.1'	5483
	North flank of northwest GAOR. Strong lineations and current smoothing by SE current. Spoke burrows (see Fig. 4.4), echinoid and echinoid trails, holothurian trails, worm burrows and tubes, plow marks, shrimp, actinarian. Several photographs indicate mud waves of 0.5 - 1 m height and of unknown spacing.			

TABLE A2.1. BOTTOM PHOTOGRAPHS (Cont'd.)

Cruise	Station	Lat. °N	Long. °W	Depth (m)
KN 25	K7*	23°43.5'	68°41.5'	5311
	North flank of northwest GAOR. Moderate to strong E to SE current producing smoothed, lineated, mud bottom. Worm burrows and tubes, plow marks, burrow mounds, spoke burrows, pennatulid, echinoid, sponge, holothurian trails. Rare indication of mud waves of about 1 m amplitude.			
KN 25	K8*	23°57.2'	68°59.0'	5446
	North flank of northwest GAOR. Mud bottom smoothed and lineated by easterly current. Plow marks, worm tubes and burrows, obscure echinoid trails, tunicate (?), spoke burrows.			
KN 25	K9*	23°24.0'	69°06.1'	5394
	South flank of northwest GAOR. Current-smoothed mud bottom with lineations showing moderate NW current. Burrow mounds, echinoid trails, worm burrows and tubes, spoke burrows.			
LL 8	5*	22°57.4'	68°20.0'	5349
	South flank of northwest GAOR. Soft mud bottom with NW-SE current lineations indicating moderate current. Worm burrows and tubes, plow marks.			
LL 8	6*	20°12.5'	65°45.4'	6484
	North slope of Puerto Rico Trench. Mud bottom with no current evidence. Echinoid and echinoid trails, worm burrows, pennatulid, plow marks.			

TABLE A2.1. BOTTOM PHOTOGRAPHS (Cont'd.)

Cruise	Station	Lat. °N	Long. °W	Depth (m)
LL 8	7	20°02.5'	65°48.9'	7346
	North slope of Puerto Rico Trench. Fairly flat, soft, mud bottom smoothed by currents of unknown direction. Holothurians and their trails, fecal coils.			
LL 8	8A*	19°58.7'	65°56.0'	7623
	North slope of Puerto Rico Trench. Fairly flat, soft, mud bottom with no current evidence. Worm burrows, mounds, and tubes. Minor N-S undulations.			
LL 8	8B*	19°57.0'	65°57.4'	8143
	Puerto Rico Trench. Flat mud bottom with few angular rocks. Weak current to west. Fecal coils, few trails, holothurians.			
LL 8	9*	20°05.6'	65°59.0'	7071
	North slope of Puerto Rico Trench. Nearly flat, soft mud bottom. Numerous worm burrows and burrow mounds. Holothurians and trails.			
LL 8	11*	20°05.2'	66°00.5'	7015
	North slope of Puerto Rico Trench. Soft, flat mud bottom with no current evidence. Holothurian and echinoid trails, fecal coils, worm burrows.			
SA	K4*	19°51.0'	63°56.0'	7577
	Floor of Puerto Rico Trench. Coarse-textured mud bottom with lineations indicating moderate current to west. Fossil ripple marks (?) oriented NE-SW. Worm tubes and burrows.			

TABLE A2.1. BOTTOM PHOTOGRAPHS (Cont'd.)

Cruise	Station	Lat. °N	Long. °W	Depth (m)
SA	K5*	20°04.5'	63°47.0'	6167
	North slope of Puerto Rico Trench. Soft mud bottom with worm burrows, spoke burrows, few fecal coils and plow marks, actinarians, one rat-tail fish.			
SA	K6*	20°25.0'	63°47.0'	5009
	Crest of eastern GAOR. Fairly flat mud bottom with little current evidence. Scattered, half-buried manganese nodules. Spoke burrows, worm burrows, acorn worm.			
SA	K7*	22°59.0'	63°50.0'	5842
	Nares Abyssal Plain. Flat mud bottom with no current evidence. Fresh to obscure echinoid trails, worm burrows, spoke burrows.			
WS	E7	22°05.0'	68°05.0'	~5420
	West flank of west-central GAOR. Current-smoothed and lineated, flat mud bottom. Worm burrows and tubes, plow marks.			

APPENDIX III SUSPENDED PARTICULATE MATTER

Suspended particulate matter samples were obtained from depths greater than 4500 m over the Greater Antilles Outer Ridge on three cruises: MT. MITCHELL RP-13-MI-71 (January, 1971), ATLANTIS II 60, leg 8 (August, 1971), and KNORR 25, leg 1 (February, 1972). Sample handling procedures are described in the text.

All samples were taken as part of standard hydrographic casts, and the hydrographic station numbers are listed in parentheses (Table A3.1). N before a filter number denotes a Nuclepore filter, SF denotes a silver filter, and all others are Millepore filters. Sample depths were calculated from the hydrographic data, and these depths and the water depths are in corrected meters.

TABLE A3.1. SUSPENDED PARTICULATE MATTER SAMPLES

Cruise	Station	Filter No.	Sample Depth (m)	Temp. °C	Concentration (µg/l)	Volume Filtered (liters)	Lat. °N	Long. °W	Water Depth (m)
MM	2	71-1	4658	1.85	13	18.62	22°33.3'	66°10.3'	5823
		71-2	4736	1.84	15	18.07			
		71-3	1405	-	17	18.64			
MM	6	71-4	5103	1.64	40	25.44	22°17.5'	67°20.8'	5515
		71-5	5221	1.60	31	25.46			
		71-6	5308	1.58	19	24.19			
MM	7	71-7	4762	1.78	25	20.49	21°54.0'	67°40.0'	5190
		71-8	4867	1.75	16	19.68			
		71-9	4942	1.68	37	20.48			
MM	9	71-12	5168	1.70	55	20.50	21°15.9'	68°07.4'	5456
		71-11	5270	1.70	48	20.49			
		71-10	5341	1.69	47	20.63			
AII 60	2(1826)	234	5072	1.76	16	21.86	23°53.0'	69°48.0'	5417
		233	5170	1.73	15	22.45			
		232	5293	1.63	24	25.92			
		231	5361	1.58	16	25.49			
AII 60	4(1828)	238	4927	1.82	13	27.10	23°43.7'	69°12.1'	5271
		237	5025	1.75	18	22.50			
		236	5149	1.68	14	28.00			
		235	5233	1.61	23	27.30			

TABLE A3.1. SUSPENDED PARTICULATE MATTER SAMPLES (Cont'd.)

Cruise	Station	Filter No.	Sample Depth (m)	Temp. °C	Concentration (µg/l)	Volume Filtered (liters)	Lat. °N	Long. °W	Water Depth (m)
AII 60	5(1829)	242	5420	1.59	7	27.50	24°12.0'	68°21.6'	5763
		241	5520	1.56	35	24.00			
		240	5645	1.54	6	27.80			
		239	5730	1.54	18	27.90			
AII 60	6(1830)	246	5254	1.67	22	25.80	23°56.6'	68°30.6'	5600
		245	5355	1.63	44	26.60			
		244	5475	1.55	14	27.95			
		243	5556	1.54	17	26.70			
AII 60	7(1831)	250	4993	1.72	14	26.50	23°46.0'	68°43.5'	5345
		249	5093	1.67	40	28.70			
		248	5218	1.59	10	22.00			
		247	5303	1.54	>21	25.30			
AII 60	8(1832)	254	4857	1.80	9	27.20	23°35.6'	68°55.7'	5197
		253	4955	1.77	29	27.40			
		252	5078	1.73	16	27.00			
		251	5162	1.69	>19	27.60			
AII 60	9(1833)	258	5047	1.78	15	27.60	23°25.6'	69°04.5'	5397
		257	5145	1.76	32	27.25			
		256	5267	1.72	25	26.65			
		255	5350	1.68	21	23.70			

TABLE A3.1. SUSPENDED PARTICULATE MATTER SAMPLES (Cont'd.)

Cruise	Station	Filter No.	Sample Depth (m)	Temp. °C	Concentration (µg/l)	Volume Filtered (liters)	Lat. °N	Long. °W	Water Depth (m)
AII 60	10(1834)	262	5146	1.76	16	28.25	23°11.0'	69°18.7'	5496
		261	5244	1.72	31	23.55			
		260	5366	1.64	12	27.80			
		259	5450	1.59	16	27.55			
AII 60	11(1835)	267	5151	1.73	14	27.30	22°50.2'	68°43.8'	5499
		268	5249	1.69	42	27.35			
		264	5371	1.61	24	27.05			
		263	5454	1.58	18	25.80			
AII 60	12(1836)	272	5070	1.77	15	25.10	22°59.8'	68°32.7'	5400
		271	5169	1.74	55	26.20			
		270	5291	1.67	26	25.90			
		269	5375	1.64	63	25.75			
AII 60	13(1837)	276	4940	1.77	16	27.35	23°10.0'	68°19.3'	5241
		275	5039	1.73	49	28.10			
		274	5164	1.64	37	26.15			
		273	5248	1.63	61	25.75			
AII 60	14(1838)	280	5074	1.79	14	27.10	23°19.5'	68°05.5'	5434
		279	5172	1.73	34	24.75			
		278	5294	1.60	19	27.20			
		277	5377	1.56	22	27.00			

TABLE A3.1. SUSPENDED PARTICULATE MATTER SAMPLES (Cont'd.)

Cruise	Station	Filter No.	Sample Depth (m)	Temp. °C	Concen- tration (µg/l)	Volume Filtered (liters)	Lat. °N	Long. °W	Water Depth (m)
AII 60	15(1839)	284	5280	1.60	6	20.55	23°28.8'	67°51.5'	5630
		283	5378	1.56	15	17.90			
		282	5525	1.53	12	26.40			
		281	5608	1.54	5	26.65			
AII 60	16(1840)	288	5411	1.56	6	25.45	23°39.7'	67°41.3'	5766
		287	5509	1.55	16	26.10			
		286	5632	1.54	8	26.70			
		285	5715	1.55	8	25.95			
AII 60	17(1841)	292	5366	1.59	10	25.90	23°53.2'	68°03.4'	5713
		291	5463	1.57	24	27.00			
		290	5585	1.54	11	27.80			
		289	5633	1.54	20	28.30			
AII 60	18(1842)	297	5120	1.70	18	25.85	23°43.4'	68°16.6'	5452
		295	5219	1.65	>15	25.20			
		294	5341	1.57	13	27.20			
		293	5391	1.56	12	26.55			
AII 60	20(1844)	301	4867	1.78	18	25.00	23°29.4'	68°35.0'	5223
		300	4965	1.73	37	23.15			
		302	5088	1.64	-	26.90			
		298	5137	1.63	23	25.00			

TABLE A3.1. SUSPENDED PARTICULATE MATTER SAMPLES (Cont'd.)

Cruise	Station	Filter No.	Sample Depth (m)	Temp. °C	Concentration (µg/l)	Volume Filtered (liters)	Lat. °N	Long. °W	Water Depth (m)
AII 60	21(1845)	306	4962	1.80	21	27.10	23°15.7'	68°43.6'	5333
		305	5061	1.78	26	22.30			
		304	5185	1.73	21	26.60			
		303	5235	1.70	23	26.60			
AII 60	22(1846)	310	4938	1.80	13	22.35	22°51.5'	68°17.1'	5313
		309	5037	1.76	24	26.40			
		308	*	*	16	27.00			
		307	*	*	9	26.50			
AII 60	23(1847)	314	4997	1.78	26	26.90	22°45.2'	67°55.8'	5320
		313	5096	1.74	27	26.50			
		312	5218	1.67	21	26.40			
		311	5266	1.64	27	26.45			
KN 25	1(94)	N52	5351	1.57	22	22.80	25°01.5'	68°03.5'	5519
		N51	5439	1.56	14	25.60			
KN 25	2(95)	71-14	4580	1.79	6	18.85	24°42.2'	68°08.0'	5680
		71-13	4662	1.77	10	16.45			
KN 25	3(96)	71-16	5593	1.54	10	17.73	24°23.8'	68°11.4'	5727
		71-15	5679	1.53	6	17.78			

* Bottom 4 Nansen bottles pre-tripped.

TABLE A3.1. SUSPENDED PARTICULATE MATTER SAMPLES (Cont'd.)

Cruise	Station	Filter No.	Sample Depth (m)	Temp. °C	Concen- tration (µg/l)	Volume Filtered (liters)	Lat. °N	Long. °W	Water Depth (m)
KN 25	6(99)	SF#1	5340	1.56	-	32.70	23°52.6'	68°35.1'	5484
		71-18	5425	1.54	13	15.90			
KN 25	7(100)	SF#2	5166	1.67	-	25.30	23°43.5'	68°41.5'	5308
		71-19	5253	1.62	27	24.92			
KN 25	9(102)	SF#3	5232	1.71	-	21.20	23°24.0'	69°06.1'	5388
		N53	5318	1.64	24	27.15			
KN 25	11 104	SF#4	5326	1.74	-	24.30	23°48.0'	69°56.0'	5411
		71-20	5412	(1.67)	30	24.30			
KN 25	13(106)	SF#5	5124	1.77	-	16.00	22°15.4'	67°56.9'	5374

APPENDIX IV PHYSICAL PROPERTIES OF CORES

WATER CONTENT

Water content is determined as percent dry weight according to the formula

$$w = (W_w/W_s) 100 \text{ percent}$$

where W_w is the weight of water present in the sediment sample, and W_s is the weight of the sediment solids.

Samples were oven dried at 105°C.

The values of water content for the cores from the Greater Antilles Outer Ridge (Figs. A4.1-A4.13) are generally greater than or equal to values for other deep-ocean cores taken in the Atlantic and Pacific Oceans (Richards, 1962; Buchan and others, 1967). The high water content of the sediment probably results from the rapid sedimentation on the Greater Antilles Outer Ridge.

SHEAR STRENGTH

The shear strength of a sediment is the maximum shear stress which the sediment can withstand. Most measurements of shear strength were made with a manually operated Torvane device on the vertically-split surface of the cores. The vanes on this apparatus project 0.8 cm into the sediment and thus test only a shallow section of the core. Measurements were also made on the KNORR cores with a motorized

vane which penetrated deeper into the cores, and the values obtained in this manner are less than or equal to those of the Torvane (Figs. A4.1, A4.2). The reasons for this discrepancy are undetermined, although the Torvane may not have been accurately calibrated.

The shear strength values determined for the cores from the Greater Antilles Outer Ridge (Figs. A4.1-A4.13) are comparable to values for other deep-ocean sediments in the Atlantic and Pacific Oceans (Richards, 1962; Hamilton, 1970). The very high values determined in the lower part of core KN25-3GGC (Fig. A4.1) are most likely due to compaction of the sediment during the coring process.

Figure A4.1. Plots of water content and shear strength for gravity core AII60-8:2GC.

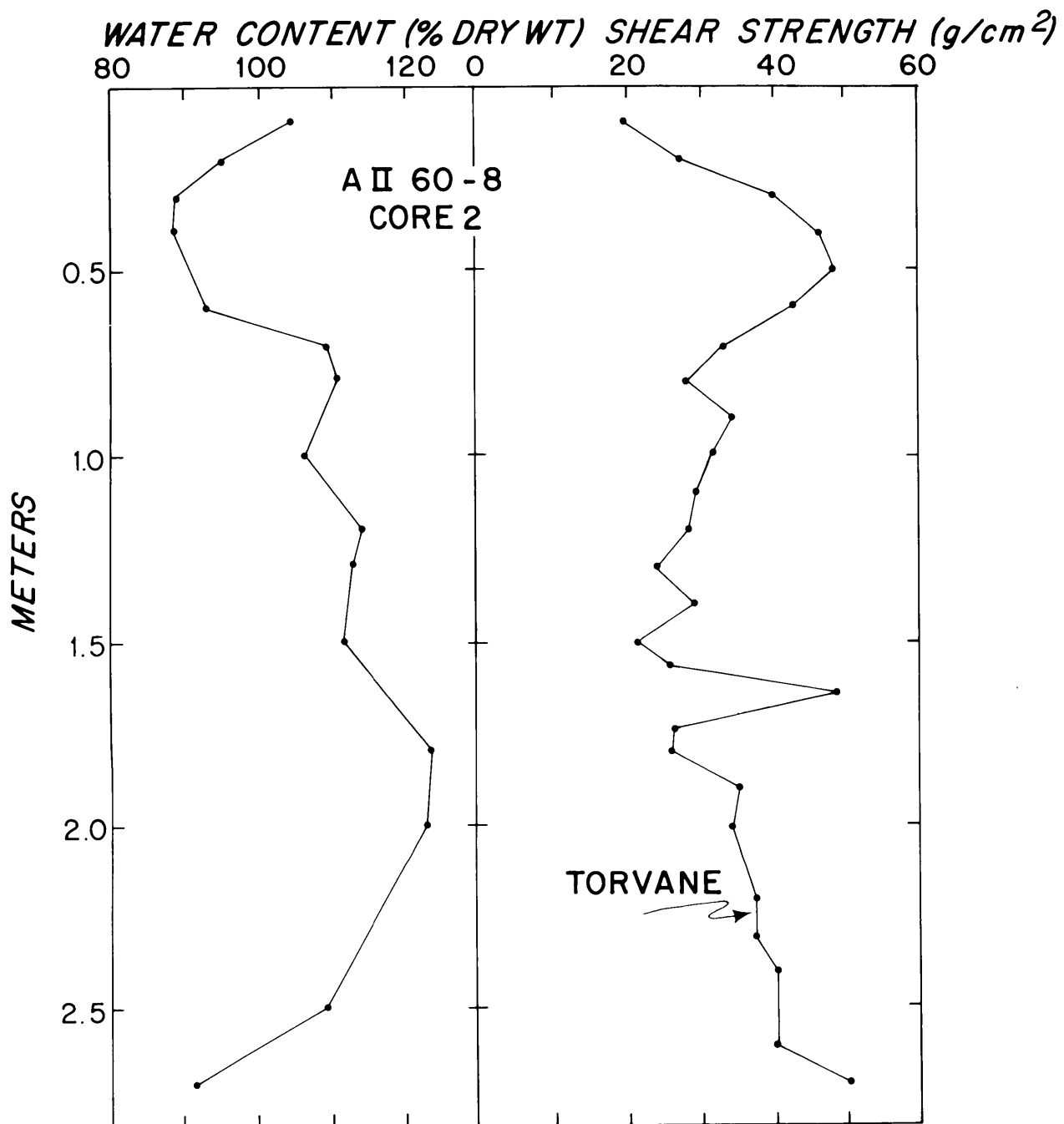


Figure A4.2. Plots of water content and shear strength for gravity core 4B, taken on leg 8 of ATLANTIS II Cruise 60.

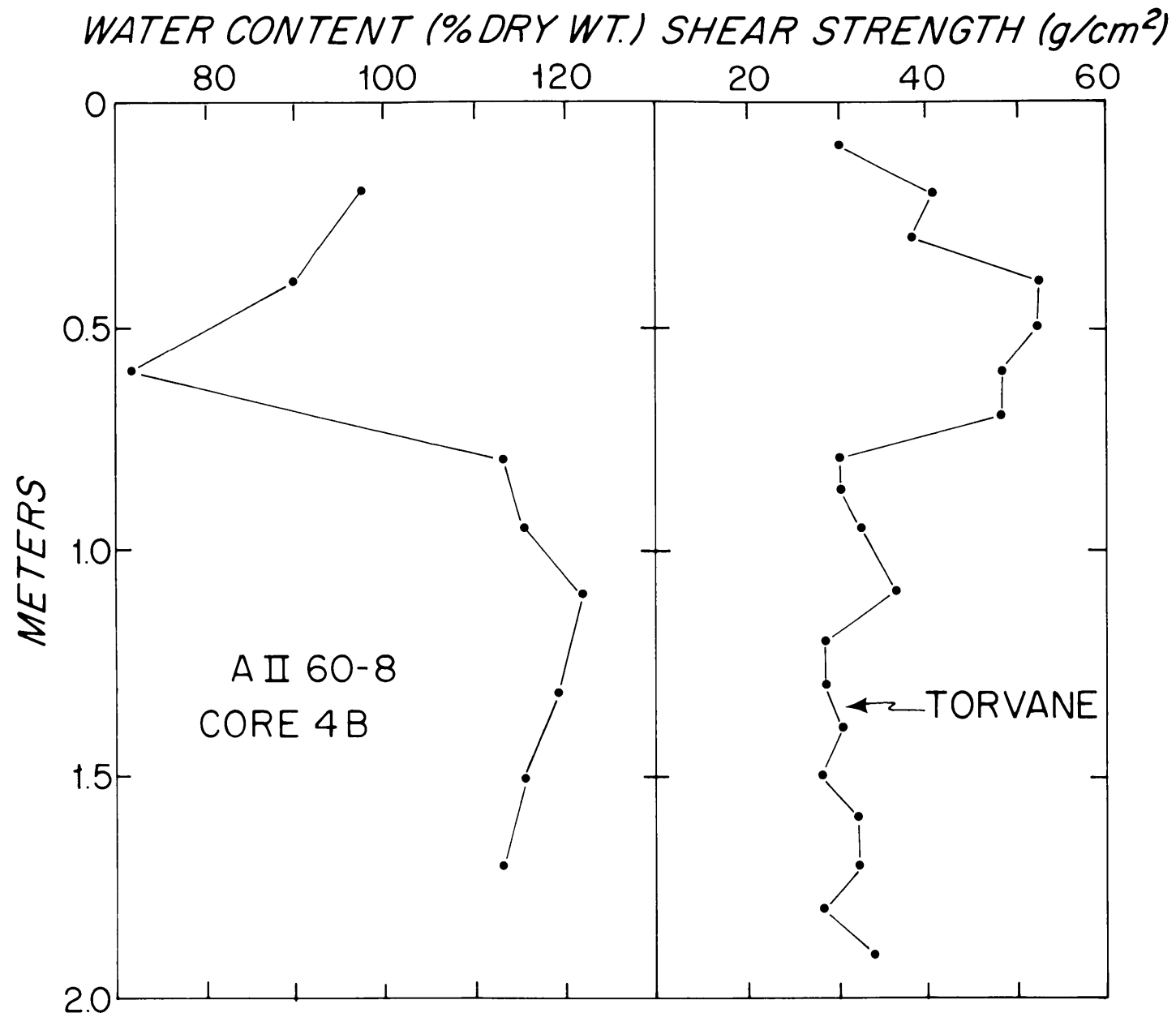


Figure A4.3. Plots of water content and shear strength for gravity cores 6A and 6B, taken from the southwest flank of the northwestern Greater Antilles Outer Ridge on ATLANTIS II Cruise 60, leg 8. A and B are the two barrels of a dual-barrel corer; the two cores thus represent sediment samples taken 23 cm (center to center) apart.

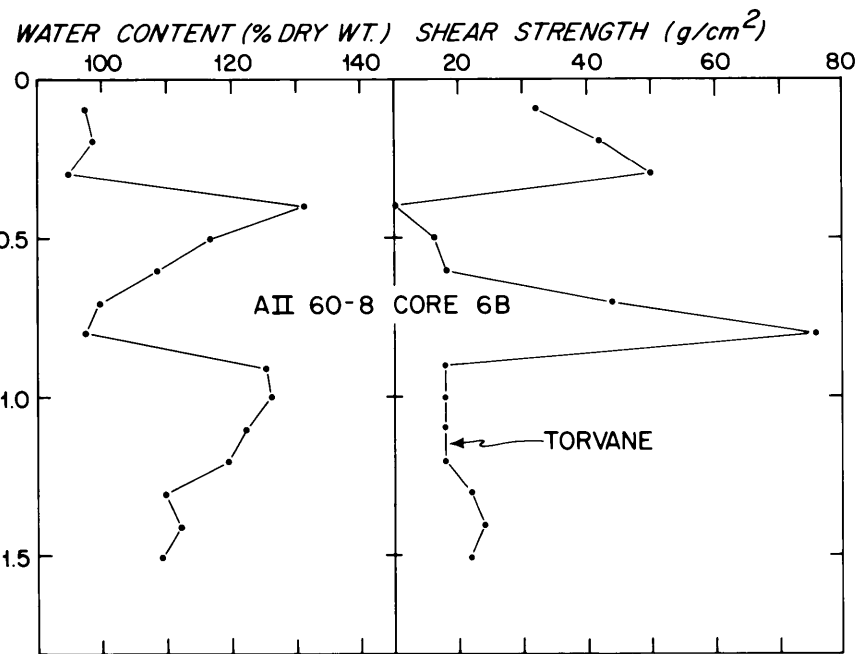
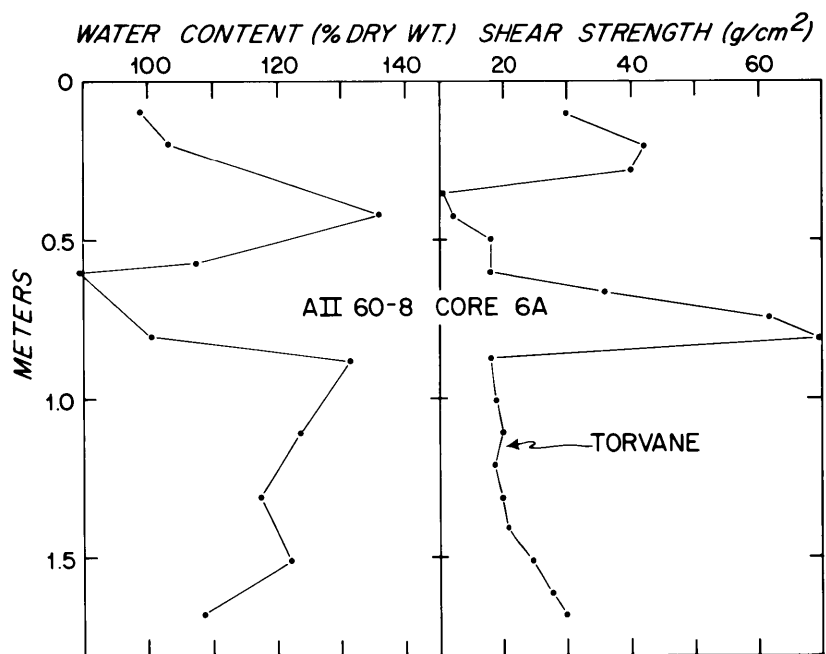


Figure A4.4. Plots of water content and shear strength for gravity core AII60-8:7GC. This core was taken 70 km southeast of cores AII60-8:6GC and at the same depth. Note the very close resemblance of physical property variations in this core to those in cores AII60-8:6GC (Fig. A4.3); the lithologies of the cores are also very similar.

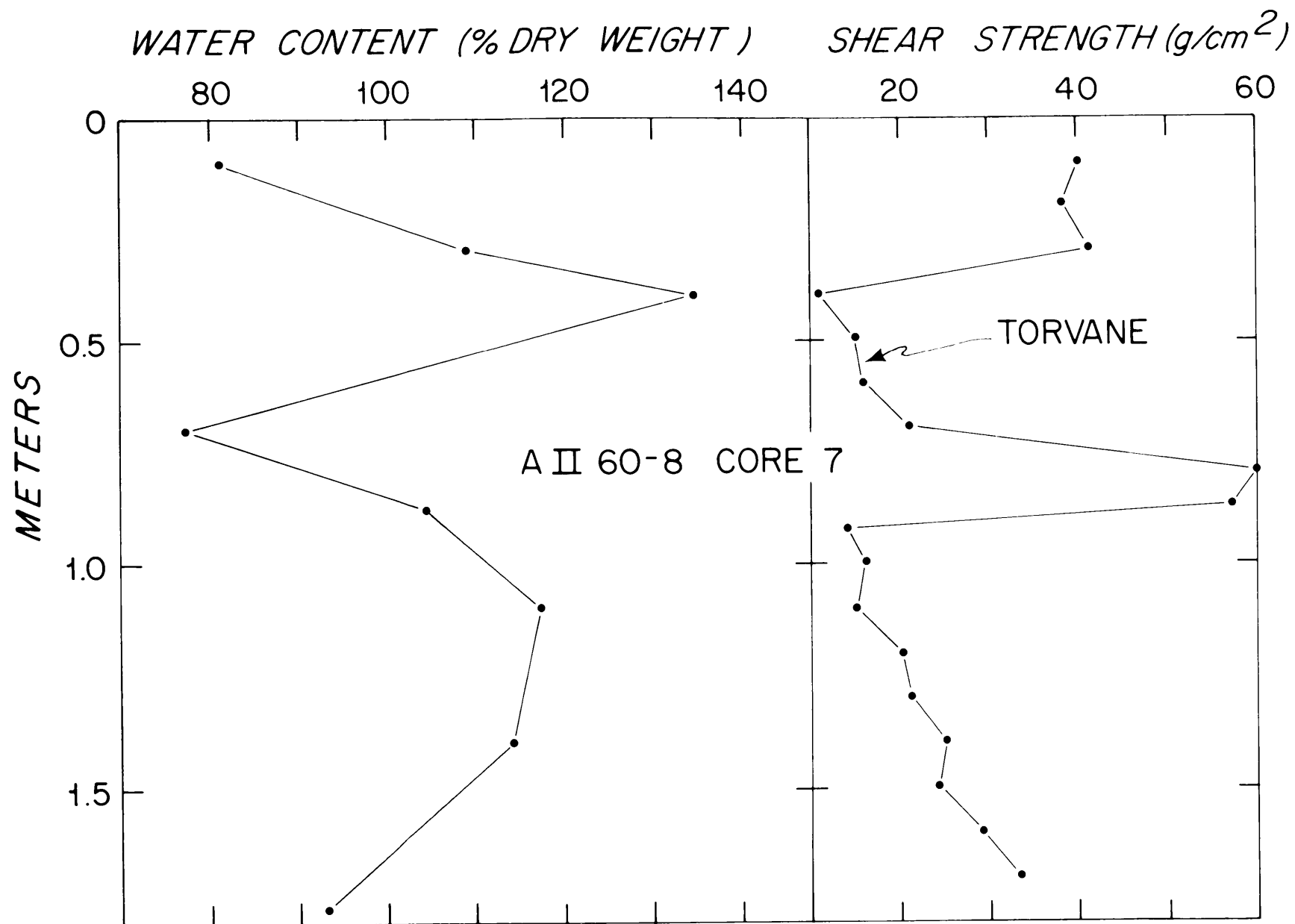


Figure A4.5. Plots of water content and shear strength for gravity core 10A (AII60, leg 8).

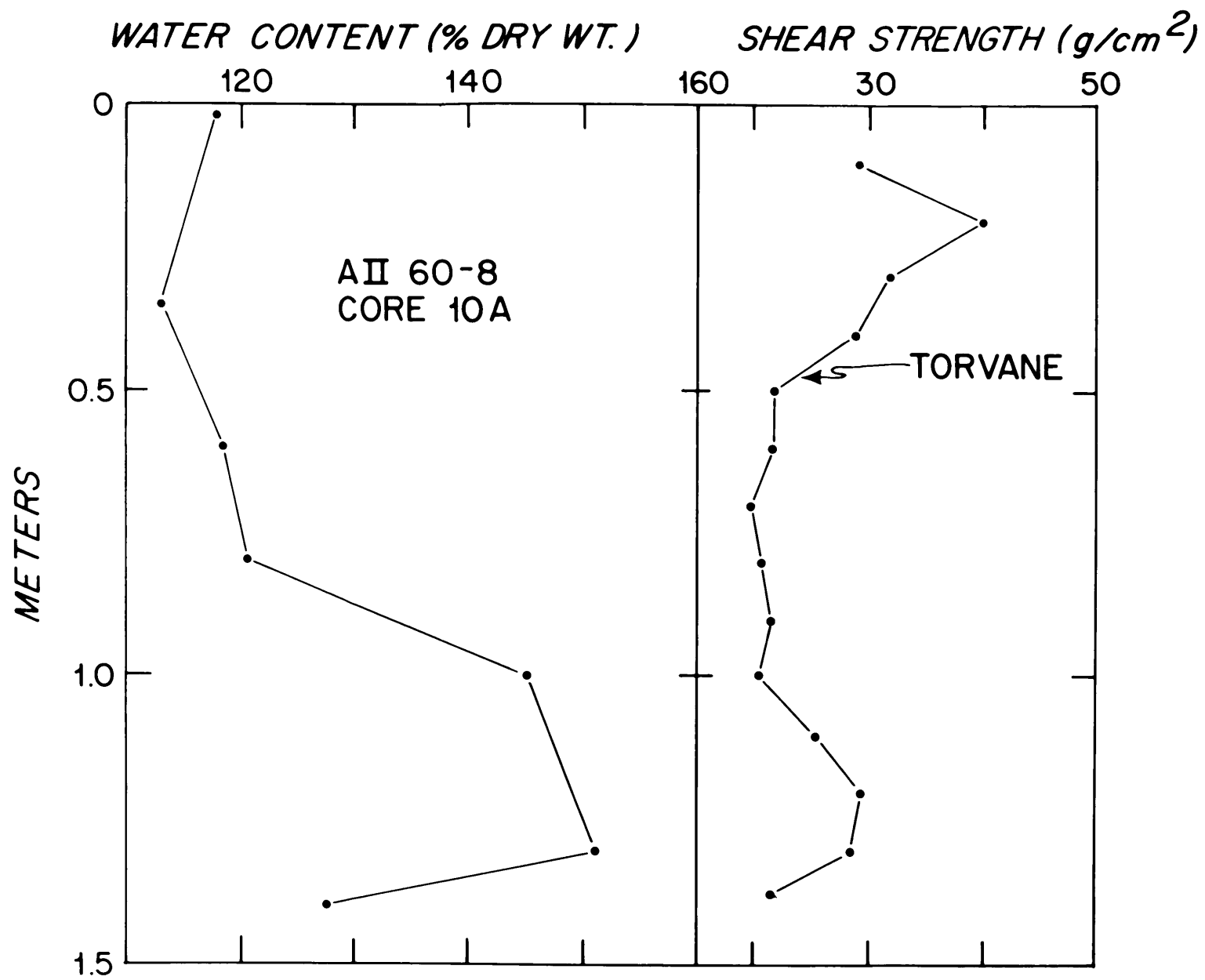


Figure A4.6. Plots of water content and shear strength for gravity core AII60-8:11GC.

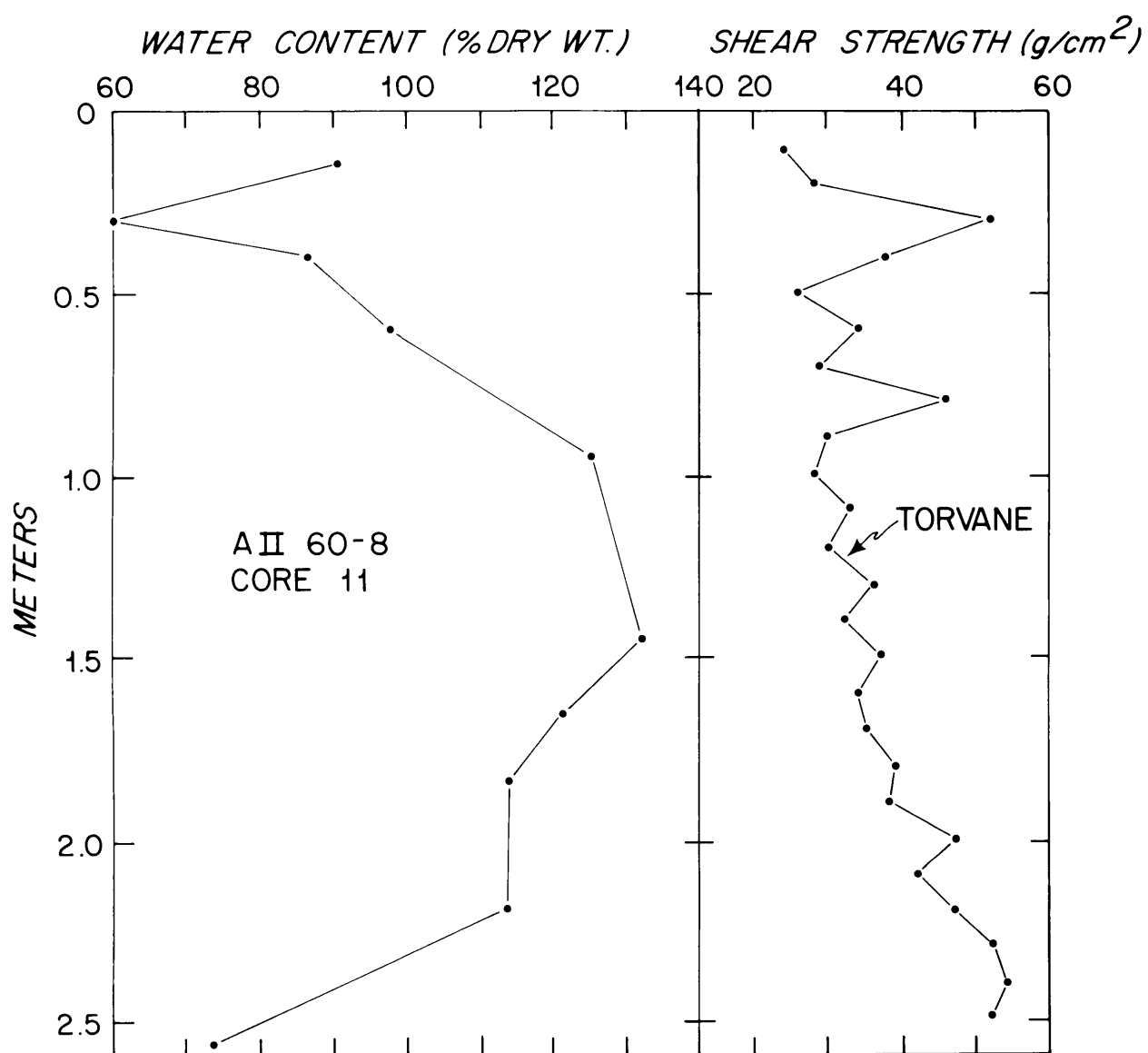


Figure A4.7. Plots of water content and shear strength for gravity core AII60-8:13GC.

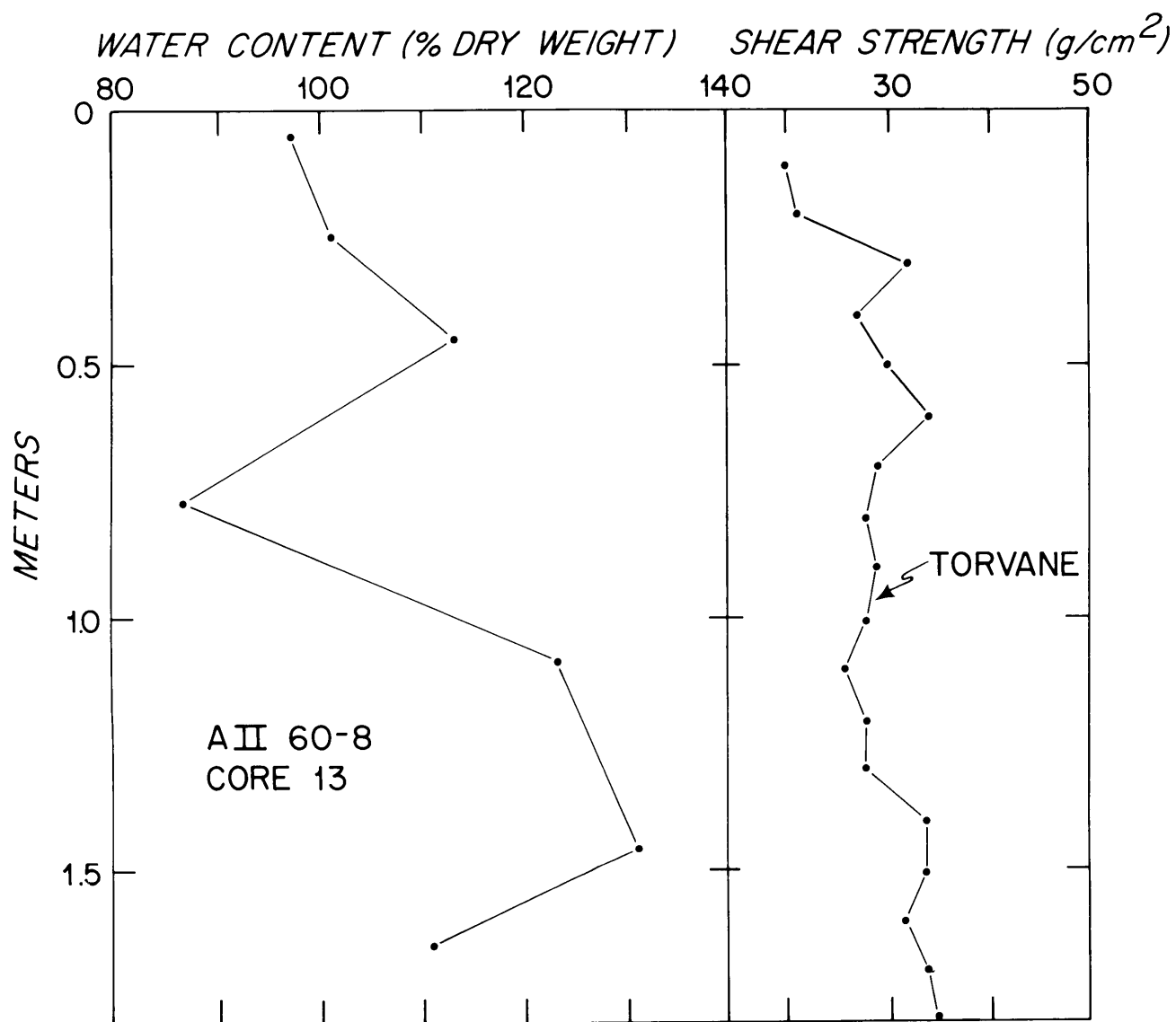


Figure A4.8. Plots of water content and shear strength for gravity core AII60-8:18GC.

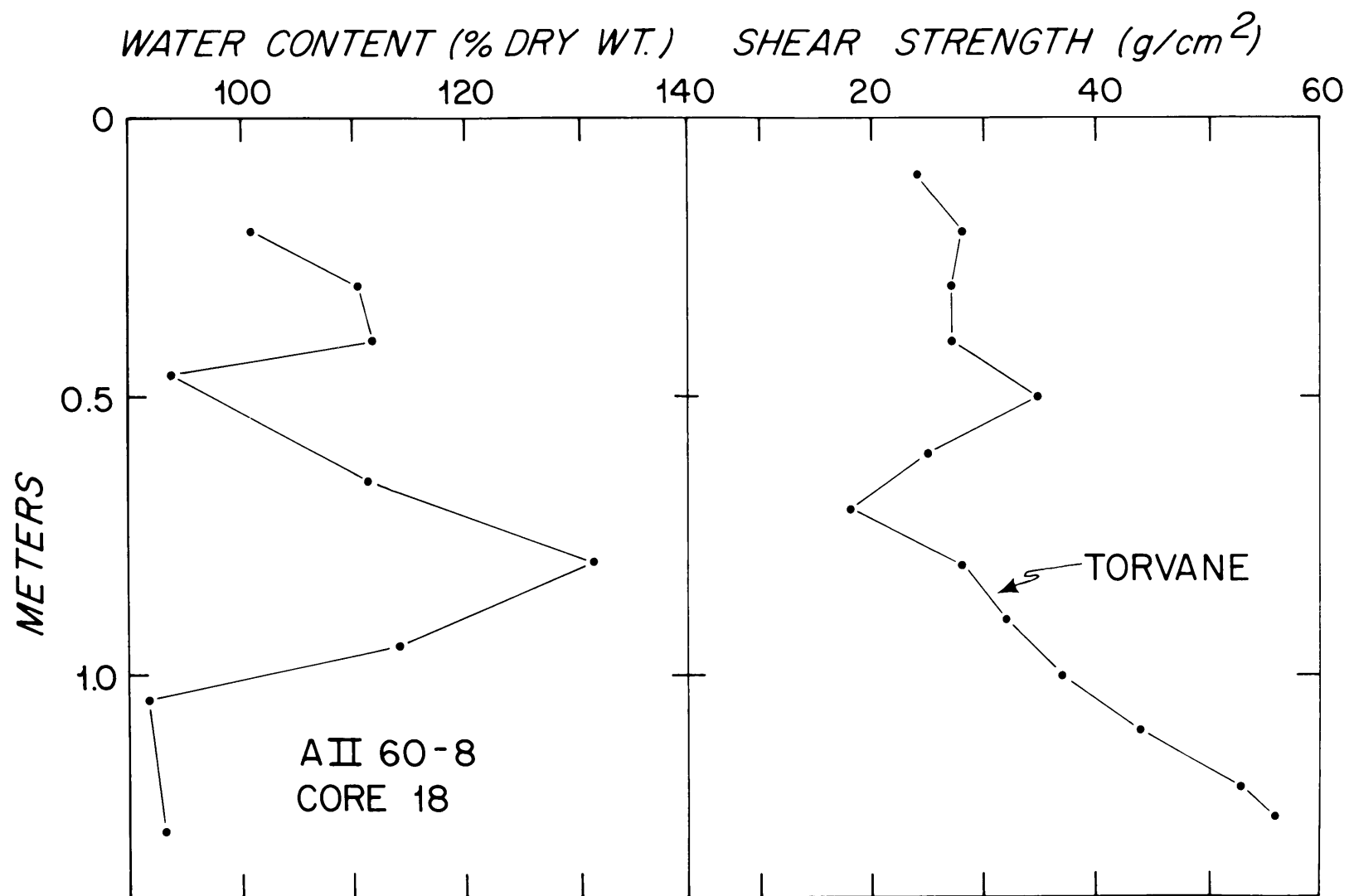


Figure A4.9. Plots of water content and shear strength for giant gravity-core KN25-3GGC. Note the sharp drop in water content and the increase in shear strength in the lower half of the core, possibly indicating compaction and incomplete recovery during the coring process. At right, filled circles are Torvane measurements; open circles are measurements made with the motorized vane.

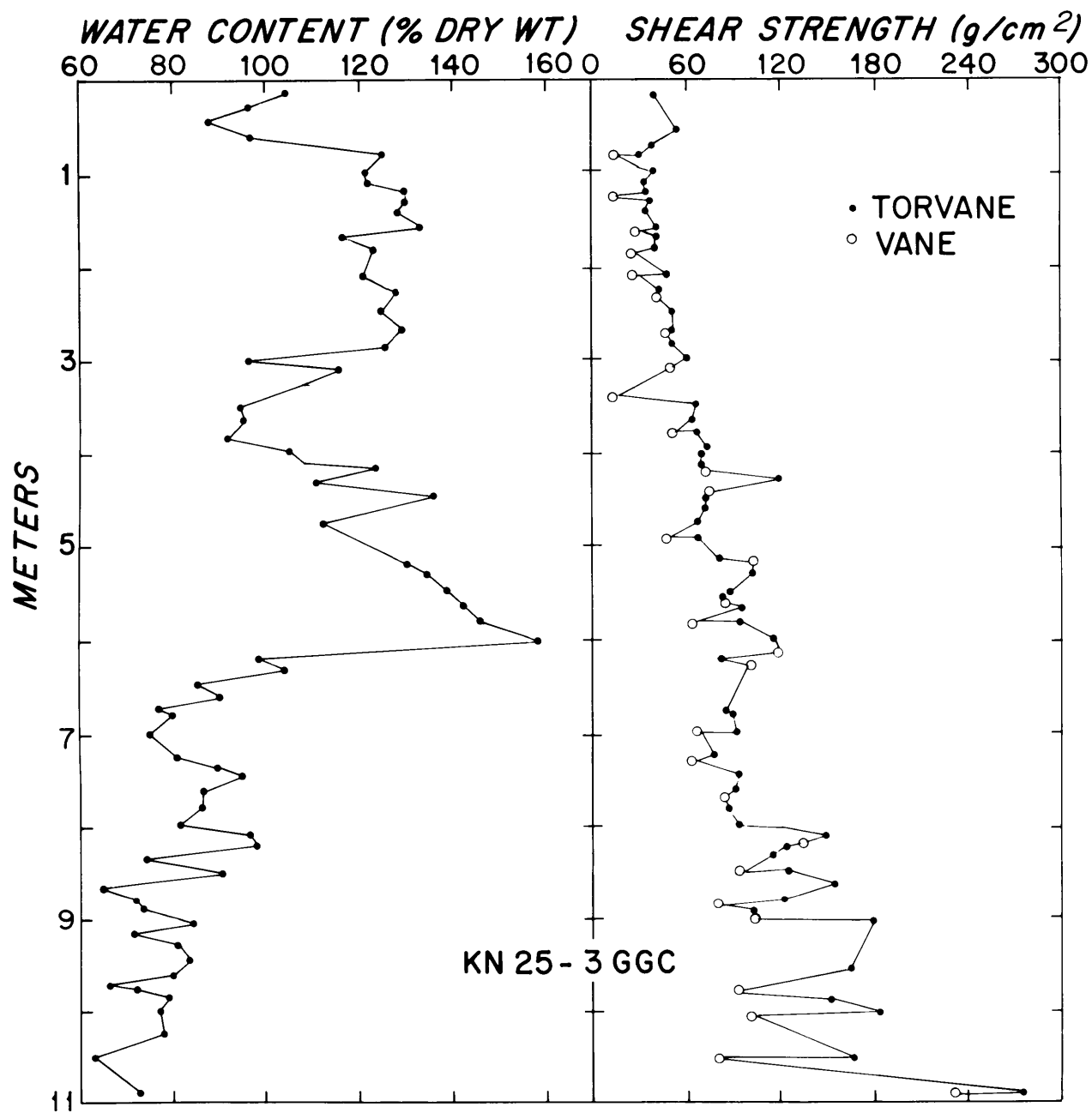


Figure A4.10. Plots of water content and shear strength for giant piston-core KN25-4GPC. At right, filled circles are Torvane measurements; open circles are measurements made with the motorized vane.

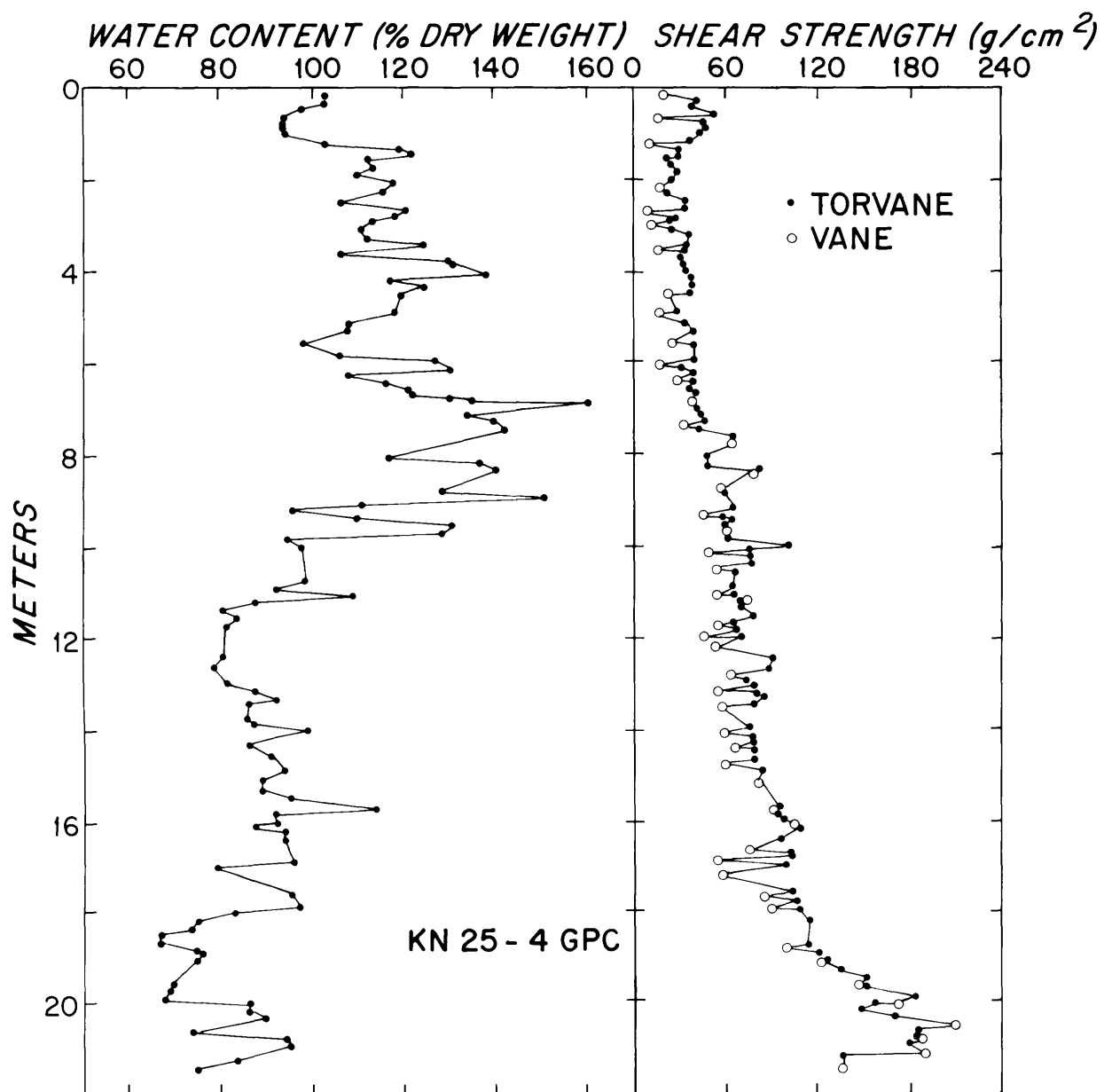


Figure A4.11. Plots of water content and shear strength for gravity core MM-1GC.

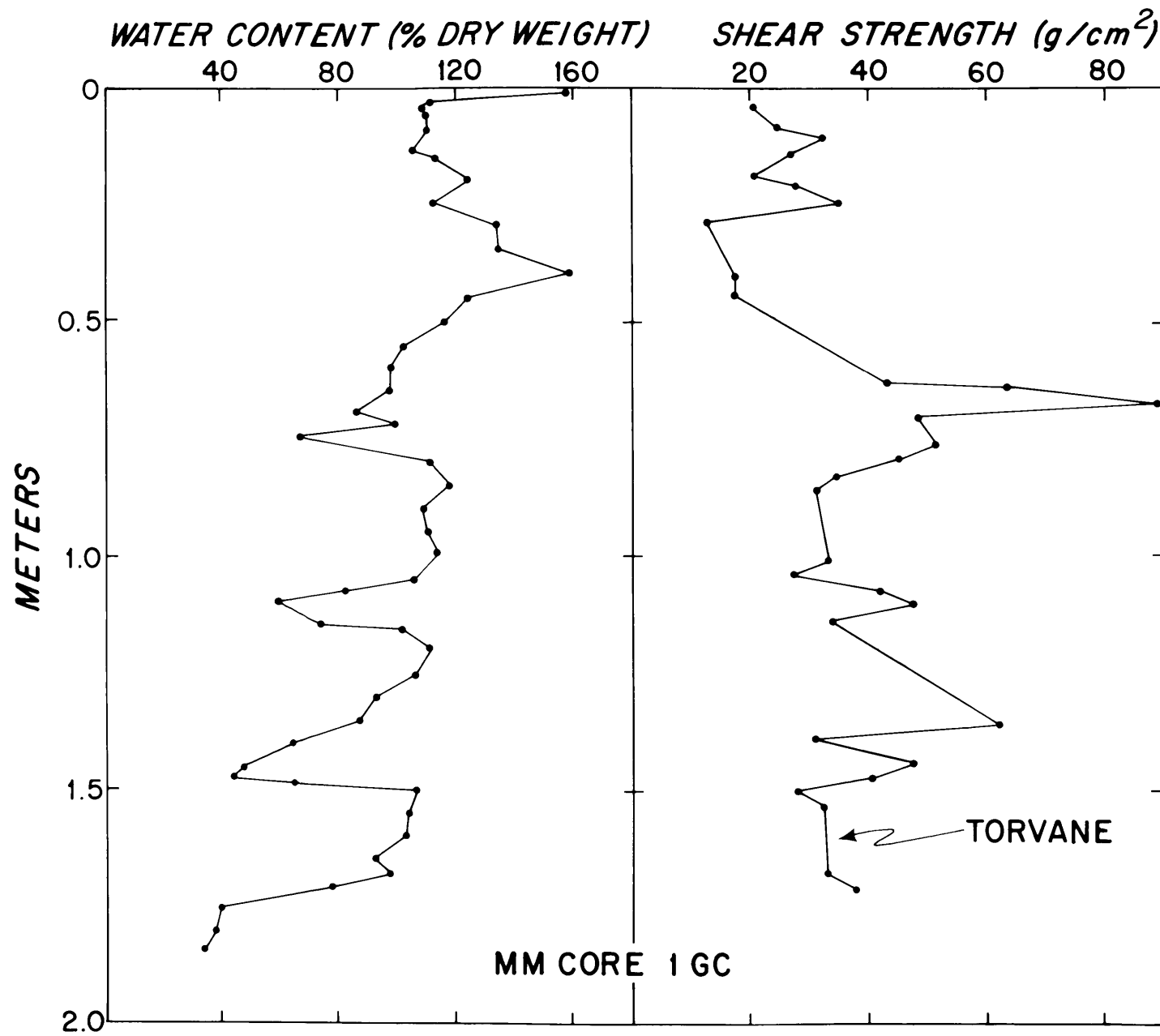


Figure A4.12. Plots of water content and shear strength for gravity core MM-2GC.

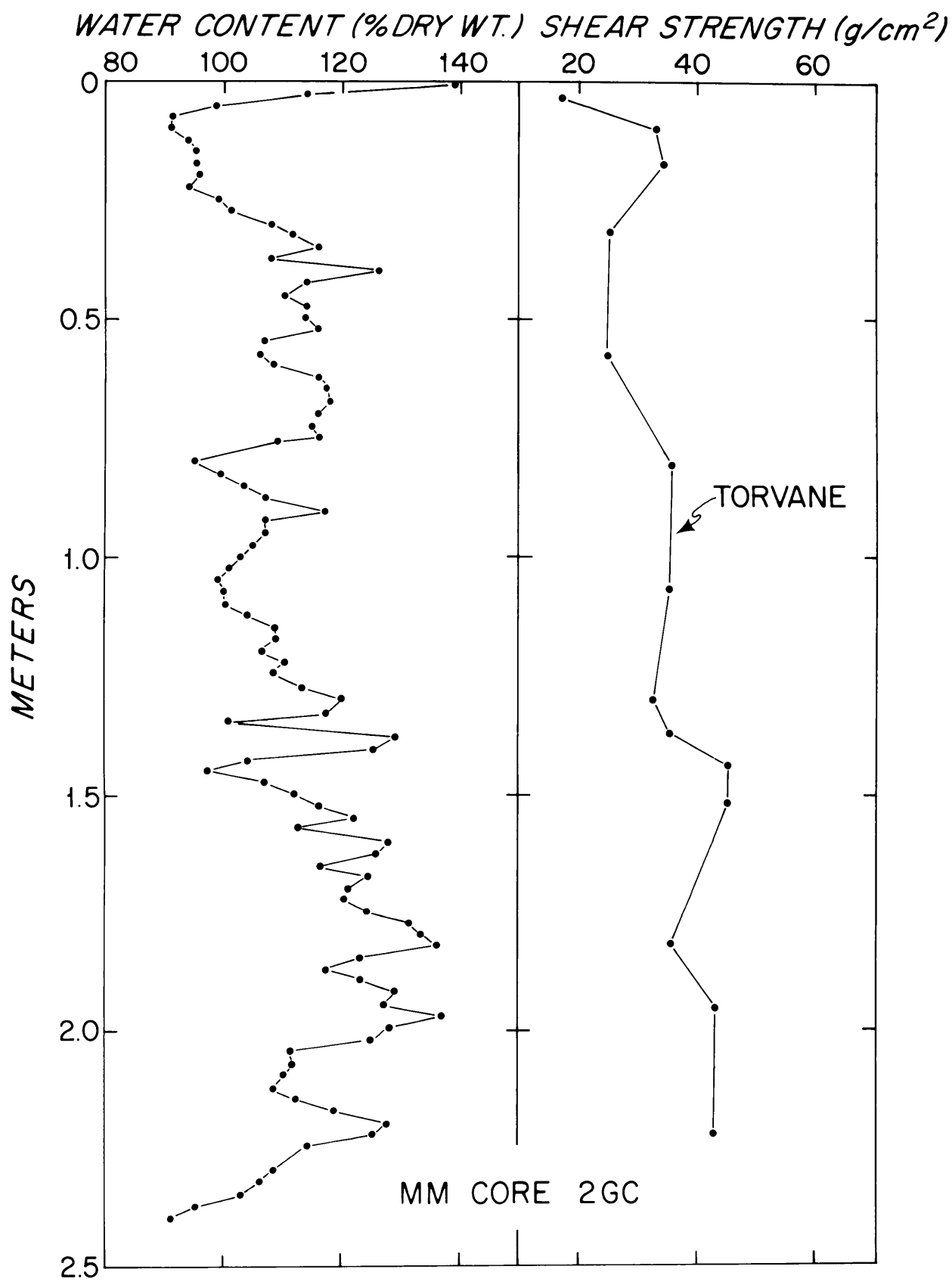
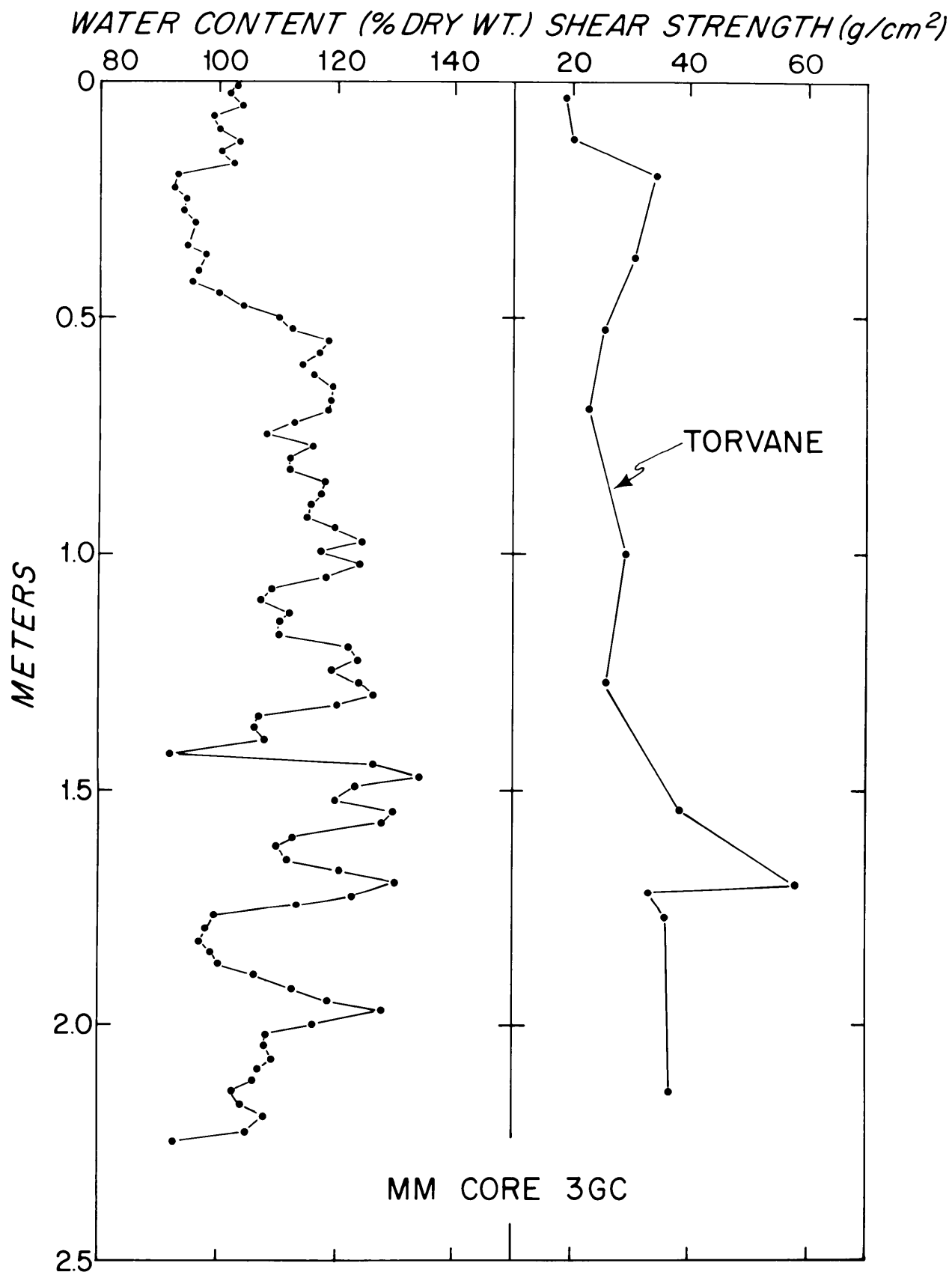


Figure A4.13. Plots of water content and shear strength for gravity core MM-3GC.



BIOGRAPHY

Born: March 19, 1946, Hot Springs, South Dakota

1966-1967 (Summers) Professional Assistant in Geophysics,
Pan American Petroleum Corporation

1968 B.S. in Geology with high honors,
South Dakota School of Mines and
Technology. Elected to Who's Who in
American Universities and Colleges
and the Society of Sigma Xi.

1968 (Summer) Geophysical Assistant, Western
Geophysical Corporation

1968-1972 Full-Time Teaching Assistant,
Massachusetts Institute of Technology
and Woods Hole Oceanographic
Institution.

1972-1973 Graduate Research Assistant, Woods
Hole Oceanographic Institution.

PUBLICATIONS

Wilson, R.W. and B.E. Tucholke (1966) A first record of an
alligator from the Middle Oligocene of the Big Badlands
of South Dakota (abstract): Proc. S.D. Acad. Sciences,
v. 45, p. 287-288.

Tucholke, B.E. and C.D. Hollister (1970) Deposition and com-
position of acoustically transparent deep-sea sediments
(Greater Antilles Outer Ridge)(abstract): Geol. Soc.
America Abs. with Programs, v. 2, p. 710.

Hollister, C.D., B.E. Tucholke, and A.J. Silva (1971)
Results of Giant Piston Coring in the Gulf of Maine
(abstract): Trans. Am. Geophys. Union, v. 52, p. 259.

Tucholke, B.E. and C.D. Hollister (1972) Late Pleistocene
and Holocene sedimentation in the western Gulf of
Maine (abstract): Trans. Am. Geophys. Union, v. 53,
p. 422.

Tucholke, B.E., R.N. Oldale, and C.D. Hollister (1972)
Acoustical survey of Massachusetts and Cape Cod Bays,
Western Gulf of Maine: U.S. Geol. Surv. Misc. Geol.
Investigations, Map I-716.

- Tucholke, B.E., C.D. Hollister, and J.I. Ewing (1972) Deep circulation and sedimentation north of Puerto Rico (abstract): Geol. Soc. America Abs. with Programs, v. 4, p. 693.
- Tucholke, B.E. and C.D. Hollister (1973) Late Wisconsin glaciation of the southwestern Gulf of Maine: new evidence from the marine environment: Geol. Soc. America Bull., v. 84, (in press).
- Tucholke, B.E., W.R. Wright, and C.D. Hollister (1973) Abyssal circulation over the Greater Antilles Outer Ridge: Deep-Sea Res., v. 20, (in press).